European Maritime Safety Agency

NAVISON FINAL REPORT

CALCULATION AND ANALYSIS OF SHIPPING SOUND MAPS FOR ALL EUROPEAN SEAS FROM 2016 TO 2050

EMSA

About this study:

This report was commissioned by the European Maritime Safety Agency (EMSA) under contract number 2021/EMSA/OP/18/2021

Authors:

Özkan Sertlek[1], Alexander MacGillivray[1], Thomas Lloyd[2], Marjolein Hermans[2], Michael Wood[1], Max Schuster[3], Michael Ainslie[1], and Federica Pace[1].
[1] JASCO Applied Sciences (JASCO); [2] Maritime Research Institute Netherlands (MARIN); [3] JASCO Shipconsult.

Recommended citation:

European Maritime Safety Agency (2024), NAVISON Final Report: Calculation and analysis of shipping sound maps for all European seas from 2016 to 2050, EMSA, Lisbon

Legal notice:

Copyright notice:

Table of Contents

List of Tables

List of Figures

List of Abbreviations and Symbols

ADEON	Atlantic Deepwater Ecosystem Observatory Network
AIN	Air INjection
AM	Arithmetic Mean
ASL	areic source level
avg	average
BIAS	Baltic Sea Information on the Acoustic Soundscape
CAR	cargo vessel
CD	Commission Decision
CeNoBS	Support MSFD implementation in the Black Sea through establishing a regional monitoring system of cetaceans (D1) and noise monitoring (D11) for achieving GES
COMPASS	Collaborative Oceanography and Monitoring for Protected Areas and Species
CON	container ship
CPU	central processing unit
dB	decibel
EL	Excess Level
EMSA	European Maritime Safety Agency
END	Environmental Noise Directive
EU	European Union
GES	Good Environmental Status
GiB	gibibyte
GIS	Global Information System
GHG	Greenhouse Gas
HELCOM BLUES	Helsinki Commission Biodiversity, Litter, Underwater noise and Effective regional measures for the Baltic Sea
HOLAS	Holistic assessment
HPC	Hull and Propeller Cleaning
ICES	International Council for the Exploration of the Sea
IQOE	International Quiet Ocean Experiment
JOMOPANS	Joint Monitoring Programme for Ambient Noise North Sea
JONAS	Joint framework for Ocean Noise in the Atlantic Seas
MARIN	Maritime Research Institute Netherlands
MEP	More Efficient Propeller
mo	month
MPA	Marine Protected Area
MS	Member States
MSFD	Marine Strategy Framework Directive
NAVISON	NAVIs SONus
NAVSRCMAP	NAVISON source map
netCDF	network Common Data Form
NPS	National Park Service
NRS	Noise Reference Station

OCS	Outer Continental Shelf
OHF	Optimised Hull Form
PAS	passenger vessel
q	quarter
QGIS	Quantum GIS
QRP	QuieteR Propeller
RANDI	Research Ambient Noise Directionality
RRO	roll on-roll off
SATURN	Solutions @ Underwater Radiated Noise
SOW	spatial observation window
SPL	sound pressure level
SRD	Speed ReDuction
SSP	Sound speed profile
SSSPL	Steady state sound pressure level
TAW	Temporal analysis window
TGC	tanker or gas carrier
TOW	temporal observation window
UNLV	Underwater Noise Limit Value
URN	Underwater Radiated Noise
y	year

Executive Summary

The Navis Sonus (NAVISON) project, sponsored by the European Maritime Safety Agency (EMSA), aims to predict Underwater Radiated Noise (URN) from vessels in European seas. This project was undertaken as a collaborative work between JASCO Applied Sciences (Deutschland) GmbH (JASCO), DW-ShipConsult, and the Maritime Research Institute Netherlands (MARIN).

The main output of the NAVISON project is a collection of sound map layers that can be used to analyse past trends of underwater sound from shipping and investigate the future impact of different technologies and operational measures.

Hindcast (2016 to 2023) and forecast (2030, 2040, and 2050) sound map layers are calculated on a quarterly basis for five selected regions of European waters:

- Baltic Sea,
- Black Sea,
- Mediterranean Sea,
- North Sea, and
- Northeast Atlantic Ocean.

Sound maps are calculated for two one-tenth decade (or decidecade) frequency bands (63 and 125 Hz) corresponding to the European Union's (EU's) Marine Strategy Framework Directive (MSFD) environmental status criterion D11C2 for low-frequency continuous sound. These bands were identified as important frequencies for anthropogenic noise in EU waters. In these two bands, sound map layers are calculated for five vessel types:

- Cargo vessels and bulk carrier (CAR).
- Container ships (CON).
- Cruise and passenger vessels (PAS).
- Tankers and gas carriers (TGC).
- Roll-on-roll-off (Ro-Ro) vessels (cargo and passenger) (RRO).

Underwater radiated noise emissions for these vessels are computed using a semi-empirical source level model, developed during the NAVISON project, called PIANO (Propulsion-Induced Acoustic Noise at Operating conditions). PIANO uses ship design and operational parameters to compute the separate contributions from cavitation and mechanical noise to vessel URN. The PIANO model is used to compute source levels for vessels in European seas from archival ship tracking data from the Automatic Identification System (AIS). Source level tracks are used to compute maps of time-averaged source level density for each region, over a temporal observation window (TOW) of one quarter of a year. The NAVISON approach is based on modelling sound from shipping source level density, rather than from individual ships.

Hindcast sound map layers for 2016–2023 are computed from shipping source level density using JASCO's ARTEMIA (Acoustic Real-Time Exposure Model Involving Ambient) soundscape model. ARTEMIA calculates sound propagation using the parabolic equation (PE) method, based on detailed databases of sound speed, sediment type and bathymetry for European seas. Depth-averaged SPL maps are calculated by averaging the squared sound pressure within the water column across 20 evenly spaced receiver depths, ranging from 5 m to 195 m.

Forecast sound maps layers for 2030, 2040, and 2050 are computed for four different future scenarios for a single frequency band (63Hz):

- Business as usual (BAU).
- Greenhouse gas emissions roadmap (GHG).
- Underwater radiated noise management (URN).
- URN management in addition to GHG roadmap (U&G).

Under BAU, no mitigation measures are applied, with only estimated changes in ship traffic volume contributing to changes in the soundscape. The GHG and URN scenarios focus on intentional abatement of these two sources of emissions separately, while U&G represents a combined scenario striving for reduction of both GHG and URN. The GHG scenario is inspired by the International Maritime Organization's (pre-July 2023) targets for carbon intensity

reduction of shipping by 2050, whereas no such roadmap currently exists for URN. Each forecast scenario involves varying penetration rates for six different mitigation measures as well as long-term changes in shipping traffic volume (relative to a 2022 AIS baseline). The six mitigation measures considered by NAVISON are as follows:

- Speed reduction.
- More efficient propellers.
- Quieter propellers.
- Air injection systems.
- Optimised hull forms.
- Hull and propeller cleaning.

Sound maps for the forecast scenarios are calculated using a novel approach that combines sound map layers for each mitigation measure, based on their penetration rates and joint probabilities of adoption. Separate layers for cavitation and machinery noise are computed for each measure, to predict their effect more accurately on the total soundscape. The mitigation layers are combined, according to the penetration rate of each measure, to produce sound maps for each forecast scenario. This computationally efficient approach allows an arbitrary number of forecast scenarios to be evaluated without re-computing the underlying sound map layers.

During NAVISON, new methods and tools were developed for producing large-scale shipping sound maps in European waters. Innovations introduced by NAVISON include:

- The development of a novel source level model (PIANO) for vessel URN emissions.
- The development of methods to determine the effect of GHG and URN reduction measures on vessel URN.
- A new sound mapping approach, based on source density layers, to make calculations practical over large spatial and temporal scales.
- The implementation of spatial averaging within the receiver cells.
- The use of high-performance computing systems and development of parallelised sound mapping models.
- The use of the arithmetic mean for calculating quarterly averages, following the TG Noise (Dekeling et al. 2014) and IQOE (2019) recommendations.
- A novel forecasting approach based on a probabilistic method for combining sound map layers for different source mechanisms and mitigation measures.
- The use of sound energy density for the analysis of sound maps.

Both the hindcast and forecast sound map layers are provided as network Common Data Form (netCDF)-formatted files. Python scripts are provided for visualising and analysing the sound map layers using the Quantum GIS (QGIS) software package. The sound map layers are analysed in terms of sound energy density, which offers a practical metric to assess the contribution of different vessel categories to underwater sound within the selected regions. In addition to the sound maps, sound energy density is used to answer the following questions:

- Where are the noisiest and quietest spots in the sound maps for all European seas? Which region has the greatest sound energy density?
- How do environmental parameters affect the sound maps? (i.e. bathymetry effects, seasonal changes due to SSP, etc)
- What non-environmental factors are responsible for temporal changes in the sound maps (i.e., including COVID effects, changes in ship routes etc.)?
- What is the ranking of different vessel categories based on their acoustic energy density (for each region and over all of Europe)?

Noisiest and quietest spots:

- The areas with the highest SPL values in Europe appear to be the English Channel, Strait of Gibraltar, Adriatic Sea, Dardanelles, and some regions in the Baltic Sea, where the annually averaged SPL is between 120 and 130 dB for most of the years between 2016 and 2023.
- The areas with the lowest SPL values seem to be the northwest part of the northeast Atlantic Ocean (around Denmark Strait and Irminger Sea), southern part of Mediterranean Sea and east of Black Sea. However, some of the low SPL values could be related to limited AIS coverage in these regions.

- The Baltic Sea exhibits the highest sound energy density, attributed to its combination of high vessel density and shallow water.

Effect of environmental parameters:

- Seasonal temperature variations result in high sea surface temperatures in the summer and low ones in the winter. In turn this leads to strong sound propagation in the winter (and spring) and weak propagation in the summer, corresponding to highest sound energy density observed during the winter and spring quarters (quarters 1 and 2), and lowest in the summer quarter (quarter 3). This seasonal effect is weaker in shallow water regions such as the Baltic Sea and the North Sea.
  The effect of bathymetry can be observed in the sound map layers. For instance, even though there is no large change in the ASL in the same area, estimated SPL values are lower in the deeper parts of the Ionian Sea and the Bay of Biscay.

Effect of non-environment parameters:

Seasonal cycles in sound energy density caused by changes in temperature are sometimes disrupted. One potential disrupting factor is the COVID-19 pandemic, most clearly visible for the PAS vessel category. Moreover, alterations in shipping routes, passenger timetables, changes in the AIS data coverage, and vessel operating speed can introduce variability into source level, which affects the sound energy density.

Ranking of vessel categories:

The percentage contributions to sound energy density from different vessel categories in Europe are ranked from the largest to the lowest contribution:

- At 63 Hz, TGC (about 65 %), CAR (about 30 %), RRO, CON, PAS vessels (about 5 % for all three categories combined).
- At 125 Hz, CAR, RRO, CON (about 30 % for each category), CON and PAS (about 5 % for both categories combined).

Temporal changes in the forecast sound energy density depend on the scenario being considered, with differences between regions and ship types also observed. While under the URN scenario the sound energy density decreased consistently over time compared to BAU for all regions and ship types, this was not observed for the GHG scenario. In this case, the sound energy density for the whole of Europe increased up to 2050 when considering all vessels together, with this effect predominantly caused by TGC vessels, as well as a smaller contribution from CON vessels. For U&G – considered the most realistic scenario – the sound energy density for all vessels across the whole of Europe decreased over time, although TGC showed increases in certain regions (particularly the North Sea), mainly in 2030 and 2040.

The contrasting forecast results between regions and ship types can be attributed to differences in the input data used in the source level modelling. Parameters including vessel age, operating speed and propeller efficiency contribute to the effectiveness of each of the mitigation measures. This, together with the penetration rates adopted for each ship type under the three mitigation scenarios, determines the magnitude and direction of the changes in sound energy density. More specifically, the increases in sound energy density for TGC result from a larger average increase in source level due to the More Efficient Propeller measure than for other ship types, with other measures providing insufficient mitigation effect to compensate for this increase. While this was observed for all forecast years under the GHG scenario, in the U&G scenario, following an initial increase, the sound energy density decreases for the later forecast years as an increasing proportion of vessels are equipped with a Quieter Propeller rather than a More Efficient Propeller.

Comparing NAVISON results with other ship sound mapping projects in Europe, such as BIAS, HELCOM BLUES/HOLAS 3, and JOMOPANS, presents a challenge due to the use of different metrics, specifically arithmetic mean versus median. The 90th percentile maps of JOMOPANS are more similar to the arithmetic mean based on the results of NAVISON, while the 50th percentile (median) maps of JOMOPANS appear lower than the NAVISON maps (arithmetic mean).

Based on the lessons learned during the NAVISON project, the following primary recommendations are listed:

- Harmonise metrics to facilitate quantitative comparisons between different projects.
- Produce sound maps for frequencies other than 63 and 125 Hz for both hindcast and forecast: in particular,
    - investigate the contribution of CON vessels at frequencies below 63 Hz.
    - investigate the performance of GHG and URN mitigation measures for the intermediate bands, 80 and 100 Hz.
- Further develop the PIANO model to improve its usability and extend its applicability.
- Calculate contribution from wind –essential for quantifying exceedance level and potentially important for higher frequencies.
- Validate the existing maps with measurements by quantifying the difference between modelled and measured SPL.

1. Introduction

The Navis Sonus (NAVISON) project, sponsored by the European Maritime Safety Agency (EMSA), aims to predict Underwater Radiated Noise (URN) from vessels in European seas. To achieve this aim, hindcast (2016 to 2023) and forecast (2030, 2040, and 2050) sound map layers are calculated for selected time periods, frequency bands, and vessel types based on vessel traffic data, environmental data, source level models, and propagation loss models (Ainslie et al. 2022, Wood 2022, Lloyd et al. 2024a). This project was undertaken as a collaborative work between JASCO Applied Sciences (Deutschland) GmbH (JASCO), DW-ShipConsult, and the Maritime Research Institute Netherlands (MARIN). Sound map layers are calculated for five selected regions of European waters:

- Baltic Sea,
- Black Sea,
- Mediterranean Sea,
- Northeast Atlantic Ocean, and
- North Sea.

Appendix A describes how and why the borders of these regions are chosen based on the geophysical features (e.g. Dover-Calais crossing or Strait of Gibraltar).

URN is calculated in two one-tenth decade (or decidecade) frequency bands (63 and 125 Hz) corresponding to the European Union's (EU's) Marine Strategy Framework Directive (MSFD) environmental status indicators for low-frequency continuous sound (2008/56/EC)[1]. These bands were identified by Tasker et al. (2010) as important frequencies for anthropogenic noise in EU waters and were identified by Ainslie et al. (2021a) as bands dominated by shipping in the coastal NE Pacific region.

Source levels for the sound map calculations are computed using the PIANO model (Lloyd et al. 2024b, Lloyd et al. 2024a), which was developed during the NAVISON project. PIANO is a semi-empirical model that calculates source levels considering the separate contributions from cavitation noise of the propeller and mechanical noise of the main and auxiliary engines. Inputs to PIANO include ship design parameters, such as propeller type and design, engine type and engine mountings, and wake field quality, as well as operational conditions such as propeller speed and current power. This model is used to compute source levels for five vessel categories using information from archival Automatic Identification System (AIS) tracks:

- Cargo vessels and bulk carrier (CAR),
- Container ships (CON),
- Cruise and passenger vessels (except Roll-on Roll-off (Ro-Ro)) (PAS),
- Tankers and gas carriers (TGC), and
- Ro-Ro vessels (cargo and passenger) (RRO).

Map layers of areic source level (ASL) are computed for each category by processing the outputs of the PIANO model with the NAVSRCMAP tool (MacGillivray et al. 2023a). JASCO's Acoustic Real-Time Exposure Model Involving Ambient (ARTEMIA) software is used to calculate sound map layers for different ship types, years, and seasons from the ASL data. ARTEMIA calculates sound propagation using a wave-equation model, based on detailed databases of environmental inputs (sound speed, sediment type and bathymetry) for European seas. The sound map layers are analysed in terms of sound energy density, which offers a practical metric to assess the contribution of these five vessel categories to underwater sound within the selected regions.

The modelling approach for forecast sound map layers involves combining baseline layers (based on 2022 AIS tracks) for different URN and greenhouse gas (GHG) reduction measures. Each forecast scenario involves varying penetration rates for six different mitigation measures as well as changes in ship traffic volume. The mitigation measures considered by NAVISON are as follows:

- Speed reduction,
- More efficient propellers,
- Quieter propellers,
- Air injection systems,

[1] The MSFD indicators are expressed in terms of 1/3-octave bands. These are functionally equivalent to decidecade bands.

- Optimised hull forms, and
- Hull and propeller cleaning.

Sound maps for the forecast scenarios are calculated using a novel approach that combines map layers based on the joint probabilities of adoption of these six mitigation measures.

This report omits detailed descriptions of the modelling approach and sound map layer outputs, which were already covered in the previous progress reports (Wood 2022, Lloyd et al. 2023, MacGillivray et al. 2023a, Lloyd et al. 2024a, Sertlek and MacGillivray 2024). This report primarily focuses on highlighting the novelty of the modelling approach (Chapter 2), and on the analysis of both hindcast and forecast sound map layers (Chapter 3). Limitations of the modelling approaches and on how to use the results are discussed in Chapter 4.

In addition to the sound maps, sound energy density is used to answer the following questions:

- Where are the noisiest and quietest spots in the sound maps for all European seas?
- How do environmental parameters affect the sound maps? (i.e. bathymetry effects on the Mediterranean Sea maps, seasonal changes due to SSP, etc)
- What non-environmental factors are responsible for temporal changes in the sound maps (i.e., including COVID effects, changes in ship routes etc.)?
- What is the ranking of different vessel categories based on their acoustic energy density (for each region and over all of Europe)?
- Which region has the greatest sound energy density?

Further review of NAVISON is then made through comparisons with other sound mapping projects in Chapter 5 and discussion of the outcomes in Chapter 6, with conclusions and recommendations for future projects summarised in Chapter 6.5.

2. Modelling Approach

During NAVISON project various methods and tools have been developed to calculate sound maps for all European waters (Figure 1). These tools perform the following tasks:

- AIS vessel traffic data processing
- Source level calculations for selected vessel categories
- Calculating source density (i.e., areic source level) map layers
- Acoustic environmental model automation
- Sound propagation modelling
- Sound mapping and visualisation in GIS software
- Post -processing of sound map layers

To meet the NAVISON project's requirements, existing tools from MARIN and JASCO (such as DECS and ARTEMIA) have been improved with new capabilities and databases specific to NAVISON regions. First, based on the AIS inputs, the PIANO model calculates the source levels. The NAVSRCMAP[2] tool processes the output of PIANO model to produce ASL map layers by analysing ship track data and source levels corresponding to various ship categories across a specified timeframe. The NAVISON sound map layers are calculated from the ASL map layers and environmental parameters (sound speed profiles, sediment properties and water depth). During the post-processing, sound energy density is calculated from the sound maps to analyse temporal trends and the contributions of different vessel categories to underwater sound. Sound energy density is also used to assess the performance of GHG and URN mitigation measures for the forecast scenarios.

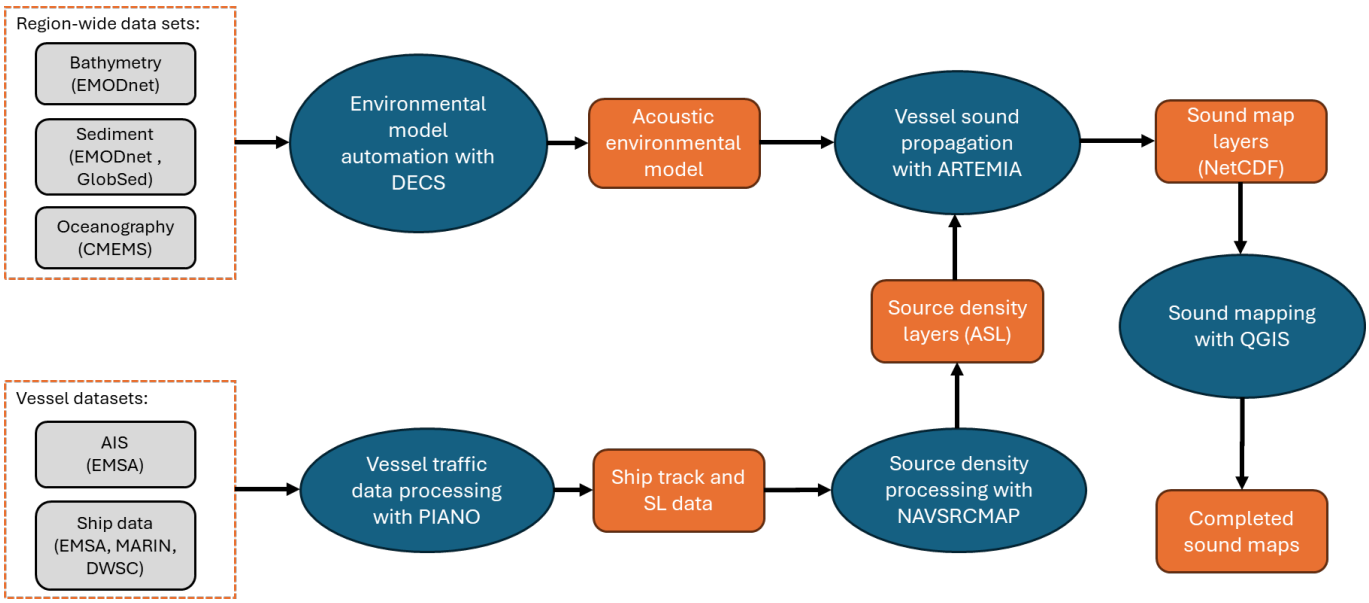

Figure 1 Diagram showing the process flow for producing the NAVISON sound maps. Blue ovals indicate processes, grey boxes indicate process input data, and orange boxes indicate process outputs.

Sound map layers are calculated for:

- 5 regions.
- 2 frequencies (63 and 125 Hz).
- 5 ship categories and sum of all categories.
- 4 quarters of each year and annual average.
- 8 hindcast years (2016 to 2023, inclusive).
- 3 forecast years (2030, 2050 and 2050).
- 4 GHG and URN management scenarios.

[2] Details of the NAVSRCMAP tool are described in the Task 1.3 progress report (MacGillivray et al. 2023a),.

The sound map layers are provided as network Common Data Form (netCDF)-formatted data files. The computations are performed on JASCO's high performance computing cluster infrastructure which accelerates the sound maps computations by running the sound field calculations on multiple computing nodes, with up to 96 CPU cores and 256 GiB of memory per node. Once all calculations are completed, ARTEMIA model outputs are converted to netCDF file format. The detailed content of netCDF files is described in Appendix G. The sound maps are calculated in WGS-84 geographic coordinates (coordinate reference system EPSG:4326); the netCDF files, therefore, also use the same coordinate system. These netCDF files for sound map and areic source level layers for different regions, period, vessel categories and frequency band are visualised using Python scripts in the Quantum GIS (QGIS) software package.

The NAVISON project involved a number of innovations:

- Development of a novel source level model (PIANO) for vessel URN emissions
- Development of methods to determine the effect of GHG and URN reduction measures on vessel URN.
- A new sound mapping approach, based on source density (ASL) layers, to make calculations practical over large spatial and temporal scales.
- Implementation of spatial averaging within the receiver cells (following the approach of Sertlek et al. (2019b) for large scale sound maps).
- The use of high-performance computing systems and development of parallelised sound mapping models
- The use of the arithmetic mean for calculating quarterly averages, following the TG Noise (Dekeling et al. 2014) and IQOE (2019) recommendations (although the arithmetic mean was used by (Sertlek et al. 2019b), it is first time implemented for a regional or larger scale sound mapping project).
- A novel forecasting approach based on probabilistic method for combining sound map layers for different source mechanisms and mitigation measures.
- The use sound energy density for the analysis of sound maps.

More details about these approaches will be given in the following subsections.

2.1 Source Modelling

We describe how the source level information required for sound mapping is obtained in the NAVISON project. This covers the development of a new source level model, processing of ship traffic and data and derivation of source density information.

2.1.1 Source Level

A key development of the NAVISON project is a new semi-empirical source level model for broadband machinery and propeller cavitation noise of ships, called the Propulsion-Induced Acoustic Noise at Operating conditions, or PIANO model. The PIANO model adopts a physics-based approach, making it suitable for application to both hindcast and forecast sound mapping studies, as well as early design stage URN estimations, through its ability to model the effects of changes in ship design and operating parameters on source levels. Important improvements on existing point source models include the ability to model machinery noise of two-stroke engines (which are used by the majority of the world fleet) and model changes in source level of controllable-pitch propellers (CPPs) when operating at reduced pitch. PIANO is inspired by, and combines and improves on features from, several existing ship source level models:

- The Wittekind model (Wittekind 2014), a semi-empirical model which models machinery and cavitation noise source mechanisms separately, but does not model noise from two-stroke engines;
- The JOMOPANS-ECHO (J-E) model (MacGillivray and de Jong 2021) an empirical model which distinguishes between different ship types, but does not take the engine or propeller operating condition into account; and
- The Empirical Tip Vortex (ETV) model (Bosschers 2018), which models broadband cavitation noise based on the propeller design and operating condition, but requires detailed simulations of the propeller geometry as input.

An overview of how the total source level is predicted using the PIANO model is given in Figure 2. To derive the operating condition of the engine(s) and propeller(s) a higher number of input parameters are required than for existing point source models. Much of this information can be obtained from a ship particulars database, with the rest obtained using regression formulae and empirical relationships. These are provided in Lloyd et al. (2024a).

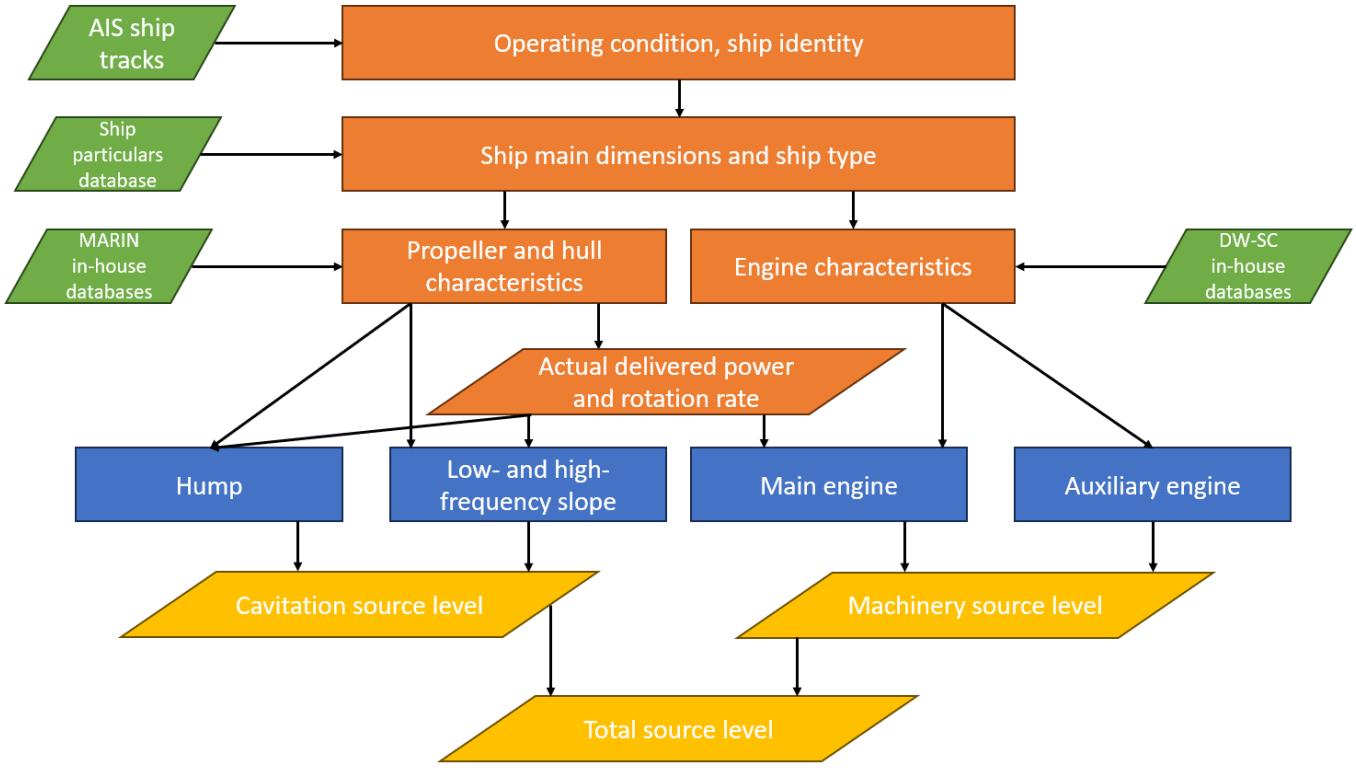

Figure 2 PIANO source level model flow chart. Model inputs shown in green, processes and intermediate results in orange, individual spectral components in blue, and outputs in yellow.

Example source level spectra obtained using the PIANO model are shown in Figure 3 and compared to measurement data and predictions using two existing point source models. The two graphs cover different ship types and operating conditions: the container ship is equipped with a two-stroke engine and fixed-pitch propeller and is operating close to its service speed, while the general cargo ship is powered by a (resiliently mounted) four-stroke engine and controllable-pitch propeller, with the CPP operated at reduced pitch due to the low ship speed.

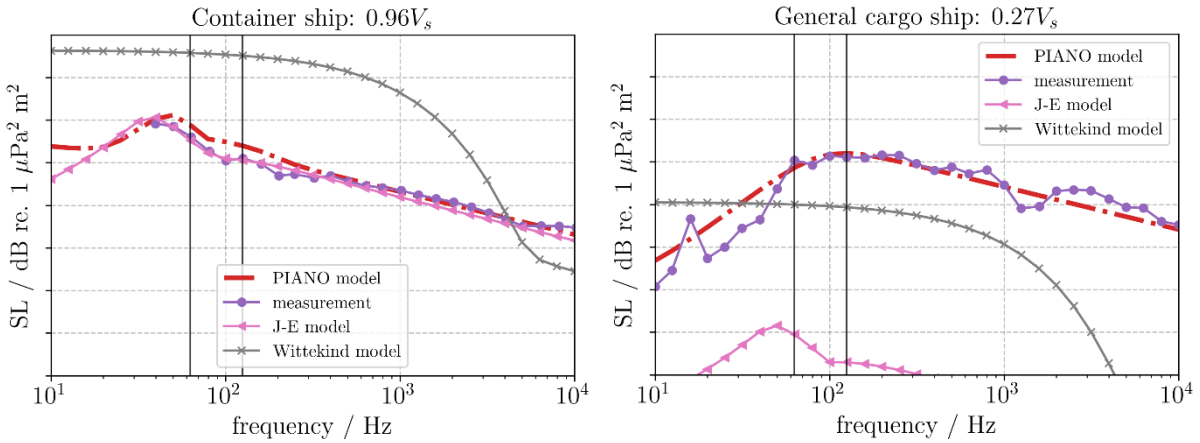

Figure 3 Example source level spectra in dB as a function of frequency in Hz for the PIANO model, compared to measured data and existing ship point source models: containership (left) and general cargo vessel (right). The vessel operating speed is shown in the plot titles as a decimal fraction of the service speed V_s. No scale is shown on the ordinate for confidentiality reasons relating to the measurement data. Scale divisions of the ordinate are 10 dB, such that the total y axis range is 80 dB. Measurement data made available to MARIN through the Cooperative Research Ships (CRS) framework.

In both cases shown in Figure 3 the PIANO model results agree well with the measurement data while also displaying improved predictions compared to the existing models. For the container ship, the SL spectra from the PIANO and J-E models are very similar, while the Wittekind model overpredicts the SL significantly since it was not intended for modelling two-stroke engines. In the case of the general cargo ship, the PIANO model was empirically tuned to account for changes in the spectral level and shape of cavitation sound for propellers operating below design pitch. Since it is the first model to include this behaviour, the predicted source levels are more accurate for this ship/propeller

type and operating condition. For the operating condition shown, the Wittekind model assumes that the propeller is not cavitating, and therefore only models machinery noise, while the SL of the J-E model simply reduces with decreasing speed with no change in the spectral shape depending on the propeller type.

Further validation and tuning of the PIANO model were performed using a large database of ship URN measurements provided by the ECHO Program. Model SL predictions were compared to measured spectra for almost 6000 transits involving about 1400 individual vessels covering a wide range of ship types. Comparison error statistics were used to manually adjust the model empirical constants and coefficients per ship type in order to reduce the comparison error as much as possible. The resulting comparison error statistics for the final tuned PIANO model were found to be similar to those reported for the J-E model, with a frequency-averaged absolute error and standard deviation of 5.6 dB and 7.1 dB respectively for the PIANO model, compared to 5.0 dB and 6.0 dB for the J-E model. The slightly increased error level of the PIANO model compared to the J-E model was deemed to be acceptable given the much higher predictive capabilities offered by the newly developed model.

2.1.2 Ship Tracks

Source information for generating the sound maps was obtained by applying the PIANO model to ship traffic data in European waters for the selected ship types and time periods. A brief overview of the procedure is provided here with a full description given in MacGillivray et al. (2023a).

The ship traffic was based on Automatic Identification System (AIS) data provided by EMSA. An overview of the raw AIS data set used for generating the ship tracks is provided in Appendix B.

Before the source information could be generated, several processing steps were performed in order to convert the raw AIS messages into so-called journeys. Firstly, the messages were converted from National Marine Electronics Association (NMEA) format to human-readable text files of ship tracks containing both static (e.g. IMO number) and dynamic (e.g. speed over ground) AIS messages, covering the entire European region. This process also filters out data deemed to be unreliable, e.g. duplicate messages, incorrect position updates and speed over ground data.

Next, additional input parameters required by the PIANO model were linked to the track data using the IMO number of each vessel present in the AIS data set. These additional parameters were available from a ship particulars database provided by EMSA. Where required data fields were not available in the database, or entries for a particular vessel were missing, these parameters were estimated using regressions derived from the database as part of the NAVISON project, or existing empirical relationships available from the open literature or in-house databases. For example, the propeller diameter was not available and was estimated as a function of design draft for each ship type. At this stage, each unique vessel was also assigned a ship type category for generating the sound maps, i.e. a broader categorisation than the ship types listed in the ship particulars database.

Following this, the track data was filtered into journeys, using criteria based on position, draft, and speed. In this way, vessels berthed in ports – which were not included in the study – were omitted from the data set. Vessels anchored offshore (assumed to be when speed over ground was less than 3 knots) were retained. The journeys were then filtered to obtain the monthly traffic for each of the five regions separately.

Finally, source information was appended to each track point, namely the source level at 63 and 125 Hz and the source depth. The source depth is taken to be equal to the propeller shaft immersion, which is obtained from the operating draft provided in the ship tracks and the estimated propeller diameter. A single source depth is used, which is assumed to be representative of the combined machinery and propeller cavitation noise sources.

2.1.3 Areic Source Level

The NAVISON approach is based on modelling sound from time-averaged shipping source density, rather than from individual ships. The density-based approach is practical for large areas and long temporal durations (i.e., over time scales of quarters and years). In this approach, the sources are assumed to be distributed uniformly within each map cell and the corresponding source levels are based on the integrated sound source energy inside the cell. This is a novel and computationally efficient method that can be used to assess many different combinations of seasons, years, ship types, traffic scenarios, and technical and operational measures. The alternative approach is to calculate sound maps using the time-dependent locations of individual ships in AIS data sets (e.g., as in BIAS and JOMOPANS; Folegot et al. 2016, de Jong et al. 2021). This method is practical for small regions or limited numbers of sound sources but comes with a significant computational burden when modelling shipping sound propagation for thousands of sources over ocean basin scales and multiple years. Generating such data products with sufficiently fine time resolution is infeasible for NAVISON given the large spatiotemporal scope of the project. Thus, the shipping-density-based modelling approach is preferred, due to the large area, number of regions, and number of years involved.

For NAVISON, georeferenced layers of gridded source density data are used to quantity the sound energy originating from different categories of vessel, for a specified region, season, and frequency band. These source density layers are calculated by applying post-processing to the ship track data and associated source levels (Section 2.1.2). This post-processing is implemented using a bespoke software tool, called *Navsrcmap*. which outputs raster files of georeferenced source density grids, by vessel type and frequency band. Source density is represented in terms of the areic source factor (ASF; symbol $F_{S,A}$; units of Pa^2), which is defined as the mean vessel source factor per unit area within a single grid cell. The ASF within each layer is adjusted to a reference source depth, based on the mean source depth of the vessel tracks, to facilitate the sound propagation modelling (Table 1). For visualisation purposes, the ASF data can be represented as areic source level (ASL; symbol $L_{S,A}$) data by converting to decibels (Figure 4).

Table 1 Average source depth (m) by vessel category, used for computing ASL.

Category	ASL Source Depth (m)
CAR	3.8
CON	5.1
PAS	3.2
RRO	3.8
TGC	5.1

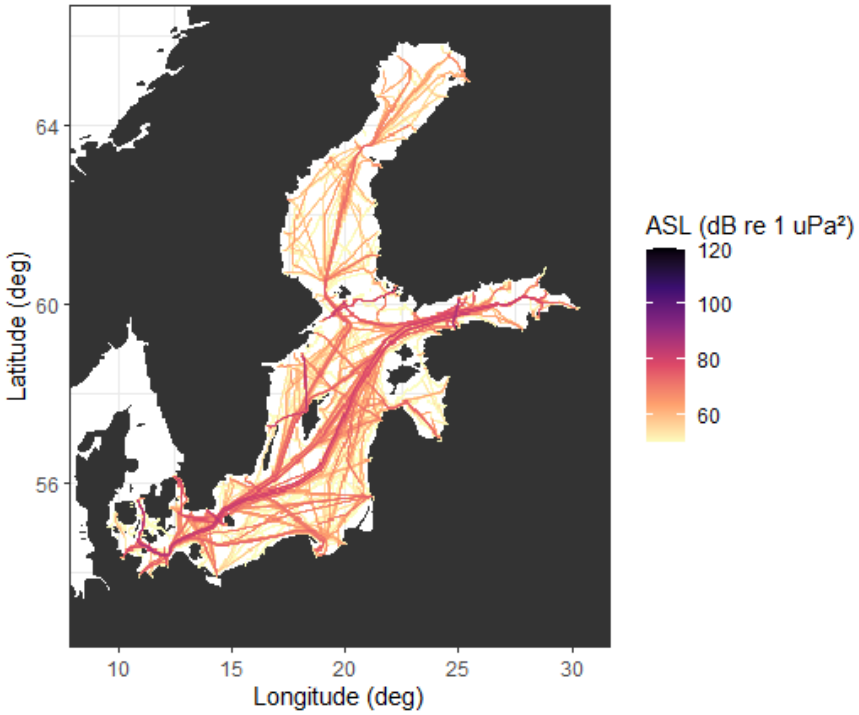

Figure 4 Example grid of areic source level for the Baltic Sea in the 63 Hz decidecade band.

2.2 Propagation Modelling

Sound propagation modelling was conducted using JASCO's Acoustic Real-Time Exposure Model Incorporating Ambient (ARTEMIA). ARTEMIA is a soundscape mapping model that accurately simulates underwater sound levels generated by large ensembles of vessels (and other marine sound sources) on a regional scale. ARTEMIA can be configured to compute propagation loss using different methods. For NAVISON, propagation loss calculations were conducted using the parabolic equation (PE) method. The implementation of the PE method in ARTEMIA is called CRAM (Complex-density Range-dependent Acoustic Model), and it computes acoustic propagation via a wide-angle split-step Padé parabolic equation solution to the acoustic wave equation. CRAM is based on the RAMGEO1.5 (Collins 1993a) source code but includes many enhancements over the original version:

- Simulation of bottom loss from an elastic seabed using the complex-density equivalent fluid approximation (Zhang and Tindle 1995).
- Inclusion of seawater attenuation using the frequency-dependent Horton-Thorp-Urick formula (equation 1.47 in Jensen et al. 2011).
- Consideration of the Earth's curvature using Tappert's effective sound speed (Collins 1993b).
- Variable range step for enhanced short-range accuracy.
- Adaptive vertical grid for more efficient field calculations.
- Thread safety, dynamic memory allocation, and several bug fixes.

ARTEMIA generates acoustic fields in three dimensions by modelling propagation loss using CRAM within two-dimensional (2D) vertical planes aligned along radials covering a 360° swath from the source, an approach commonly referred to as *N*×2D. These vertical radial planes are separated by an angular step size of $\Delta\theta$, yielding $N = 360°/\Delta\theta$ number of planes (Figure 5). N is chosen as 36 for the NAVISON sound map computations.

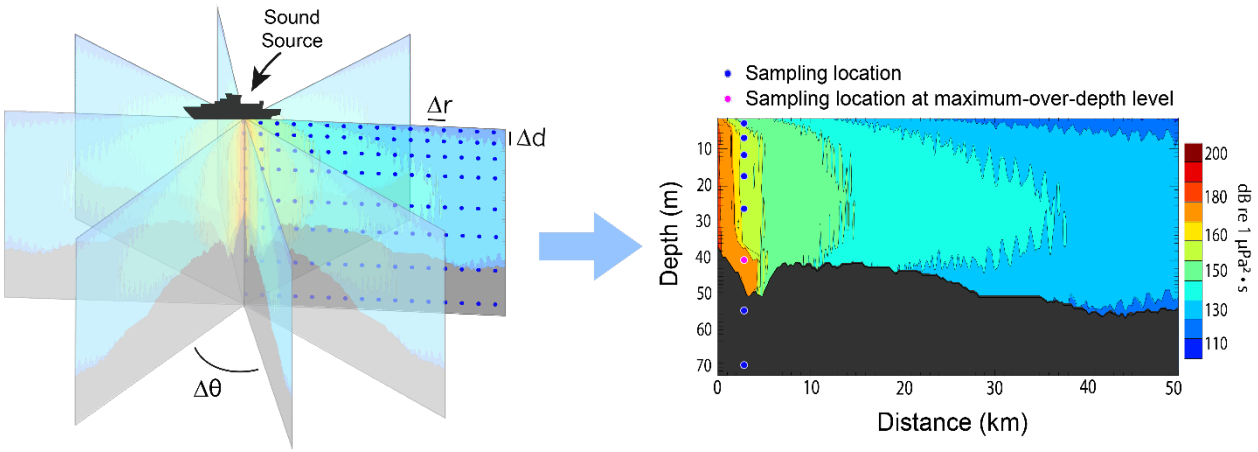

Figure 5 The N×2-D modelling in ARTEMIA, with each transect computed using CRAM.

The PE method has several advantages that make it well suited to modelling low-frequency sound propagation (63 and 125 Hz). These include explicit range dependence of bathymetry and environmental properties, arbitrary vertical stratification of sound speed profile in the water column, arbitrary stratification of geo-acoustic properties in the seabed, and computational efficiency at low-to-intermediate frequencies dominated by vessel URN (below approximately 500 Hz). Furthermore, the complex-density PE implemented by CRAM can accurately simulate elastic seabed properties for most common seabed sediments, which increases the accuracy of long-range PL calculations at continental shelf locations. For PE models, the most important factors affecting model accuracy are the range step and depth increment, and the number of Padé terms that effectively defines the maximum steepness angle of sound propagation. A battery of convergence tests was used to select appropriate computational parameters for each region (Table 2), as detailed in the Task 1.2 report (Wood 2022).

Table 2 PE computational parameters for the 63 and 125 Hz bands.

Parameter	Baltic Sea	North Sea	Black Sea	Mediterranean Sea	Northeast Atlantic Ocean
Fine range step (m)	-	-	10	10	10
Coarse range step (m)	50	50	50	50	50
Max. range of fine range step (m)	-	-	10000	10000	10000
63 Hz depth increment (m)	3	3	3	3	3
125 Hz depth increment (m)	1.5	1.5	1.5	1.5	1.5
Padé terms	4	2	3	4	4
Maximum range (m)	300000	400000	500000	600000	900000

Different approaches to modelling sound propagation for sound mapping have similarly been demonstrated in EU seas. BIAS used the parabolic equation method to model underwater acoustic propagation (Folegot et al. 2016), whereas the JOMOPANS and Sertlek et al. studies used a hybrid normal mode energy flux approach (Sertlek et al. 2019a). Verification benchmarks performed by the JOMOPANS project demonstrated the consistency of these two PL methods in the North Sea region. The parabolic equation approach (Wood 2022) has been adopted for NAVISON

as this method retains its accuracy in deep-water basins (i.e., Black Sea, Mediterranean Sea, and northeast Atlantic Ocean) without modification.

The environmental inputs required for the computing propagation loss in CRAM are bathymetry, sound speed profiles, and geo-acoustic profiles. Fully range-dependent inputs for all relevant environmental parameters are generated automatically using a version of JASCO's Digital Environmental Catalogue System (DECS), specially adapted to the requirements of NAVISON. The regions were divided into environmental zones (5 × 5′), with each containing the location-specific sound speed profile and geo-acoustic profile. DECS is configured to use the best-available set of databases covering the NAVISON study area:

- Bathymetric data for the regions are obtained from EMODnet. The bathymetric data sets provided are composed of numerous aggregated studies from numerous public and research organisations and are collated into a single Digital Terrain Model (DTM) of European seas (https://www.emodnet-bathymetry.eu/). The grid resolution of the EMODnet bathymetry is 1/16 × 1/16′ (one arc minute (1′) corresponds to approximately one nautical mile (1852 m) at the equator).
- Sound speed profiles for the modelling are calculated from time-dependent and depth-dependent profiles of temperature and salinity from the Global Ocean Physics Reanalysis data set from the Copernicus Marine Environment Monitoring Service (CMEMS). These data provide the year-specific monthly-averaged temperature and salinity profiles at a horizontal resolution of 5′ and at water depths from 0 to 5500 m. Where the sound speed profile does not reach the maximum water depth within that environmental zone, it is extrapolated to the sea floor presuming constant temperature and salinity.
- Geo-acoustic profiles for the modelling area are based on a location-dependent two-layer system that consists of a sediment layer and a basement layer. The composition of the sediment layer is based on the Folk classification from the EMODnet Seabed Substrate data set; where there were gaps in the data, the seabed material was presumed to be the most common sediment type seen across the data at the same water depth. The substrate layer is based on the EMODnet Seafloor Geology data set. The sediment layer thickness is from the “GlobSed: Updated total sediment thickness in the world's oceans” data set (Straume et al. 2019). The descriptions of the substrate were converted to numeric inputs using sediment property values from by Ainslie (2010), and depth-dependent equations by Hamilton (1980); the median sound speed at the sea floor across the environmental zone.

To provide environmental data for all regions, seasons, and years, the entire process was automated to generate the suite of environments required for propagation modelling. Additional details regarding the environmental databases used by DECS are provided in the Task 1.2 progress report (Wood 2022).

2.3 Sound Map Layers and Sound Energy Density

To calculate the sound map layers, the inputs of Areic Source Level (ASL) layers are used for each vessel category for a specified timeframe. The calculations are performed individually for the 63 and 125 Hz decidecade centre frequencies. Sound map layers are calculated, including:

- 5 regions.
- 2 frequencies (63 and 125 Hz).
- 5 ship categories and sum of all categories.
- 4 quarters of each year and annual average.
- 8 years (2016 to 2023).

The ARTEMIA soundscape model computes sound pressure at 20 evenly spaced receiver depths, ranging from 5 m to 195 m. These depths were selected to align with the typical habitat range of marine animals and the depth recommendations provided by IQOE guidelines (2019). The depth-averaged Sound Pressure Level (SPL) is then calculated by averaging the squared sound pressures within the water column across these specified receiver depths. The resulting sound map layers display the depth-averaged SPL values for all regions. The depth averaging is only relevant to sound map layers; no depth averaging is applied to the ASL map layers.

Sound map layers are generated by accumulating all vessel sound emissions within a specified time interval, referred to as the temporal observation window (TOW). TOW is the interval of time within which a statistic of the sound field

is calculated or estimated[3] (Ainslie et al. 2021b). For NAVISON map layers, the TOW was chosen as one quarter of a year. Annually averaged sound map layers are computed by averaging the four quarterly sound map layers for a single year. The chosen TOW values for each quarter and year are listed in Table 3.

Table 3 Temporal Observation Window (TOW). The number of days for each TOW varies between quarters because it is determined by the number of calendar days corresponding to the AIS data inputs.

TOW	Quarter abbreviation	Start and end date	TOW in days	TOW in seconds
First quarter	q1	1 January – 31 March	90 days (or 91 days in leap years)	7776000 s (or 7862400 s in leap years)
Second quarter	q2	1 April – 30 June	91 days	7862400 s
Third quarter	q3	1 July – 30 September	92 days	7948800 s
Fourth quarter	q4	1 October – 31 December	92 days	7948800 s
Annual average	avg	1 January – 31 December	365 days (or 366 days in leap years)	31536000 s (or 31622400 s in leap years)

At every location, sound propagation is computed using a representative monthly average sound speed profile for each quarter[4]. The months of February, May, August, and November are used to represent quarters 1 through 4. Sound speed profiles are not averaged over the TOW, as to do so would smooth out vertical gradients within the thermocline that are important for accurately capturing the effect of refraction on sound propagation. Use of a single month to represent the sound speed profile for each quarter more accurately represents water-borne propagation paths over long distances and provides an acceptable trade-off between computational time and model accuracy.

The source level and sound map layers are computed on a regular computational grid specified in latitude and longitude coordinates. The latitude and longitude increments are chosen so that the spatial observation window (SOW) is approximately square at the centre of the map layers. SOW is a region of space within which a spatially averaged power quantity is calculated or estimated, for a specified duration of the TOW. The size of a SOW is specified by means of an area, expressed in km^2, and a depth range (e.g., 50 to 200 m) (Ainslie et al. 2021b). Table 4 shows the chosen SOW and map resolutions for each region.

[3] Examples of statistic include rms sound pressure, peak sound pressure, and sound pressure kurtosis. An example is rms sound pressure calculated using a temporal observation window of 1 min.
[4] Sound speed is computed from mean temperature and salinity profiles from the Copernicus Marine Environmental Modelling Service (CMEMS 2023), at a spatial resolution of 1/12° as described in the Task 1.3 progress report (MacGillivray et al. 2023a),.

Table 4 Sound map layer resolution. The spatial observation window (SOW) is equal to the map layers resolution.

Region	Longitude (degrees)		Latitude (degrees)		SOW size (Lon degrees x Lat degrees)	Mean SOW area of map layer (km²)
	min	max	min	max		
Baltic Sea	9.0	30.52	53.0	66.0	0.08 x 0.04	20 km²
North Sea	-5.0	13.56	50.0	60.8	0.08 x 0.04	22.3 km²
Black Sea	27	42.03	40.8	48.01	0.09 x 0.07	55.6 km²
Mediterranean Sea	-5.5	37.16	29.0	47.06	0.09 x 0.07	61.1 km²
Northeast Atlantic Ocean	-30.0	36.66	24.0	74.54	0.22 x 0.14	240 km²

The map resolutions and SOW areas vary across regions. The choice of different resolutions is driven by the need for efficient utilisation of computational time and resources. Sound mapping tends to be computationally demanding, contingent on factors such as the size of the mapping region, the number of sound sources, and frequencies involved. To handle optimally the extensive computations, different map resolutions are required: the sound map layers of the northeast Atlantic Ocean have the largest spatial extent but the lowest spatial resolution. Nevertheless, even with varying resolutions, the computational method based on the representation of vessels as a spatially distributed (i.e., areic) sound source. As described in detail in the Task 1.3 Progress Report (MacGillivray et al. 2023a) the SPL for a spatially distributed source is computed by means of spatial averaging of the propagation factor within the SOW; this operation, referred to as "box-averaging", ensures the preservation of consistent sound energy in each map layer. This approach ensures that sound levels are represented consistently between map layers, even when those layers are computed with different spatial resolutions. For sound maps, spatial averaging is applied to ensure the conservation of total sound energy (Sertlek et al. 2019b) within each map layer cell, using selected spatial observation windows (SOW; i.e., the area over which spatial averaging is applied) equal in size to the map resolution.

2.4 Forecast Scenarios and Modelling Approach

Forecast sound maps can be used to examine the effects of potential changes in ship traffic and design and operational variables on future soundscapes under various assumed scenarios. To achieve this capability within the NAVISON project, the existing soundscape modelling framework outlined in Sections 2.1–2.3 was adapted such that the effects of a number of mitigation measures on URN could be simulated. Several scenarios were developed such that the effects of differences in regulatory policy could be compared. This section is a summary of the work reported in MacGillivray et al. (2023a).

2.4.1 Forecast Scenarios

A number of forecast scenarios up until the year 2050 were devised based on different assumptions regarding the future regulatory environment for shipping. This considered policy related both to GHG and URN emissions. The International Maritime Organization (IMO) has published a clear roadmap for the decarbonisation of shipping (2022)[5], with several performance indices already in force for the majority of the world fleet. On the other hand, regulation of ship URN (within the EU) is currently limited to the MSFD, with no firm plans for the future implementation of a mitigation strategy[6]. Several scenarios were developed, recognising that the existing GHG emissions regulations represented the highest certainty in terms of future regulatory environment, while also assuming that there are ambitions for the development of URN mitigation policy. To reflect this uncertainty, and account for different possible future outcomes, the following four scenario descriptions were used:

- Business as usual (BAU).
- Greenhouse gas emissions roadmap (GHG).
- Underwater radiated noise management (URN).
- URN management in addition to GHG roadmap (U&G).

Under BAU, no mitigation measures are applied, with only estimated changes in ship traffic volume contributing to changes in the soundscape. This acts as a reference scenario since changes in ship traffic volume are included in all scenarios. The GHG and URN scenarios focus on intentional abatement of these two sources of emissions separately, while U&G represents a combined scenario striving for reduction of both GHG and URN levels. This last scenario might be considered the most realistic given expected future policy developments. Only changes in URN were investigated, with any consequences on GHG emissions being outside of the project scope.

A flowchart describing the high-level process behind the generation of forecast sound maps in shown in Figure 6. The following main steps are required:

- Select baseline AIS ship track data set. This data is used as basis for the future ship traffic. The year 2022 was chosen for NAVISON, since it contained the highest (terrestrial and satellite) AIS data coverage at the time the work was performed (2023 was not yet available).
- For each year, estimate the change in ship traffic volume for each ship type and model the effect thereof on URN.
- For each year of each scenario, the effects of a combination mitigation measures on URN are modelled. Temporal changes in the adoption level of mitigation measures are modelled by the so-called penetration rate, which can vary differently for each ship type. The penetration rate is explained further in Lloyd et al. (2023)
- Having obtained new sound maps for each year of each scenario, changes in SPL under the three scenarios involving mitigation can be obtained by subtracting the equivalent results for the BAU scenario.

[5] This work was conducted prior to the publications of IMO's revised GHG reduction strategy (MEPC 80/WP.12) (IMO, 2023a).This means that the decarbonisation targets assumed in NAVISON are less stringent than those in force today. Specifically, a target of net-zero GHG emissions in 2050 compared to a 2008 baseline has now been set, whereas the equivalent target in the initial strategy was a 50 % reduction. On the other hand, the carbon intensity reduction target for 2030 compared to 2008 has been reduced from 40 % to 30 %.

[6] This work was conducted prior to the publication of IMO's Revised guidelines for the reduction of underwater noise from shipping (MEPC.1/Circ.906)(IMO, 2023b). At the time of writing IMO is in the process of initiating implementation of the guidelines through a so-called experience-building phase. Despite this, the guidelines are non-mandatory.

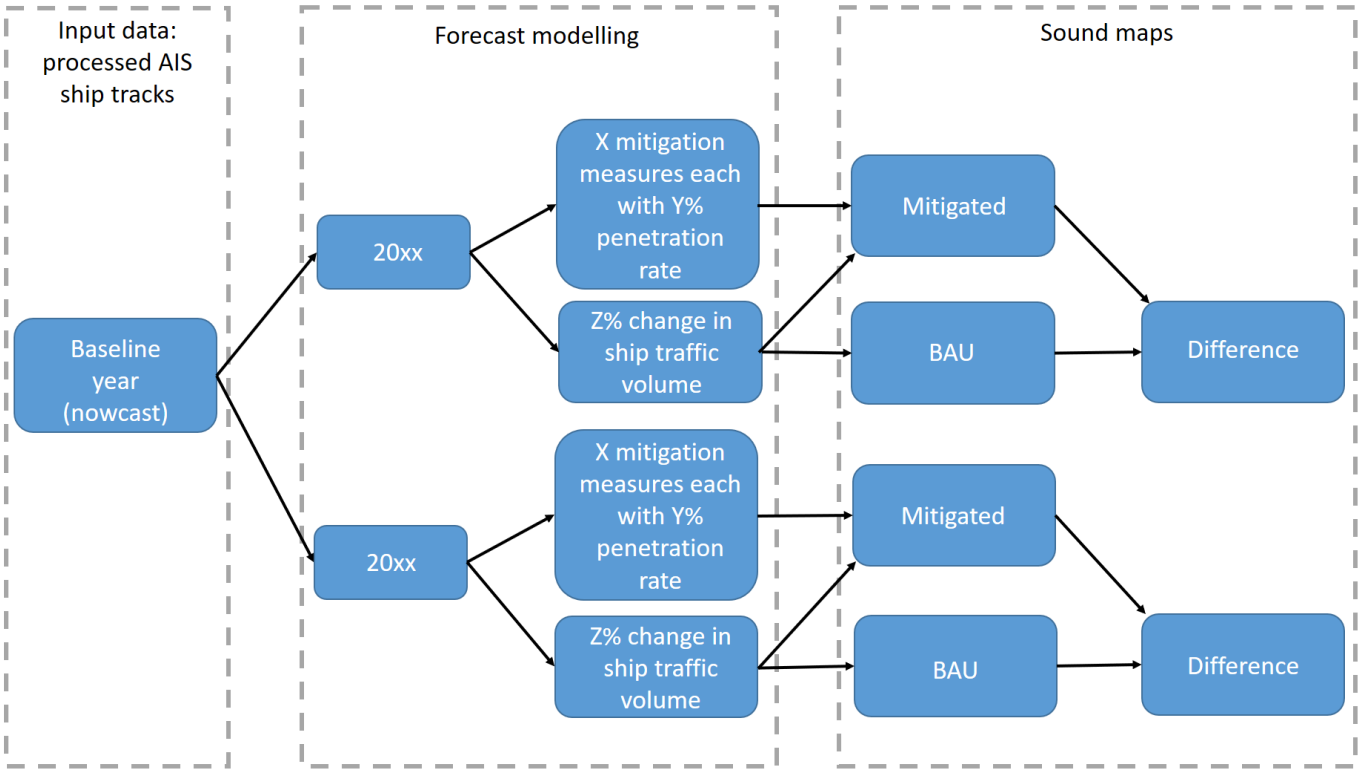

Figure 6 Generic process diagram for defining a forecast scenario. 'AIS' refers to Automatic Identification. The variables X, Y and Z are a function of the year (20xx).

To model realistic scenarios the combined effects of multiple mitigation measures should be included. This reflects the real-world development of both GHG and URN abatement efforts by a diverse range of stakeholders and covers both operational and (retrofit and newbuild) technical measures. Furthermore, it was recognised that certain approaches for reducing GHG emissions can result in an increase in URN levels, while for others a concurrent mitigation effect on GHG and URN can be expected. Since a finite number of measures could be modelled within the project, a review of possible measures was conducted, with a final selection of six measures made ensuring that the combination was relevant to the scenarios under consideration. An overview of the selected measures is provided in Table 5. Cavitation and machinery source levels were modelled separately so that the effect of each measure on mitigating the two source mechanisms could be studied both in isolation as well as in combination.

Under each scenario, appropriate combinations of mitigation measures were selected. For the GHG scenarios, these were speed Reduction (SRD), More efficient propeller (MEP), optimised hull form (OHF) and hull and propeller cleaning (HPC). In the URN scenarios, SRD, quieter propeller (QRP) and air injection (AIN) were applied, while under U&G scenarios, all six measures were included. The associated penetration rates for 2030, 2040, and 2050 were estimated using data from literature (Hoffmann 2020, IMO 2021). Where information for a particular measure was not available, which was particularly the case for the URN-related measures, this was taken from a similar measure or based on best estimates. Changes in ship traffic volume were estimated based on predicted changes in transport work for different ship types up until 2050 (DNV 2022). Appendix F gives full details of the scenario input data.

Table 5 Summary of mitigation measures selected for further modelling. The final selection includes both GHG and URN mitigation measures, technical and operational measures, covers a wide range of stakeholder groups, is relevant for the entire time period considered and allows for mitigation of both propeller cavitation and machinery noise.

Measure name	Measure code	Category	Type	Main stakeholder group(s)	2022	2030	2040	2050	Cavitation	Machinery
Speed reduction	SRD	GHG/URN	Operational	Regulatory bodies	×	✓	✓	✓	✓	✓
Hull and propeller cleaning	HPC	GHG	Operational	Ship operators	×	✓	✓	✓	✓	✓
More efficient propeller	MEP	GHG	Technical	Propeller designers	×	✓	✓	×	✓	✓
Optimised hull form	OHF	GHG	Technical	Ship builders/naval architects	×	×	✓	✓	✓	✓
Air injection (for propeller and machinery noise)	AIN	URN	Technical	Equipment manufacturers/ship builders	×	×	✓	✓	✓	✓
Quieter propeller	QRP	URN	Technical	Propeller designers	×	×	✓	✓	✓	×

The NAVISON project considers six distinct mitigation measures, with varying degrees of overlap (Figure 7). For evaluating the forecast scenarios, these measures have been divided into two sets:

1. Set A, consisting of speed reduction, more efficient propellers, and quieter propellers. The two measures related to propeller design, MEP and QRP, are assumed to be mutually exclusive. Furthermore, it is assumed that most vessels implementing MEP also implement SRD.
2. Set B, consisting of air injection systems, optimised hull form, and hull and propeller cleaning. All measures in this set are assumed to be independent of other measures.

Combining sets A and B, it is possible to compute the total sound reduction associated with applying all possible combinations of measures.

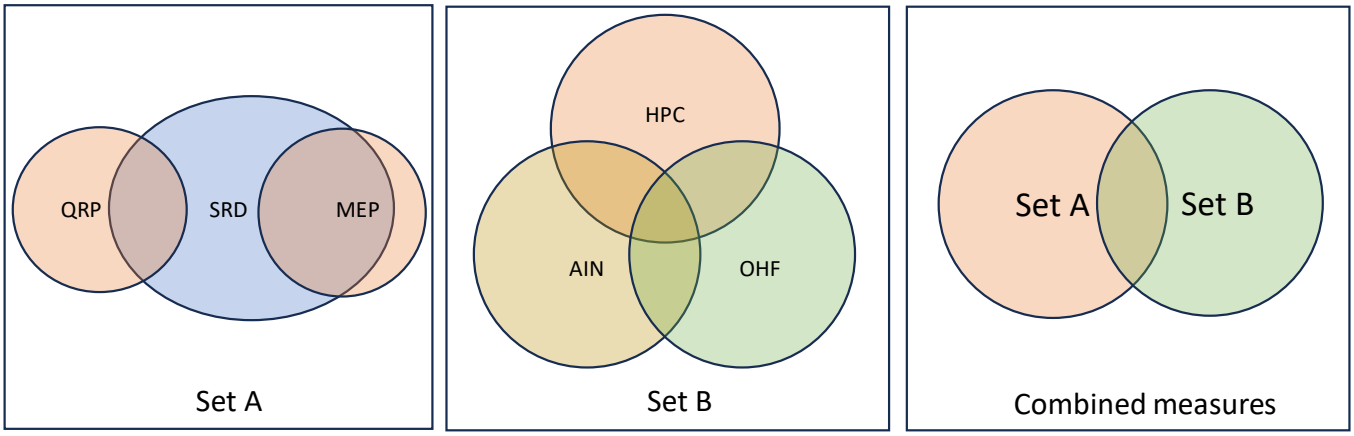

Figure 7 Venn diagrams showing how the mitigation measures considered by NAVISON are divided into two sets for evaluating forecast scenarios. In Set A, measures QRP and MEP (both related to propeller design) are assumed to be mutually exclusive, with most vessels implementing MEP also implementing SRD. In Set B, measures AIN, OHF, and HPC are assumed independent of each other. Forecast scenarios are based on combinations of all measures from Sets A and B, according to their penetration rates. QRP = quieter propeller; SRD = speed reduction; MEP = more efficient propeller; AIN = air injection system; OHF = optimised hull form; and HPC = hull and propeller cleaning.

2.4.2 Modelling Approach

The forecast modelling approach consists of two main elements: generation of ship track data for each of the mitigation measures included and generation of sound maps for the mitigation scenarios using the areic source level layers for each measure. First the probabilistic approach for obtaining the forecast sound maps is described, following which details of how each mitigation measures was modelled are provided.

2.4.2.1 Scenario-based Sound Map Generation

Sound maps for the forecast scenarios are calculated using a novel method for combining pre-computed layers for the different URN and GHG mitigation measures. The pre-computed layers represent the effect of different mitigation measures on underwater radiated noise from propeller cavitation and machinery. Propeller cavitation and machinery are captured in separate layers because the various mitigation measures affect cavitation and machinery noise differently, depending on vessel design and operational parameters. Changes in adoption rates for the different measures are captured by combining the pre-computed layers with different weighting factors, according to a penetration matrix for each scenario (Appendix F). The penetration matrix defines how the layers should be combined under each scenario, according to a probabilistic method that also considers the joint probabilities between different mitigation measures (see Figure 7). This approach allows an unlimited number of different forecast scenarios to be generated from only a limited number of sound map layers without re-running the underlying acoustic model.

The sequence of steps involved in creation of the forecast sound maps is shown in the flow chart diagram of Figure 8. The process for generating the forecast sound maps involves three high-level steps:

1. Starting from the 2022 vessel track data, additional processing is applied to the vessel tracks to calculate new cavitation and machinery source levels after applying the six different URN and GHG reduction measures. Separate processing is applied for each of the six measures, assuming a penetration rate of 100 % for each measure. An ASL and then an SPL map layer is computed from the processed track data for each measure. The

baseline SPL map layer is subtracted from the result, yielding a maximum mitigation factor layer ($\Delta L(x, y)$) for each measure.
2. The mitigation factor layers for the six different measures are combined in a probabilistic fashion, yielding the total mitigation factor for a particular forecast scenario. A penetration matrix defines the actual penetration rates (between 0–100 %) used to combine the various URN and GHG reduction measures (see Appendix F). Details of the probability calculations involved in the forecast scenarios are provided in the Task 1.4 status report (MacGillivray et al. 2023b). The resulting mitigation factor is added to the baseline SPL layer, yielding the total cavitation or machinery noise for the specified forecast scenario.
3. The cavitation and machinery noise map layers are summed together, and an adjustment is applied to the result to account for net changes in traffic volume relative to the 2022 baseline. The final output is a forecast sound map layer representing the total underwater sound (from both cavitation and machinery sources) for one of the five different vessel categories under the specified scenario.

2.4.2.2 Mitigation Measure Modelling

The pre-computed layers for each of the mitigation measures are obtained from a separate set of ship tracks for which the mitigation effect on cavitation and machinery noise is predicted using the PIANO model. The mitigation measures were modelled as follows:

- Speed reduction: a speed limit of 75 % of the vessel design speed was set, based on Nelissen et al. (2022). For each journey, the timestamps of the AIS ship tracks are first updated to ensure that the vessel remains under the speed limit. The source levels are subsequently re-computed using the adjusted speed information. Any delay in arrival time at the end of a journey is corrected for by computing the relative increase in the number of vessels required to maintain ship traffic volume per ship type.
- Hull and propeller cleaning: the effect of fouling was modelled by assuming changes to vessels' power requirement and propeller rotation rate, equivalent to use of the engine and light running margins, respectively. Due to a lack of information regarding fouling level and maintenance schedule of vessels, these changes were modelled per ship type and assumed to be constant over time. Under the HPC scenario, no fouling penalty was included, with this contribution added when modelling all other measures. For cases with fouling, an increase in power requirement per ship type was assumed, while a fixed change in rotation rate was used for all vessels, with the selected values based on literature.
- More efficient propeller: for this measure, propeller performance was modelled as a trade-off between efficiency (power requirement) and source level. Based on MARIN data, a change in source level of 1.5 dB per percent change in efficiency was assumed for all vessels. By comparing the propeller efficiency estimate of each individual vessel to the mean for each ship type, a relative efficiency improvement, and associated increase in cavitation source level could be determined. This change was applied to the cavitation SL computed by the PIANO model. Furthermore, the cavitation inception speed (CIS) was assumed to reduce as a function of the change in SL, by 5 % for every percent increase in efficiency.
- Optimised hull form: this measure was assumed to affect two input parameters of the PIANO model: the installed power and the propeller tip loading wake peak parameter (a measure of the quality/uniformity of the propeller inflow). The former affects both cavitation and machinery source levels and was modelled by deriving a linear trend for change in vessel installed power as a function of age from the ship particulars database used as input for the PIANO model. The result was a 1 % reduction in installed power per year. The total achievable installed power reduction per vessel was then modelled by assuming a mean scrapping age per ship type and computing the source levels for the case in which all vessels have been replaced (at least once). The wake peak parameter only affects cavitation source levels and is modelled in PIANO using three values (quality categories). To model the effect of OHF on this parameter it was assumed that the value of the wake peak parameter improved by one category level when a vessel was replaced. No correction was made for vessels which already had the highest wake quality, i.e. cruise vessels.
- Air injection: air injection systems for mitigation of both cavitation and machinery noise were modelled, the so-called Prairie and Masker systems, respectively. Data measured by MARIN was used (Lloyd et al. 2024c), with a fixed reduction of 3 dB at 63 Hz applied to both the cavitation and machinery source levels. This correction was made uniformly for all vessels and ship tracks.
- Quieter propeller: quieter propellers were modelled in a similar way to more efficient propellers, except that propeller efficiency and source levels were assumed to reduce, while CIS increased.

Depending on the measure, cavitation and/or machinery source levels can increase or decrease. A summary of the change in source factors of cavitation noise and machinery noise (both two-stroke and four-stroke main engines) is provided in MacGillivray et al. (2023b).

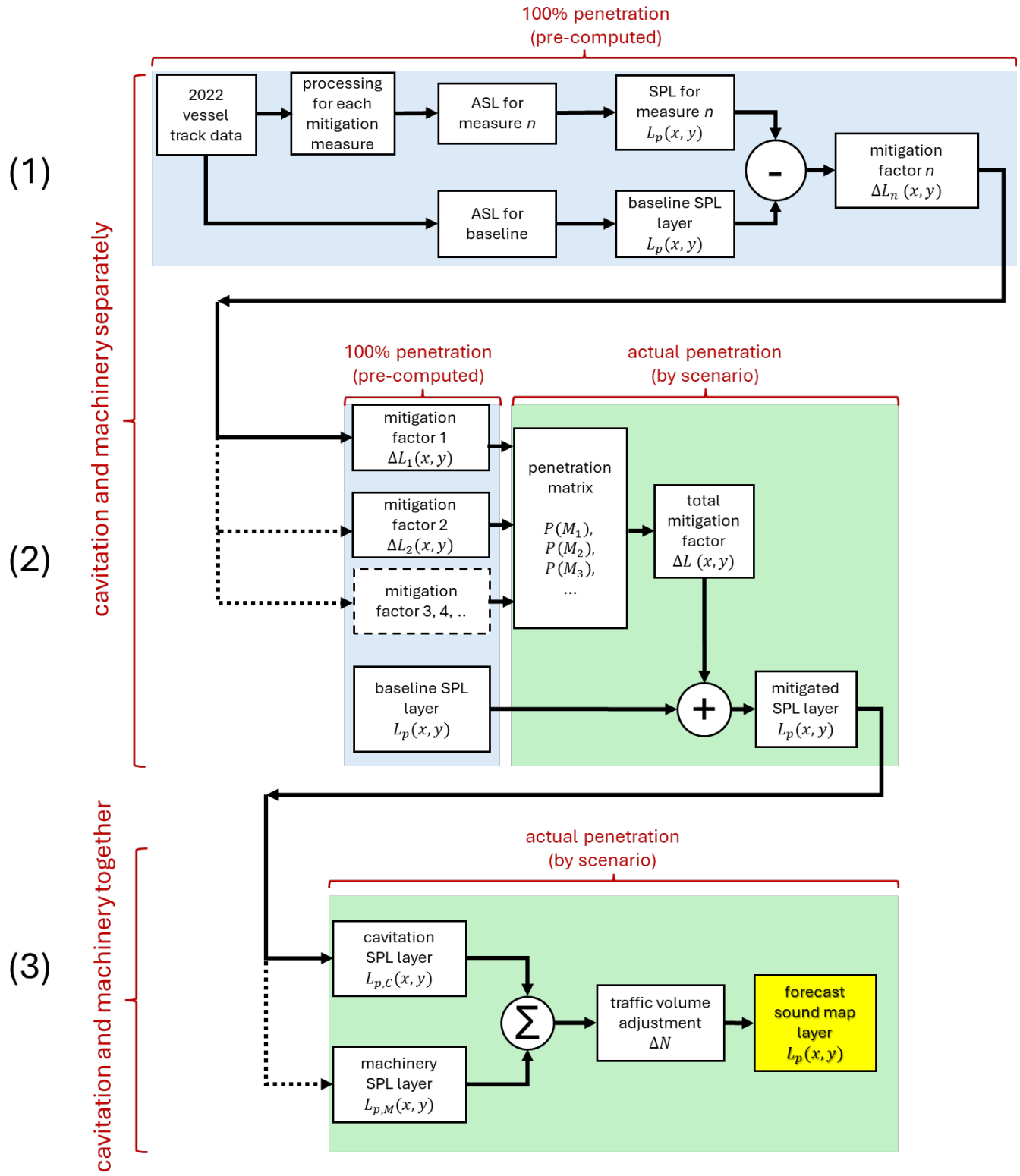

Figure 8 Flow chart diagram showing process for calculating forecast sound maps layers from pre-computed cavitation and machinery layers for different mitigation measures. The symbol "–" represents a subtraction of decibel quantities, the symbol "+" represents an addition of decibel quantities, and the symbol "Σ" represents a summation of squared sound pressure.

3. Analysing Sound Map Layers

In this section, the hindcast and forecast sound map layers are analysed. In this analysis, in addition to the sound map layers, sound energy density is used. More detailed descriptions are provided for each comparison in the following subsections. The approach used to calculate sound energy density is described in Appendix D. The sound energy density can be analysed in different ways to answer various questions related to the sound map layers. Since it is a linear quantity, sound energy density (in joules per cubic metre) provides an alternative to sound pressure level (in decibels) for comparing and visualising the sound map layers in terms of a single quantity. In this section, some examples will be provided to illustrate the potential use of sound energy density in analysing sound map layers.

3.1 Hindcast Map Layers

For each sound map layer, the quarterly sound map layer is computed from the quarterly ASL, which is obtained from a full quarter of ship track data. Annually averaged sound map layers are computed by averaging the four quarterly sound map layers for a single year. In Figure 9, sound map layers of Europe are shown at 63 Hz including all vessel categories. The same figure also displays sound energy density for each year, with the colour indicating the contribution of each included vessel category in the sound map layers. Appendix C provides the mean number of vessels present in each region, by year and quarter.

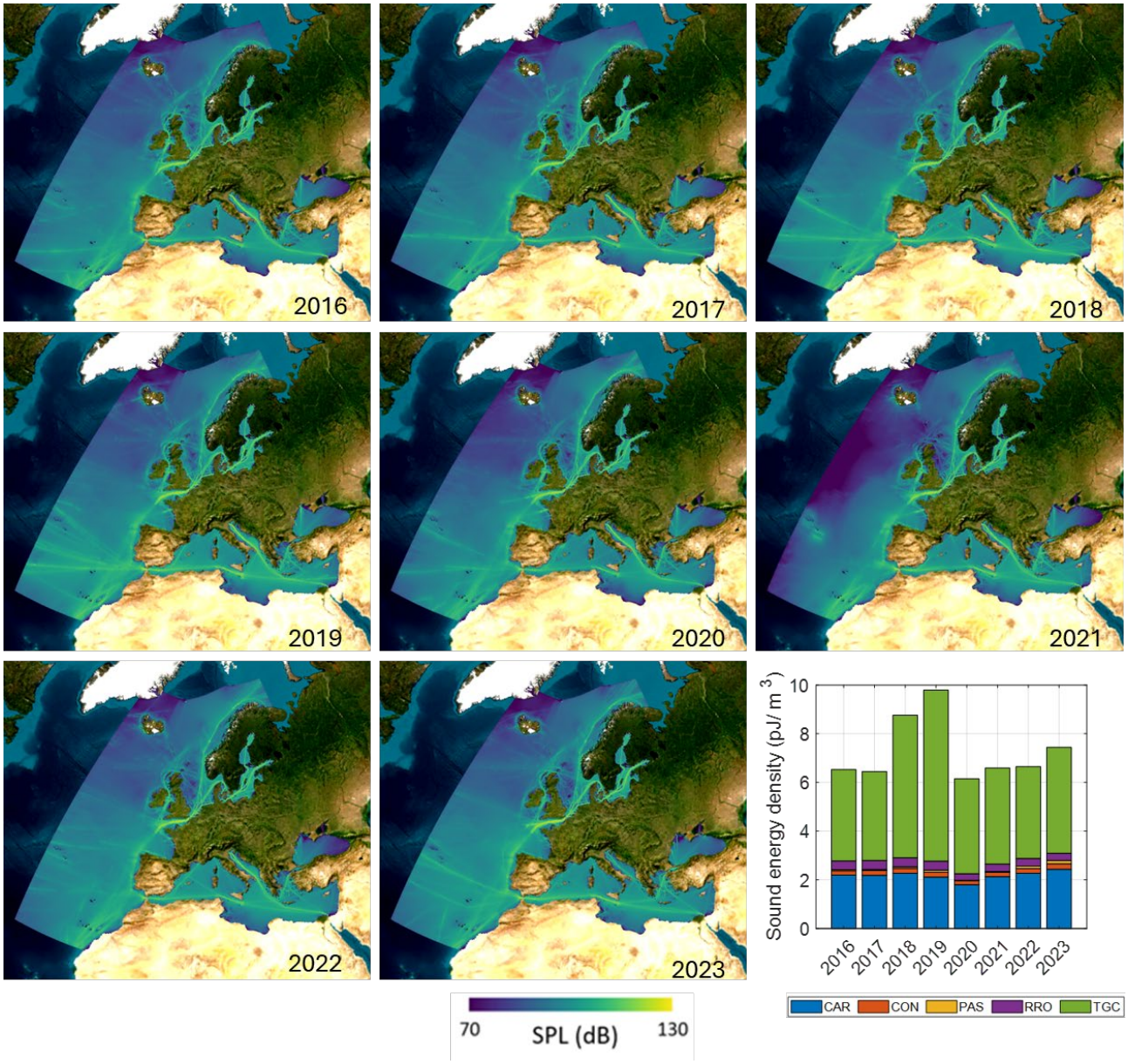

Figure 9 Annually averaged sound map layers (SPL re 1 μPa^2, in dB) including ALL vessel categories and sound energy density (in pJ/m^3) at 63 Hz. One picojoule (1 pJ) is equal to one trillionth of a joule (10^{-12} J).

Each vessel category makes a different contribution to these maps depending on their source levels and spatial distribution. To visualize these differences, annually averaged sound map layers and sound energy density are shown CAR, CON, PAS, RRO and TGC vessel categories and sum of all categories in Figures 10–14, respectively.

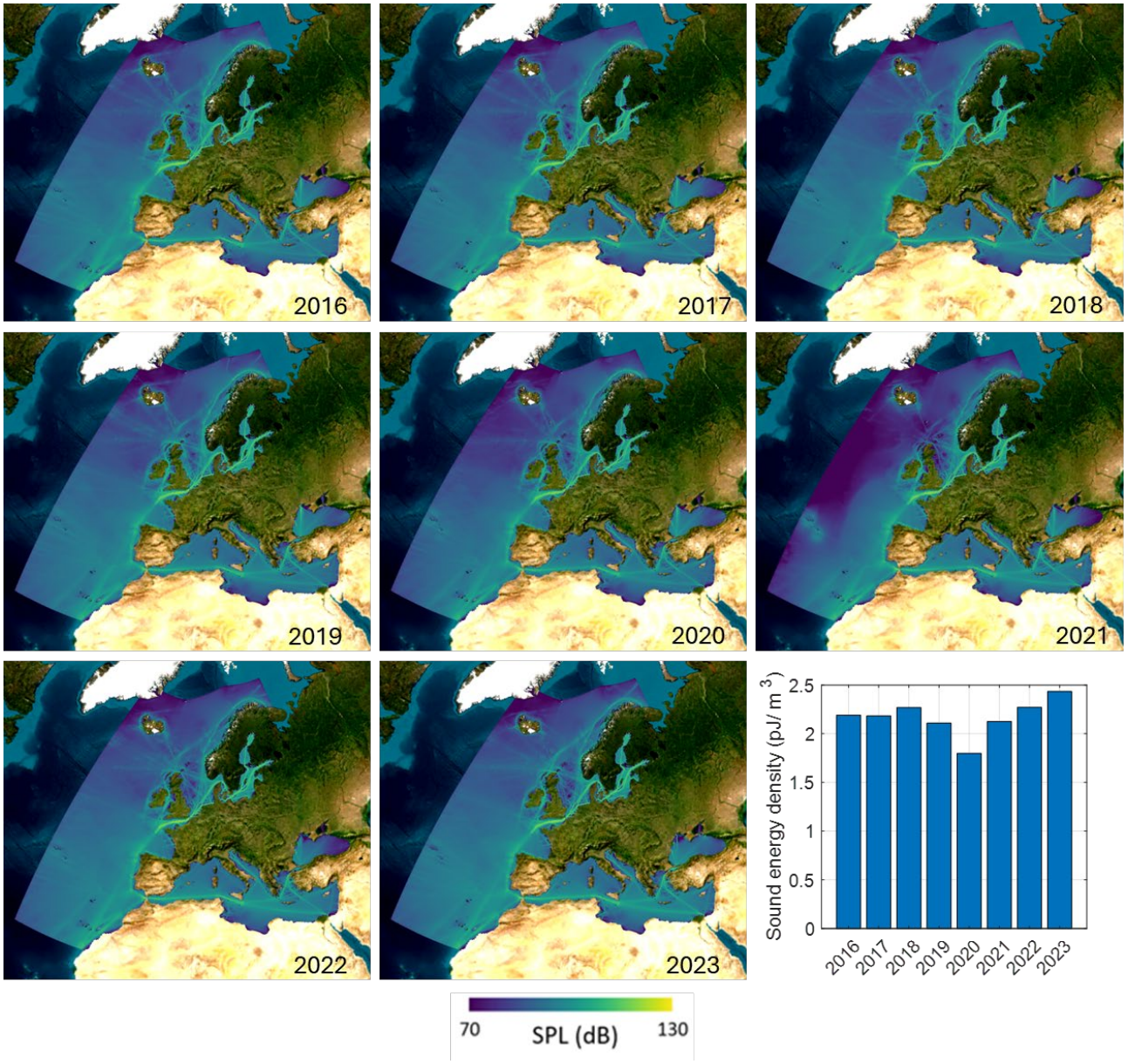

Figure 10 Annually averaged sound map layers (SPL re 1 μPa, in dB) including CAR vessel categories and sound energy density (in pJ/m^3) at 63 Hz. One picojoule (1 pJ) is equal to one trillionth of a joule (10^{-12} J).

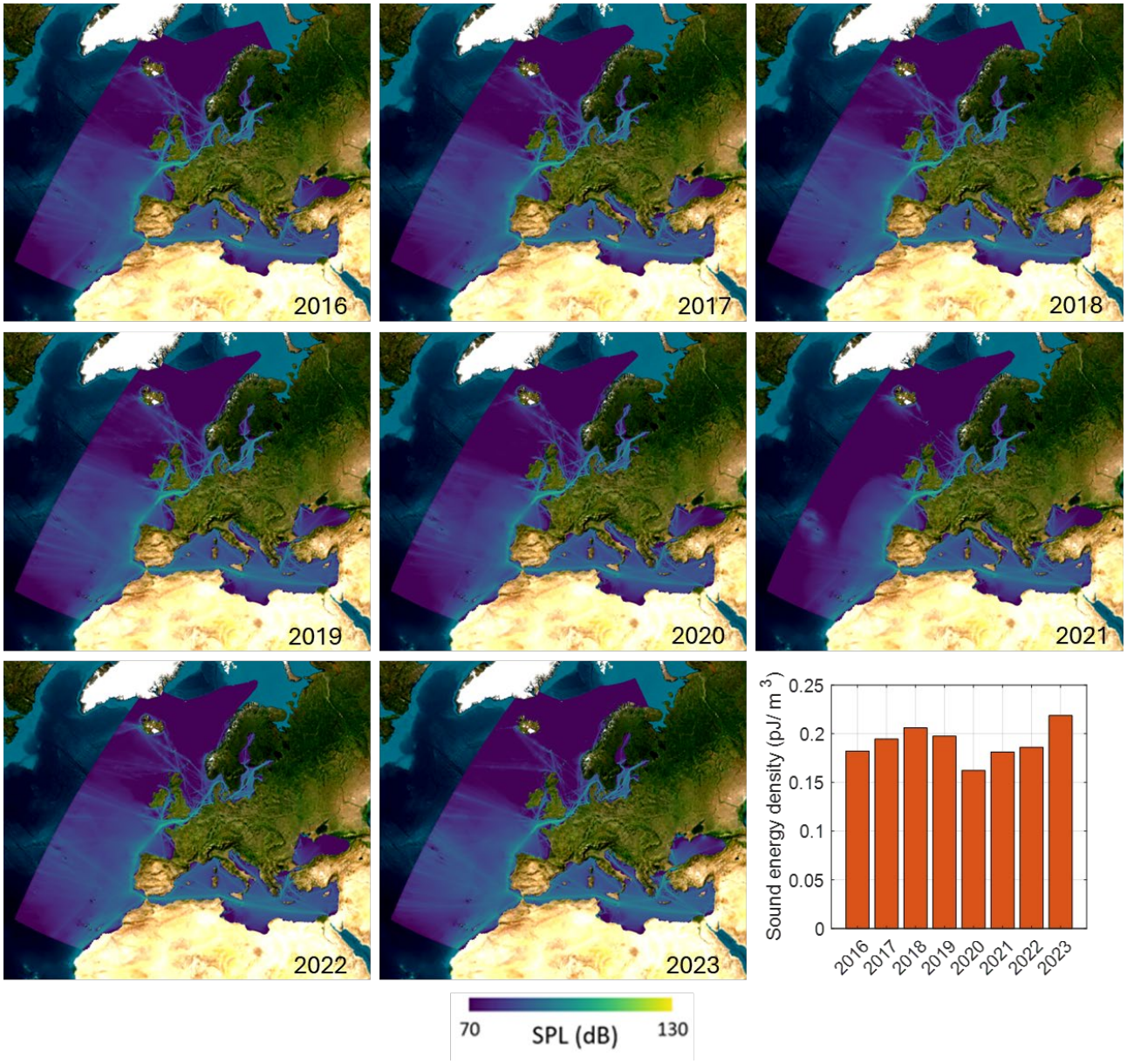

Figure 11 Annually averaged sound map layers (SPL re 1 μPa^2, in dB) including CON vessel categories and sound energy density (in pJ/m^3) at 63 Hz. One picojoule (1 pJ) is equal to one trillionth of a joule (10^{-12} J).

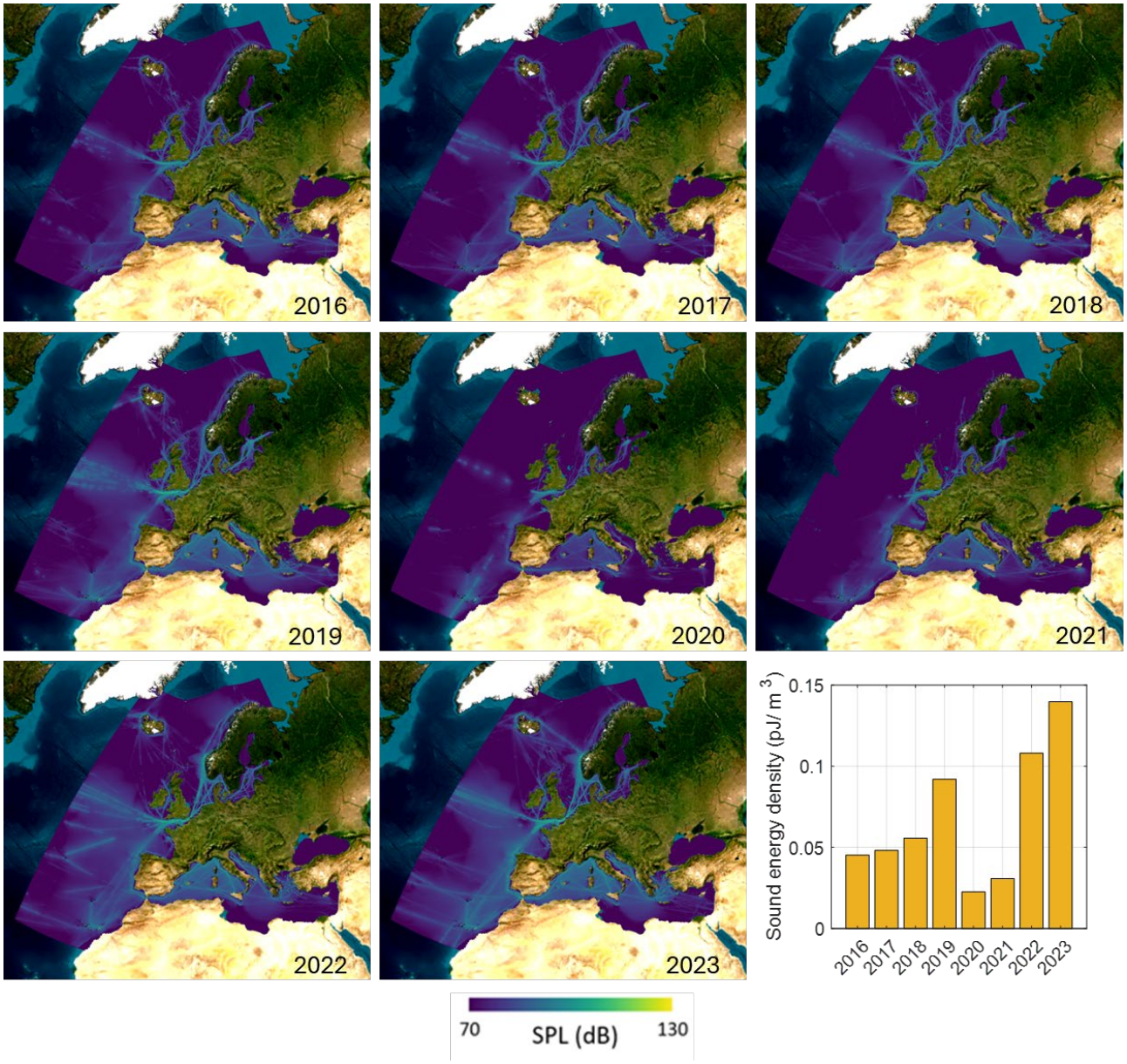

Figure 12 Annually averaged sound map layers (SPL re μPa^2, in dB) including PAS vessel categories and sound energy density (in pJ/m^3) at 63 Hz. One picojoule (1 pJ) is equal to one trillionth of a joule (10^{-12} J).

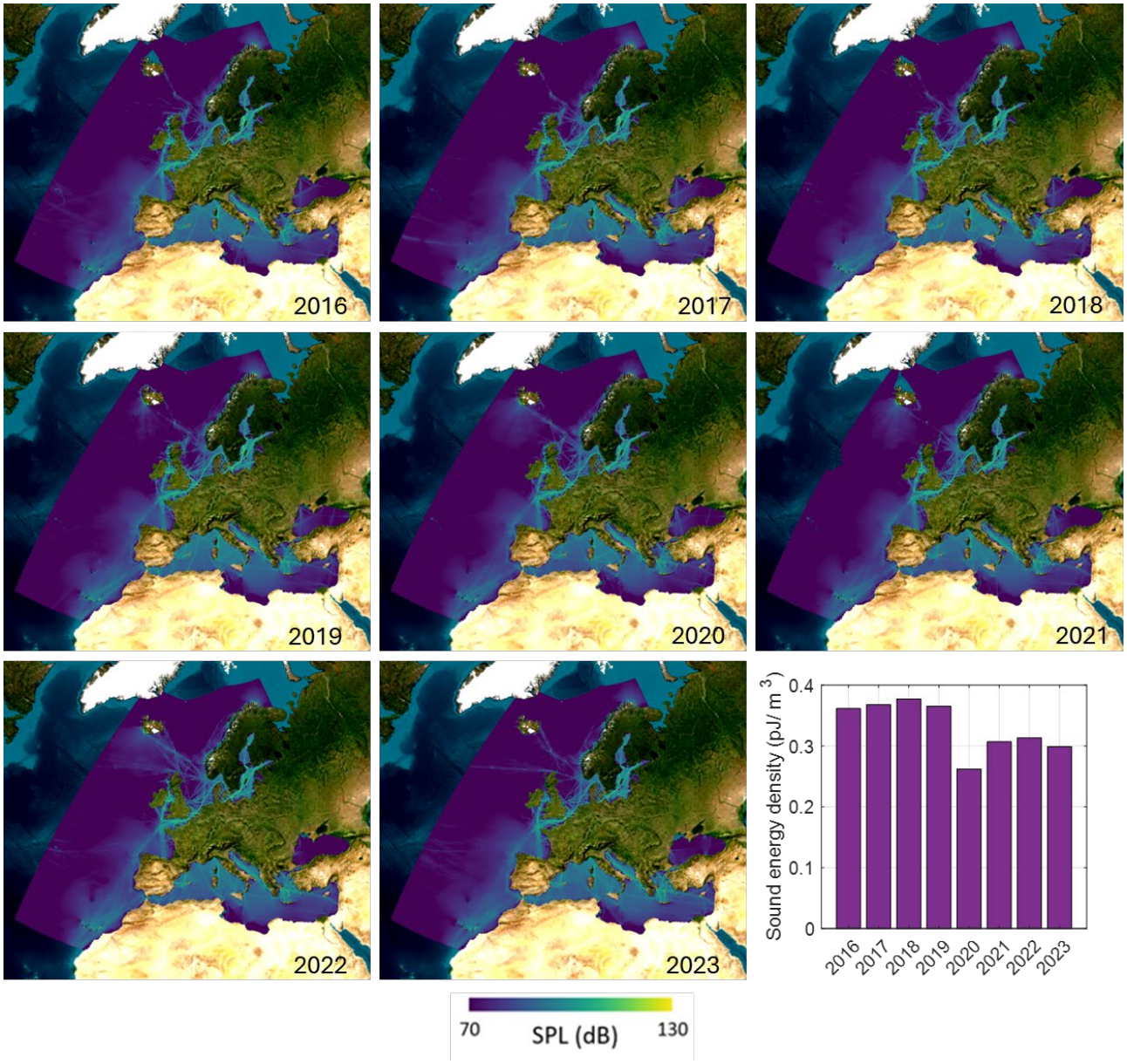

Figure 13 Annually averaged sound map layers (SPL re 1 μPa^2, in dB) including RRO vessel categories and sound energy density (in pJ/m^3) at 63 Hz. One picojoule (1 pJ) is equal to one trillionth of a joule (10^{-12} J).

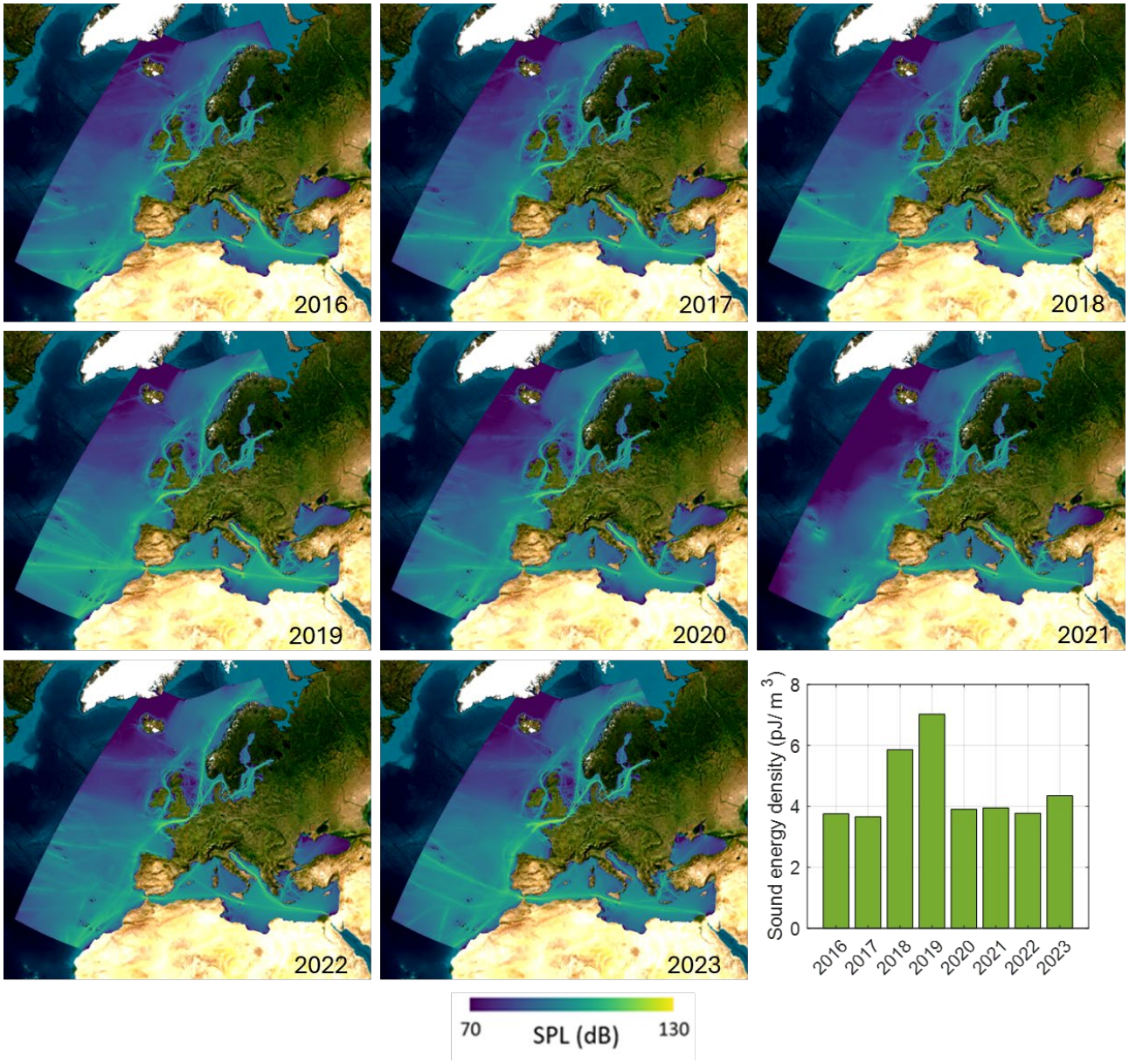

Figure 14 Annually averaged sound map layers (SPL re 1 μPa^2, in dB) including TGC vessel categories and sound energy density (in pJ/m^3) at 63 Hz. One picojoule (1 pJ) is equal to one trillionth of a joule (10^{-12} J).

These sound map layers visualise how the sound is spatially distributed for each vessel category. It is possible to visually identify the local decreases and increases for different years from these sound map layers. For instance, SPL in the sound map layers of CAR and TGC vessels appears higher than in PAS and RRO vessels. As a complementary tool to the sound map layers, sound energy density comparisons simplify the analysis process by transforming each sound map layer into a single number, thus avoiding a laborious comparison between maps or map layers. By monitoring changes in sound energy density, it is possible to focus on specific sound maps to understand more details. In the next section, a detailed analysis of the sound map layers is provided based on the sound energy density to make detailed comparisons for each region, category, and year.

3.1.1 Analysis for Hindcast Map Layers by Vessel Category

In this subsection, sound energy density is used to investigate the temporal trends and composition of shipping sound for each region in detail. For each region, two sound map layers including all vessel categories are visualized at 63 and 125 Hz, respectively. The corresponding sound energy density is also shown next to the same sound maps. To investigate the temporal trends and contribution of each vessel category to URN, quarterly and annually averaged sound energy density is calculated and visualized for each vessel category as separate comparisons for each quarter. Making separate comparisons for each quarter can facilitate a more detailed examination of shipping sound, under the assumption that the seasonal changes in the sound speed profiles corresponding to the same quarters for different years are similar. Based on the annually averaged sound energy density, the percentage distribution of sound energy density for each vessel category is calculated and provided in Appendix D. Using this information, the contribution of each vessel category and temporal trends are analysed. Additionally, quarterly averaged sound energy density is visualised, which helps to identify seasonal cycles of sound energy density.

3.1.1.1 Europe

In Figure 15, sound map layers of all regions for 2022 are shown at 63 and 125 Hz including ALL vessel categories. The modelled sound pressure level seems to be highest (between 120 dB and 130 dB) in parts of the English Channel and Baltic Sea in both frequency bands.

The effects of the sound speed profile and bathymetry on underwater sound propagation can be illustrated by these sound map layers. In deep waters (Mediterranean Sea, Black Sea, and northeast Atlantic Ocean), the seasonal change in sea surface temperature affects the angle of sound propagation paths, resulting in stronger bottom interaction (and consequently higher propagation loss) in the summer than in the winter. Consequently, different sound propagation characteristics could be observed depending on the sound speed profile:

In shallow water (e.g., the Baltic Sea and North Sea), the impact of the sound speed profile on sound maps is relatively small, as observed in different regions based on the sound energy density discussed later in this section. In contrast, the effect of sediment type could be stronger in shallow waters due to the multiple reflections of sound from the sea surface and sediment.

The effect of bathymetry can also be important. For example, a large spatial gradient in SPL is observed between the north of the Bay of Biscay and the southwest approaches to the English Channel (Figure 15), which can be explained by the rapid changes in the bathymetry. Water depth in the Bay of Biscay is more than 4000 m, decreasing abruptly to ~200 m on the continental shelf. The SPL is visibly lower in deep water because the sound energy is diluted into a larger volume. Similar effects are also observed in the Ionian Sea, where has also a rapid transition from the deep waters (exceeding 4500 m) to shallow waters (100-150 m).

As another example, shadowing effects on sound propagation are observed in the Mediterranean Sea, especially by islands, which act as a barrier to sound. A similar barrier effect is expected across the Mid-Atlantic Ridge, which was selected as the western boundary of NAVISON regions as described in Appendix A. (If sound sources west of the Mid-Atlantic Ridge had been included, some of the dark blue areas might show higher SPL values in Figure 15.)

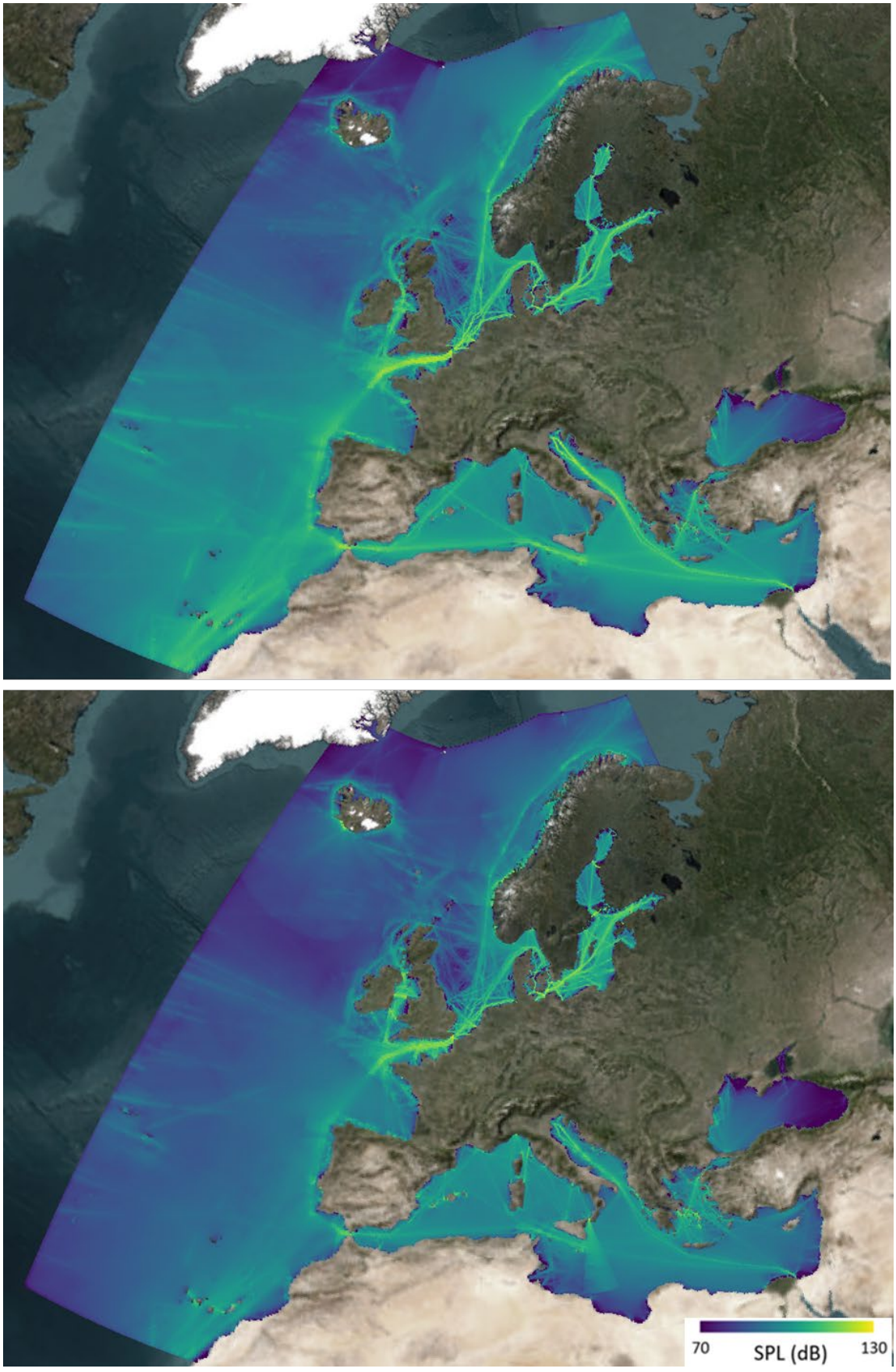

Figure 15 Sound map layers (SPL re 1 μPa^2, in dB) of all regions for 2022 including ALL vessel categories at (top) 63 Hz and (bottom) 125 Hz.

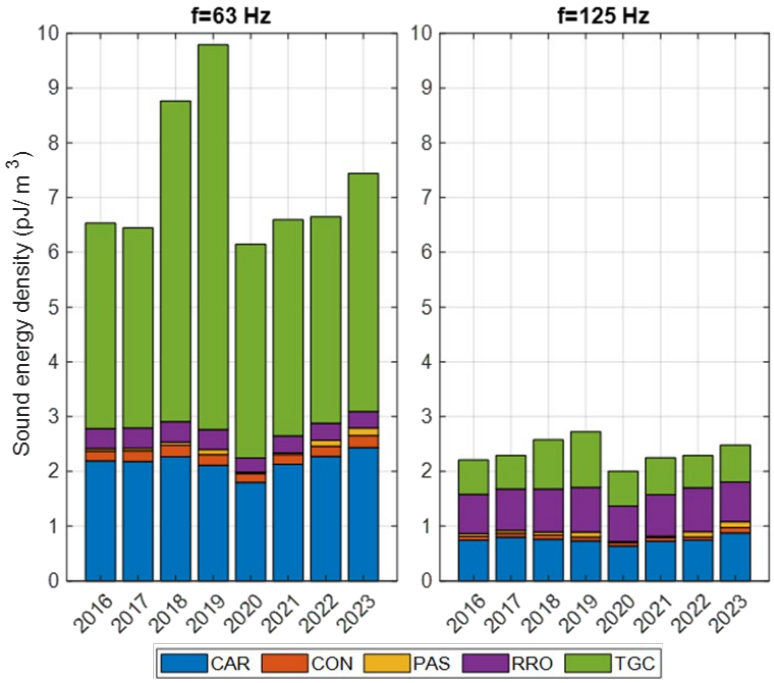

Figure 16 Annually averaged sound energy density (in pJ/m^3) in the Europe at (left) 63 Hz and (right) 125 Hz.

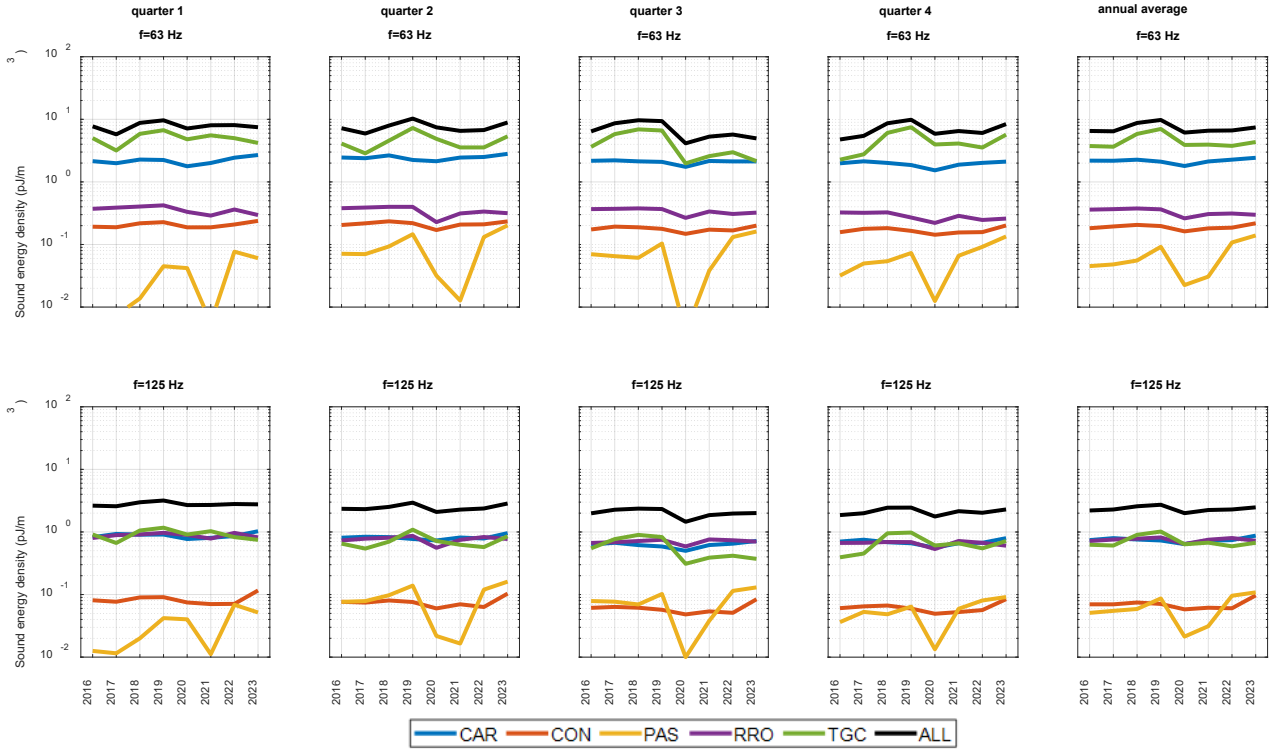

Figure 17 Sound energy density (in pJ/m^3) for the years 2016 to 2023 of different vessel categories for each quarter and year in Europe. The top panel is for 63 Hz. The bottom panel is for 125 Hz.

At 63 Hz, the TGC vessels make the largest contribution (56.7 to 71.8 %) to sound energy density, followed by CAR vessels (21.5 to 34.2 %) and RRO vessels (3.7 to 5.7 %) The PAS and CON vessel categories make the lowest contributions (0.4 to 1.9 %, and 2.0 to 3.0 %, respectively).

At 125 Hz, the largest contributions are from CAR (between 26.9 % and 35.3 %), RRO (between 29.2 % and 35.0 %), and TGC (between 25.8 % and 37.3 %). Although the temporal variations for CAR and RRO vessels are similar, TGC vessels exhibit larger changes over different years. For example, in the fourth quarter, the sound energy density rapidly decreases in 2020 and remains lower between 2020 and 2023. The lowest contributions are from CON (between 2.6 % and 3.9 %) and PAS (between 1.1 % and 4.4 %).

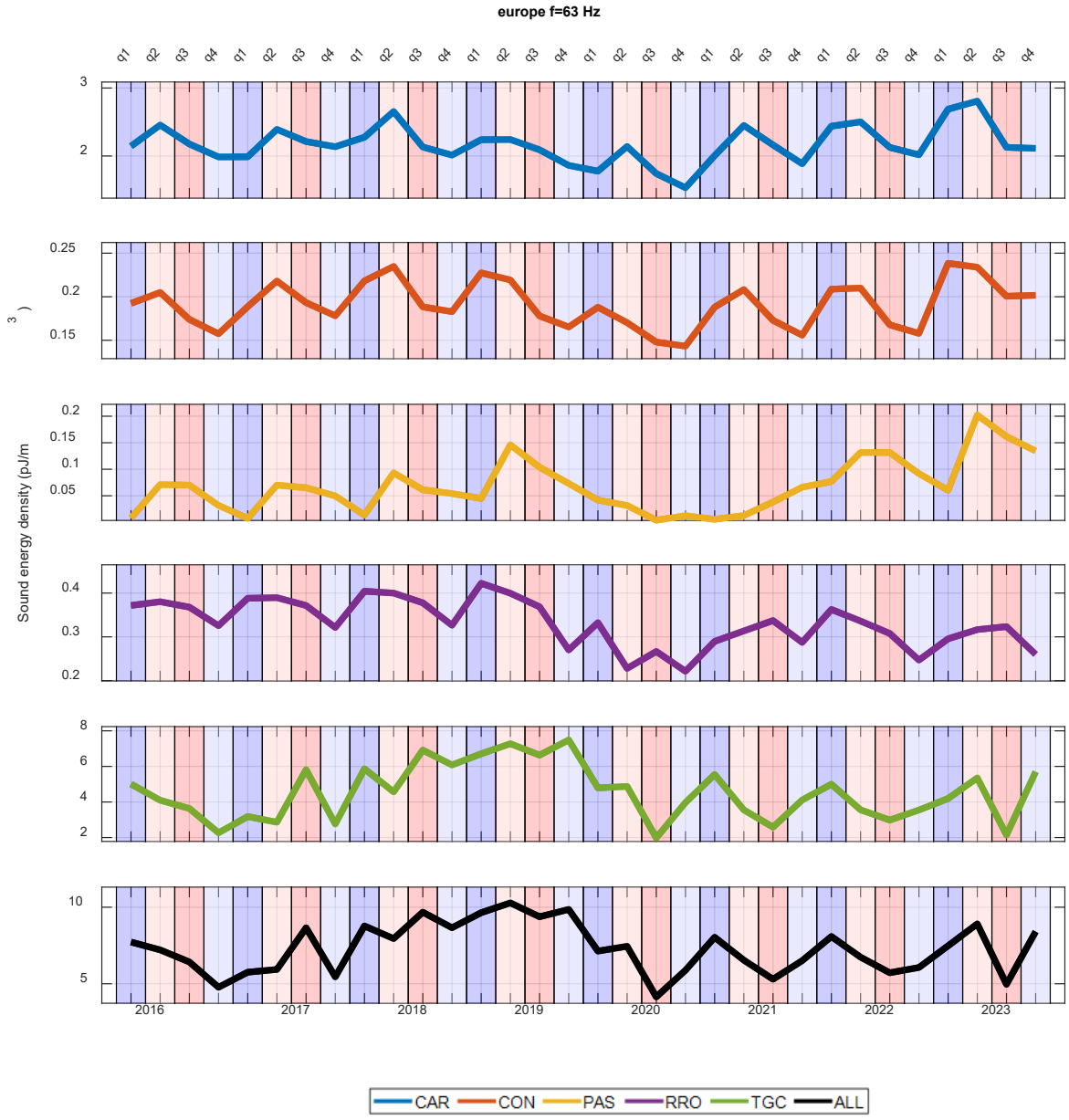

Figure 18 Sound energy density (in pJ/m^3) of different vessel categories for each quarter in chronological order at 63 Hz.

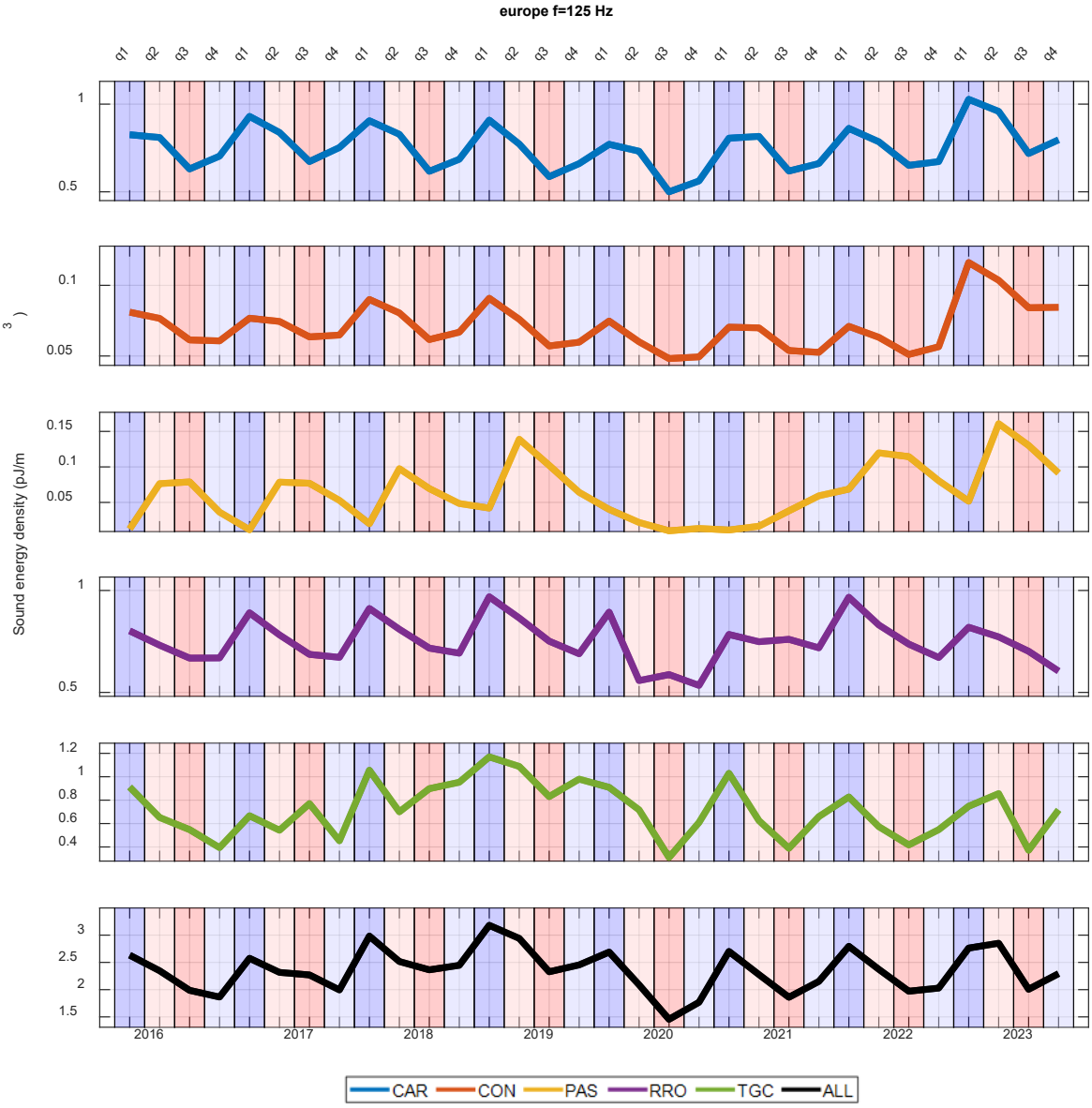

Figure 19 Sound energy density (in pJ/m^3) of different vessel categories in the Europe for each quarter in chronological order at 125 Hz.

The seasonal cycles due to changes in the sound speed profile are clearly visible for CAR and CON vessels in all years. At 125 Hz, the largest sound energy density for the same vessel categories is observed in the first quarters (shown by dark blue background). This is expected and can be explained by the effect of sound speed profile on the sound propagation, which gives lower propagation loss in winters than summers in the same region. The number of vessels and their speed can also affect the sound energy density. At 63 Hz, the largest sound energy density for CAR and CON vessels are observed in the second quarters (shown by pale red background), which is unexpected. One hypothesis to explain the peaks of sound energy density at 63 Hz in spring may be related to melting ice which may reduce the temperature of the upper water layers in deep water, thus reducing propagation loss and increasing SPL in the spring. However, one would then expect the same effect at 125 Hz, which we do not observe, shedding doubt on the hypothesis. For PAS vessels, these seasonal cycles were interrupted in 2020 and 2021, probably due to the COVID-19 pandemic (Mathieu et al. 2024). Except for this interrupted period, the largest sound energy density of PAS vessels is observed during the second and third quarters. The reason for the lower energies may be related to having lower ASL during the winter period due to the decrease in the number of PAS vessels. For TGC vessels, the seasonal cycles are not clearly visible before 2020. The lowest sound energy density for TGC vessels is observed in the third quarters after 2020. This could be related to high variability in their ASL (possibly different speed and numbers) and paths in different years.

As an additional analysis the sound energy density per vessel is estimated by dividing the sound energy density by the total number of vessels. In Figure 20 and Figure 21, the quarterly and annually averaged sound energy density per vessel are shown, respectively.

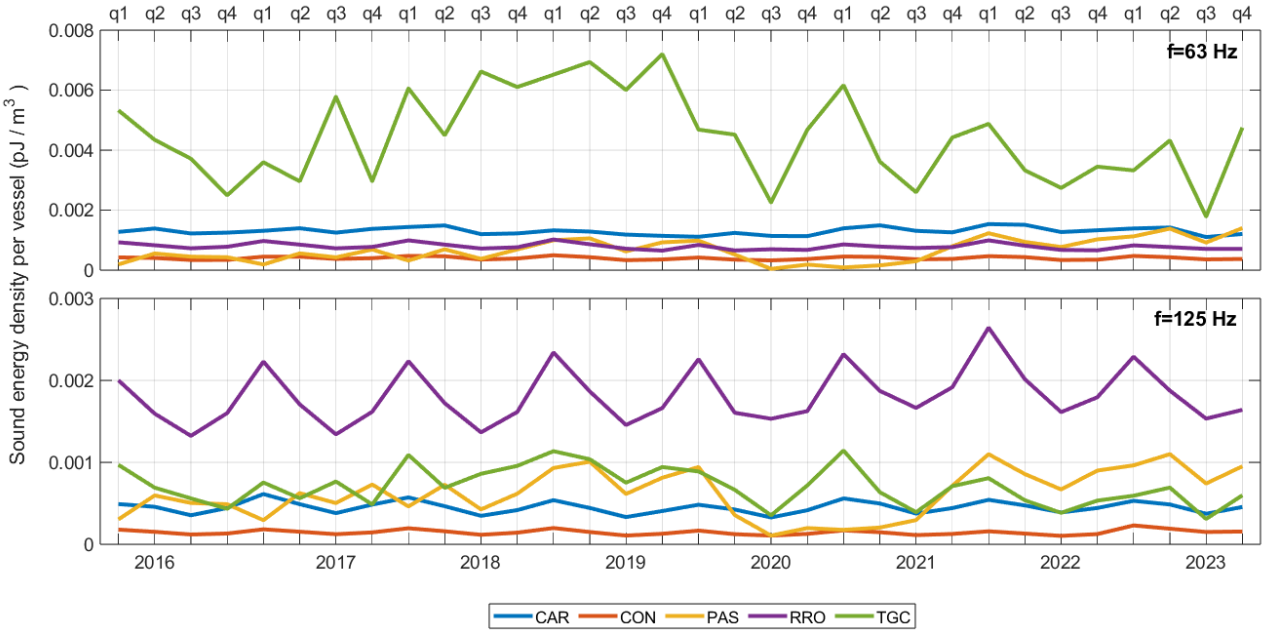

Figure 20 Quarterly variation of average contribution to sound energy density (in pJ/m^3) per vessel for each vessel category in Europe for 63 Hz (top) and 125 Hz (bottom)

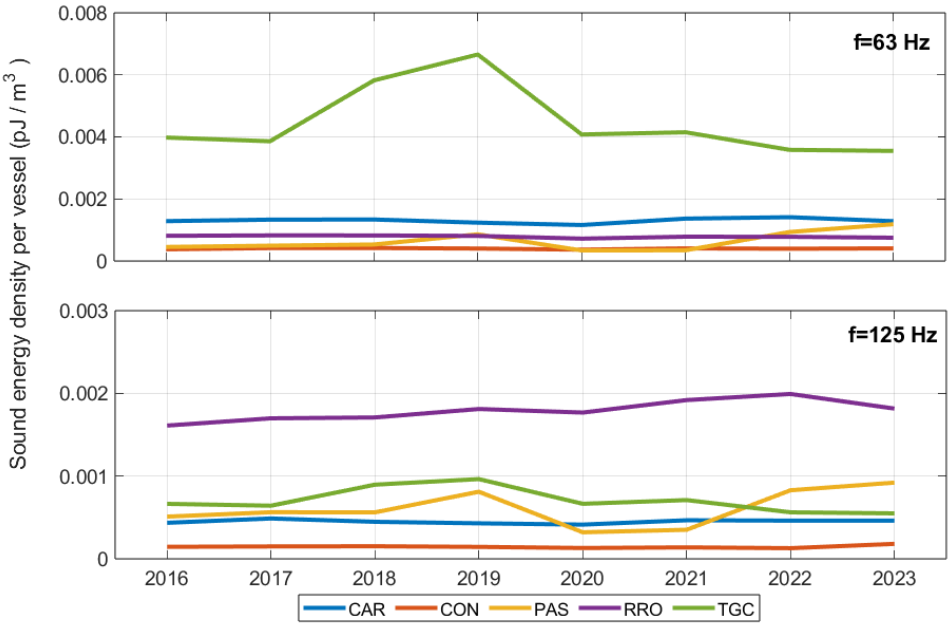

Figure 21 Annual variation of average contribution to sound energy density (in pJ/m^3) per vessel for each vessel category in Europe for 63 Hz (top) and 125 Hz (bottom)

Based on these comparisons, the TGC vessel category at 63 Hz and the RRO vessel category at 125 Hz make the largest contributions to sound energy density per vessel. The second-largest contributions come from CAR vessels at 63 Hz and TGC vessels (from 2016 to 2021) and PAS vessels (in 2022 and 2023) at 125 Hz. There are noticeable seasonal variations, especially for the RRO and PAS vessel categories, which could be related to changes in their areic source levels (due to different speed and density) and seasonal differences in sound propagation.

These comparisons show the sound energy density of single vessel from each category and do not reflect the total sound energy contribution of different vessel categories without considering the total number of vessels. For instance, although the PAS vessel category has the second-highest sound energy density per vessel at 125 Hz in Europe, their overall contribution to total sound energy is much lower than other categories, as shown in Figure 17.

3.1.1.2 Baltic Sea

Sound map layers of Baltic Sea for 2022 are shown at 63 and 125 Hz including ALL vessel categories in Figure 22. As seen in these sound maps, the Baltic Sea has busy shipping lanes, especially in the southern area.

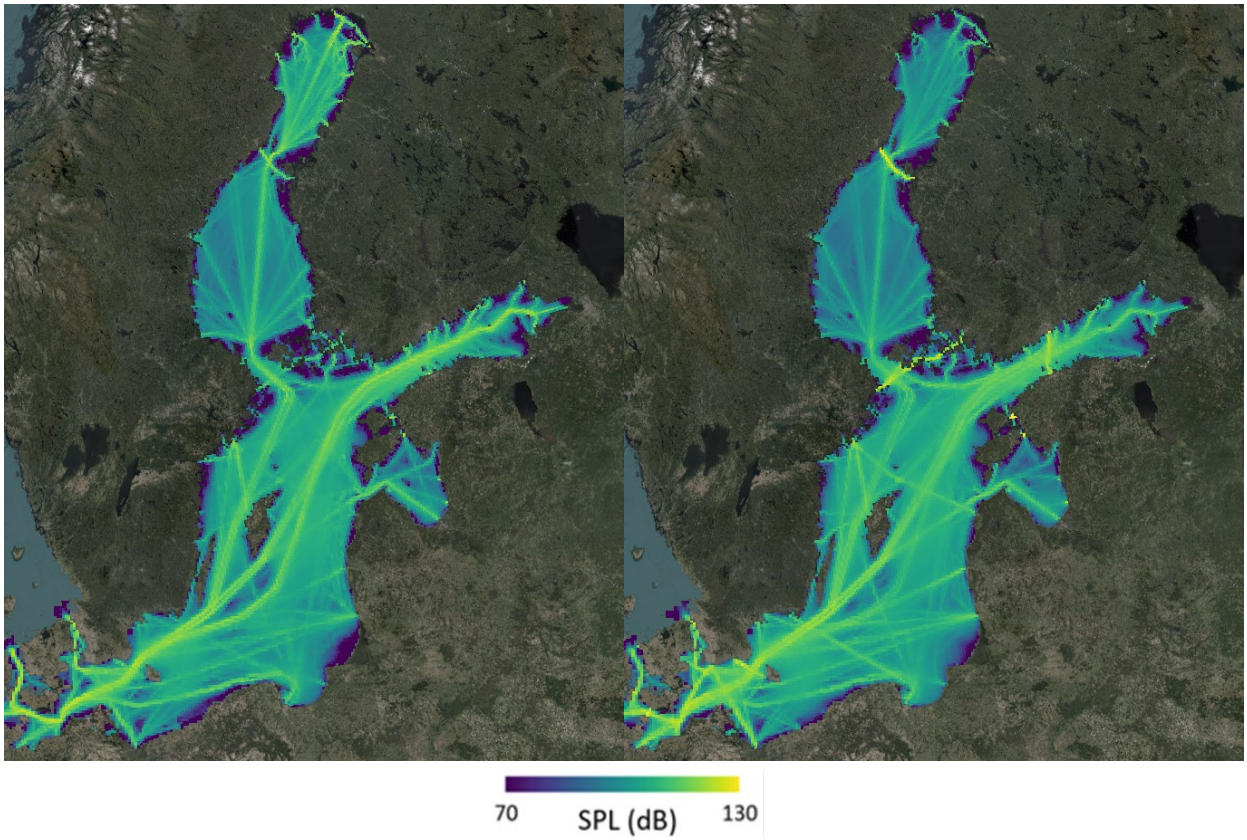

Figure 22 Sound map layers of Baltic Sea (SPL re 1 μPa^2, in dB) for 2022 including ALL vessel categories at (left) 63 Hz and (right) 125 Hz.

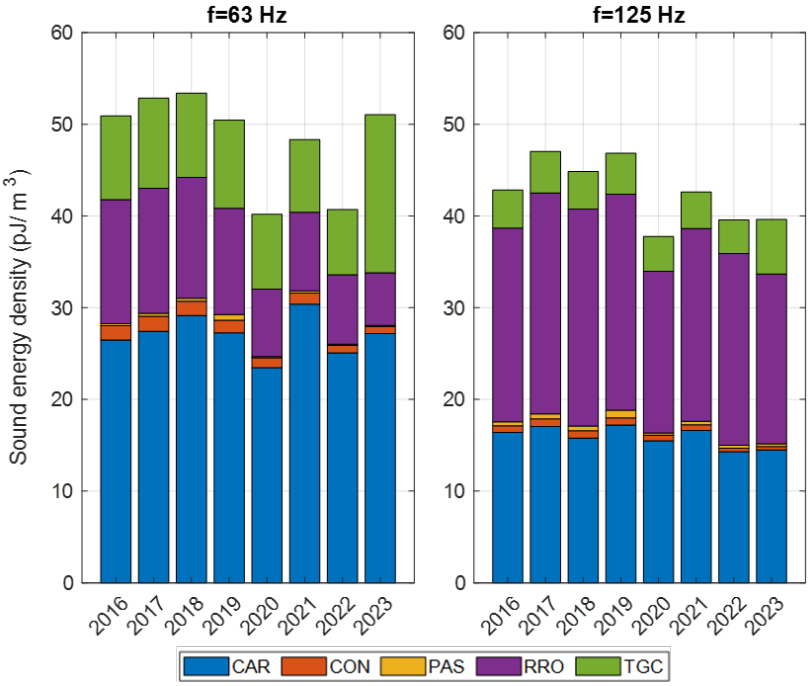

Figure 23 Annually averaged sound energy density (in pJ/m^3) in the Baltic Sea at (left) 63 Hz and (right) 125 Hz.

To quantify the contribution of individual vessel categories to the total shipping sound and temporal trend, calculating sound energy density offers a practical approach. Figure 24 illustrates the sound energy density for each vessel category, presented as quarterly and annual averages.

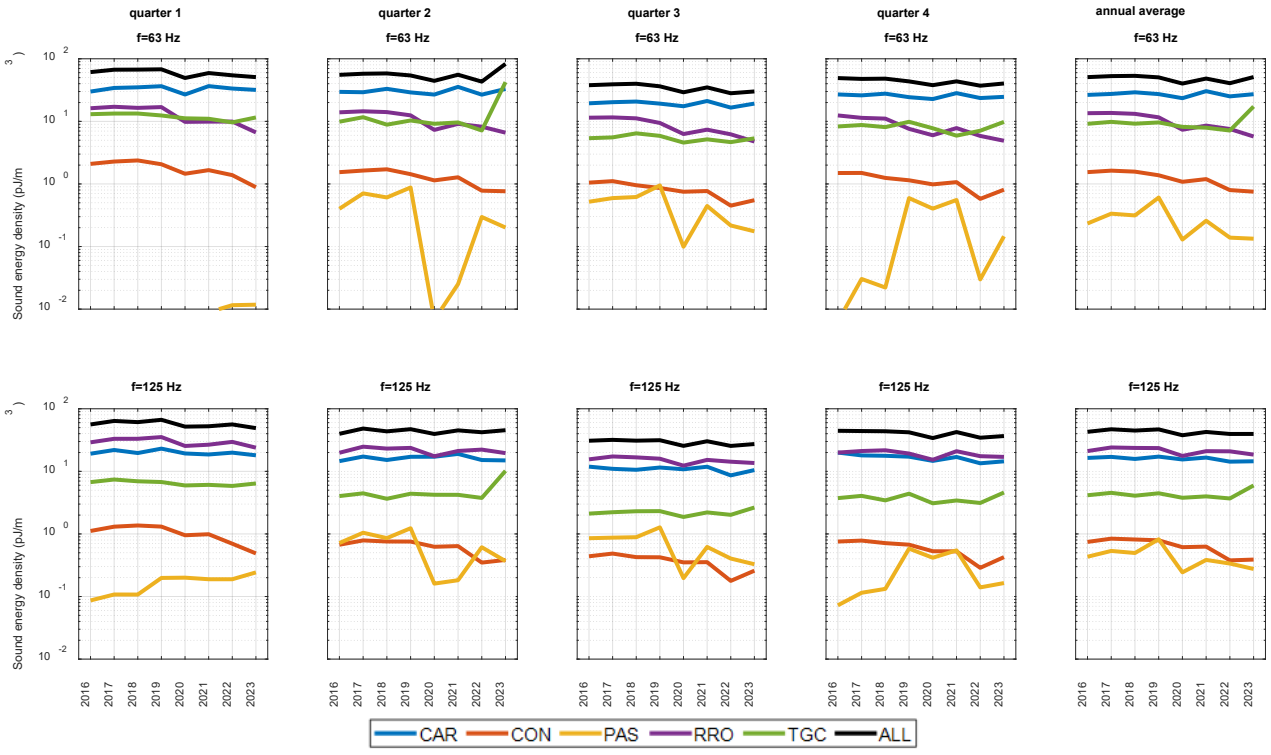

Figure 24 Sound energy density (in pJ/m^3) of different vessel categories for each quarter and year in the Baltic Sea. The top panel is for 63 Hz. The bottom panel is for 125 Hz.

At 63 Hz, the CAR vessel category consistently has the largest contribution to URN except in the second quarter of 2023. Over 50 % of sound energy density (ranging from 52 to 62.9 %) originates from the CAR vessel category.

During the first quarter, the contribution of the PAS vessel category is the lowest in both 63 and 125 Hz bands, with less than 1.2 % (fluctuating between 0.3 and 1.2 %). TGC vessels' contribution varies between 16.4 and 33.8 %, while CON vessels' contribution falls between 1.5 and 3 %. The RRO vessels' contribution ranges from 11.2 to 26.5 %.

At 125 Hz, the RRO vessels make a slightly higher contribution than CAR vessels. RRO vessels contribute to annually averaged sound energy density in the range of 46.7 to 52.8 %, CAR vessels range from 35.2 to 41 %, and TGC vessels range between 9.3 and 15 %. CON vessels range from 0.9 to 1.8 %. Additionally, the contribution of PAS vessels varies from 0.7 to 1.76 %.

To investigate the temporal trends of sound energy density, the sound energy density for each quarter is used, providing higher temporal resolution than annually averaged sound energy density. This approach can help in understanding changes in underwater sound level by matching these changes with potential causes (e.g., storms, oil and economic crises, pandemics). Additionally, plotting the sound energy density in chronological order can help to see variations more clearly due to seasonal changes in the sound speed profile. The temporal variation of quarterly averaged sound energy density is shown for different vessel categories in the Baltic Sea in Figure 25.

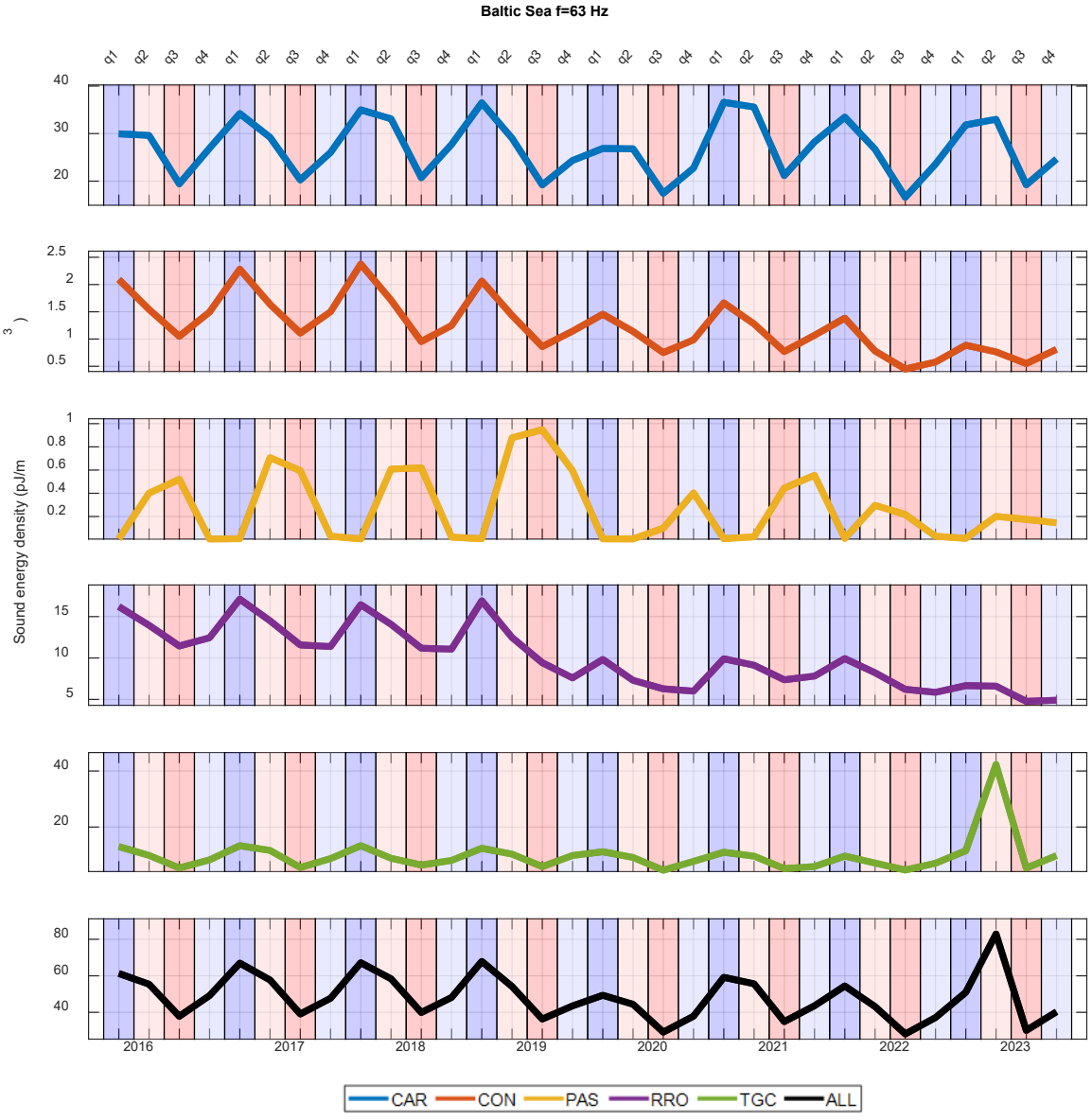

Figure 25 Sound energy density (in pJ/m^3) of different vessel categories in the Baltic Sea for each quarter in chronological order at 63 Hz.

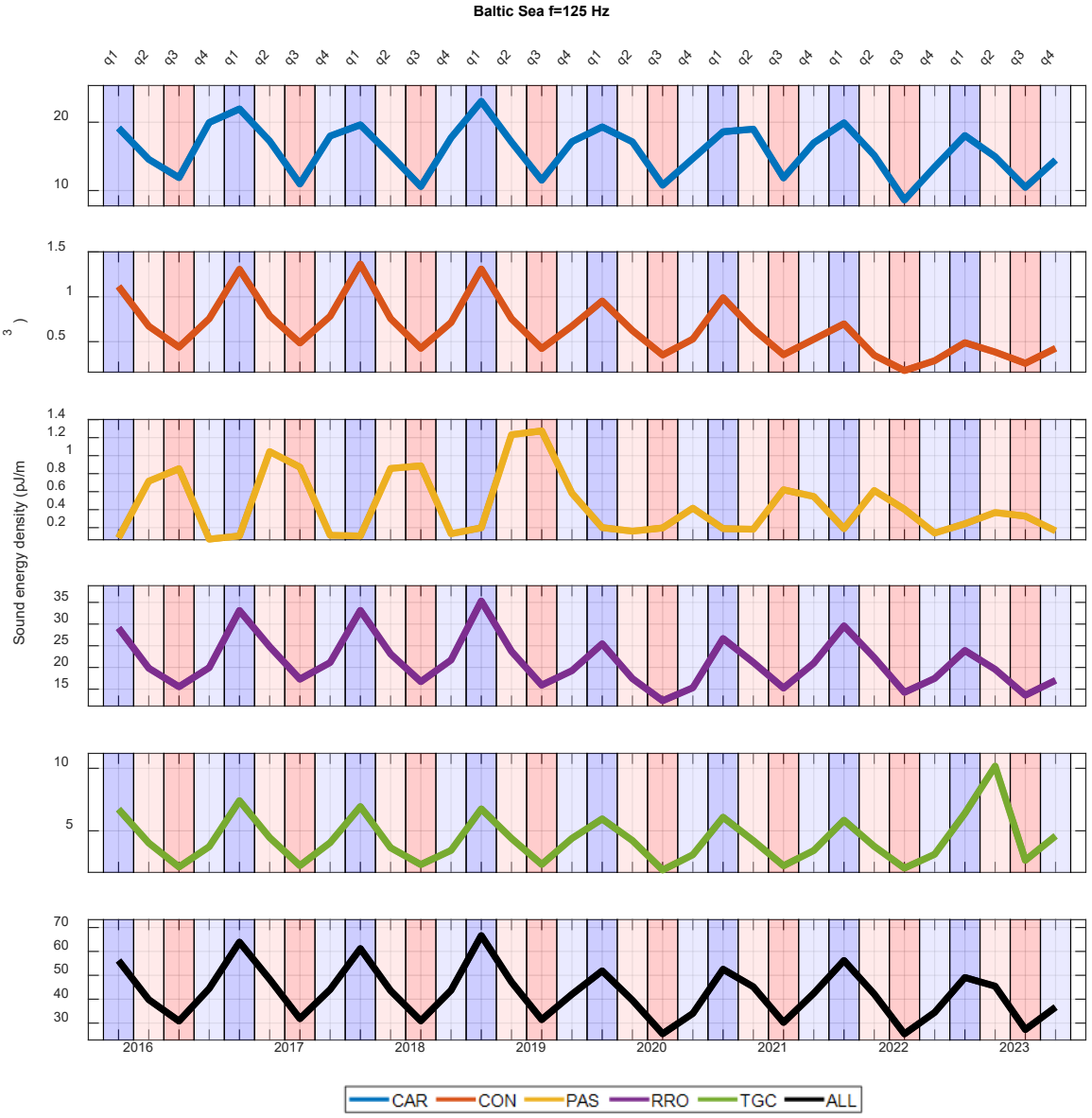

Figure 26 Sound energy density (in pJ/m^3) of different vessel categories in the Baltic Sea for each quarter in chronological order at 125 Hz.

The seasonal cycles are noticeable for all vessel categories. Except for the PAS vessel category, the sound energy density is the largest in the first quarters (shown by a darker blue background) and lowest in the third quarters (shown by a darker red background). The PAS vessels have the lowest sound energy density in the first and fourth quarters, and the largest in the second and third quarters. These cycles can be attributed to changes in the sound speed profile, vessel speed and AIS distribution specific to the selected years. However, since the Baltic Sea has shallow waters (less than 70 m on average), no strong effect of the sound speed profile is expected at 63 and 125 Hz(Sertlek et al. 2016b).

In 2020, there is a noticeable decrease in the sound energy density for almost all vessel categories, likely related to the COVID-19 pandemic. This decrease is particularly pronounced for the PAS vessel category, which is naturally one of the most affected due to limitations in travelling during the pandemic.

During the second quarter of 2023, there is a notable rapid increase in the sound energy density of the TGC vessel category. To understand this increase, an analysis of the changes in the number of TGC vessels and the areic source level (ASL) map layer during the same quarter was conducted. The ASL map layers of TGC vessels appear to be higher for the second quarter of 2023 compared to other quarters. However, no visible rapid change was observed in the number of TGC vessels. This increase may be related to changes in the speed of TGC vessels at specific local spots. Further investigation (i.e., repeating the similar sound energy density calculation at multiple frequencies in a larger frequency band) is required to understand the cause of this increase.

3.1.1.3 Black Sea

Similar comparisons performed for the Baltic Sea are also repeated for the Black Sea in this subsection. In Figure 27, sound map layers of Black Sea for 2022 are shown at 63 and 125 Hz including ALL vessel categories.

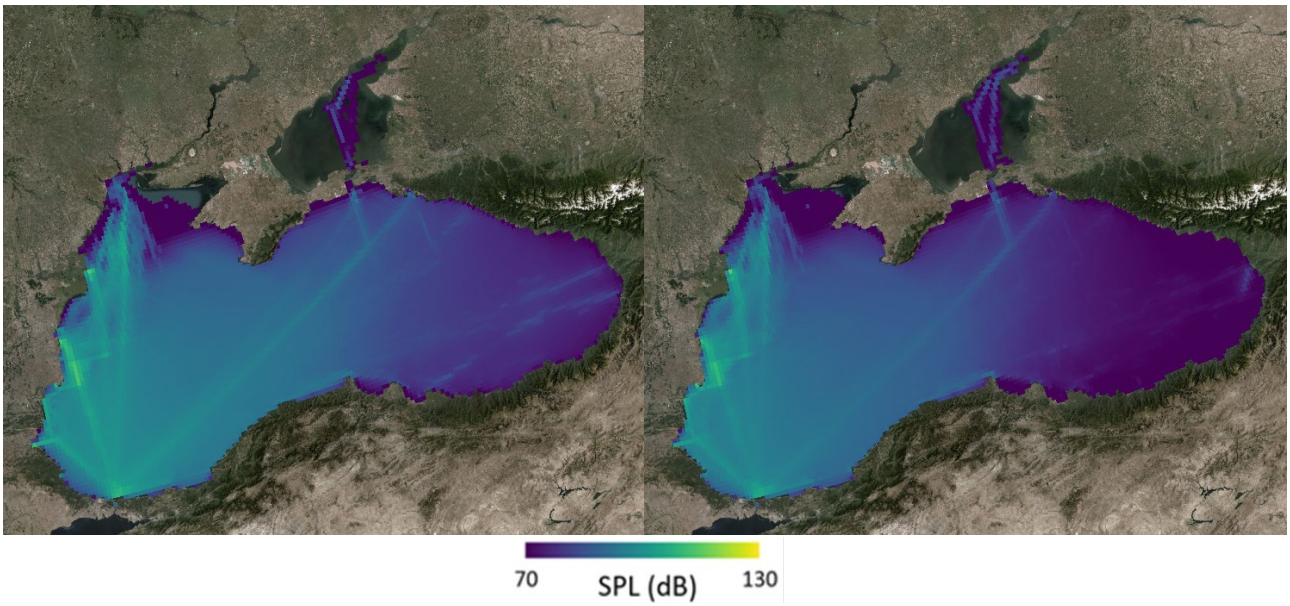

Figure 27 Sound map layers (SPL re 1 μPa^2, in dB) of Black Sea for 2022 including ALL vessel categories at (left) 63 Hz and (right) 125 Hz.

This map could provide insight into the spatial distribution of underwater sound for the year 2022. For the Black Sea, the AIS coverage appears to be low for certain years and regions, which may impact the accuracy and analysis of the data in those areas.

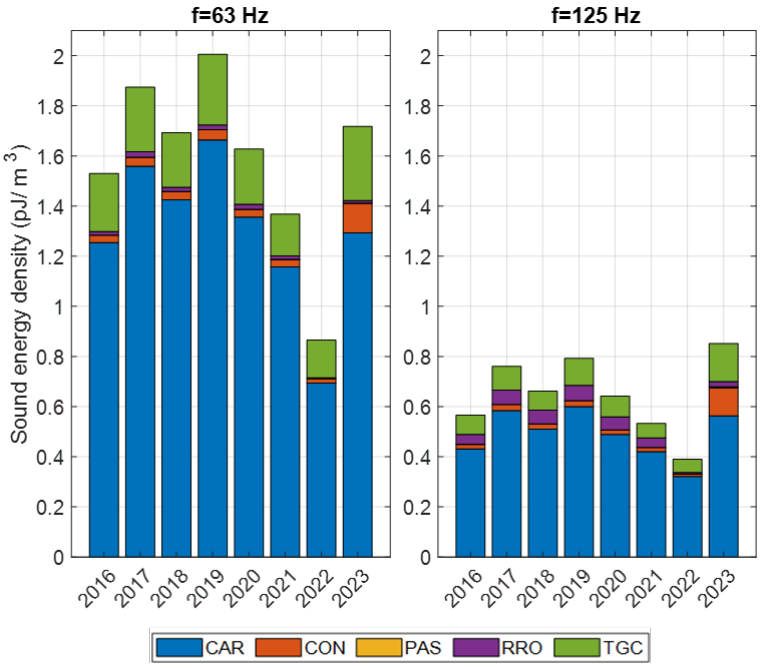

Figure 28 Annually averaged sound energy density (in pJ/m^3) in the Black Sea at (left) 63 Hz and (right) 125 Hz.

The sound energy density for each vessel category is presented as quarterly and annual averages in Figure 29.

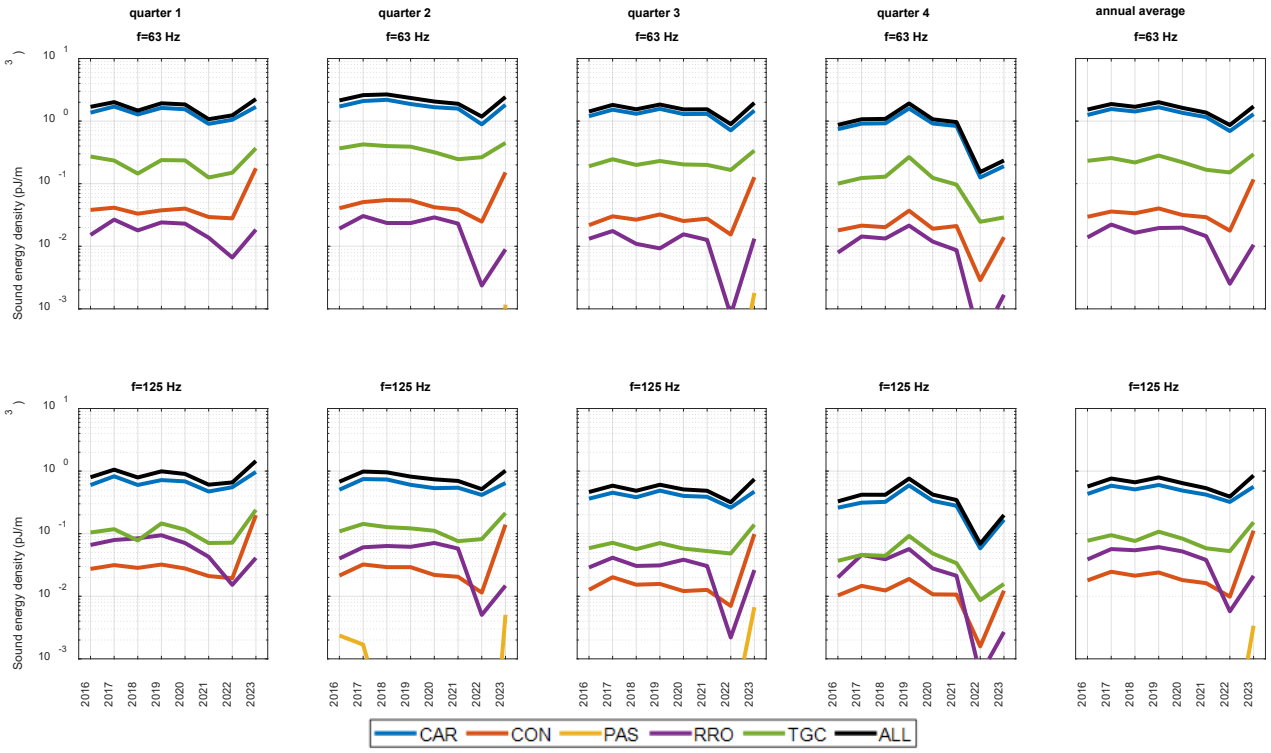

Figure 29 Sound energy density (in pJ/m^3) of different vessel categories for each quarter and year in the Black Sea. The top panel is for 63 Hz. The bottom panel is for 125 Hz.

At 63 Hz, the contribution of the CAR vessel category to sound energy density is the largest, ranging from 75.3 to 84.6 %. Meanwhile, the TGC vessel category's contribution ranges from 12.2 to 17.5 %. At 125 Hz, once again, the CAR vessel category's contribution to sound energy density is the largest, ranging from 66.1 to 82 %. TGC vessels contribute 10.9 to 17.9 % of the total energy density.

Throughout all quarters, the CAR vessel category consistently makes the largest contribution at both 63 and 125 Hz. Following the CAR vessels, TGC vessels make the second largest contributions to URN in both frequency bands. Conversely, the PAS vessel category consistently makes the lowest contribution for all quarters. The contribution of PAS vessels is so low that it falls outside the range of the y-axis in the first quarter's comparisons. The contribution of PAS vessels is close to 0 % for both frequencies.

To see the seasonal cycles, the same values are plotted in a chronological order in Figure 30.

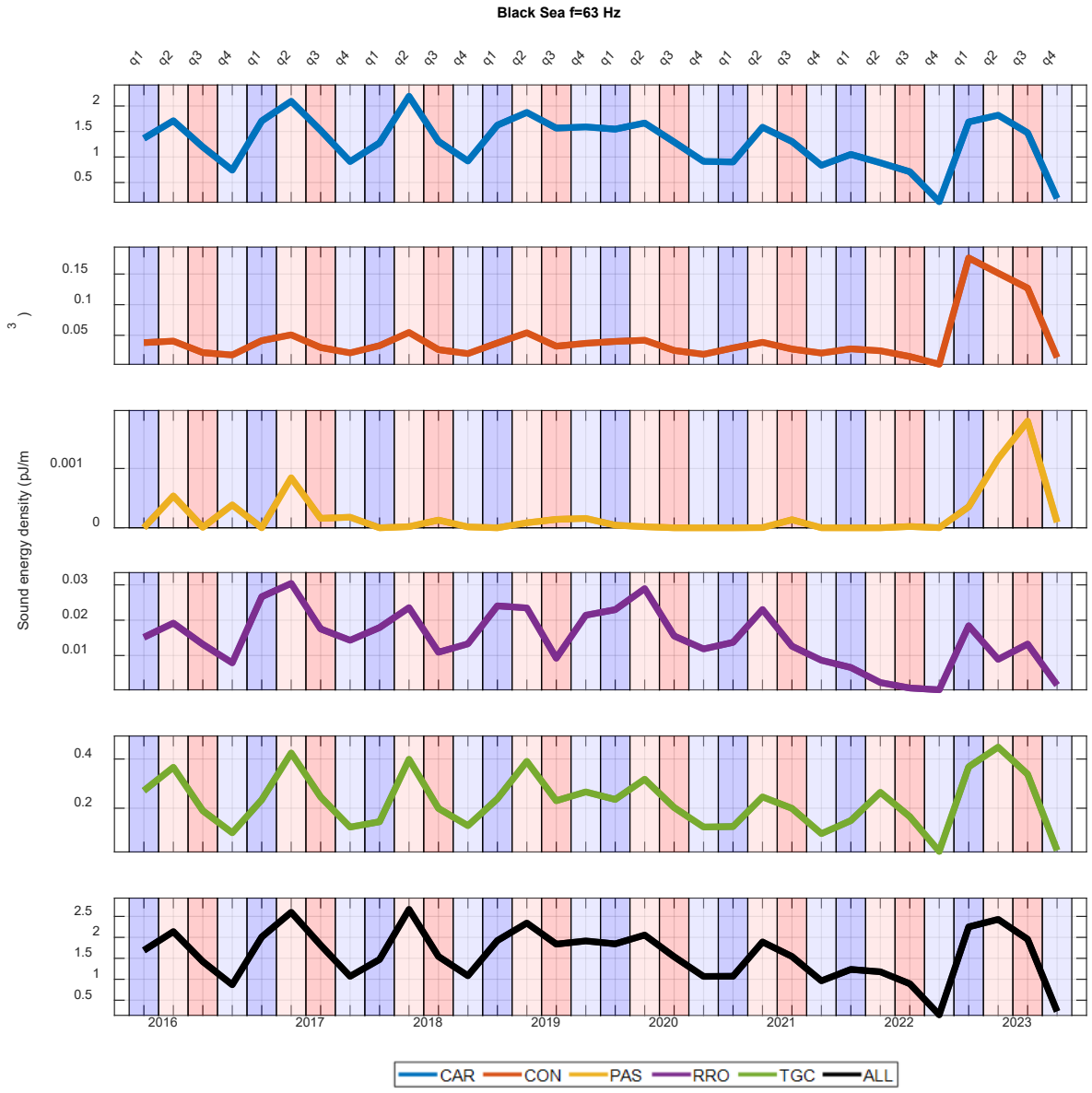

Figure 30 Sound energy density (in pJ/m^3) of different vessel categories in the Black Sea for each quarter in chronological order at 63 Hz.

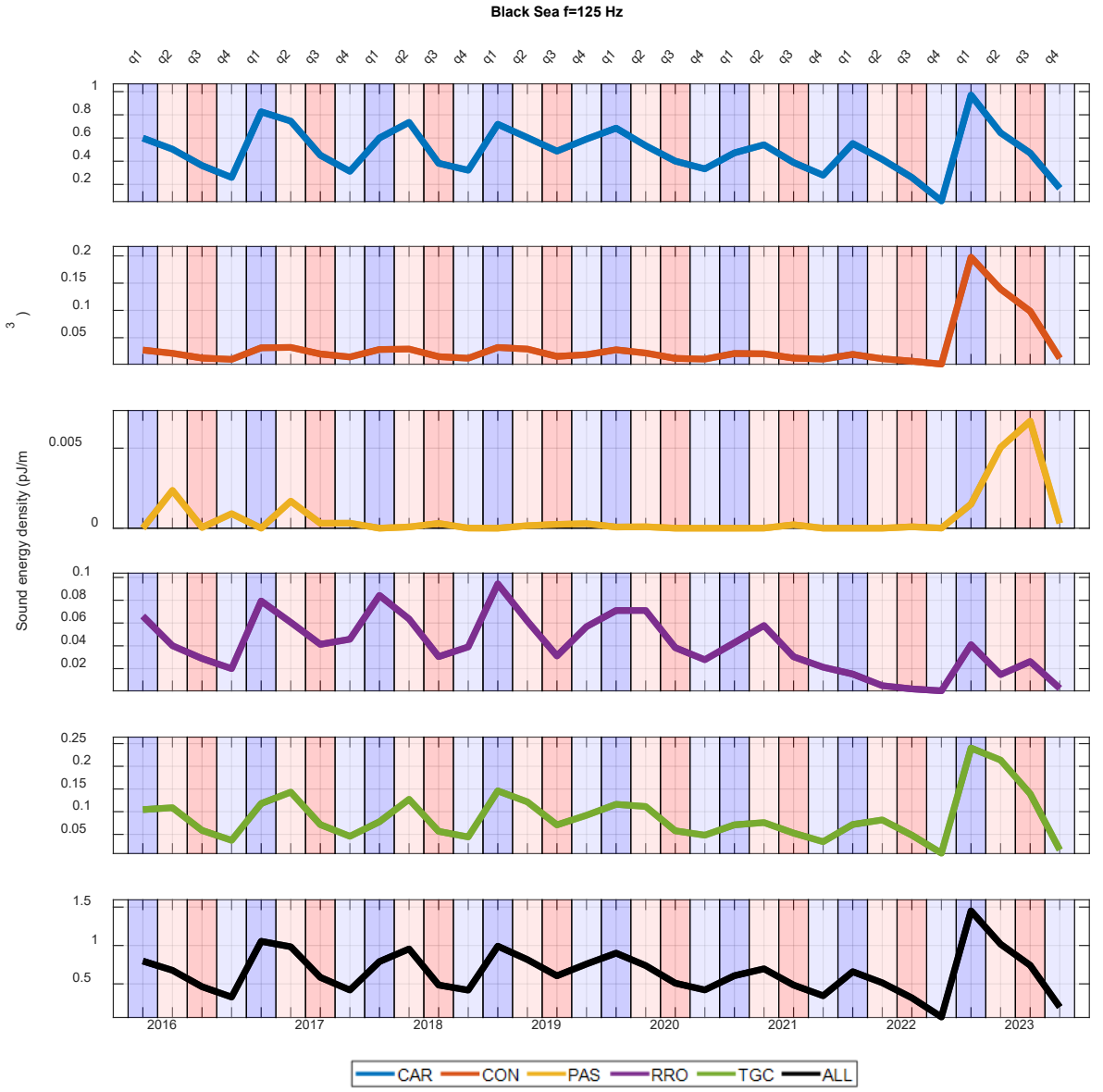

Figure 31 Sound energy density (in pJ/m^3) of different vessel categories in the Black Sea for each quarter in chronological order at 125 Hz.

The highest sound energy density at 125 Hz occurs in the first quarter, as expected. At 63 Hz, the maxima shift to quarter 2, which is not unexpected, but could be related to melting ice, as mentioned above. However, seasonal cycles are less visible in the Black Sea, perhaps because of limited AIS coverage and variations in the AIS coverage between different years.

The contribution of PAS vessels remains consistently the lowest in all quarters. For some quarters, such as the fourth quarter of 2020 and 2021, there are no AIS data available for PAS vessels in the Black Sea. Therefore, there is no contribution from the PAS vessels for these months.

As previously mentioned, there is a significant decrease in sound energy across all vessel categories during the fourth quarter of 2022. This decrease is most noticeable for RRO vessels and observed in all quarters. A similar decrease is observed for all vessel categories during the fourth quarter of 2022.

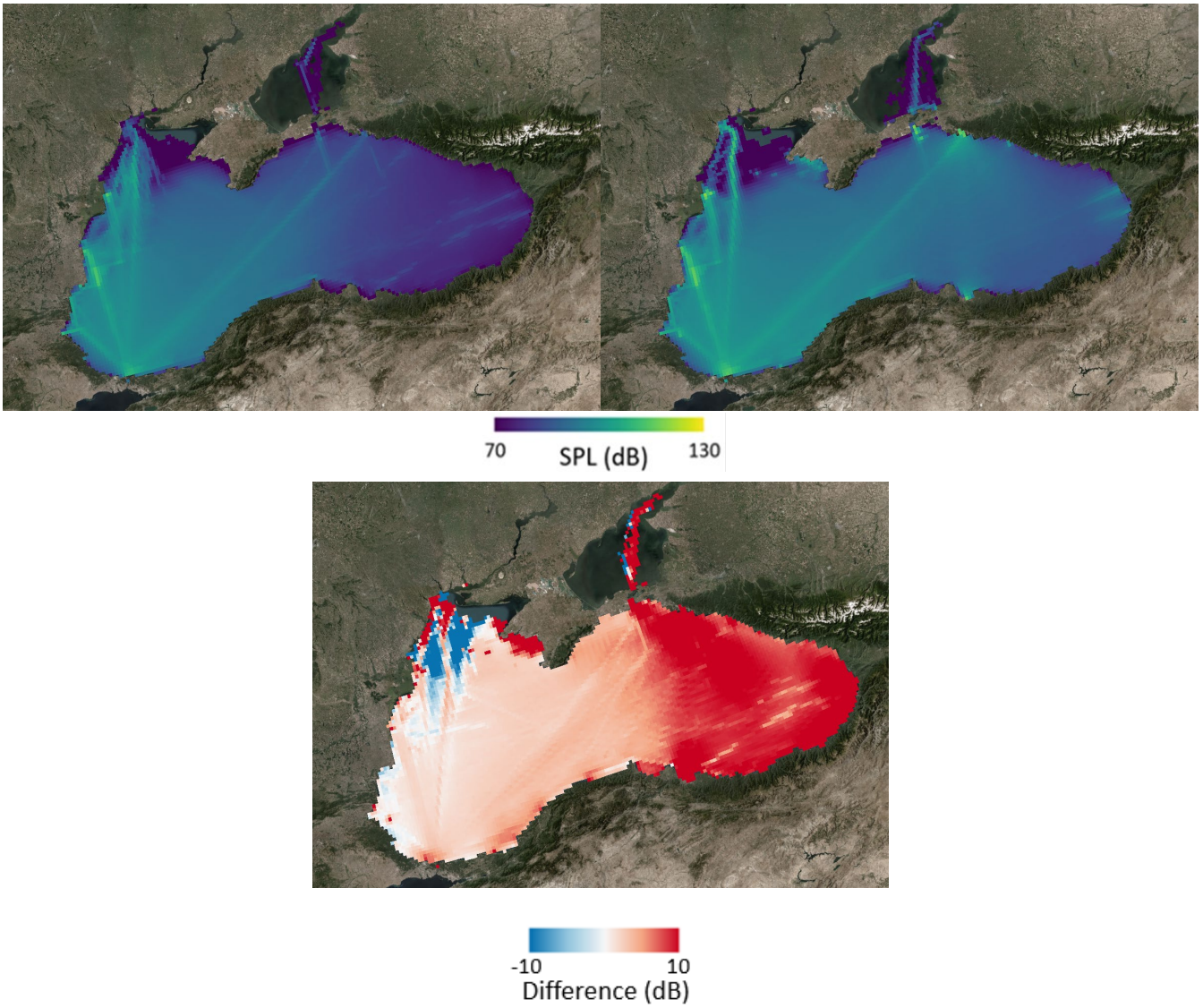

Figure 32 Sound map layers (SPL re 1 μPa^2, in dB) of the Black Sea for 2022 (top left) and 2023 (top right) at 63 Hz. The difference (2023–2022) (bottom) of these two maps.

3.1.1.4 Mediterranean Sea

In Figure 33, sound map layers of Mediterranean Sea for 2022 are shown at 63 and 125 Hz including ALL vessel categories.

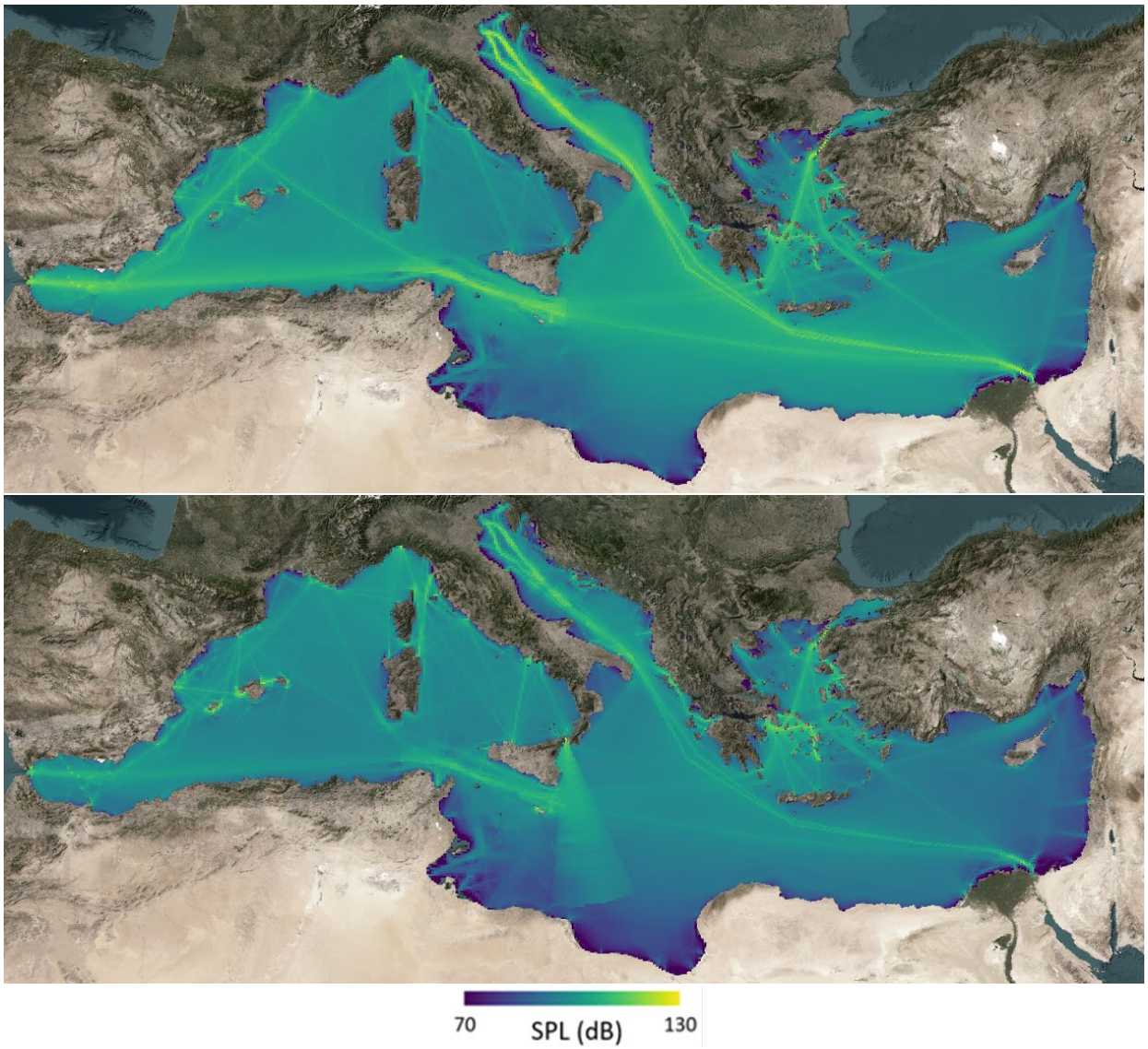

Figure 33 Sound map layers (SPL re 1 μPa^2, in dB) of Mediterranean Sea for 2022 including ALL vessel categories at (top) 63 Hz and (bottom) 125 Hz.

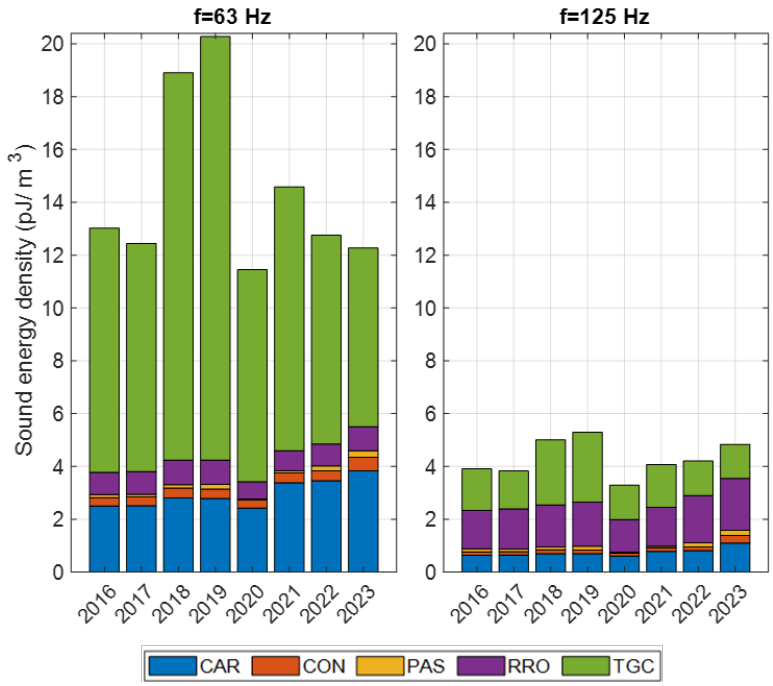

Figure 34 Annually averaged sound energy density (in pJ/m^3) in the Mediterranean Sea at (left) 63 Hz and (right) 125 Hz.

3.1.1.4.1 Ranking the Contribution of Vessel Categories to Sound Energy Density

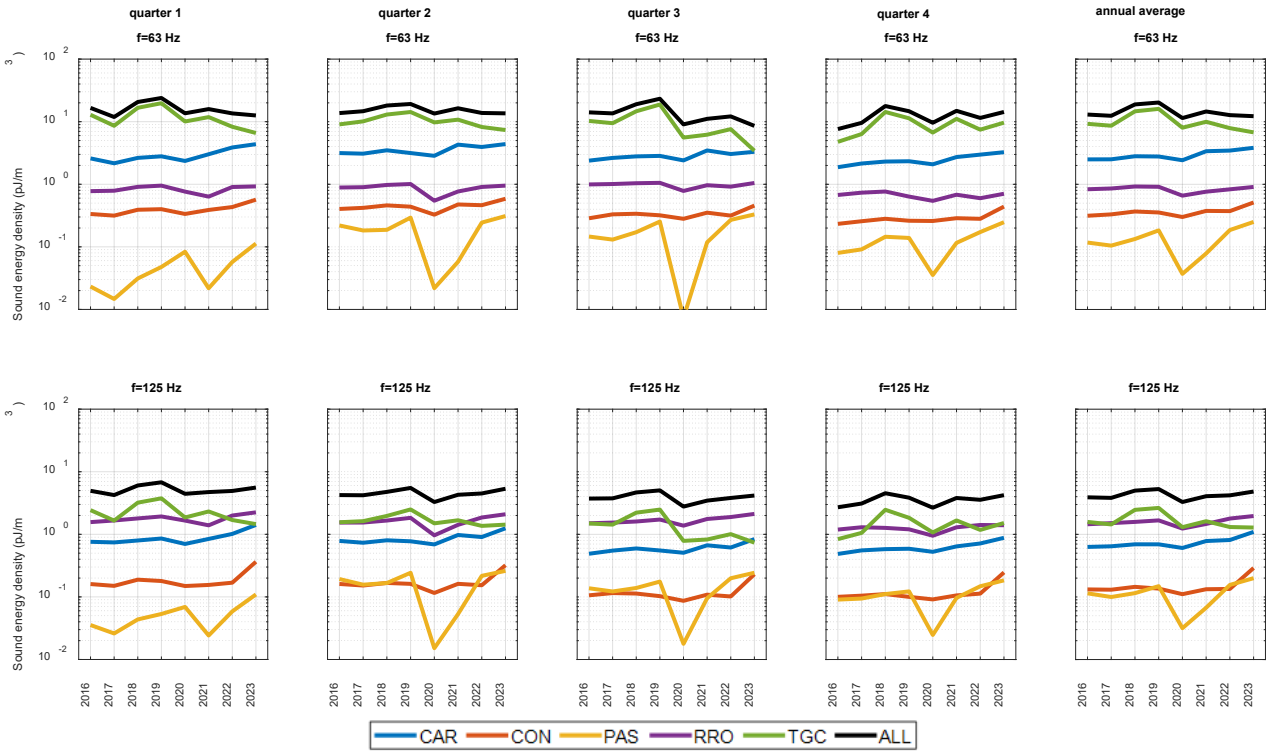

Figure 35 Sound energy density (in pJ/m^3) of different vessel categories for each quarter and year in the Mediterranean Sea. The top panel is for 63 Hz. The bottom panel is for 125 Hz.

At 63 Hz, TGC vessels make the largest contribution (ranging from 55.1 to 79.1 %), followed by CAR vessel category (between 13.7 to 31.23 %). RRO vessels' contribution ranges from 4.5 to 7.4 %. The lowest contribution, varying between 0.3 and 2.0 %, is from PAS vessels.

At 125 Hz, the largest contributions come from both RRO (31.6 to 42.6 %) and TGC vessels (26.6 to 50.0 %). The lowest contributions are from both PAS vessels (ranging from 1.0 to 4.1 %) and CON vessels (ranging from 2.6 to 6.0 %). CAR vessels' contribution falls between 13.1 to 22.6 %.

There was a notable decrease in sound energy density for PAS vessels during 2020, likely due to the restrictions imposed by the COVID-19 pandemic. Other categories have also decreased in their sound energy density during 2020; however, the decrease is not as strong as that observed in PAS vessels.

The Mediterranean Sea covers a large area, including multiple countries. There can be local increases or decreases in shipping sound. For instance, a comparison of sound map layers for 2022 and 2023 at 63 Hz is shown in Figure 36. In 2022, there are higher SPL values along the vessel tracks in the Adriatic Sea. However, there is less sound in the same region in 2023. In contrast, the Marmara Sea seems quieter in 2022 than in 2023. However, the sound energy density is calculated for the entire Mediterranean Sea. It is not directly possible to gather this information from the energy density without additional calculations for the sub-regions of the Mediterranean Sea. For this reason, area-over-specific-SPL graphs could be helpful as a complementary analysis once the choice of SOW is harmonised.

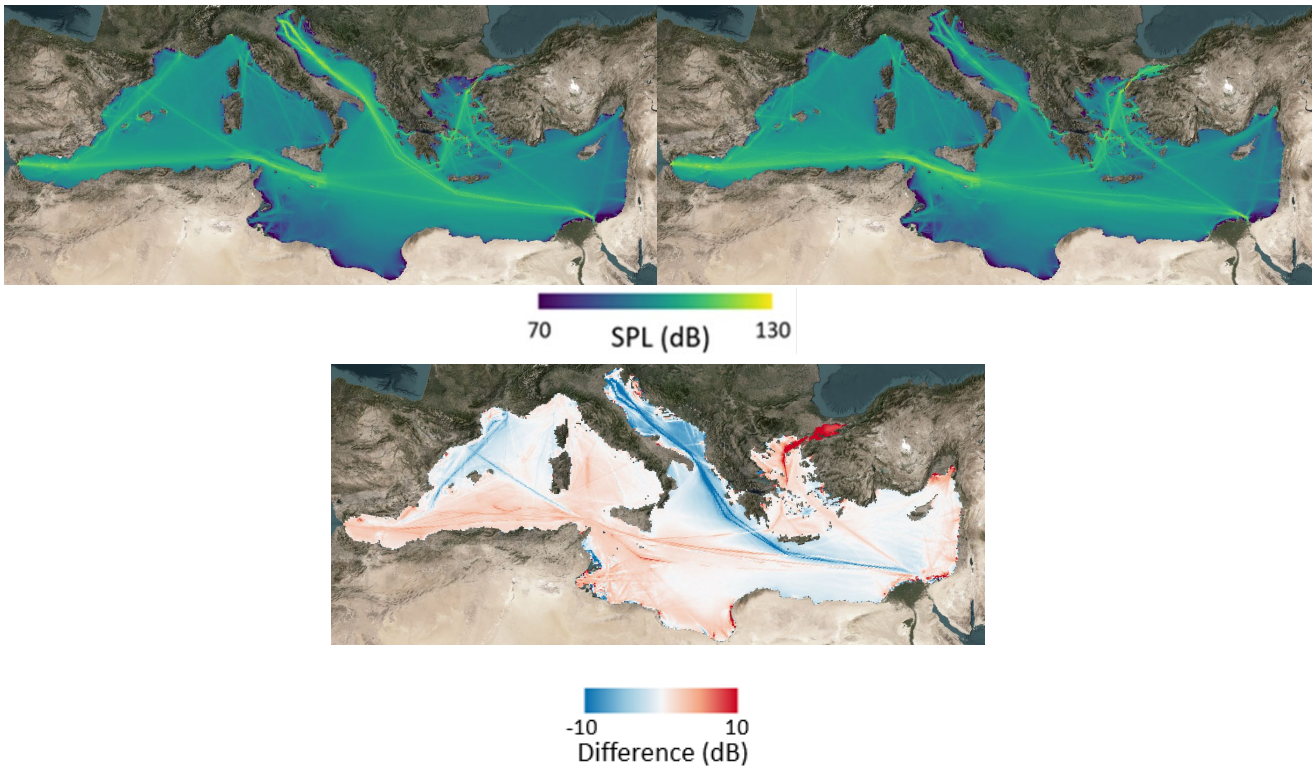

Figure 36 Comparison of sound map layers (SPL re 1 μPa^2, in dB) of Mediterranean Sea for including ALL vessel categories during (top left) 2022 and (top right) 2023 at 63 Hz. The difference (2023–2022) (bottom) of these two maps.

The quarterly averaged sound energy density in chronological order is shown in Figure 37.

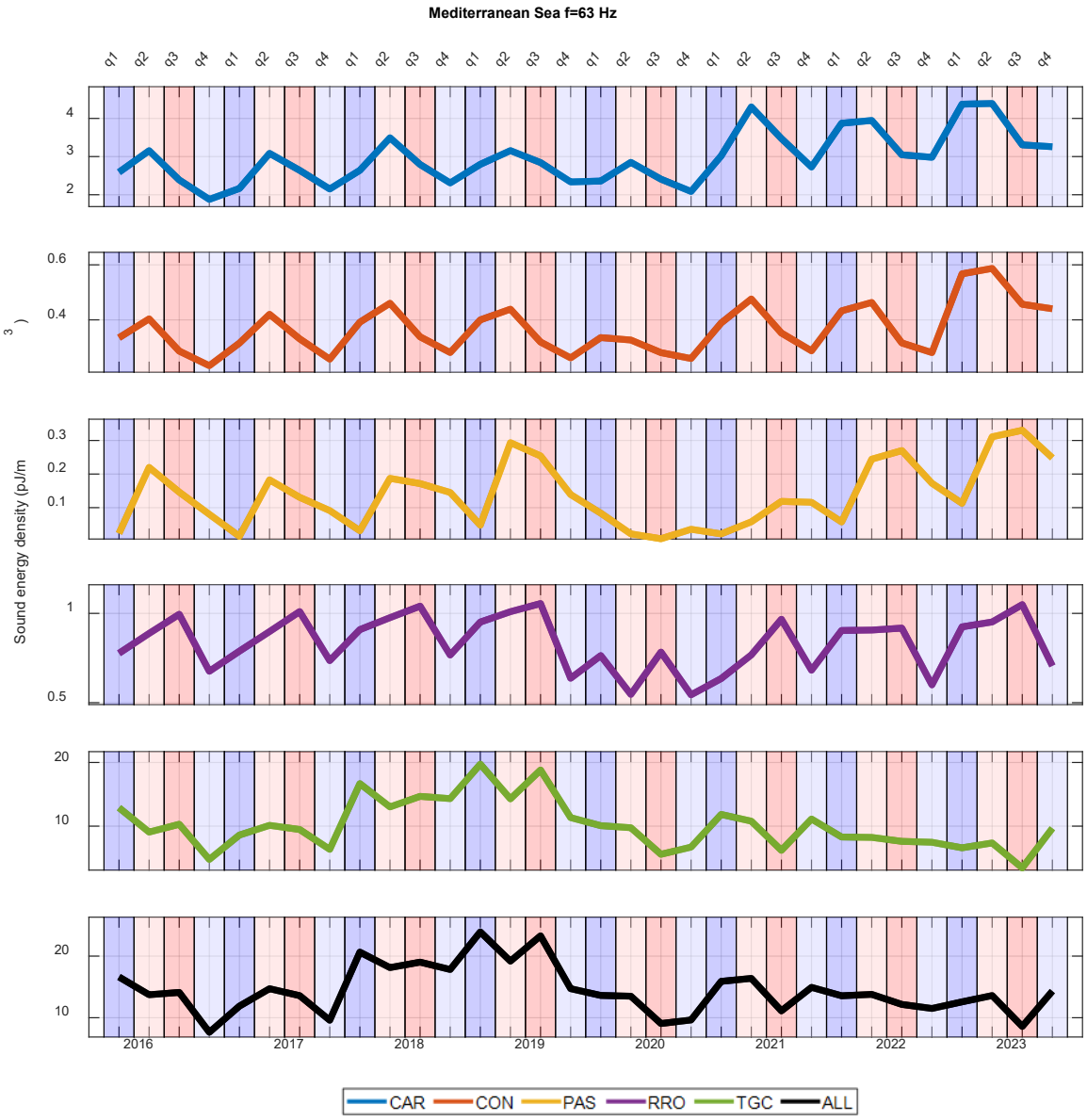

Figure 37 Sound energy density (in pJ/m^3) of different vessel categories for each quarter in chronological order for 63 Hz.

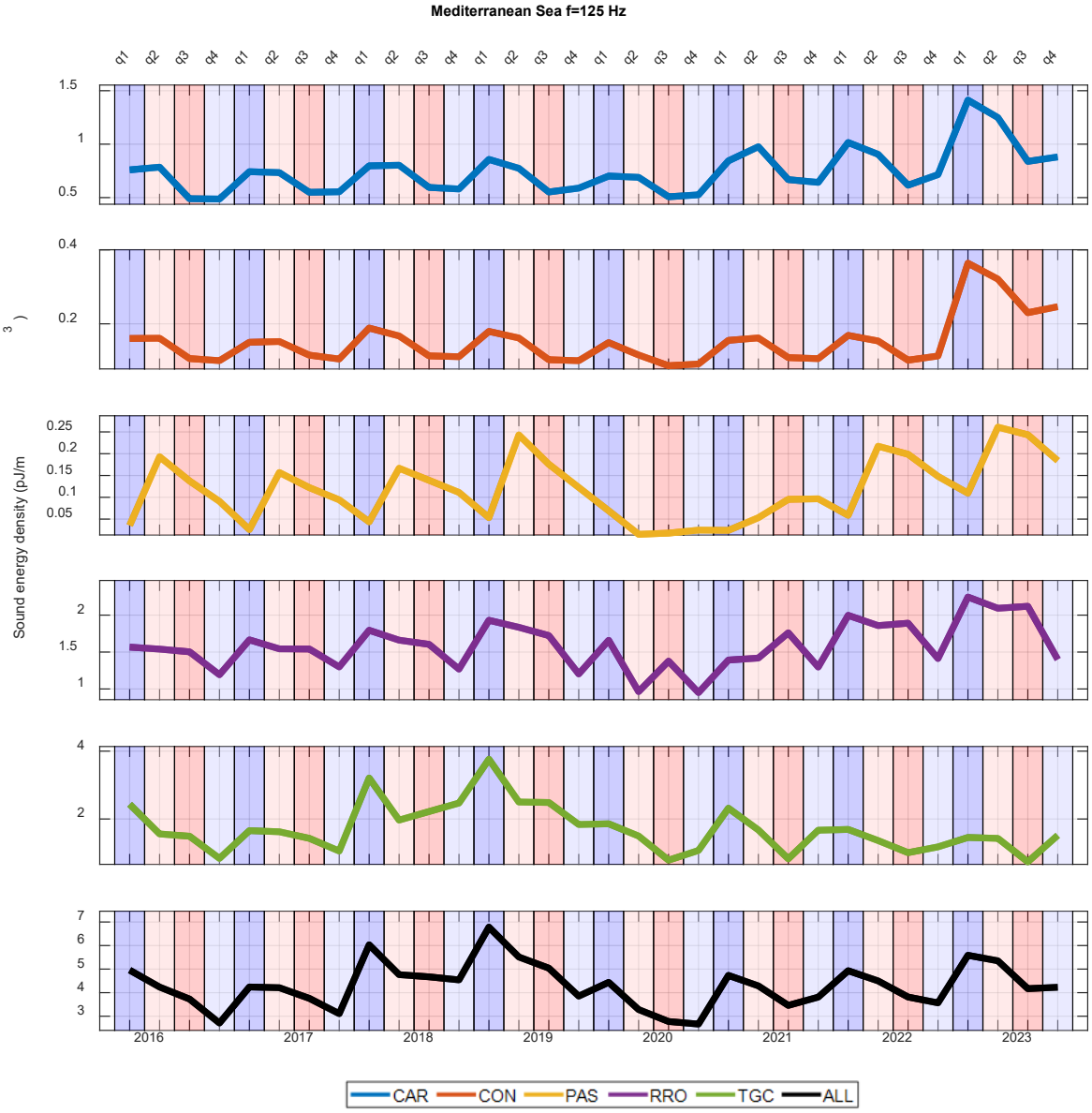

Figure 38 Sound energy density (in pJ/m^3) of different vessel categories for each quarter in chronological order for 125 Hz.

Seasonal cycles are strongly visible for the PAS vessel category until the second quarter of 2020 when the restrictions due to the COVID-19 pandemic began to appear. There is also a slight decrease during the second quarter of 2020 for other vessel categories (except RRO). However, it appears that this decrease does not strongly affect the seasonal changes observed for the PAS vessel category, and the recovery time to having seasonal patterns seems shorter. There is a large increase in sound energy density for the CAR and CON vessel categories at 125 Hz in the first quarter of 2023. However, this increase is smaller at 63 Hz for the same categories. At 63 Hz, the largest sound energy density for CAR and CON vessels is mostly observed during the second quarter. However, at 125 Hz, the largest sound energy density occurs in the first quarters. As discussed in the previous section, this difference could be related to effect of seasonal SSPs on the sound propagation. Especially during the second quarter, melting ice is hypothesised to affect the sound speed in the upper water layer, which could explain why peaks in sound energy density at 63 Hz are observed in this region. This hypothesis has not been investigated.

For the TGC vessel category, the seasonal cycles are not as visible as in other categories. This could be related to larger variations in the areic source level and the number of TGC vessels, rather than the effect of SSP on sound propagation. As the largest contribution comes from TGC vessels, its temporal pattern becomes apparent when summing the sound energies of all vessels.

3.1.1.5 North Sea

In Figure 39, sound map layers of North Sea for 2022 are shown at 63 and 125 Hz including ALL vessel categories.

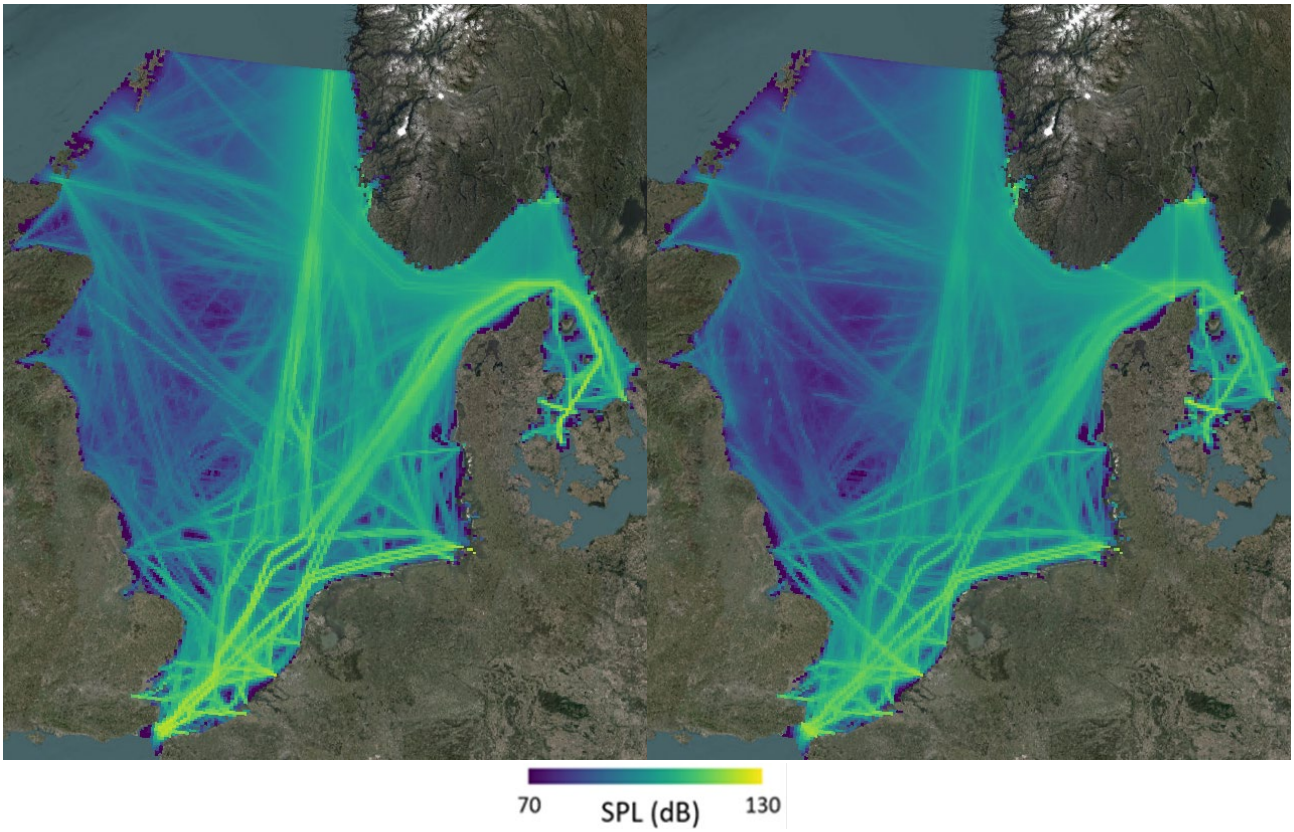

Figure 39 Sound map layers (SPL re 1 μPa^2, in dB) of North Sea for 2022 including ALL vessel categories at (left) 63 Hz and (right) 125 Hz.

The southern North Sea exhibits high shipping density around the English Channel, with strongly visible vessel traffic lines continuing into the Baltic Sea and the northeastern Atlantic Ocean. To investigate the composition of sound maps, quarterly and annually averaged sound energy density plots are produced and compared.

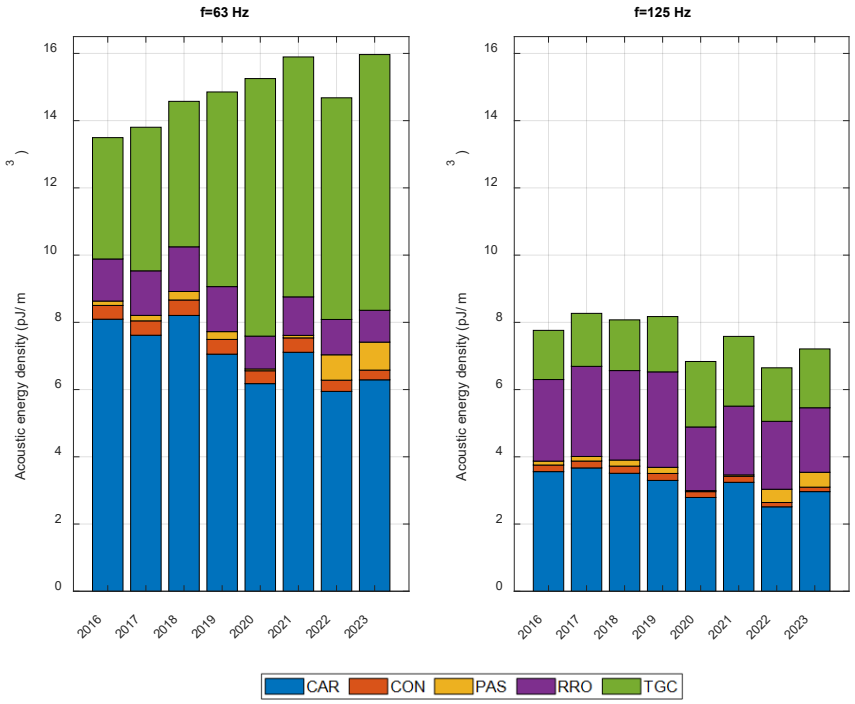

Figure 40 Annually averaged sound energy density (in pJ/m^3) in the North Sea at (left) 63 Hz and (right) 125 Hz.

3.1.1.5.1 Ranking the Contribution of Vessel Categories to Sound Energy Density

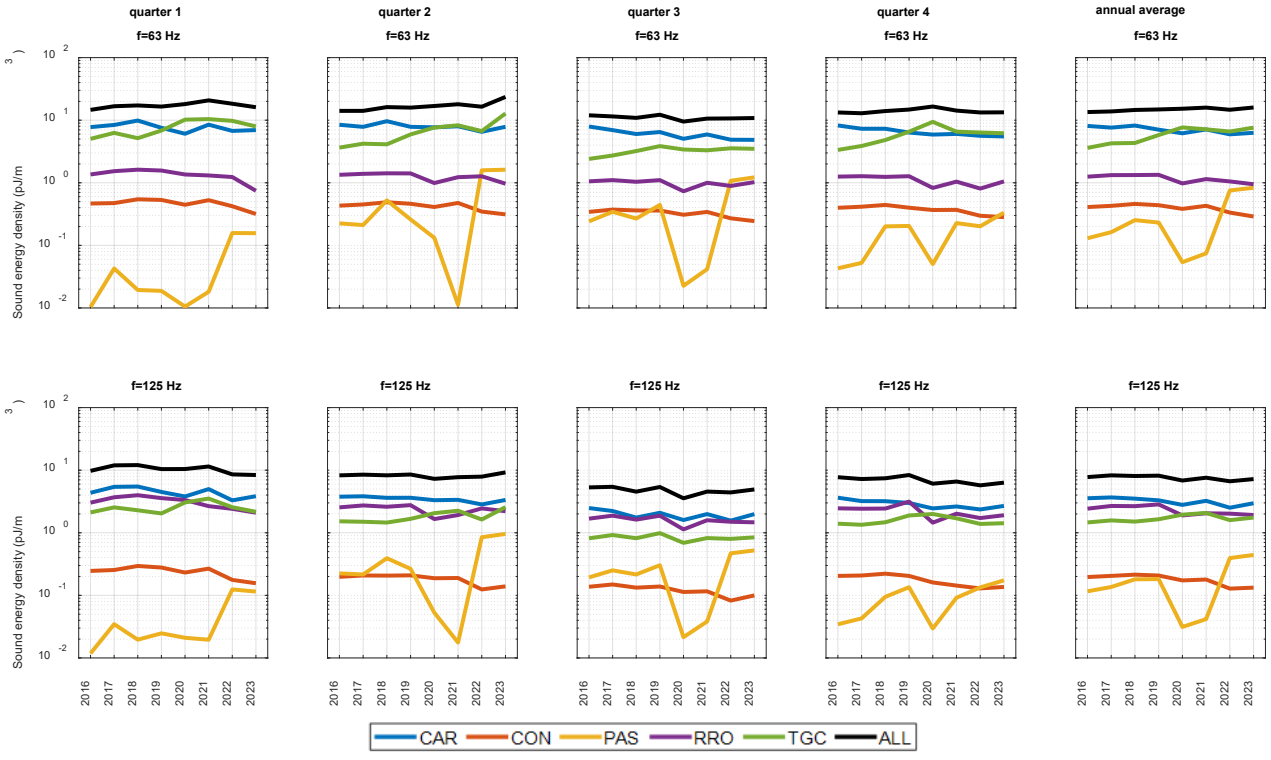

Figure 41 Sound energy density (in pJ/m^3) of different vessel categories for each quarter and year in the North Sea. The top panel is for 63 Hz. The bottom panel is for 125 Hz.

At 63 Hz, the largest contributions to sound energy density are from CAR vessels (ranging from 39.4 to 60.0 %) and TGC vessels (ranging from 26.7 to 50.2 %). The RRO vessel category's contribution varies between 5.9 and 9.6 %. The PAS and CON vessel categories have the lowest contributions, ranging from 0.3 to 5.2 % and 1.8 to 3.2 %, respectively.

At 125 Hz, the contribution of CAR vessels (ranging from 37.8 to 45.0 %) appears to be the highest for most years. The contributions of RRO vessels (ranging from 26.6 to 34.76 %) and TGC vessels (ranging from 18.7 to 28.5 %) to 28.5 %) to annual sound energy density are close to CAR vessel contributions for some years. Once again, the PAS and CON vessel categories have the lowest contributions, ranging between 0.5 to 6.1 % and 1.8 to 2.6 %, respectively.

Similar to other regions, there is a notable decrease in the sound energy density of the PAS vessel category during 2020 and 2021. However, the contribution of the PAS vessel category appears to increase after 2021. The sound energy density of TGC vessels shows an increasing trend until 2020, after which temporal variations become very small. The sound energy density of RRO and CON vessels is slightly decreasing after 2019 for both frequencies. CAR vessels exhibit a slight decrease until 2020, followed by fluctuations in their sound energy density after 2020, with a very slowly decreasing trend. For the sum of all vessel categories, there is a slowly increasing time trend at 63 Hz, whereas there is a decreasing time trend at 125 Hz. This difference in the temporal trend could be attributed to the higher sound energy density of the TGC vessel category at 63 Hz compared to other categories.

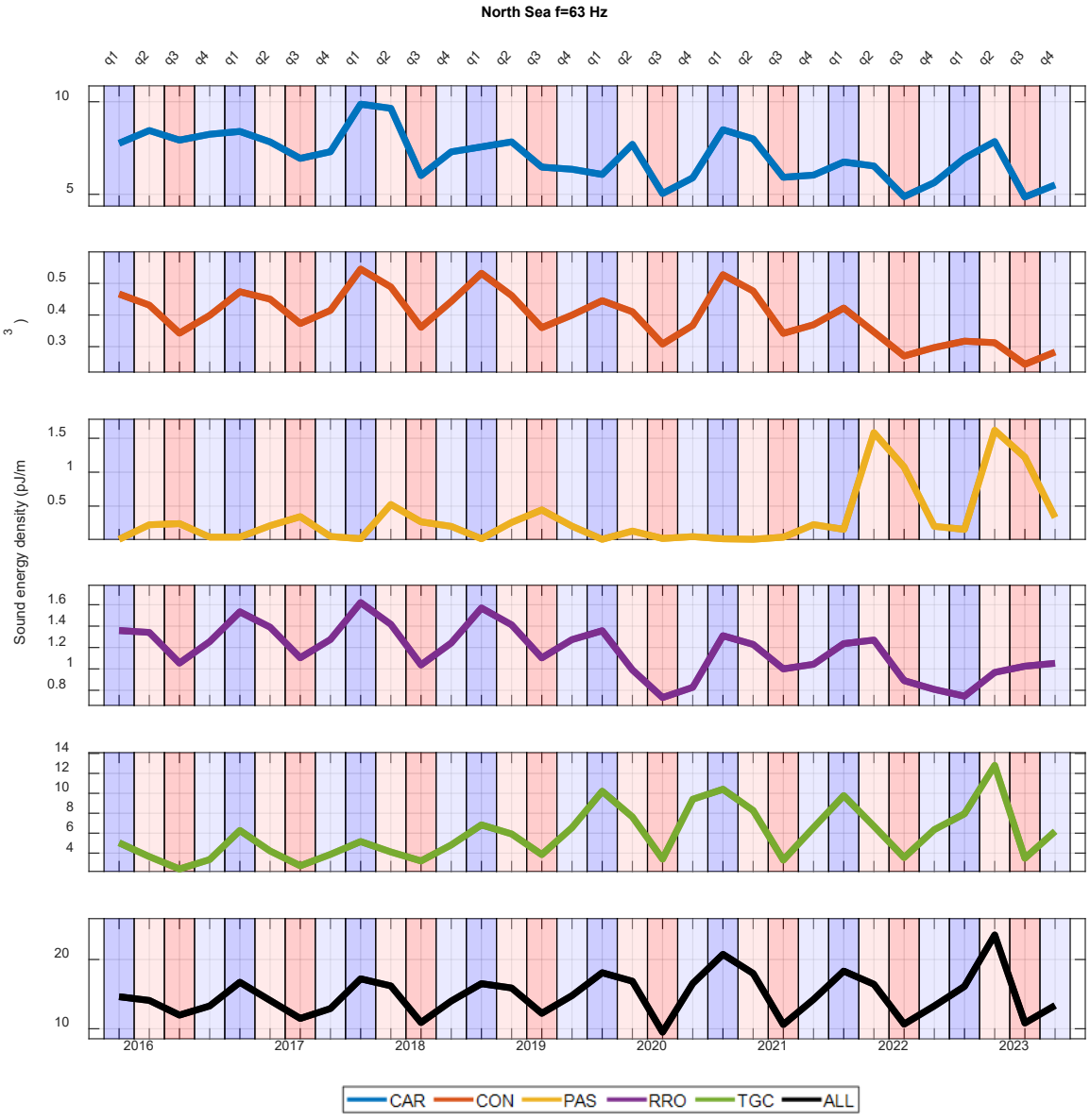

Figure 42 Sound energy density (in pJ/m^3) of different vessel categories in the North Sea for each quarter in chronological order at 63 Hz.

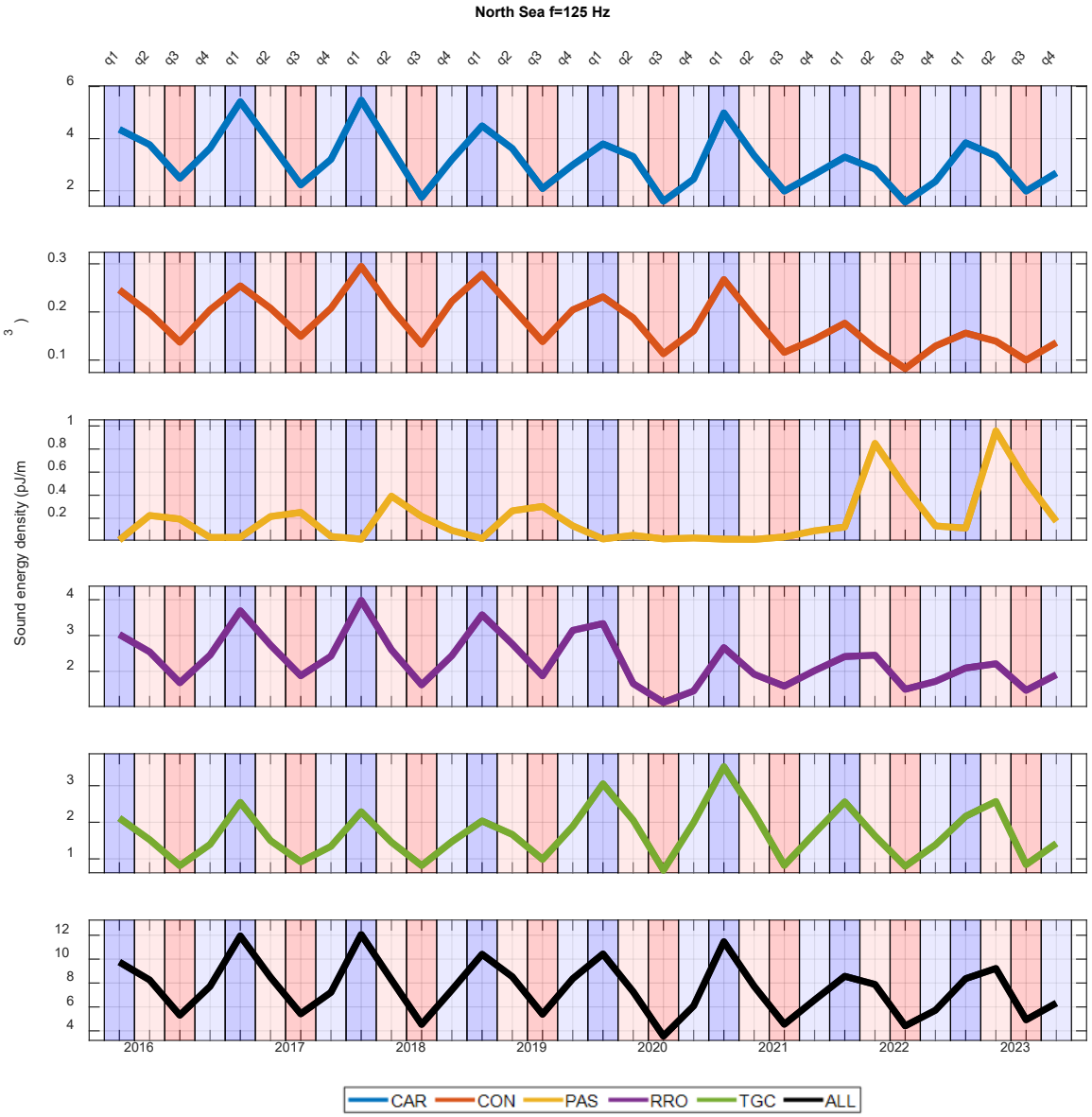

Figure 43 Sound energy density (in pJ/m^3) of different vessel categories in the North Sea for each quarter in chronological order at 125 Hz.

These seasonal cycles due to the sound speed profile are clearly visible for vessel categories at both frequencies, except PAS vessels between 2020 and 2021. The decrease in the sound energy density of the PAS vessel category could be related to the COVID-19 pandemic, as observed in other regions. Apart from the PAS and CAR (only at 63 Hz) vessel category, sound energy density is the highest in the first quarters (indicated by a darker blue background) and lowest in the third quarters (indicated by a darker red background). The influence of the sound speed profile in shallow waters is not as significant as observed in deeper waters, as discussed in previous sections.

The sound energy density of PAS vessels during the second and third quarters of 2022 and 2023 appears higher than in all other years. This may be related to better AIS coverage in 2022 and 2023. For TGC vessels, there is an increase in the sound energy density starting from the first quarter of 2020. As CAR and TGC vessels have the largest sound energy density in almost all quarters at 63 Hz, the temporal trend of all vessel categories is most influenced by CAR and TGC vessels. At 125 Hz, the contribution of RRO vessels can exceed that of TGC vessels (as shown in Figure 41)

Additionally, storms in the North Sea in early 2020 could have impacted vessel traffic and speed, directly affecting the areic source level(Sertlek 2021). Therefore, some irregular patterns (e.g., CAR vessels at 63 Hz) may be related to these strong storms.

3.1.1.6 Northeast Atlantic Ocean

In Figure 44, sound map layers of northeast Atlantic Ocean for 2022 are shown at 63 and 125 Hz including ALL vessel categories.

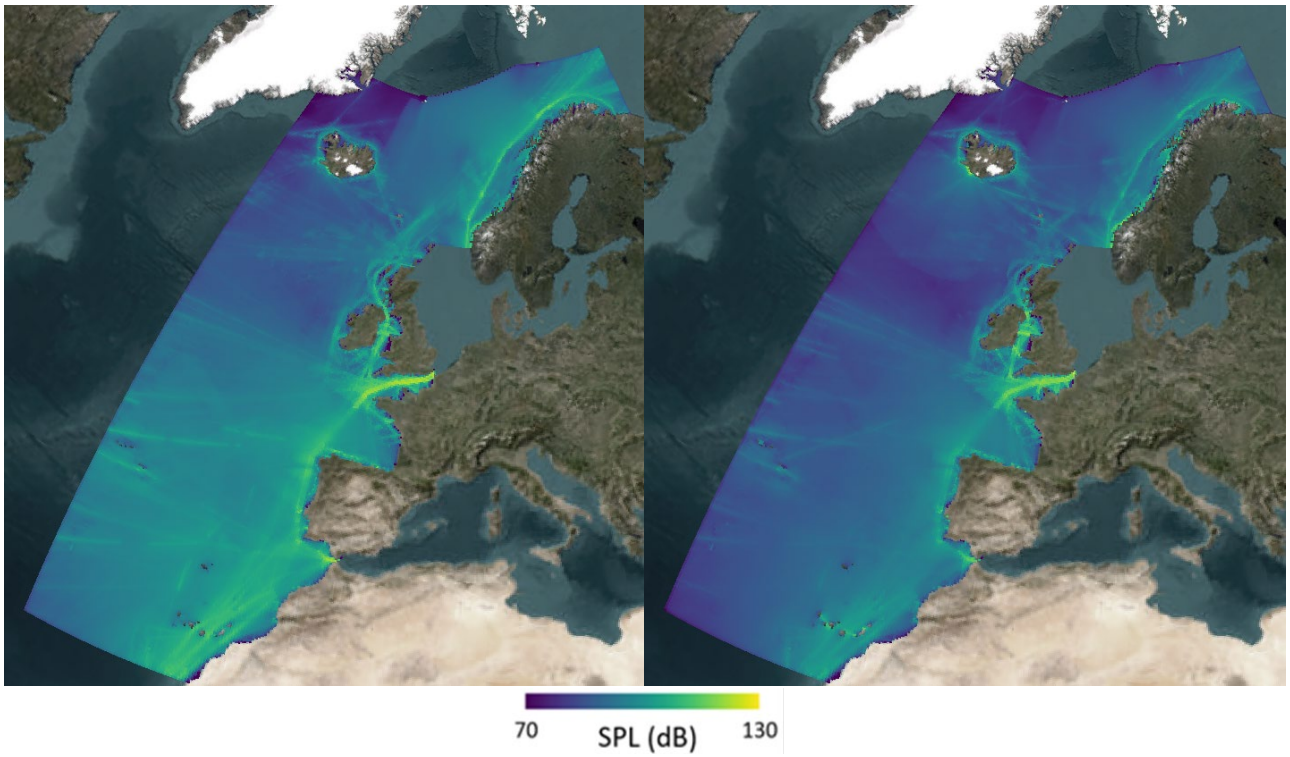

Figure 44 Sound map layers (SPL re 1 μPa^2, in dB) of northeast Atlantic Ocean for 2022 including ALL vessel categories at (left) 63 Hz and (right) 125 Hz.

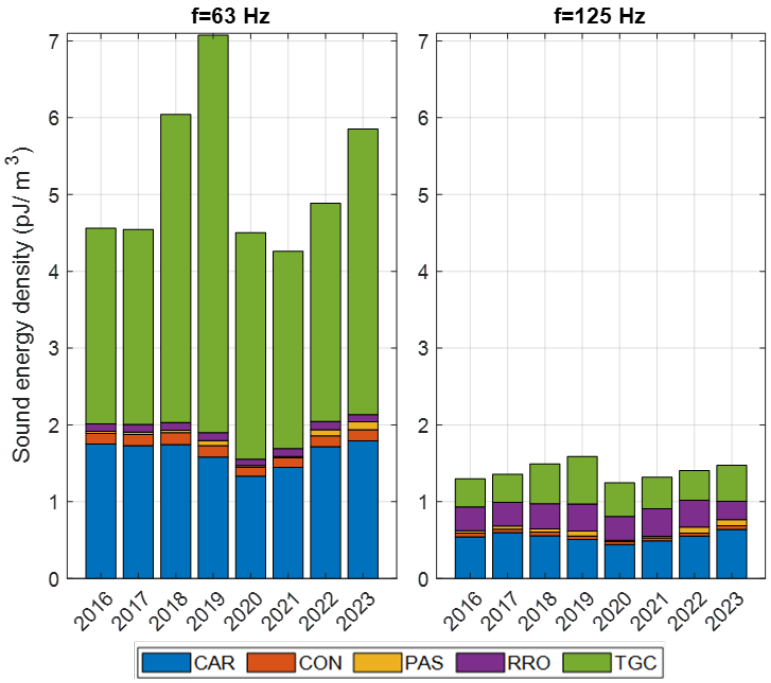

Figure 45 Annually averaged sound energy density (in pJ/m^3) in the northeast Atlantic Ocean at (left) 63 Hz and (right) 125 Hz.

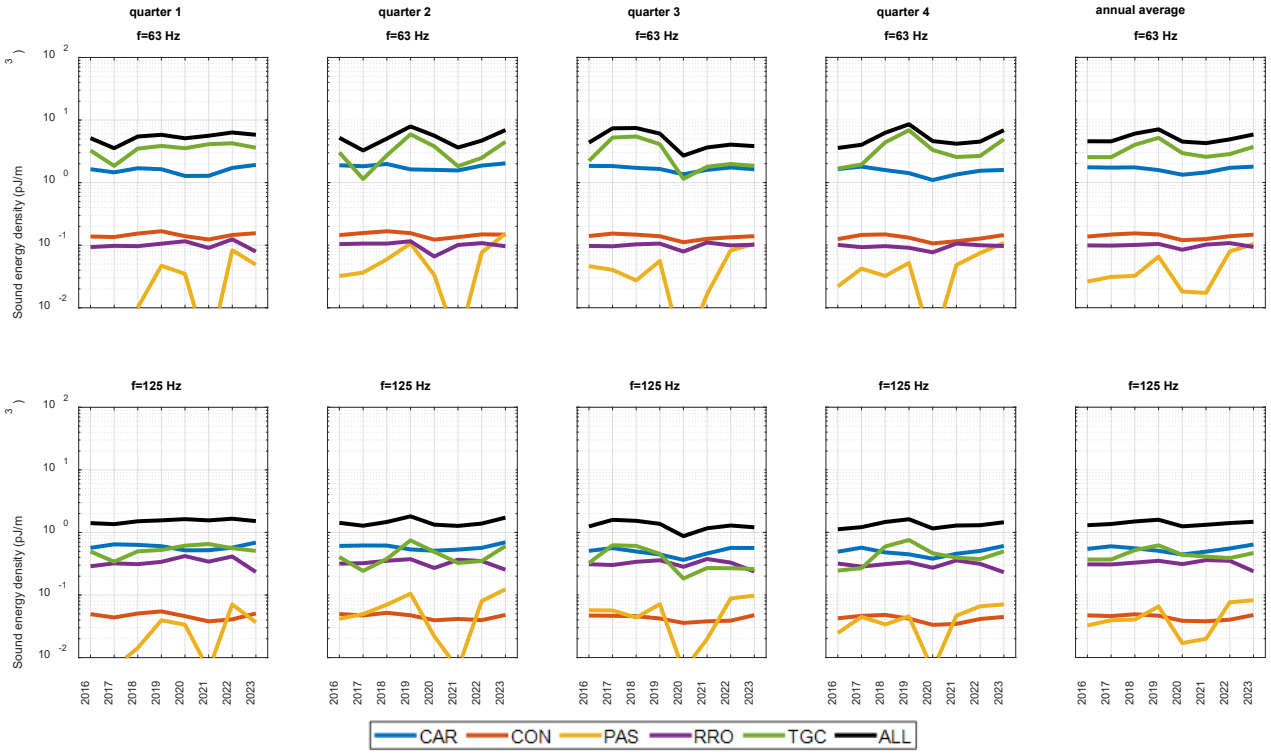

Figure 46 Sound energy density (in pJ/m^3) of different vessel categories for each quarter and year in the Northeast Atlantic Ocean. The top panel is for 63 Hz. The bottom panel is for 125 Hz.

Based on annually averaged sound energy density, at 63 Hz, the largest contribution to sound energy density is from the TGC vessel category, ranging from 55.8 to 73.2 %. The second-largest contribution is from the CAR vessel category, ranging from 22.3 to 38.4 %. The lowest contribution to sound energy density is from PAS vessels, ranging from 0.4 to 1.8 %. The contribution of RRO and CON vessels ranges from 1.87 to 2.4 % and 2.1 to 3.2 %, respectively.

At 125 Hz, the largest contributions come from the CAR vessel category (ranging from 31.9 to 44.0 %) and the TGC vessel category (ranging from 27.1 to 39.0 %), followed by RRO vessels (with contributions ranging from 16.2 to 24.9 %).

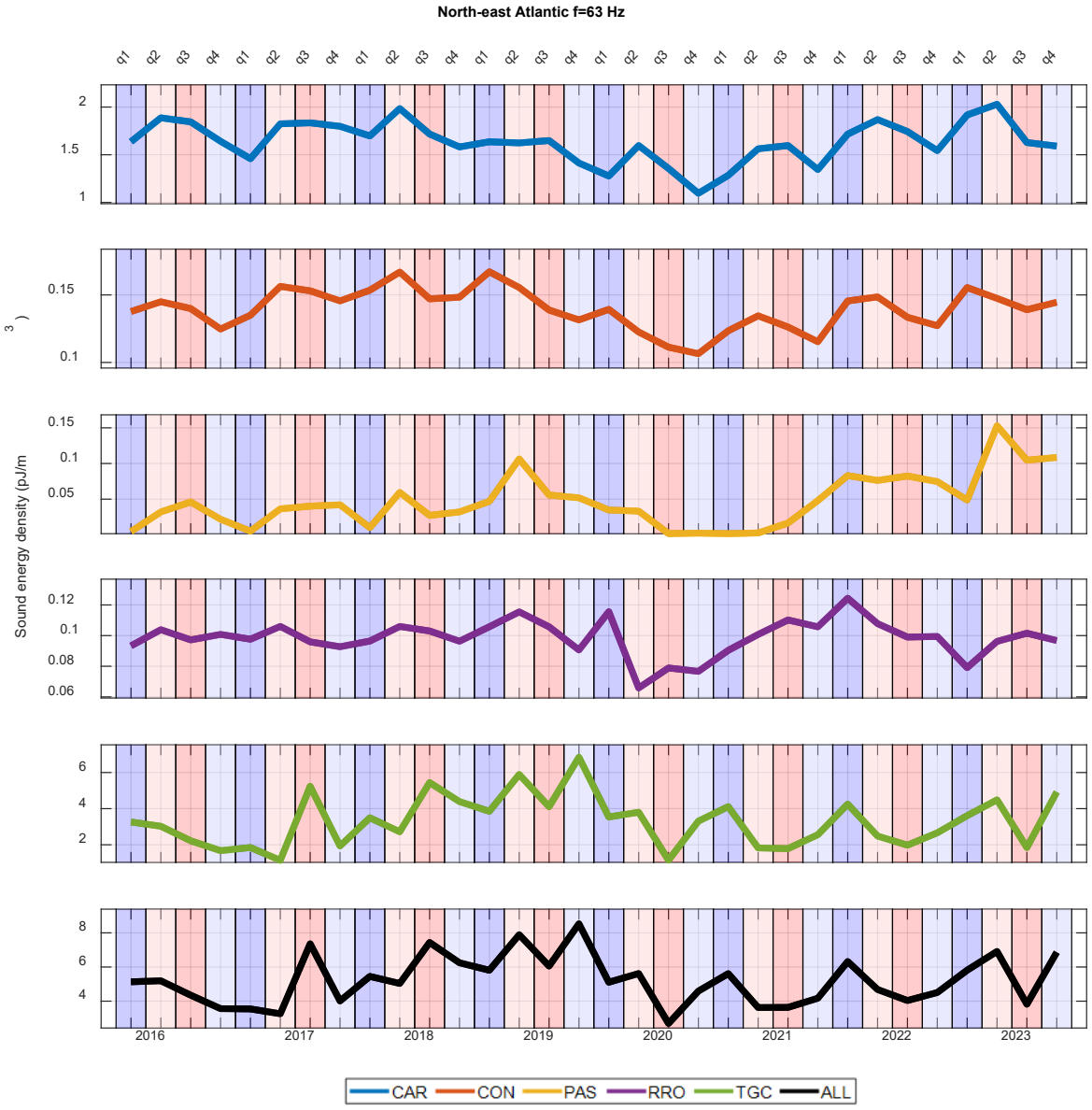

Figure 47 Sound energy density (in pJ/m^3) of different vessel categories in the northeast Atlantic Ocean for each quarter in chronological order at 63 Hz.

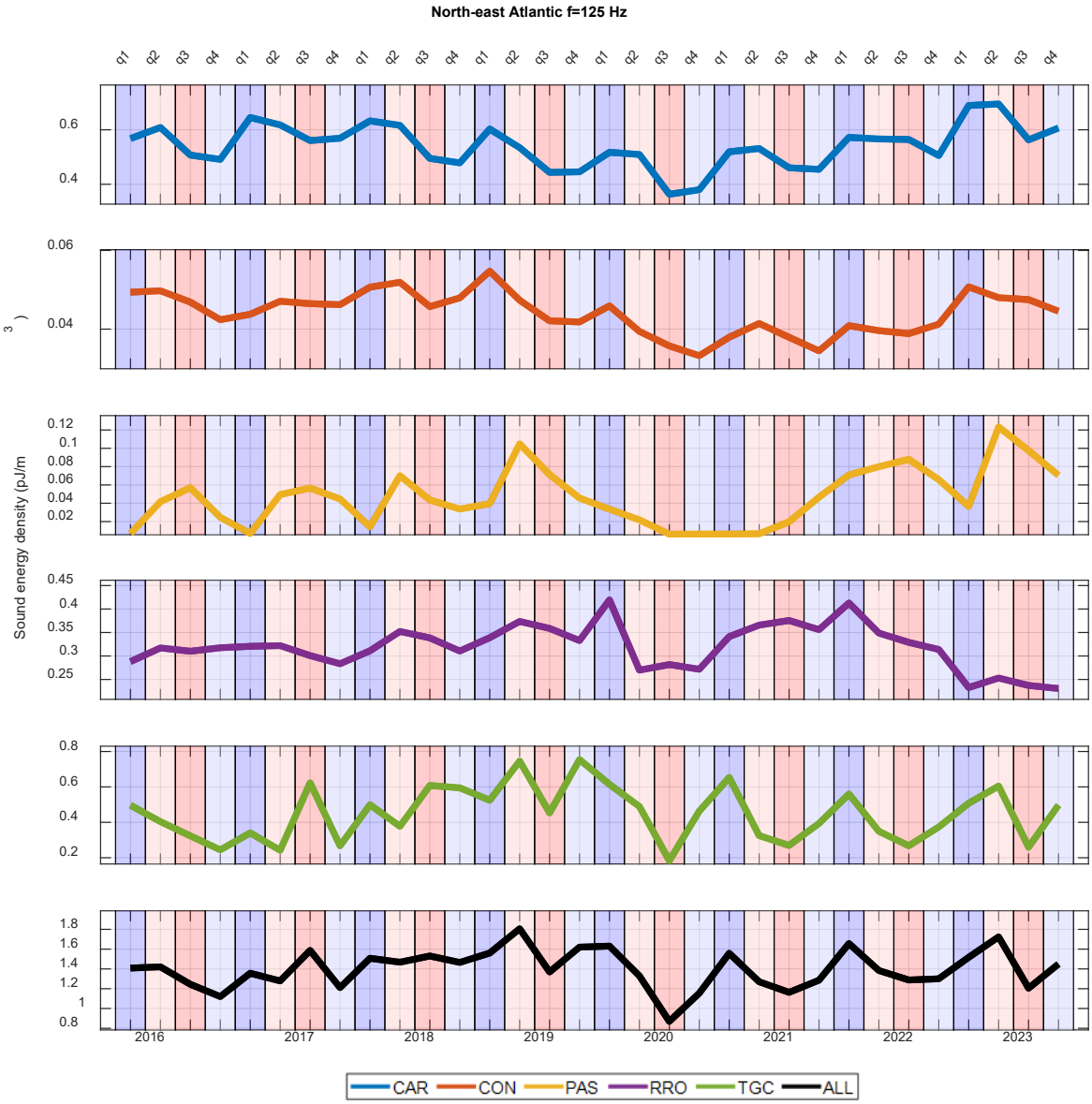

Figure 48 Sound energy density (in pJ/m^3) of different vessel categories in the northeast Atlantic Ocean for each quarter in chronological order at 125 Hz.

A strong decrease in PAS vessel category is noticeable from the second quarter of 2020 to the second quarter of 2021. A similar decrease is also visible in other vessel categories. This may be related to the COVID-19 pandemic. However, it is difficult to interpret for this region due to the lower AIS coverage during 2020, which is related to Brexit and changes in the EMSA data storage policy, as described in the discussion section.

The volume of the northeast Atlantic Ocean is the largest of all European maritime regions. The busy shipping lanes are only visible within some local regions connecting the North Sea and the Mediterranean Sea. Therefore, the sound energy density across the entire northeast Atlantic is low. However, certain local areas could have higher sound energy density.

3.1.2 Comparison of the Sound Energy Density between Different Regions

Figures 49 to 53 show the distribution of sound energy density between different regions for CAR, CON, PAS, RRO, and TGC categories, respectively.

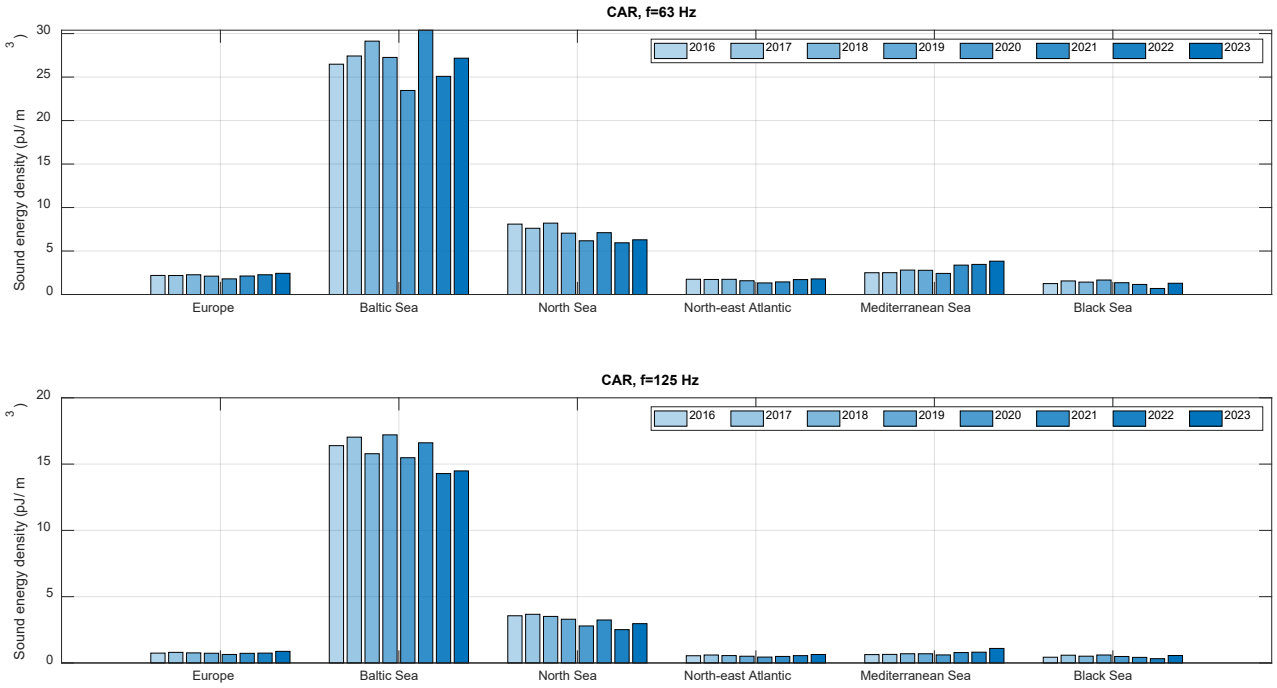

Figure 49 Sound energy density (in pJ/m^3) of CAR vessels in different regions at (top) 63 Hz and (bottom) 125 Hz.

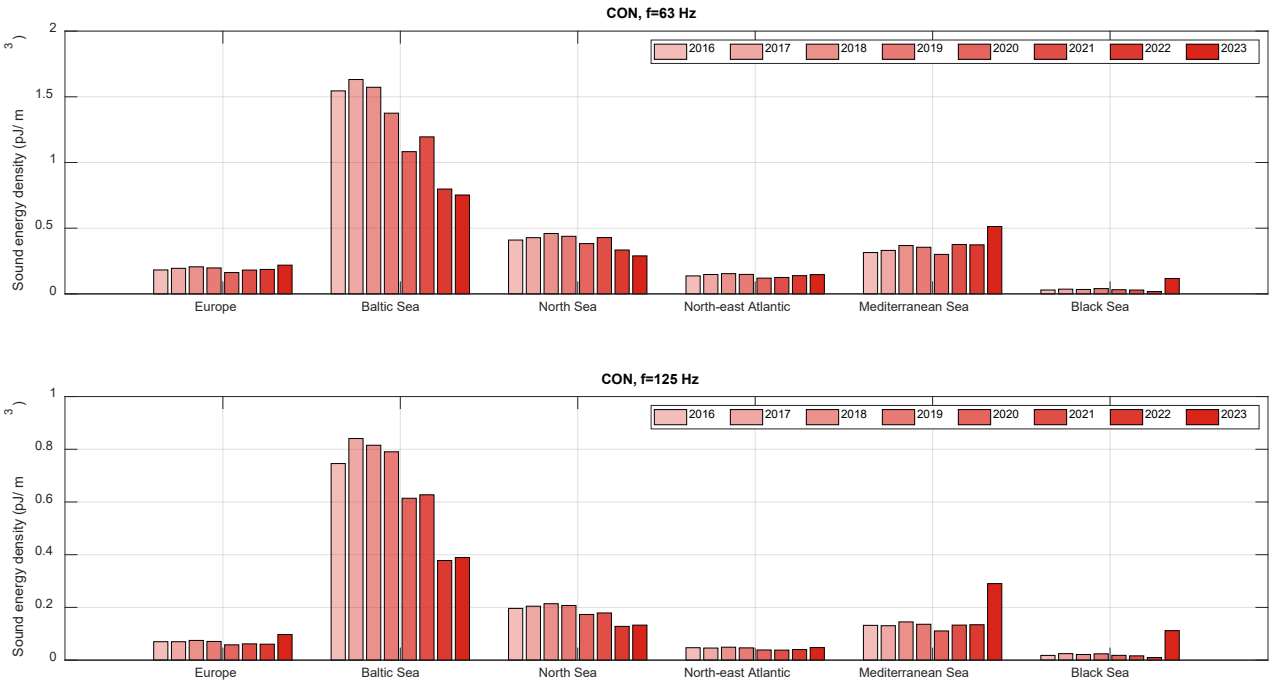

Figure 50 Sound energy density (in pJ/m^3) of CON vessels in different regions at (top) 63 Hz and (bottom) 125 Hz.

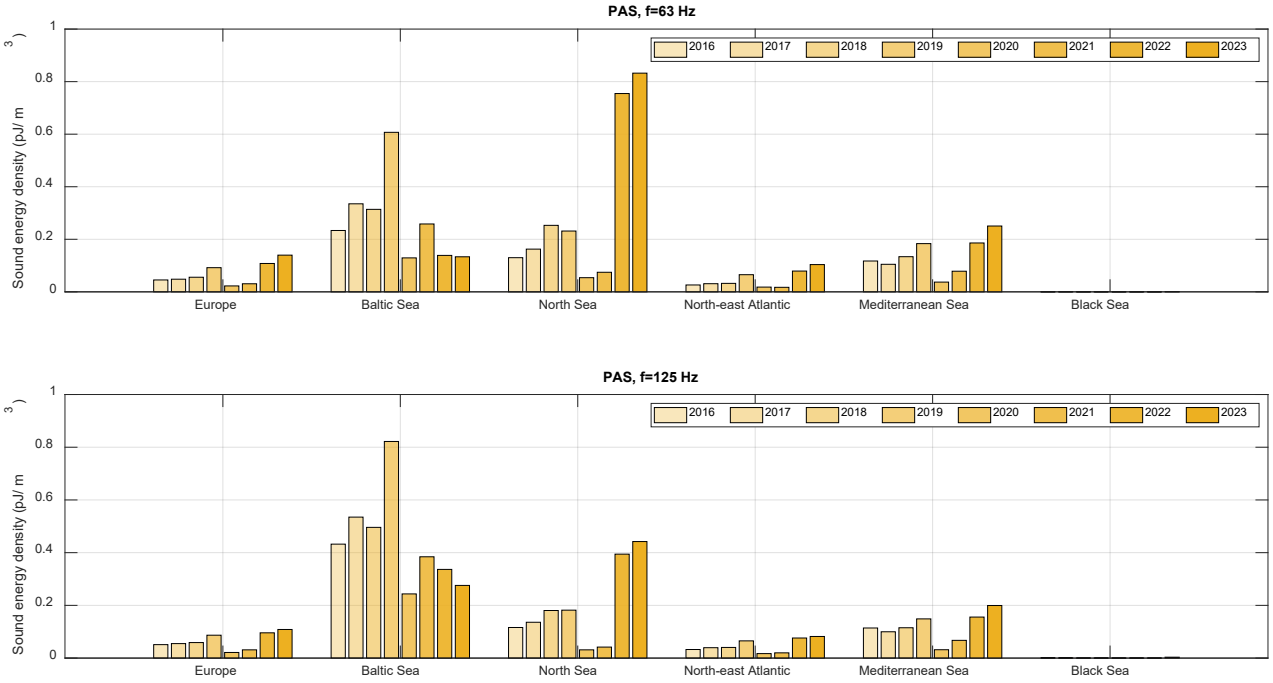

Figure 51 Sound energy density (in pJ/m^3) of PAS vessels in different regions at (top) 63 Hz and (bottom) 125 Hz.

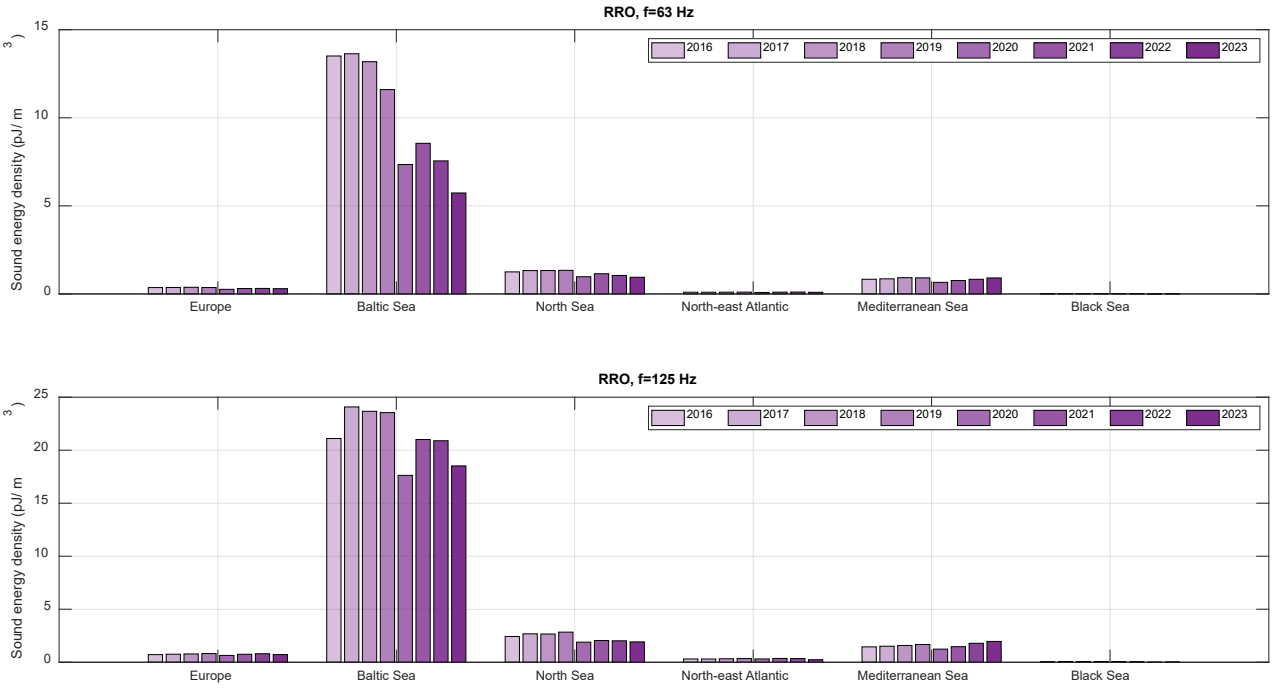

Figure 52 Sound energy density (in pJ/m^3) of RRO vessels in different regions at (top) 63 Hz and (bottom) 125 Hz.

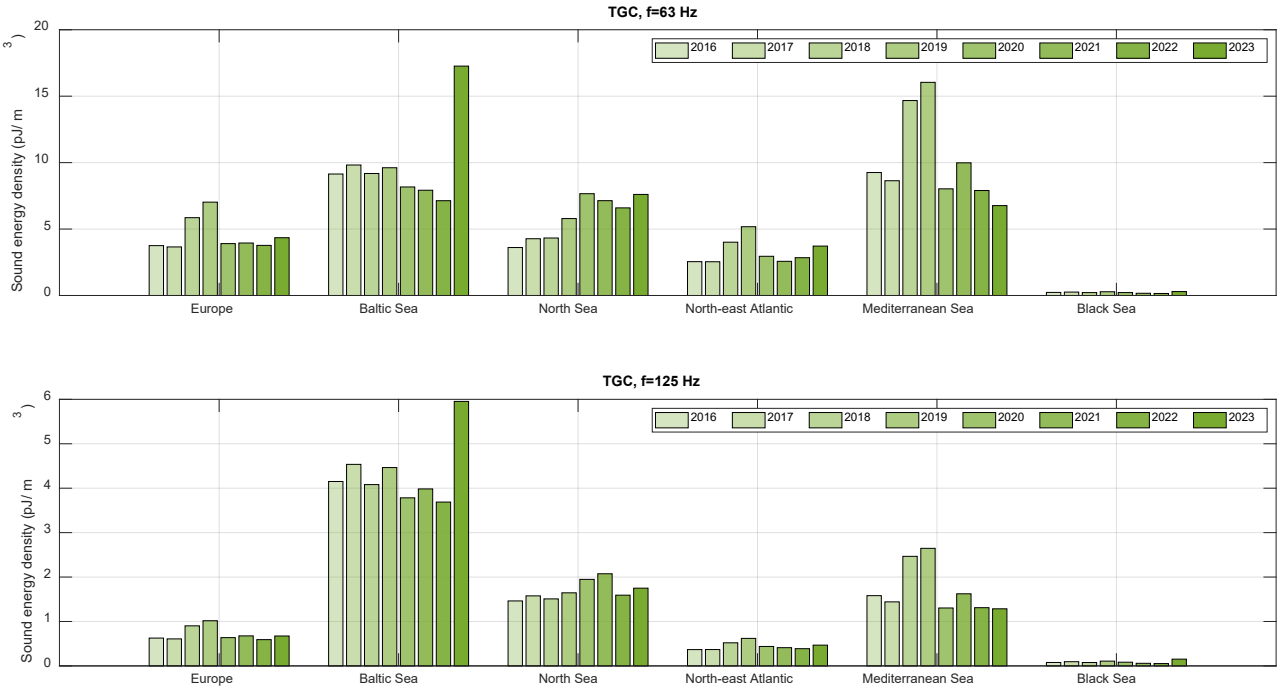

Figure 53 Sound energy density (in pJ/m^3) of TGC vessels in different regions at (top) 63 Hz and (bottom) 125 Hz.

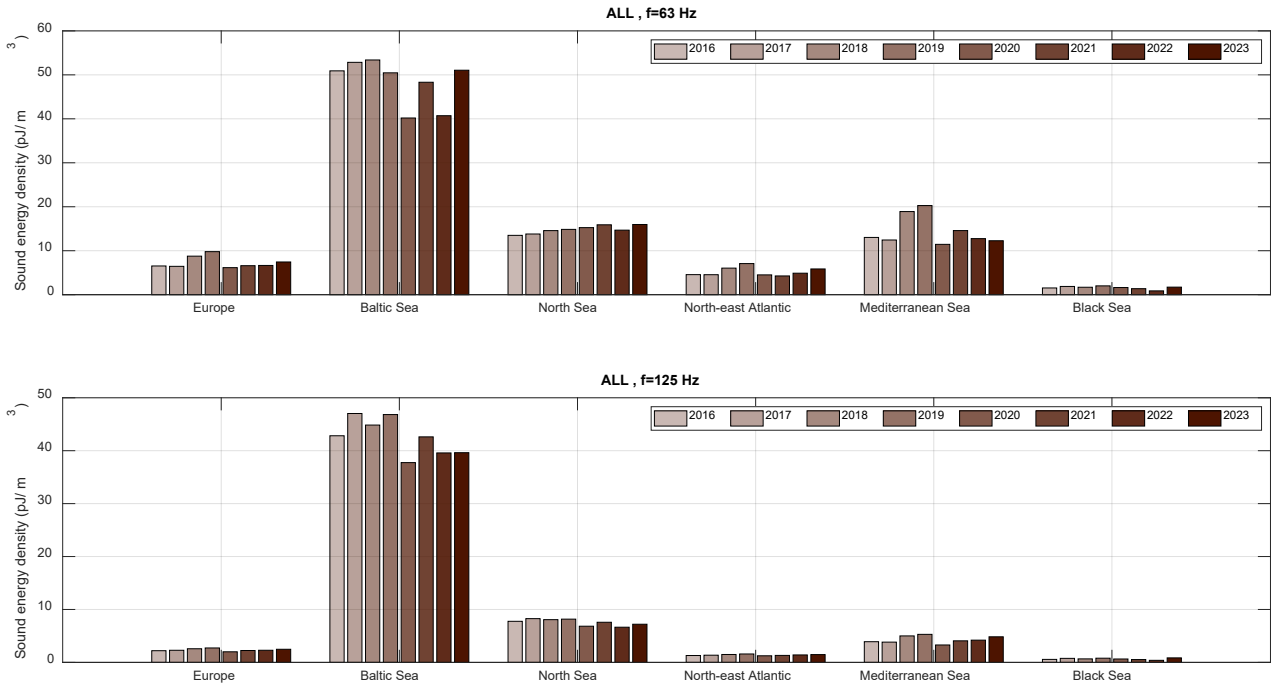

Figure 54 Sound energy density (in pJ/m^3) of ALL vessels in different regions at (top) 63 Hz and (bottom) 125 Hz.

The CAR, CON, and RRO vessel categories have the largest sound energy density in the Baltic Sea, followed by the North Sea and the Mediterranean Sea at both 63 and 125 Hz. The Black Sea has the lowest energy density for the CON vessel category. There is a decrease in the sound energy density of PAS vessels for all regions during 2020. Specifically, in the North Sea, the sound energy density appears to be increased 7–8 times at 63 Hz during 2022 and 2023 for the PAS vessel category (Figure 51). This increase may be related to better AIS data coverage. The sound energy density of TGC vessels is the highest in the Baltic Sea and the Mediterranean Sea at 63 Hz. However, at 125 Hz, the Baltic Sea has higher sound energy than the Mediterranean Sea for TGC vessels. For all vessels, the sound energy density is the highest in the Baltic Sea at both 63 and 125 Hz.

3.2 Forecast Map Layers

The calculations of forecast map layers and scenarios have been described in detail in MacGillivray et al. (2023b). Four different forecast scenarios (BAU, GHG, URN, and U&G) have been calculated for 2030, 2040, and 2050. The penetration rates and ship traffic volume changes are given for each scenario in Appendix F. To see the amount of noise reduction in more detail, the difference between the BAU sound map layers and the GHG, URN and U&G sound map layers are calculated with a narrower, diverging colour scale. Consequently, the changes in SPL for each forecast scenario can be seen more clearly for the selected years. Figure 55 shows the difference map layers of all NAVISON regions between BAU and the GHG, URN and U&G forecast scenarios.

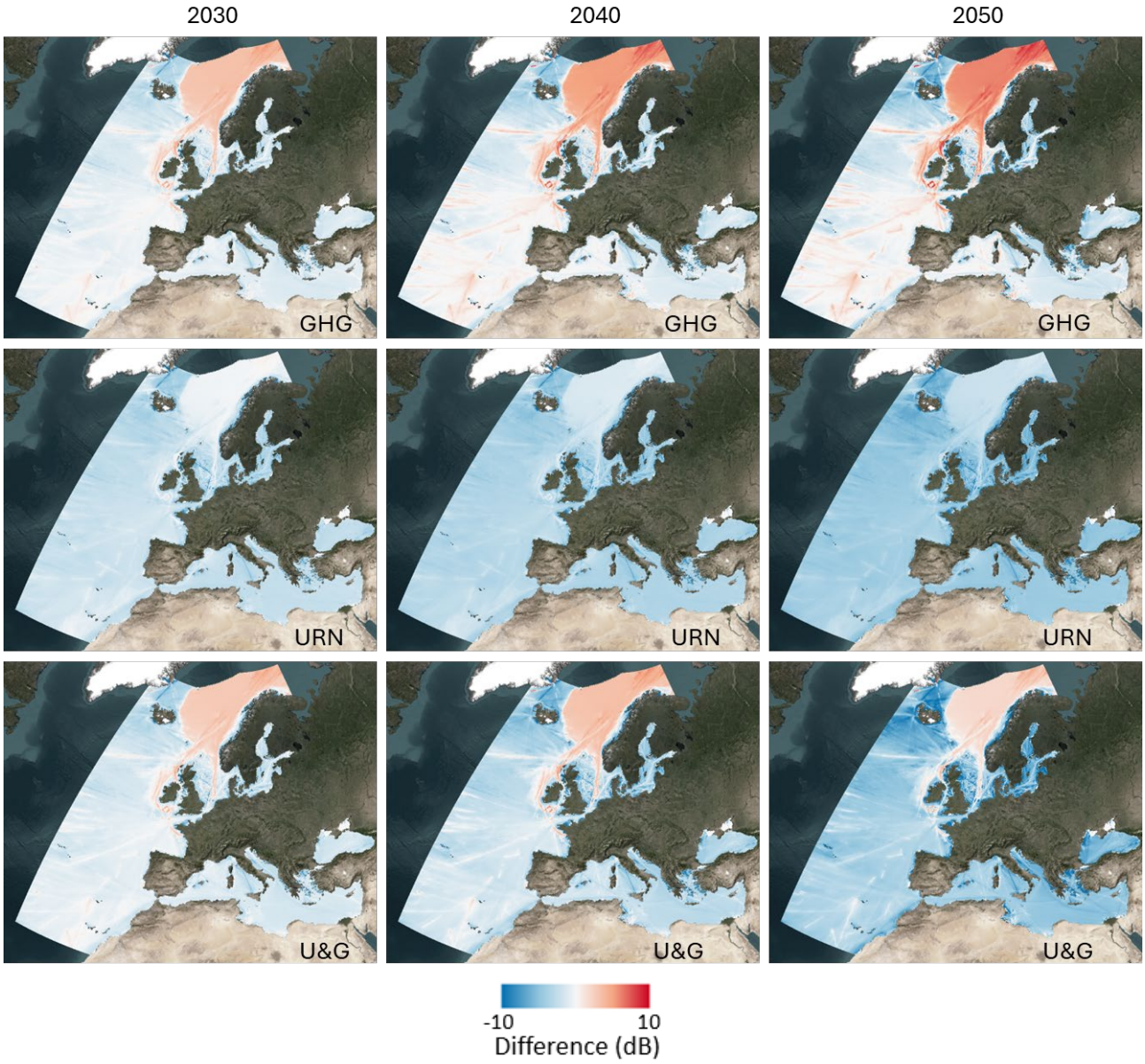

Figure 55 Difference in SPL (dB) including all vessel categories between BAU and (top) GHG, (middle) URN, and (bottom) U&G scenarios. These maps are produced for (left) 2030, (middle) 2040, and (right) 2050 at 63 Hz.

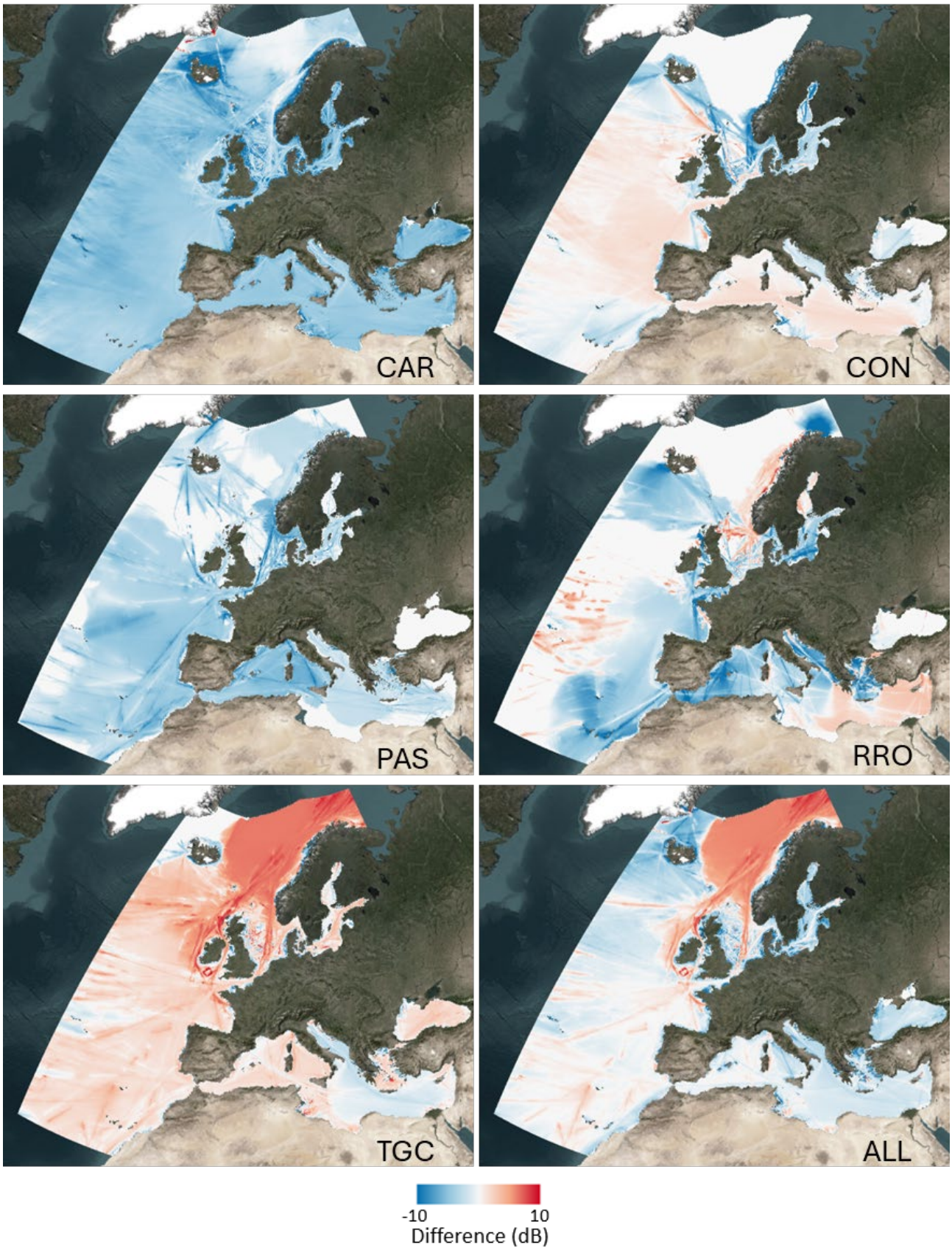

Figure 56 Difference in SPL (dB) for different vessel categories between BAU and GHG scenarios. The sound map layers are annually averaged for 2050 at 63 Hz.

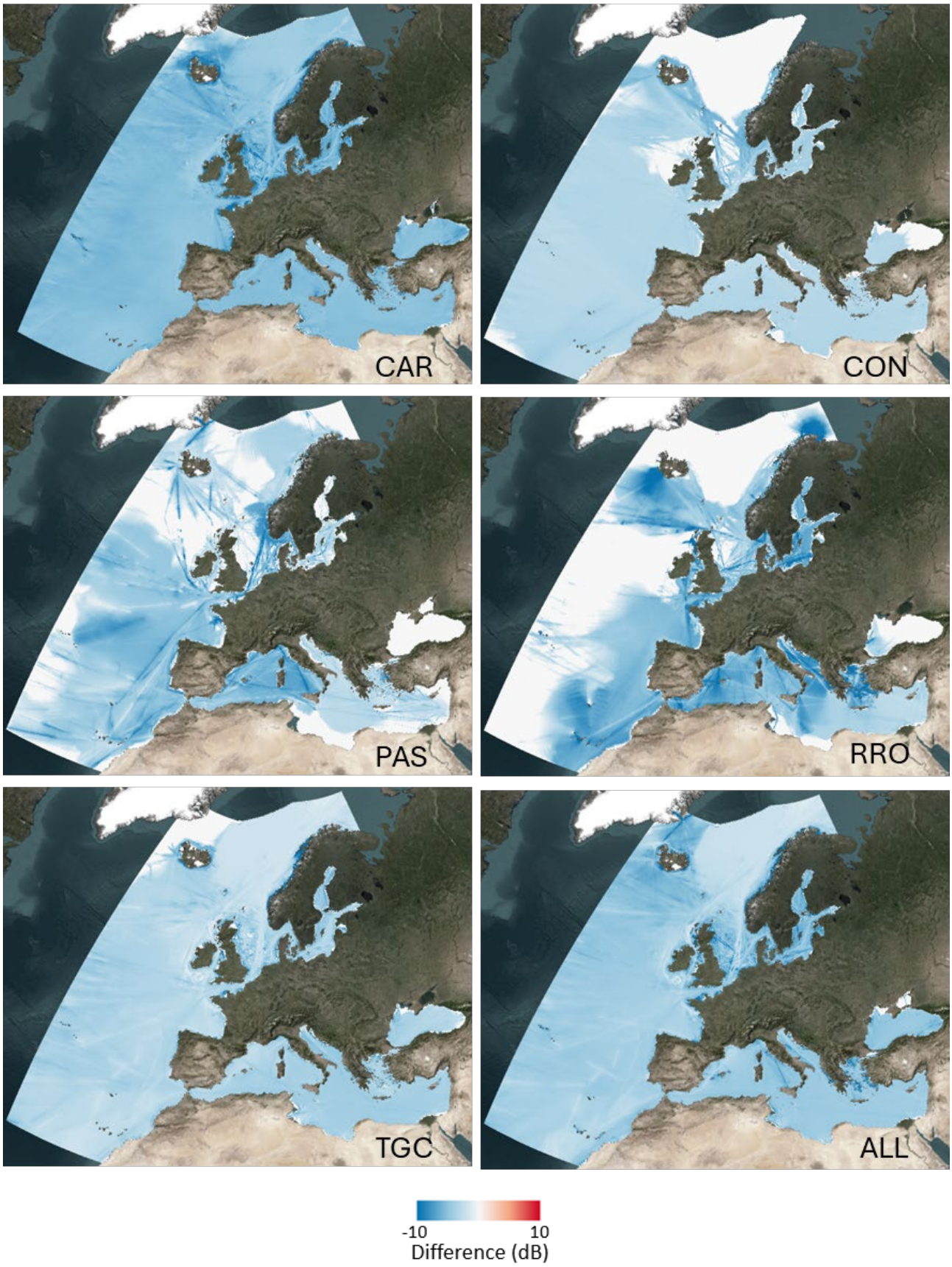

Figure 57 Difference in SPL (dB) for different vessel categories between BAU and URN scenarios. The sound map layers are annually averaged for 2050 at 63 Hz.

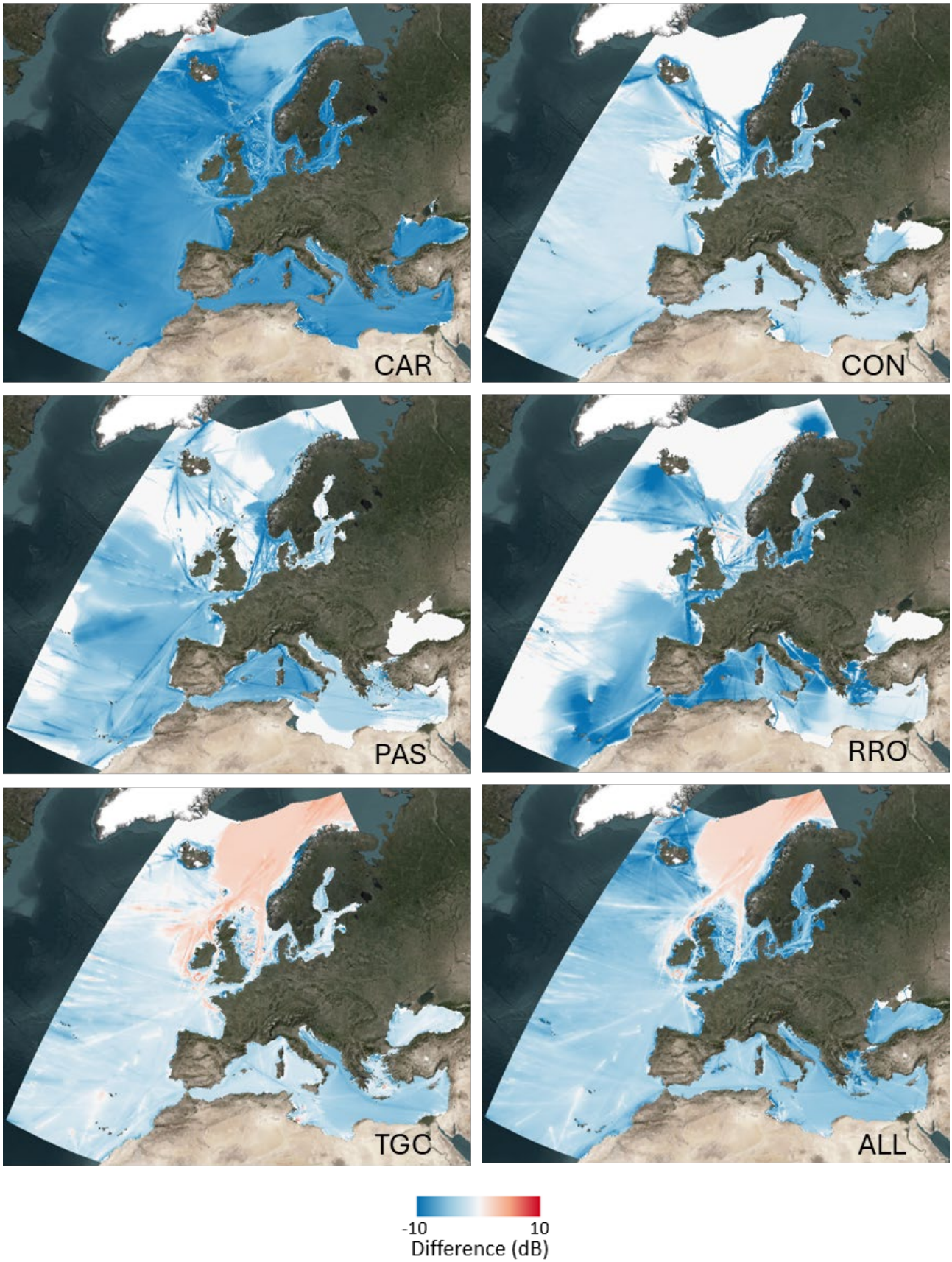

Figure 58 Difference in SPL (dB) for different vessel categories between BAU and U&G scenarios. The sound map layers are annually averaged for 2050 at 63 Hz.

3.2.1 Analysis for the Mitigation for Each Forecast Scenarios

In this section, sound energy density for each forecast scenario is analysed for different years and vessel categories. The analysis is performed individually for each region and all Europe.

Sound energy density can be used to compare the business as usual (BAU) and forecast scenarios based on different mitigation measures. For example, the percentage change compared to the BAU can be calculated for each forecast scenario based on the following formula:

$$\text{Percentage change} = 100\ \% \times \left(\frac{\mathrm{E}_{\mathrm{V}_{\mathrm{GHG,URN,U\&G}}} - \mathrm{E}_{\mathrm{V}_{\mathrm{BAU}}}}{\mathrm{E}_{\mathrm{V}_{\mathrm{BAU}}}} \right)$$

where $\mathrm{E}_{\mathrm{V}_{\mathrm{GHG,URN,U\&G}}}$ is the sound energy density for the selected forecast scenario (GHG, URN, or U&G), and $\mathrm{E}_{\mathrm{V}_{\mathrm{BAU}}}$ is the sound energy density for the BAU forecast scenario. This percentage change can be used to quantify the total noise reduction associated with each forecast scenario.

It should be noted that the performance of mitigation measures is also dependent on the frequency due to the ship-specific properties of the source level. The provided results in this section are valid for the 63 Hz decidecade frequency band. If similar computations are repeated for another frequency band, different percentage changes and temporal variations could be observed.

3.2.1.1 Europe

Figure 59 shows sound energy density calculations for BAU, GHG, URN, and U&G forecast scenarios for the baseline year (2022) and forecast years (2030, 2040, and 2050) in all European regions.

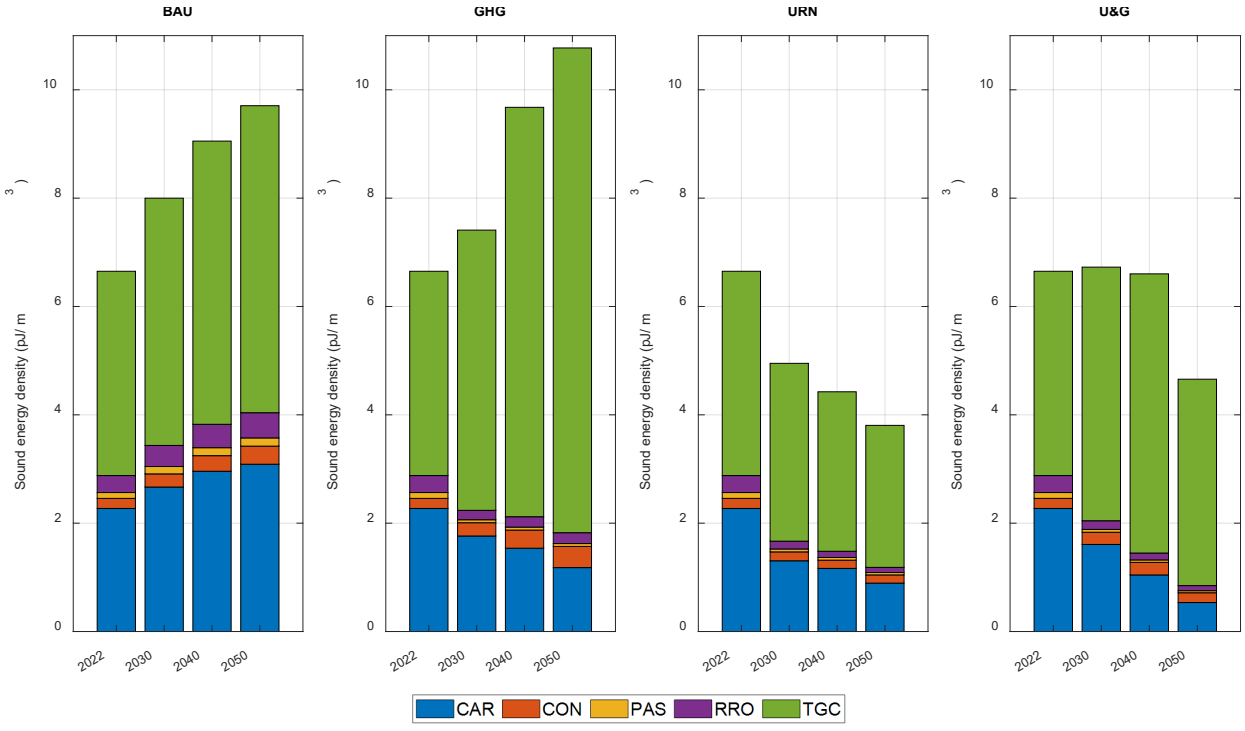

Figure 59 Sound energy density categorised for the different years at 63 Hz. (Europe)

Figure 60 shows the mitigation performance of each vessel category as quantified based on the percentage changes relative to the BAU scenario in the sound energy density for each category in Europe.

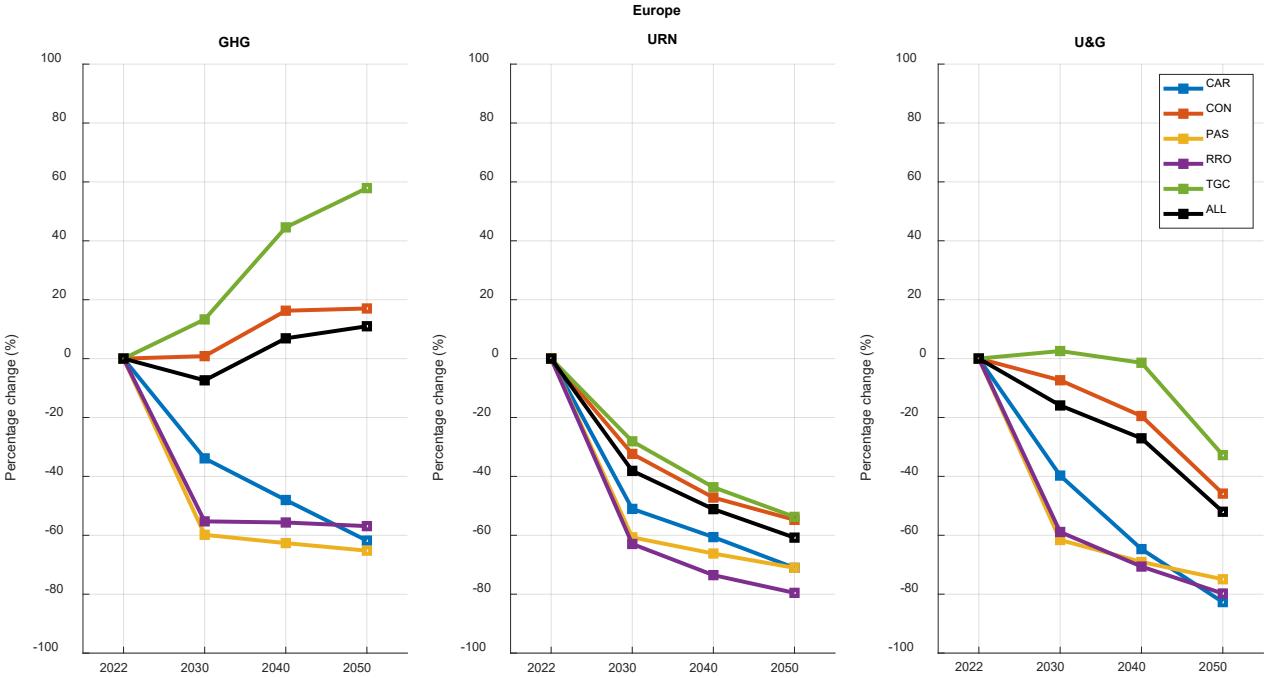

Figure 60 Percentage change in the sound energy density compared to the BAU scenario at 63 Hz. (Europe)

For GHG scenarios, sound energy density increases for TGC (13.3 % in 2030 and 57.9 % in 2050) and CON (0.9 % in 2030 and 17.0 % in 2050) vessel categories comparing to the BAU scenario. This could be related to increasing sound levels after applying the most efficient propeller measure (MEP), as described in the previous sections. When all vessel categories are considered, the sound energy density decreases comparing to the BAU scenario by 7.4 % in 2030, increases by 6.9 % in 2040, and 11.0 % in 2050. The largest declines comparing to the BAU scenario are observed for PAS (59.8 % in 2030 and 65.2 % in 2050) vessel categories, followed by RRO (55.3 and 56.9 %) and CAR (33.9 and 61.8 %).

For URN scenarios, the sound energy density comparing to BAU scenario decreases for all forecast scenarios. For the scenario including the contribution of all vessel categories, the decline comparing to the BAU scenario is 38.1 % in 2030 and 60.8 % in 2050. The largest decline comparing to the BAU scenario is observed in the RRO vessel category, ranging from 63.0 % in 2030 to 79.6 % in 2040.

For U&G scenarios, the sound energy density of TGC vessels increases comparing to the BAU scenario by 2.6 % in 2030 and decreases by 1.4 % in 2040 and 32.8 % in 2050. For the scenario including all vessel categories, the sound energy density declines comparing to the BAU scenario by 15.9 % in 2030 and 52.0 % in 2050. The decline is observed for PAS (61.6 % in 2030 and 74.9 % in 2050), CAR (39.7 % in 2030 and 82.7 % in 2050) and RRO (58.9 % in 2030 and 79.8 % in 2050).

3.2.1.2 Baltic Sea

Figure 61 shows sound energy density for BAU, GHG, URN, and U&G forecast scenarios during different years in the Baltic Sea. In these comparisons, the sound energy for the baseline year (2022) without any mitigation measure is also included. The time variation of sound energy density can be seen from these bars, which are calculated for 2030, 2040, and 2050.

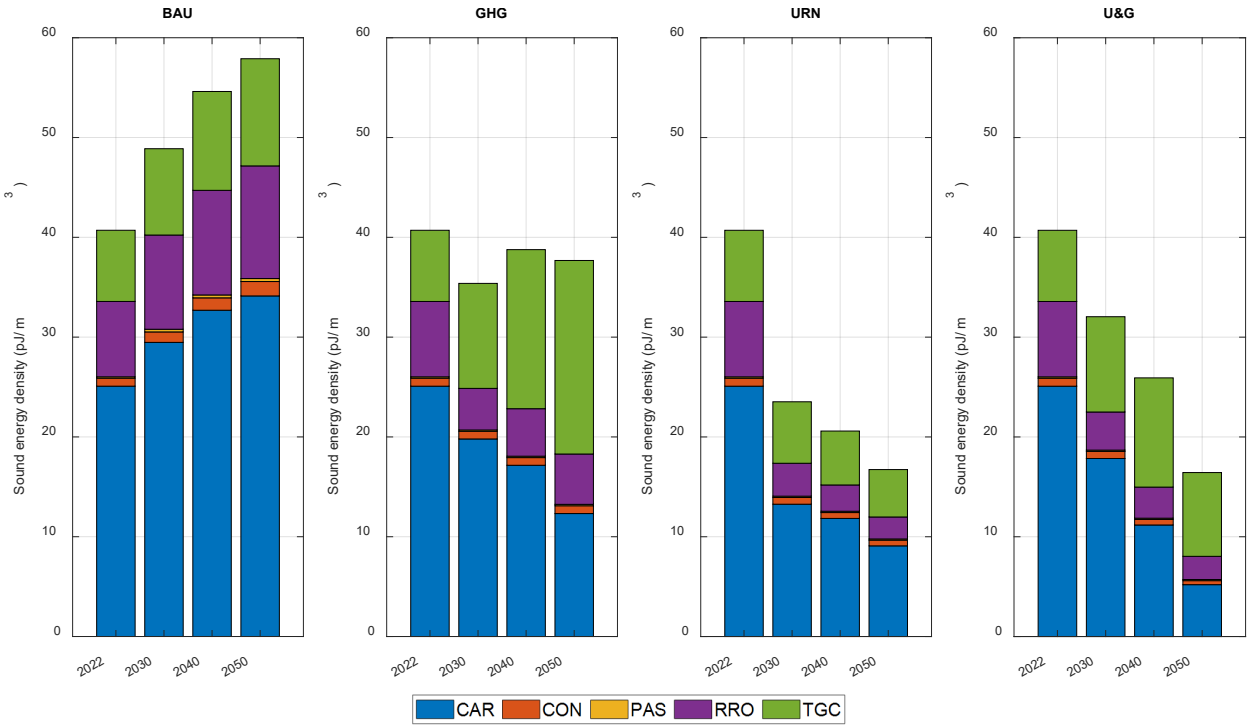

Figure 61 Sound energy density categorised for the different years at 63 Hz. (Baltic Sea)

Figure 62 shows the sound energy density of each vessel category when the different mitigation measures (for machinery and cavitation components) are applied with 100 % penetration at 63 Hz.

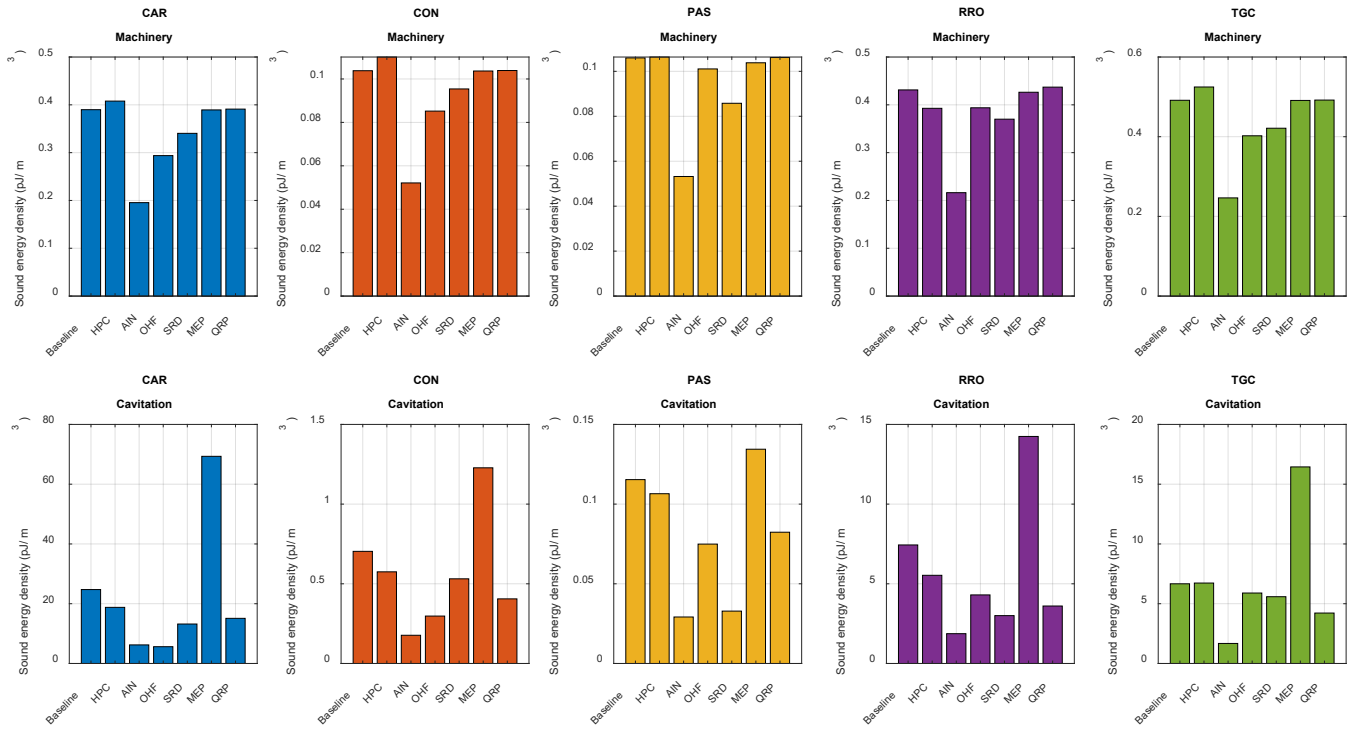

Figure 62 Sound energy density for the 100 % penetration rates for each mitigation measure at 63 Hz in Baltic Sea. Sound energy density is calculated for (top) machinery and (bottom) cavitation components.

Based on the comparisons in Figure 62, the contribution of the machinery component to sound energy density is less than the contribution of cavitation components. Comparing to the sound energy density of baseline scenarios, it is noticeable that some mitigation measures can result in larger sound energy density (i.e., Most Efficient Propeller). To quantify the changes relative to the sound energy density of the baseline scenario for each case, the percentage changes for the mitigation measures applied with a 100 % penetration rate are shown in Figure 63.

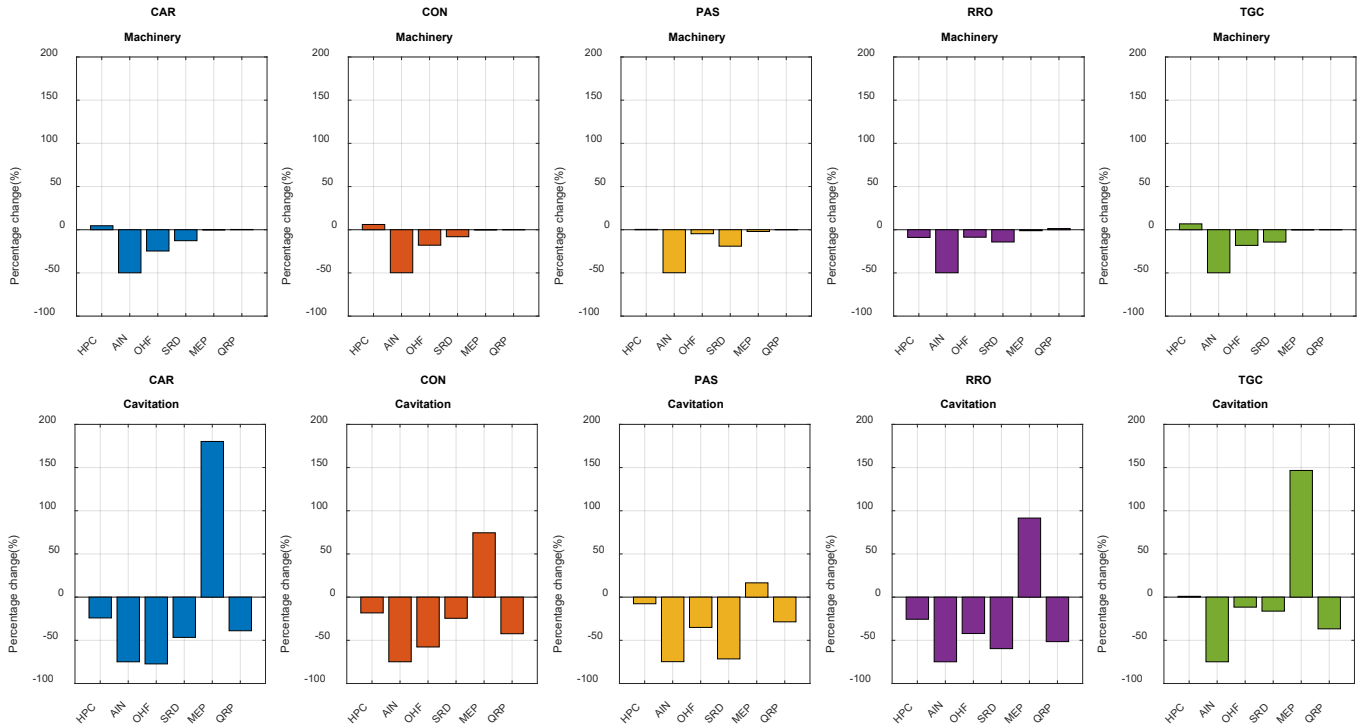

Figure 63 Percentage change in the sound energy density for (top) machinery and (bottom) cavitation components compared to the BAU scenario at 63 Hz. (Baltic Sea)

Based on these results, interpretations on the effect of each measure can be made to better understand the changes in the forecast scenarios. The sound energy density for MEP increased most for CAR and TGC vessel categories, followed by RRO, CON, and PAS. The mitigation measure for HPC has the greatest impact on RRO, followed by CAR, CON, and PAS while AIN affects all categories similarly. OHF influences CAR the most, followed by CON, RRO, PAS, and TGC. SRD has the highest impact on PAS, then RRO, CAR, CON, and TGC. QRP affects RRO the most, followed by CON, CAR, TGC, and PAS.

Large differences in trends for TGC compared to other ship types can be attributed to the observations above that several mitigation measures are less effective for this specific ship type. In combination with the modelled increases in source levels for the MEP measure, this can lead to either smaller reductions or even increases in sound energy density for TGC compared to other ship types, depending on the forecast scenario and year.

The forecast scenarios are constructed by combining the mitigation measures with different penetration rates, as outlined in Appendix F. Similar to the previous graph, Figure 61 is also reproduced by calculating the percentage change relative to BAU scenarios as shown in Figure 64. Representing sound energy density results in this manner can provide more detailed insights into the mitigation performances and temporal variations for individual vessel categories.

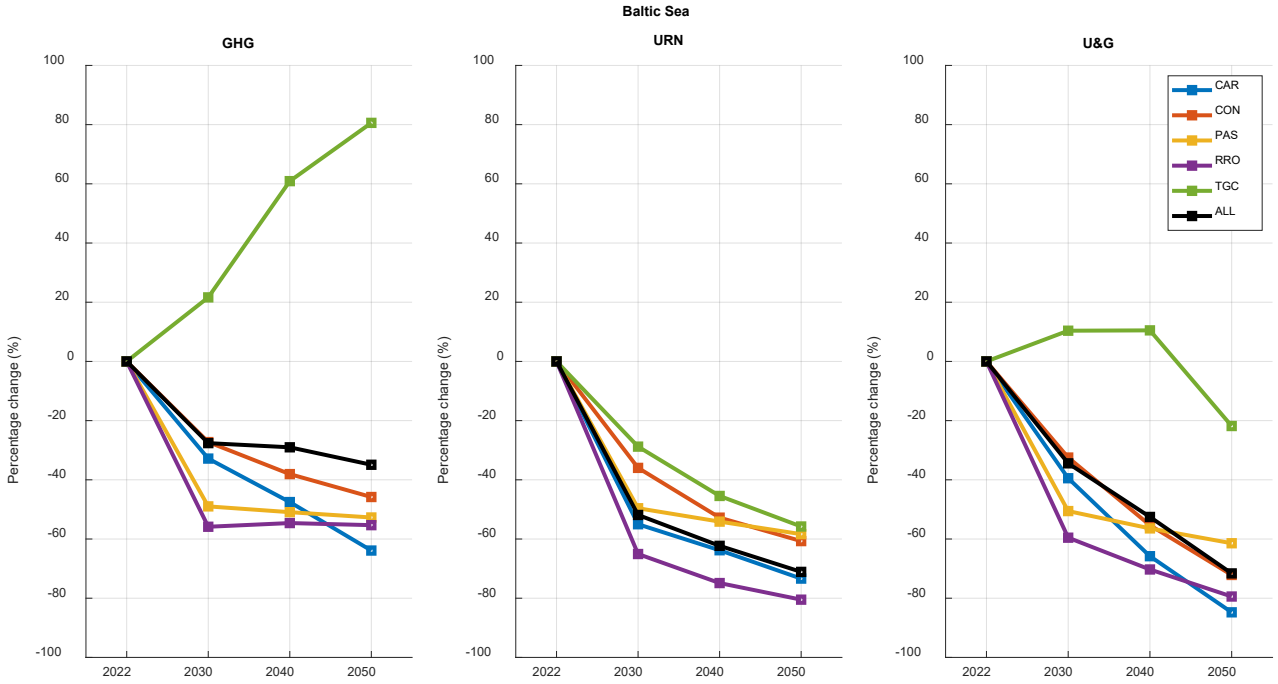

Figure 64 Percentage change in the sound energy density compared to the BAU scenario at 63 Hz. (Baltic Sea)

Based on these comparisons for different years, the sound energy density is decreasing for all scenarios when all vessel categories are included. However, the effectiveness of mitigation measures and the gradient of the temporal trend differ for individual vessel categories. The lowest mitigation performance has been observed for TGC vessels across all scenarios.

For GHG scenarios, the decrease in sound energy density ranges between 27.6 % in 2030 and 34.9 % in 2050 when all vessel categories are considered. The sound energy density of TGC vessels at 63 Hz is expected to increase by up to 80.6 % in 2050.

For URN scenarios, sound energy density decreases for all vessel categories. The highest decrease is observed for RRO (65.1 % in 2030 and 80.5 % in 2050) vessels, followed by CAR (55.0 % in 2030 and 73.4 % in 2050) vessels.

For U&G scenarios, a decrease in sound energy density is observed for all vessel categories except for TGC vessels in 2030 and 2040. The highest declines in sound energy density are observed for RRO vessels (59.6 % in 2030 and 70.3 % in 2040), and for CAR (84.8 % in 2050) vessels. The performance of mitigation measures has different effects each region for the selected vessel categories. These differences are likely attributable to broad differences in vessel design, loading, and transit speed between regions.

3.2.1.3 Black Sea

Sound energy density calculations for BAU, GHG, URN and U&G forecast scenarios are shown in Figure 65 for the baseline year (2022) and forecast years (2030, 2040, and 2050) in the Black Sea.

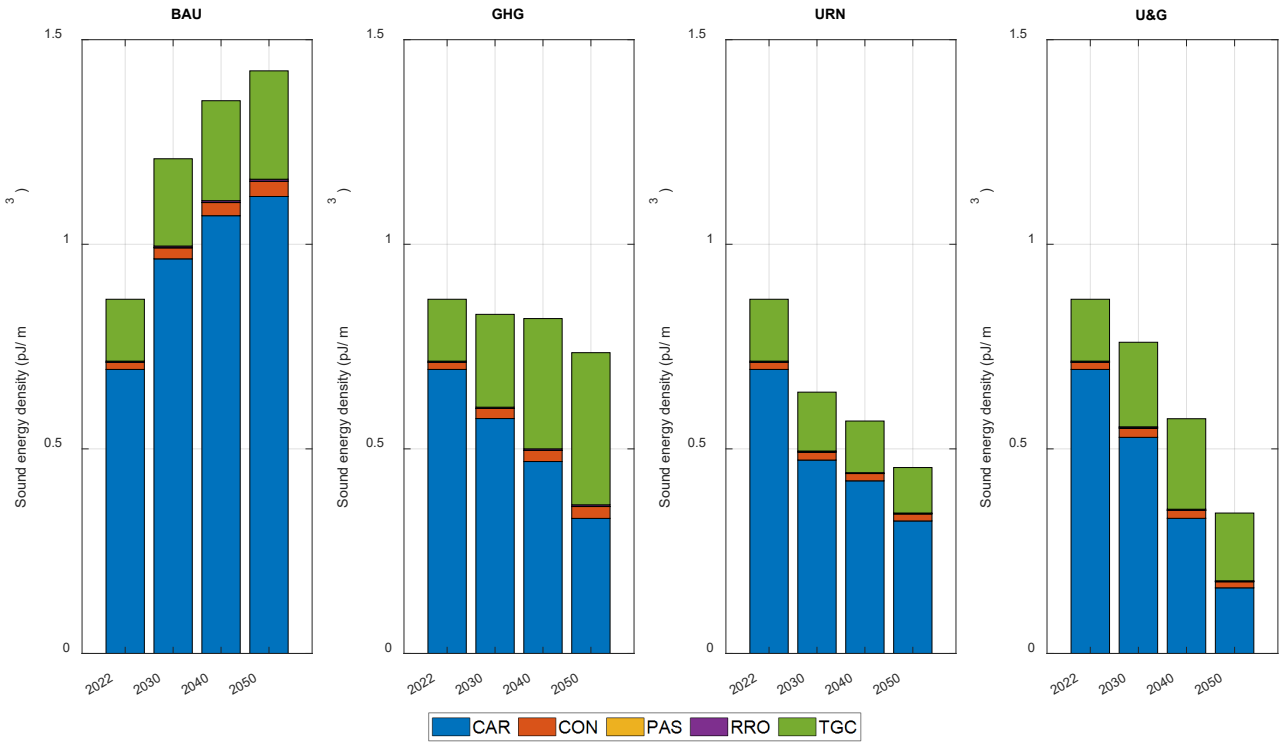

Figure 65 Sound energy density categorised for the different years at 63 Hz. (Black Sea)

The largest contributor of sound energy density in the Black Sea is CAR vessel category. Therefore, although the increase in TGC vessel category for GHG scenarios, the total sound energy density decreased for all forecast years.

Following the same structure as in the previous section, Figures 66 and 67 show the sound energy density of each vessel category when the different mitigation measures are applied with 100 % penetration at 63 Hz.

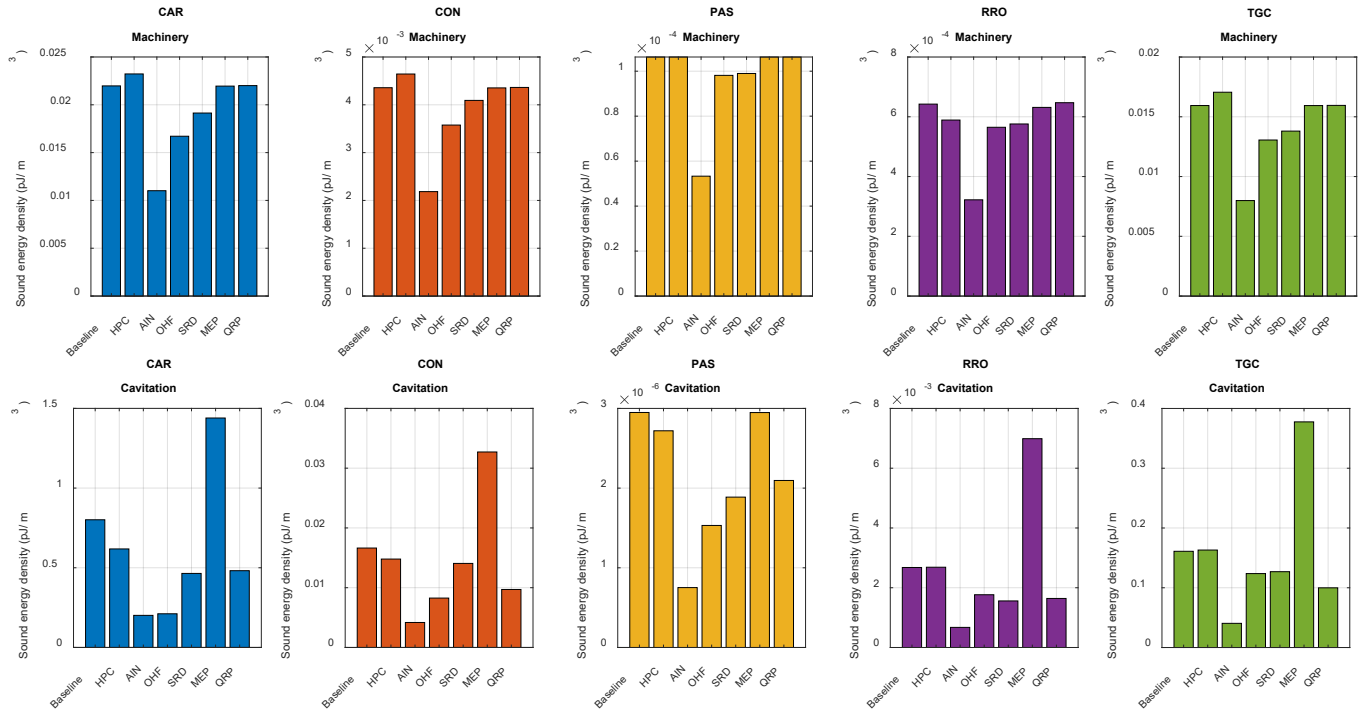

Figure 66 Sound energy density for the 100 % penetration rates for each mitigation measure at 63 Hz in Black Sea. Sound energy density is calculated for (top) machinery and (bottom) cavitation components.

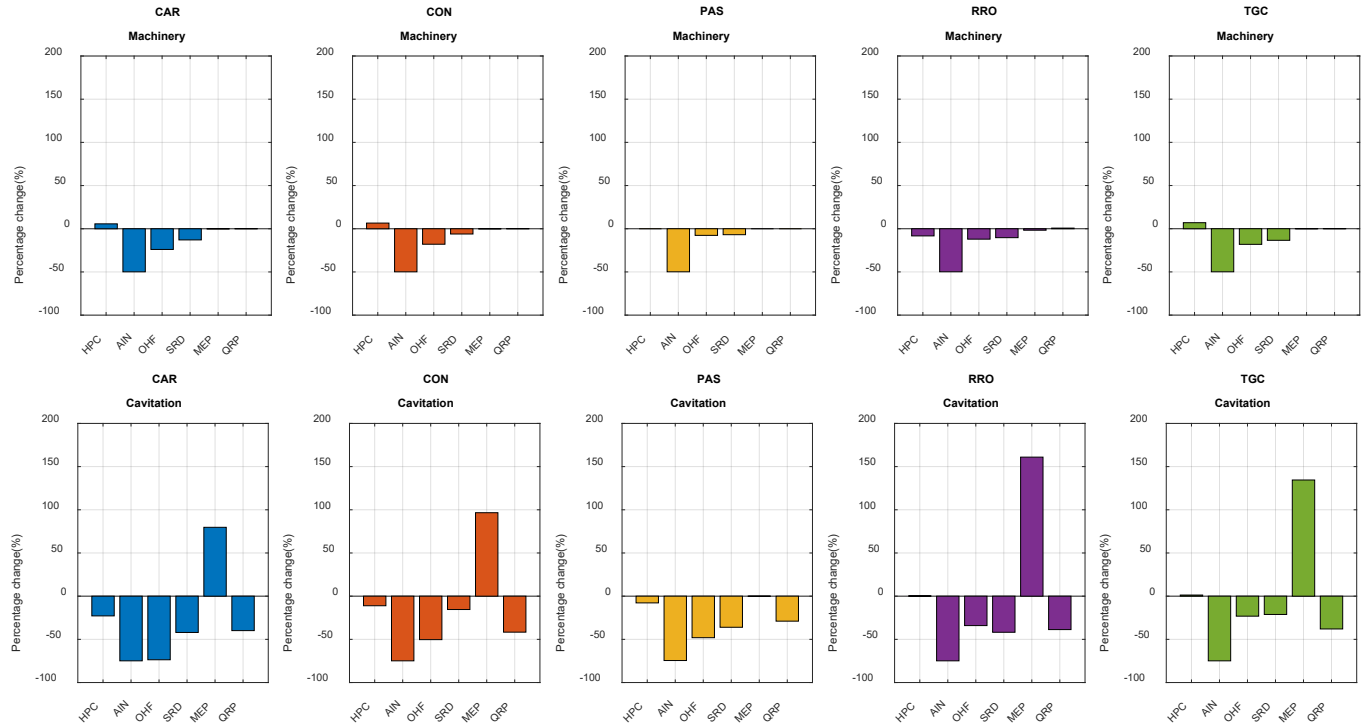

Figure 67 Percentage change in the sound energy density for (top) machinery and (bottom) cavitation components compared to the BAU scenario at 63 Hz (Black Sea).

For these comparisons, the MEP measure again leads to larger sound energy density than the baseline case for some categories. After combining the mitigation measures with different penetration rates for each mitigation scenario, the effect of these changes could be observed differently for each vessel category.

For more detailed analysis, the percentage change of sound energy density for each vessel category at 63 Hz is shown in Figure 68. It should be noted that the mitigation performances can be different at other frequencies.

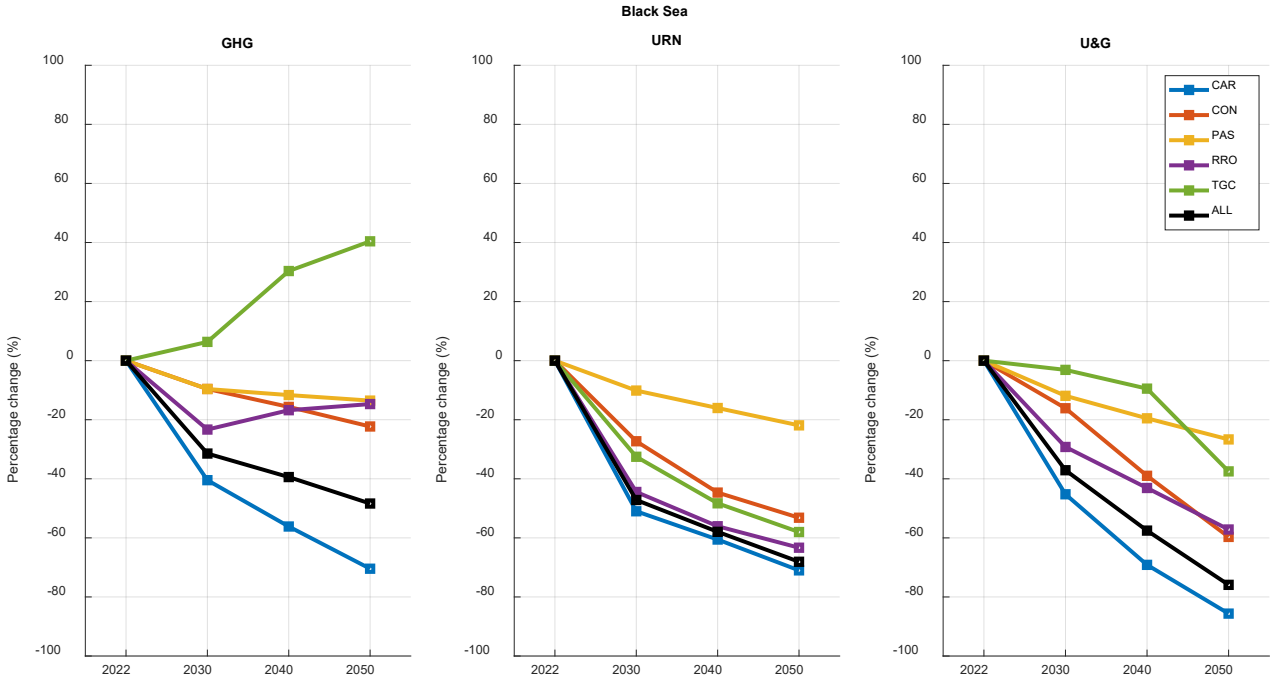

Figure 68 Percentage change in the sound energy density compared to the BAU scenario at 63 Hz. (Black Sea)

Except for the TGC vessel category in the GHG scenarios, sound energy density decreased across all forecast scenarios and vessel categories. In the GHG scenarios, the sound energy density for the TGC vessel category increases by up to 40.4 % by 2050. The PAS and CON vessel categories show the lowest reductions in sound energy density. For RRO vessels, the decrease in 2030 is greater than the decrease in 2050. The largest percentage decrease is seen in the CAR vessel category, varying between 40.5 % (2030) and 70.4 % (2050). When all vessel categories are considered, there is a decrease in sound energy density of 31.5 % in 2030 and 48.4 % in 2050.

For URN scenarios, sound energy density declines in all vessel categories. The smallest decrease occurs in PAS vessels, with reductions of 10.1 % in 2030 and 21.9 % in 2050. The largest decrease is observed in CAR vessels, ranging from 52 % (2030) to 71 % (2050). Overall, when all vessels are considered, the decrease ranges from 47.2 % (2030) to 68.1 % (2050).

For U&G scenarios, the TGC vessels show the smallest decrease in sound energy density in 2030 and 2040, while PAS vessels show the smallest decrease in 2050. The CAR vessels again exhibit the largest decrease. When all vessel categories are included, the decrease is 37.1 % in 2030 and 75.9 % in 2050.

3.2.1.4 Mediterranean Sea

Sound energy density comparisons for BAU, GHG, URN and U&G forecast scenarios are shown in Figure 69 for the baseline year (2022) and forecast years (2030, 2040, and 2050) in the Mediterranean Sea.

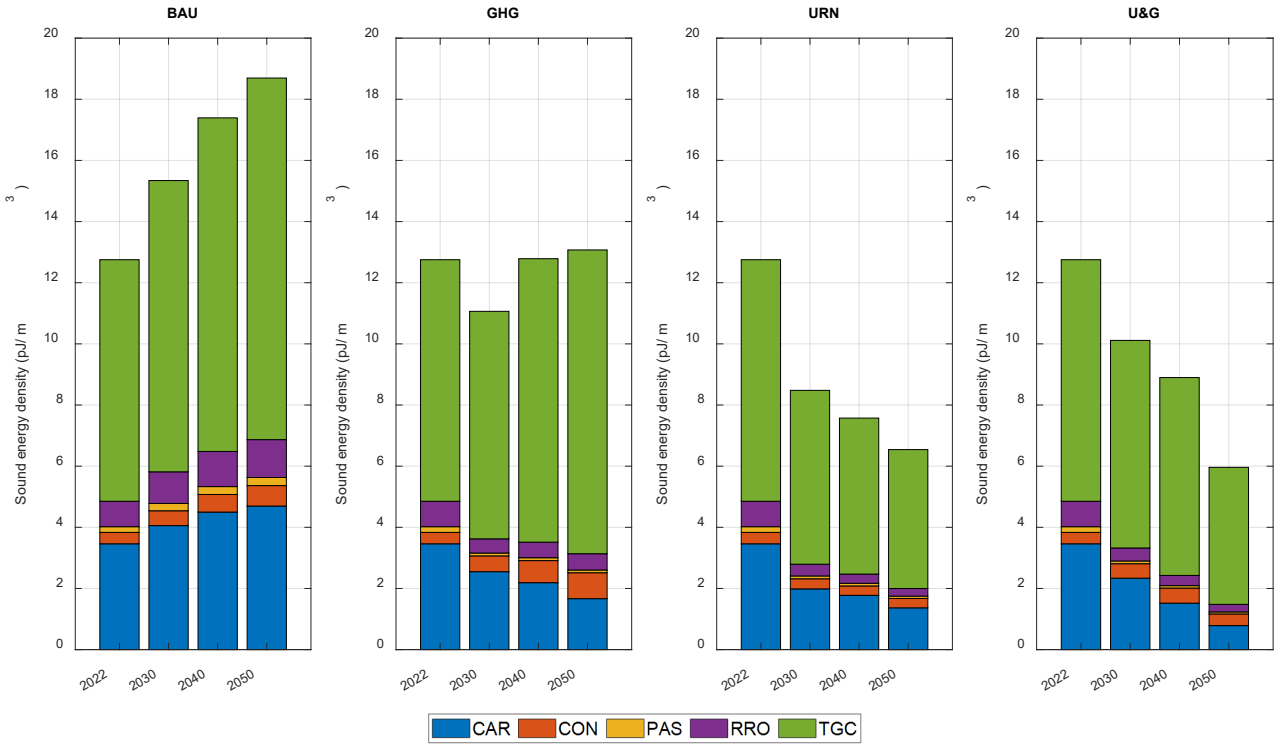

Figure 69 Sound energy density categorised for the different years at 63 Hz. (Mediterranean Sea)

The largest contribution to sound energy density is from TGC vessel category in this region. The lowest contribution is from PAS vessel category.

Figures 70 and 71 show the sound energy density of each vessel category when the different mitigation measures are applied with 100 % penetration at 63 Hz. The results are shown individually for cavitation and machinery components.

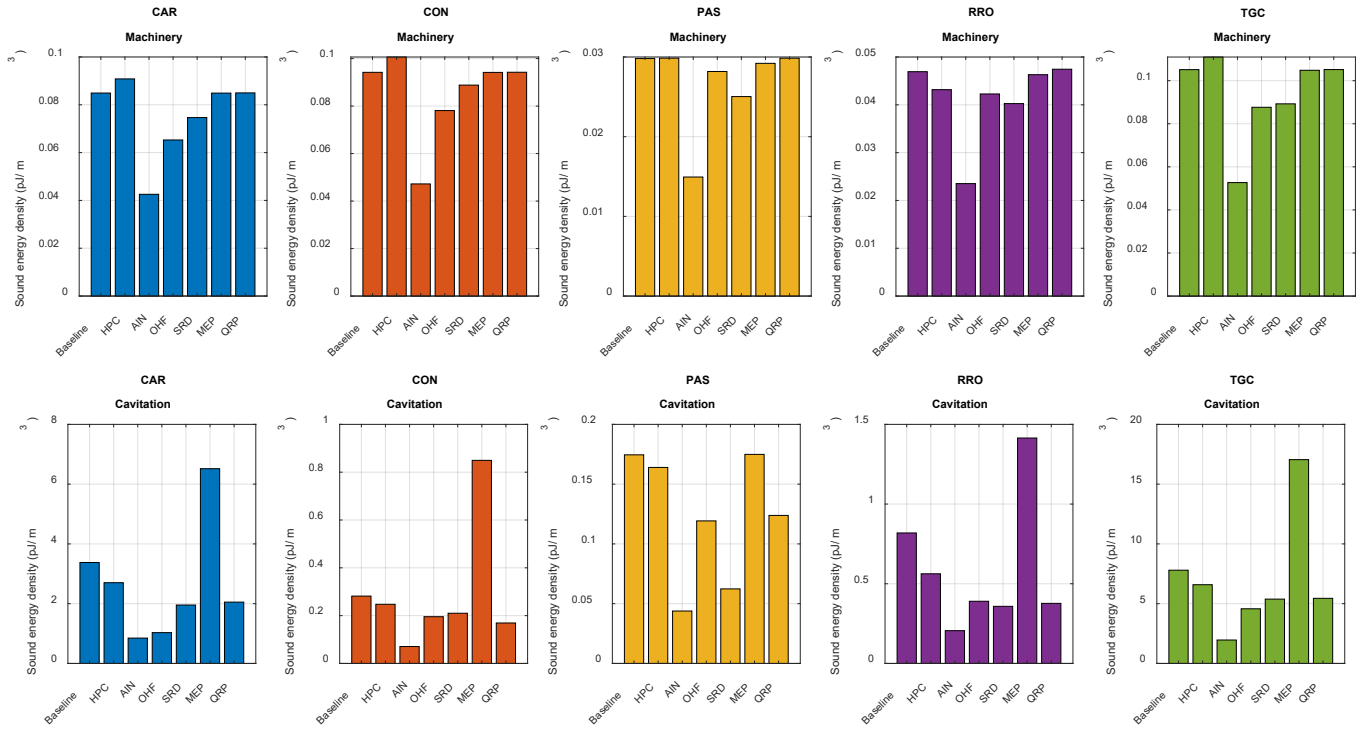

Figure 70 Sound energy density for the 100 % penetration rates for each mitigation measure at 63 Hz in Mediterranean Sea. Sound energy density is calculated for (top) machinery and (bottom) cavitation components.

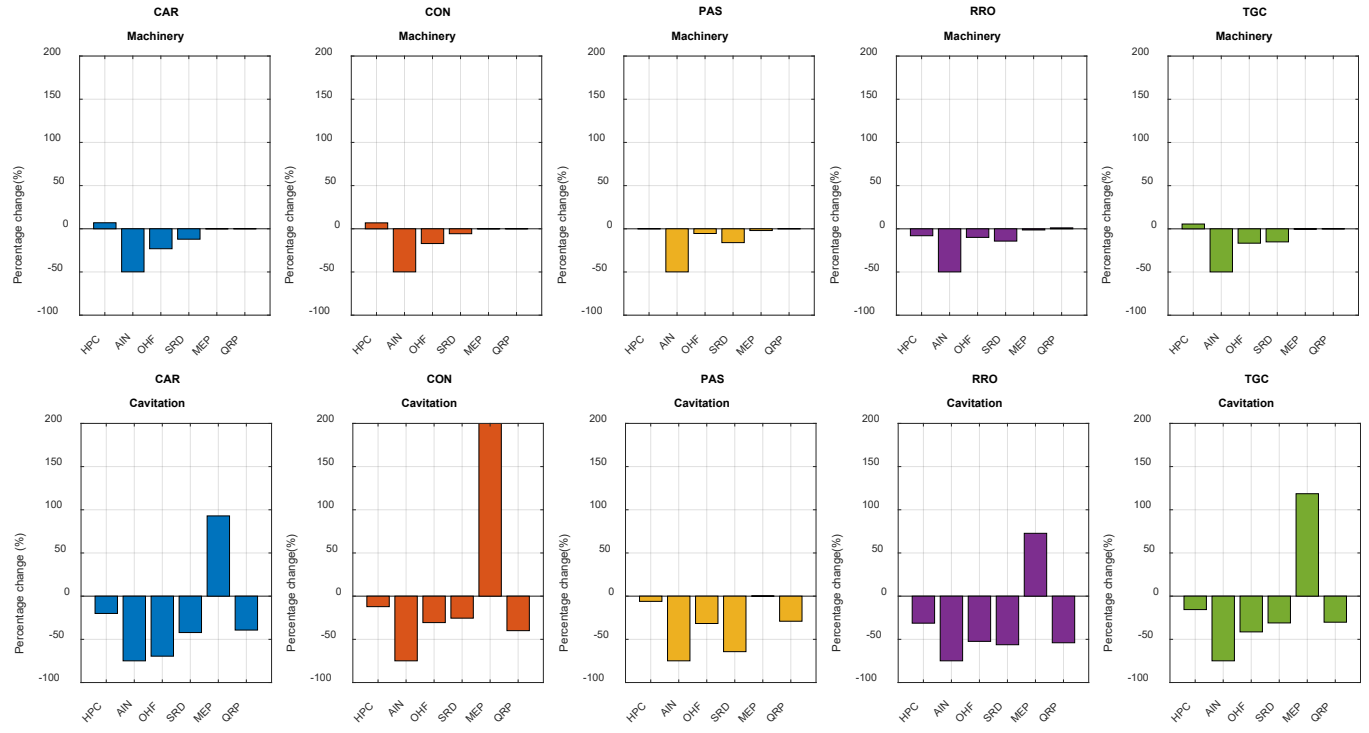

Figure 71 Percentage change in the sound energy density for (top) machinery and (bottom) cavitation components compared to the BAU scenario at 63 Hz (Mediterranean Sea).

Based on these results, the sound energy density of CON vessel category increased by more than 200 % for MEP mitigation measure. Comparing to the Baltic Sea, HPC, OHF and SRD measures have more mitigating effect for TGC vessels in the Mediterranean Sea.

For more detailed analysis regarding to the mitigation performances of each vessel category for the forecast scenarios, Figure 72 shows a percentage change graph.

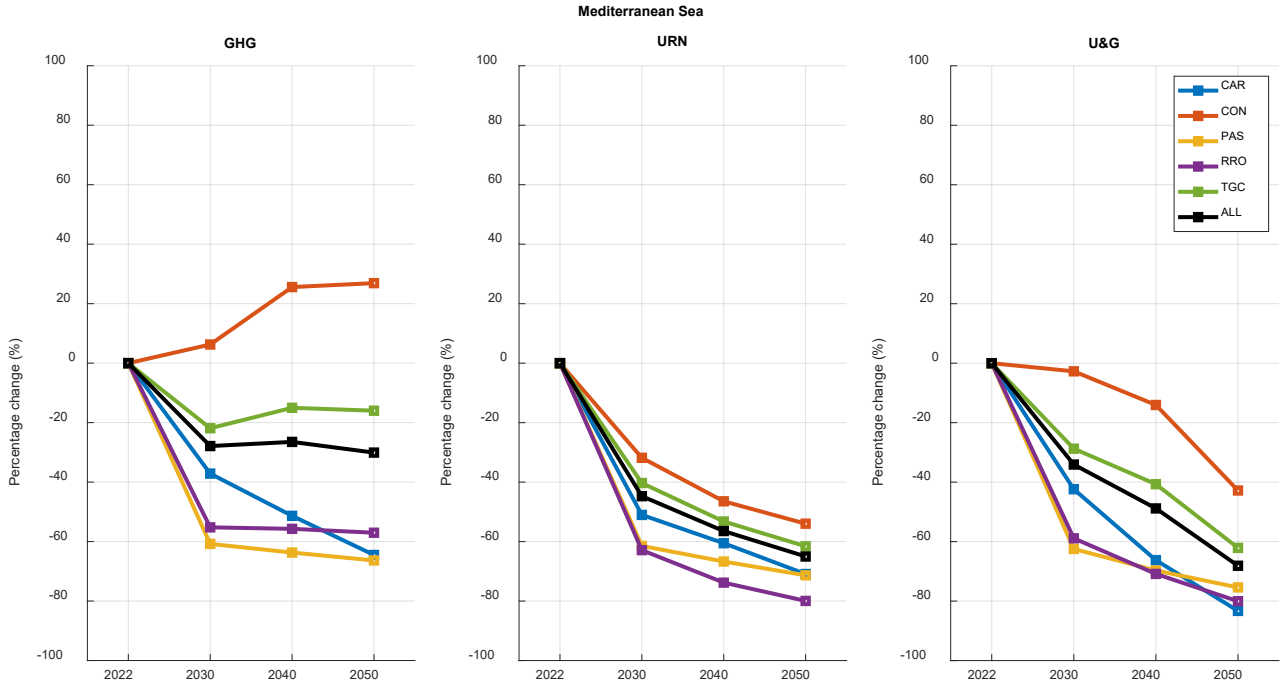

Figure 72 Percentage change in the sound energy density compared to the BAU scenario at 63 Hz. (Mediterranean Sea)

For GHG scenarios, sound energy density decreases for all vessel categories except for CON vessels. The largest decline is observed in PAS vessels, ranging from 60.8 to 66.3 %, while sound energy density increases for CON vessels, ranging from 6.3 % (2030) to 26.9 % (2050). When all vessel categories are included, the overall decrease in sound energy density varies between 27.9 % (2030) and 30.1 % (2050).

For URN scenarios, sound energy density decreases across all vessel categories. The largest decline is observed in RRO vessels, ranging from 62.9 to 79.9 % between 2030 and 2050. The lowest decline is seen in CON vessels, ranging from 31.2 % (2030) to 54 % (2050). For the scenario including all vessel categories, the decrease in sound energy density is between 44.7 % in 2030 and 65 % in 2050.

For U&G scenarios, the lowest decline is again observed in CON vessels, with reductions between 2.7 % in 2030 and 47.8 % in 2050. The largest declines are observed in RRO (58.9 % in 2030 to 80.0 % in 2050), PAS (62.5 % in 2030 to 75.4 % in 2050), and CAR (42.4 % in 2030 to 83.3 % in 2050) vessels.

It should be noted that these observations are only valid for 63 Hz. The mitigation performances can be different at other frequencies.

3.2.1.5 North Sea

Sound energy density comparisons for BAU, GHG, URN and U&G forecast scenarios are shown in Figure 73 for the baseline year (2022) and forecast years (2030, 2040, and 2050) in the North Sea.

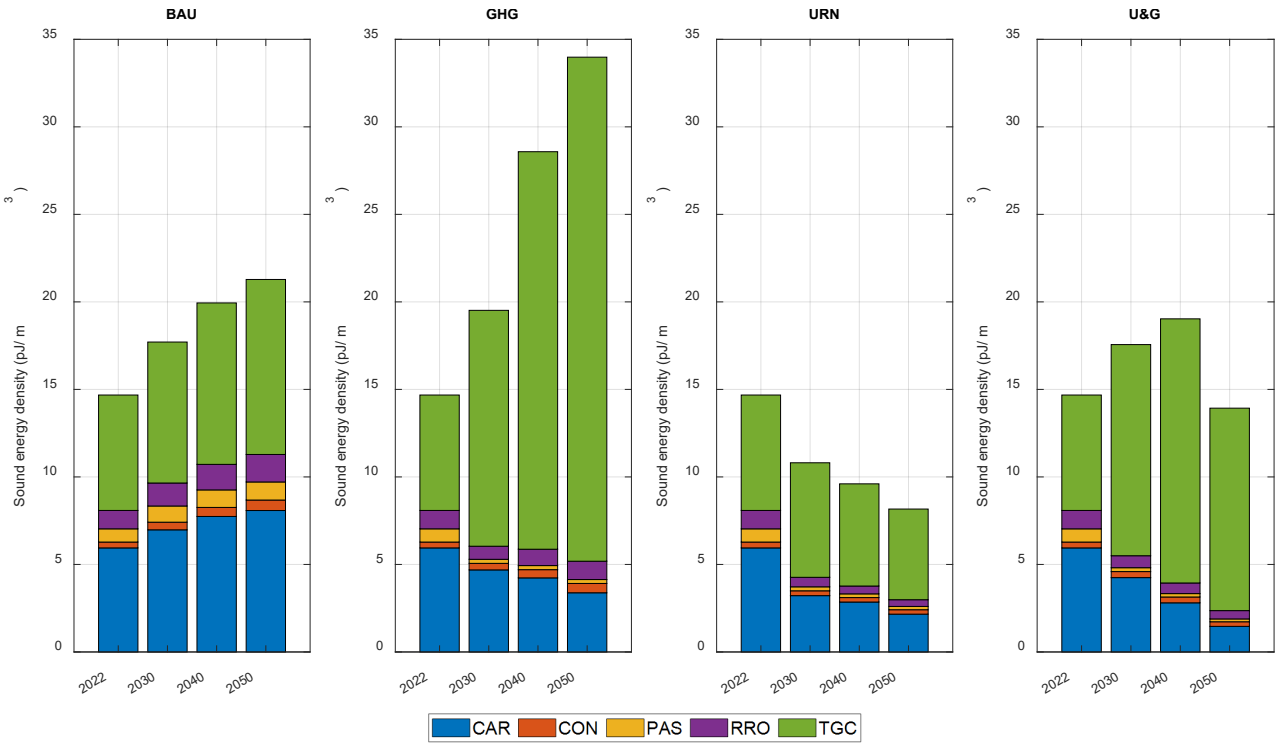

Figure 73 Sound energy density categorised for the different years at 63 Hz. (North Sea)

In 2022, the largest contributions to sound energy density are from CAR and TGC vessels. However, this ranking changes after applying mitigation measures, as each vessel category's mitigation performance varies.

Figures 74 and 75 show the sound energy density of each vessel category when the different mitigation measures are applied with 100 % penetration at 63 Hz. The results are shown individually for cavitation and machinery components.

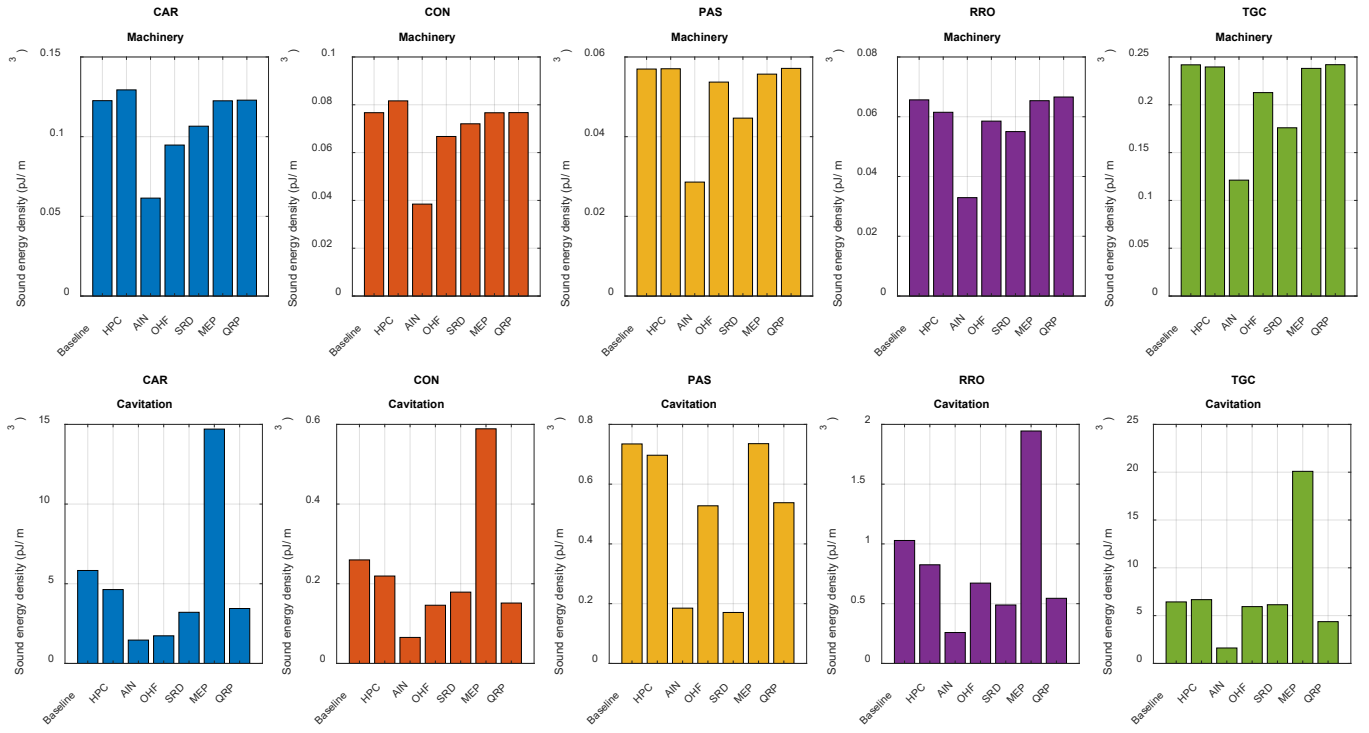

Figure 74 Sound energy density for the 100 % penetration rates for each mitigation measure at 63 Hz in North Sea. Sound energy density is calculated for (top) machinery and (bottom) cavitation components.

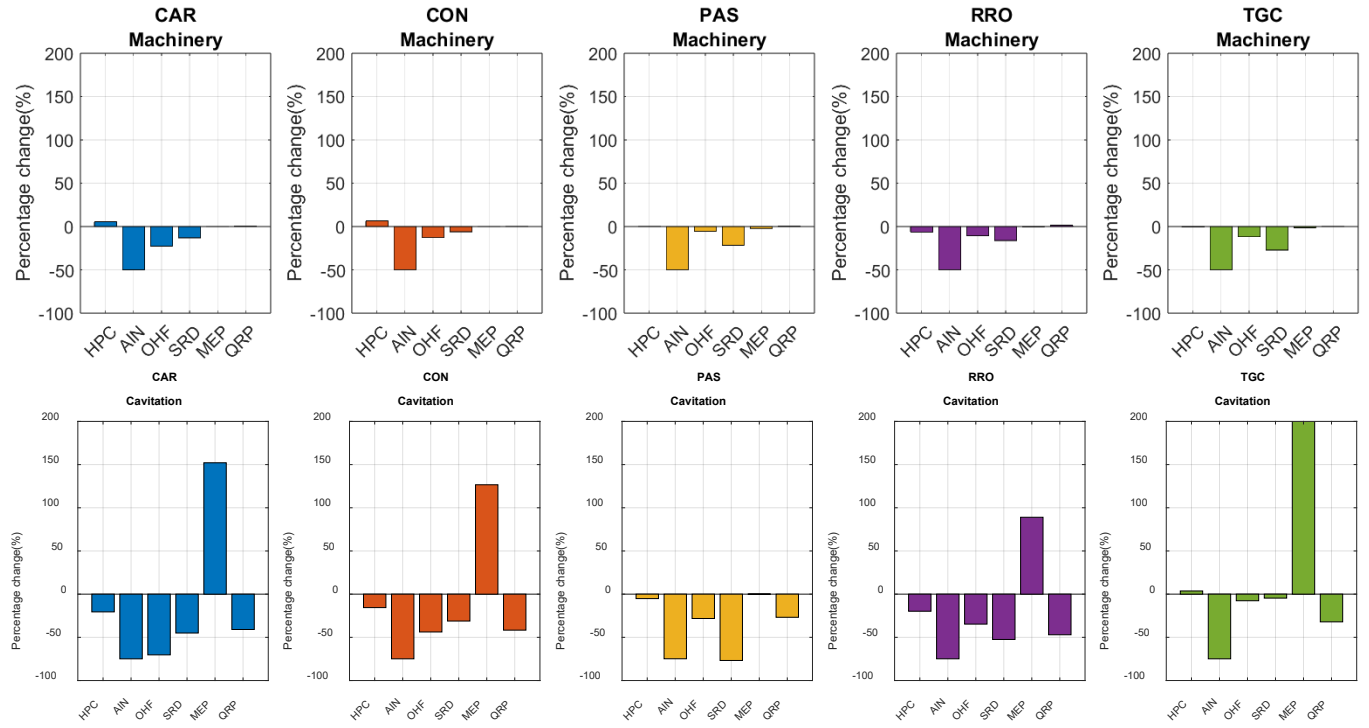

Figure 75 Percentage change in the sound energy density for (top) machinery and (bottom) cavitation components compared to the BAU scenario at 63 Hz (North Sea).

In the North Sea, the largest percentage increase (more than 200 %) in sound energy density is observed for the MEP mitigation measure applied to the TGC vessel category. Its effect will be visible in the forecast scenario results as shown in Figure 76.

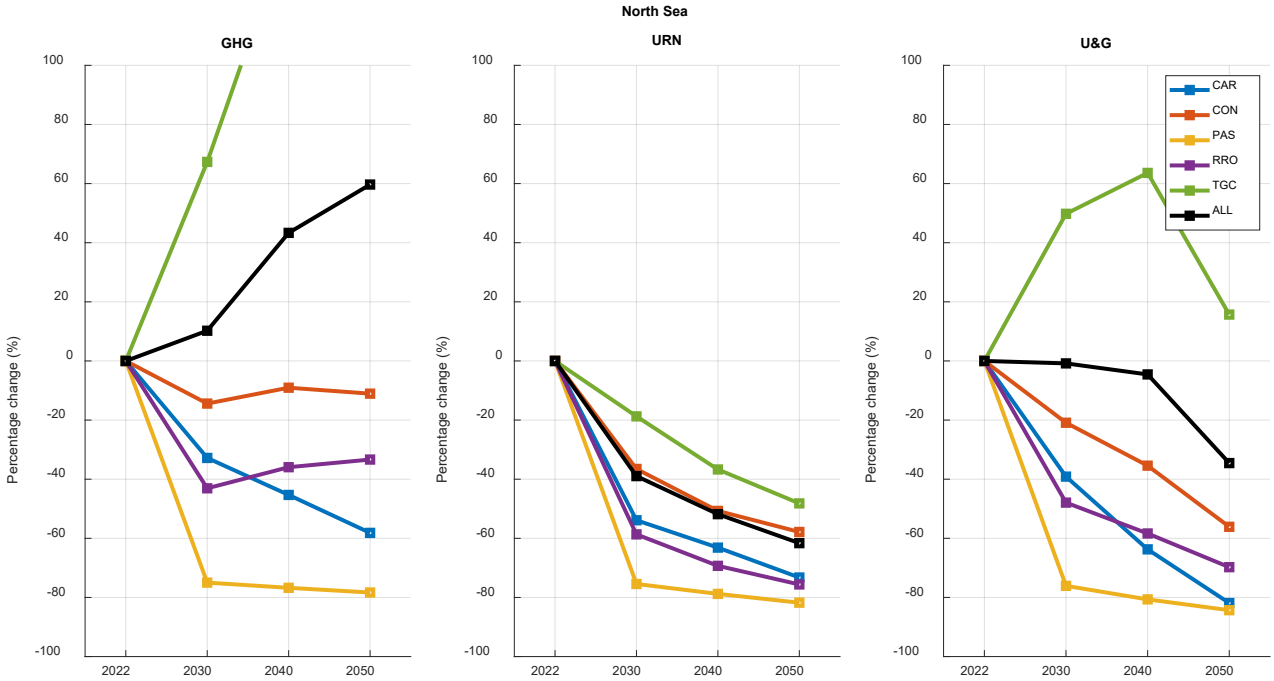

Figure 76 Percentage change in the sound energy density compared to the BAU scenario at 63 Hz. (North Sea)

For GHG scenarios, a large increase is observed in the sound energy density of the TGC vessel category, reaching 67.3 % in 2030 and surpassing 100 % in subsequent forecast years. This substantial increase in the TGC vessel category also contributes to an overall rise in sound energy density, from 10.2 % in 2030 to 59.7 % in 2050, when considering all vessel categories. Conversely, the largest decrease is observed in the PAS vessel category, ranging between 75.0 and 78.3 %. Interestingly, there is an observed increase in the sound energy density of the CON vessel category from 2030 to 2040, as well as in the RRO vessel category from 2030 to 2050, despite having lower sound energy density compared to BAU.

In URN scenarios, the sound energy density decreases for all vessel categories. The largest decline is again observed in the PAS vessel category, ranging from 71.4 to 81.8 %, while the smallest decline is observed for the TGC vessel category, ranging from 18.7 to 48.1 %. When considering all vessels, the decline in sound energy density ranges from 39.0 to 61.6 %.

For U&G scenarios, there is a decline in sound energy density for all vessel categories except TGC vessels. The decline ranges from 0.8 % in 2030 to 34.5 % in 2050 for the scenario that includes all vessel categories. The largest decline is again observed in PAS vessel categories, ranging from 76.1 % in 2030 to 84.3 % in 2050. The decline in the CON vessel category ranges from 20.9 % in 2030 to 56.1 % in 2050.

It should be noted that these observations are only valid for 63 Hz. The mitigation performances can be different at other frequencies.

3.2.1.6 Northeast Atlantic Ocean

Sound energy density comparisons for BAU, GHG, URN and U&G forecast scenarios are shown in Figure 77 for the baseline year (2022) and forecast years (2030, 2040, and 2050) in the northeast Atlantic Ocean.

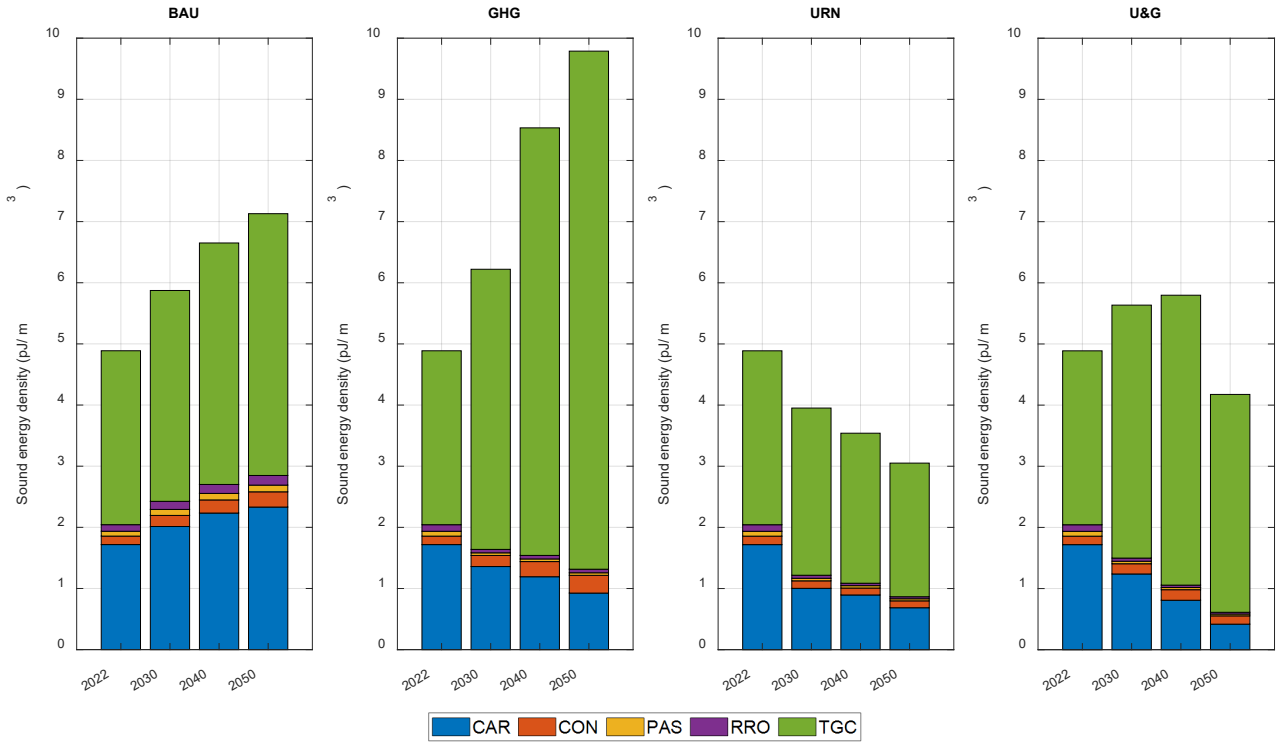

Figure 77 Sound energy density categorised for the different years at 63 Hz. (northeast Atlantic Ocean)

The TGC vessel category contributes the largest amount of sound energy density at 63 Hz, followed by the CAR vessel category in the Northeast Atlantic.

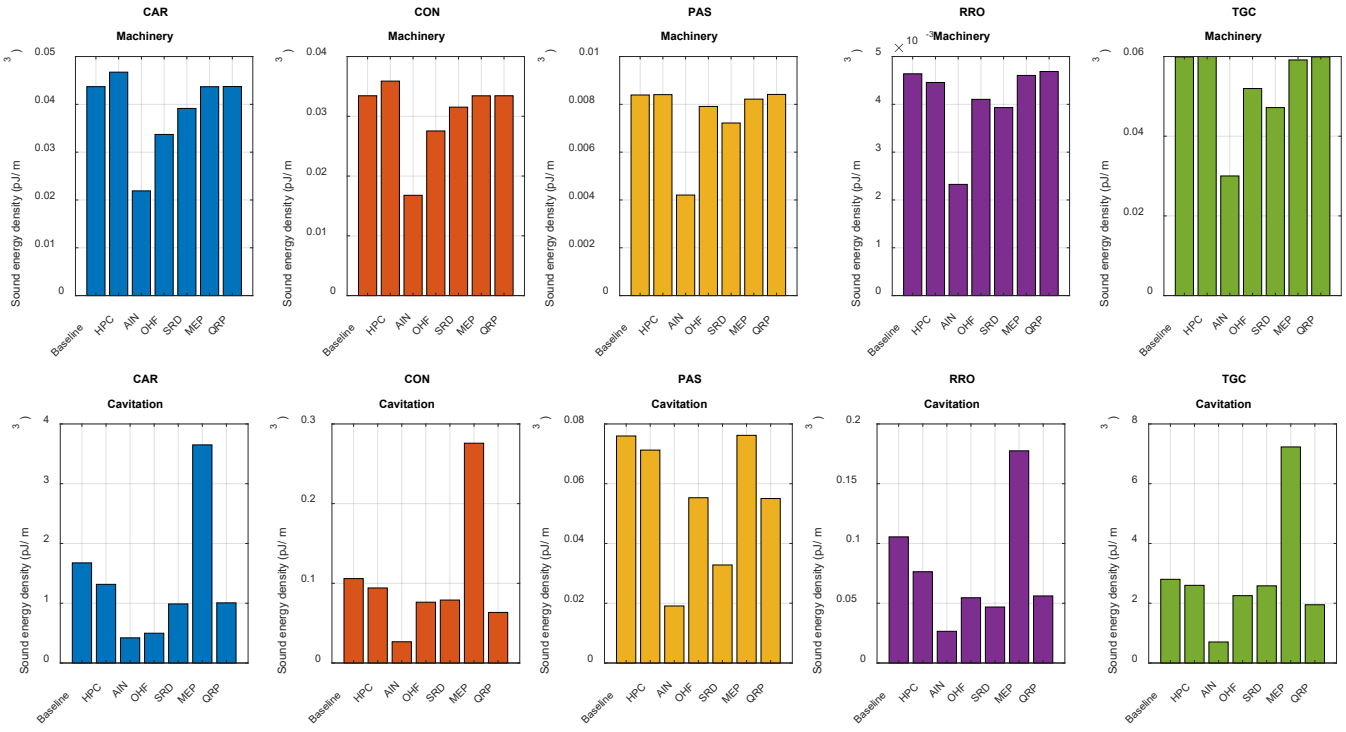

Figure 78 Sound energy density for the 100 % penetration rates for each mitigation measure at 63 Hz in the northeast Atlantic Ocean. Sound energy density is calculated for (top) machinery and (bottom) cavitation components.

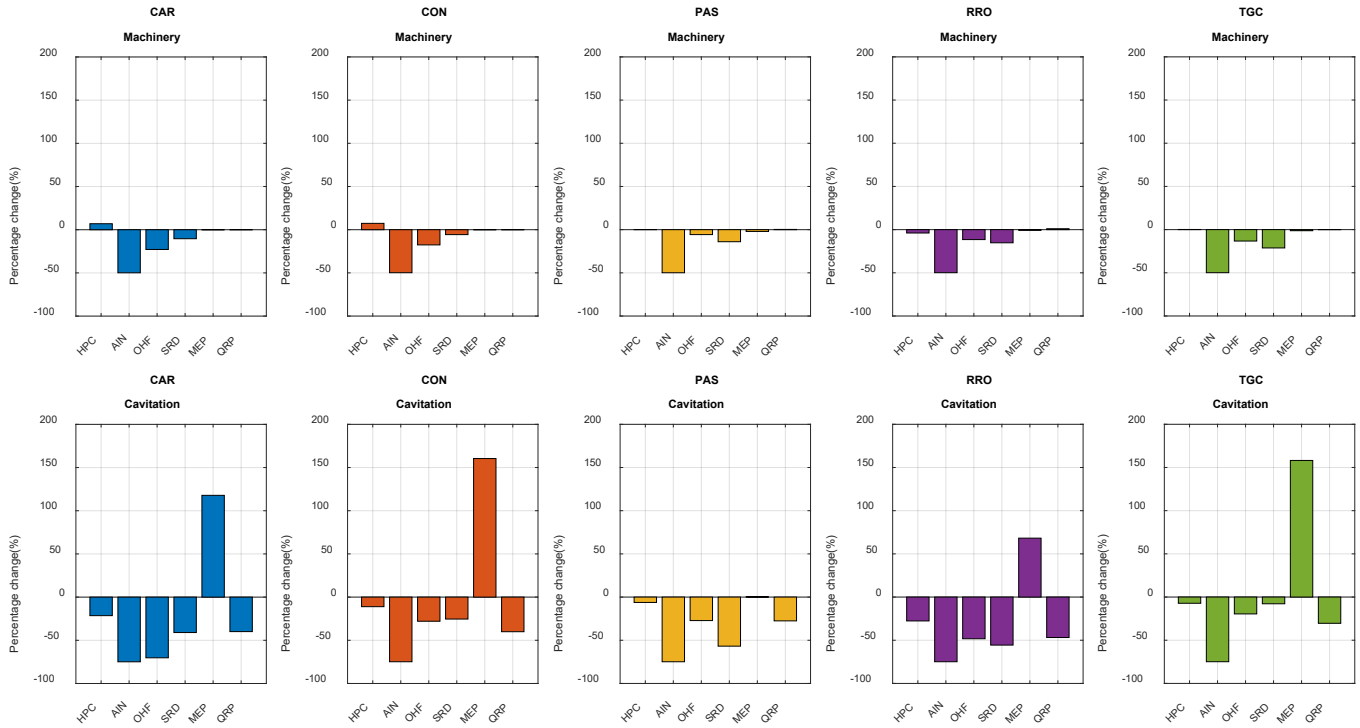

Figure 79 Percentage change in the sound energy density for (top) machinery and (bottom) cavitation components compared to the BAU scenario at 63 Hz (northeast Atlantic Ocean).

Based on these results, sound energy density for MEP increased more than 150.0 % for CON and TGC vessel categories.

For more detailed analysis for the forecast scenarios, the mitigation performance of each vessel category is quantified based on the percentage changes in the sound energy density for each category, as shown in Figure 80.

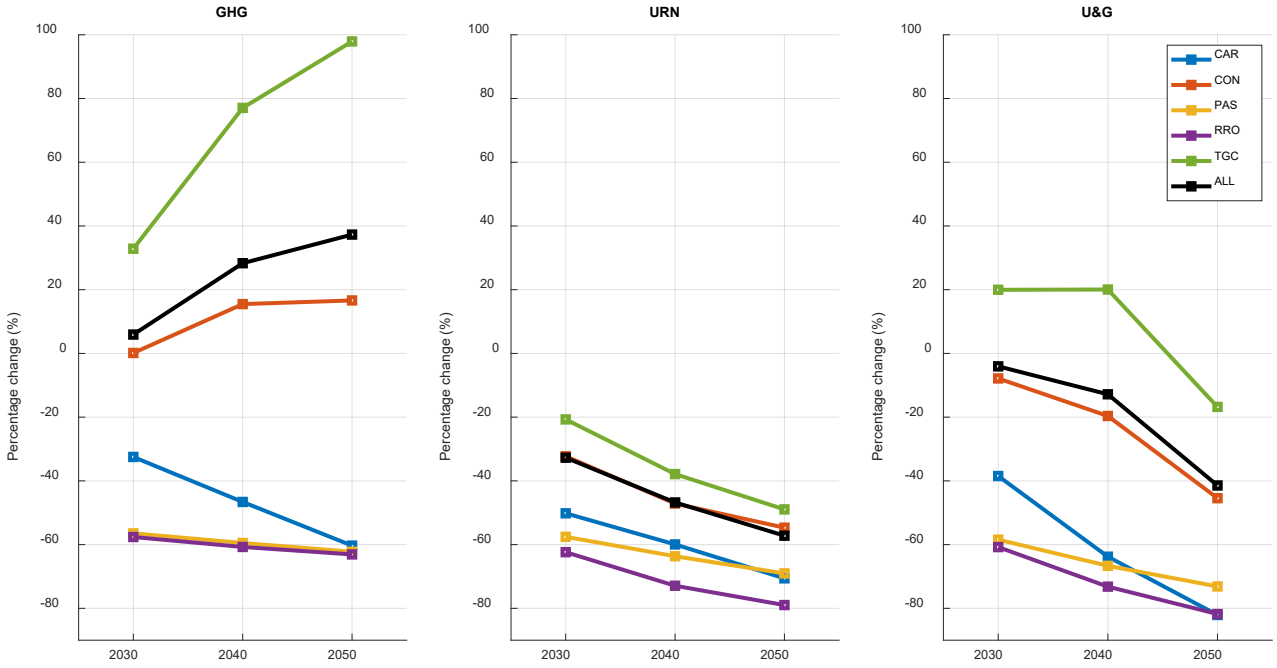

Figure 80 Percentage change in the sound energy density compared to the BAU scenario at 63 Hz. (northeast Atlantic Ocean)

In GHG scenarios, there is an increase in sound energy density for TGC vessels (32.9 to 97.9 %) and CON vessels (0.1 to 16.6 %). When considering all vessel categories, the overall sound energy density increases from 5.9 to 37.3 %. Conversely, the largest declines are observed for PAS (56.5 to 62.2 %) and RRO (57.6 to 63.0 %) vessels.

In URN scenarios, sound energy density decreases for all vessel categories. In the scenario including all vessel categories, the decrease in sound energy density ranges from 32.7 % in 2030 to 57.2 % in 2050. The largest decline is observed for the RRO vessel category (62.4 to 79.0 %), while the lowest decline is observed for the TGC vessel category (20.7 to 49 %).

In U&G scenarios, sound energy density decreases for all vessel categories except the TGC vessel category. When considering all vessel categories, the overall sound energy density decreases by 4.0 % in 2030 and 41.4 % in 2050. For TGC vessels, the sound energy density increases by about 20.0 % in 2030 and 2040 and decreases by 16.8 % in 2050.

3.2.2 Comparisons of Forecast Scenarios between Different Regions

In previous sections, the percentage changes for each mitigation measure and vessel category were highlighted for each region. In this section, the percentage changes in sound energy density for each forecast scenario are compared between the regions. The comparisons are shown for individual vessel categories.

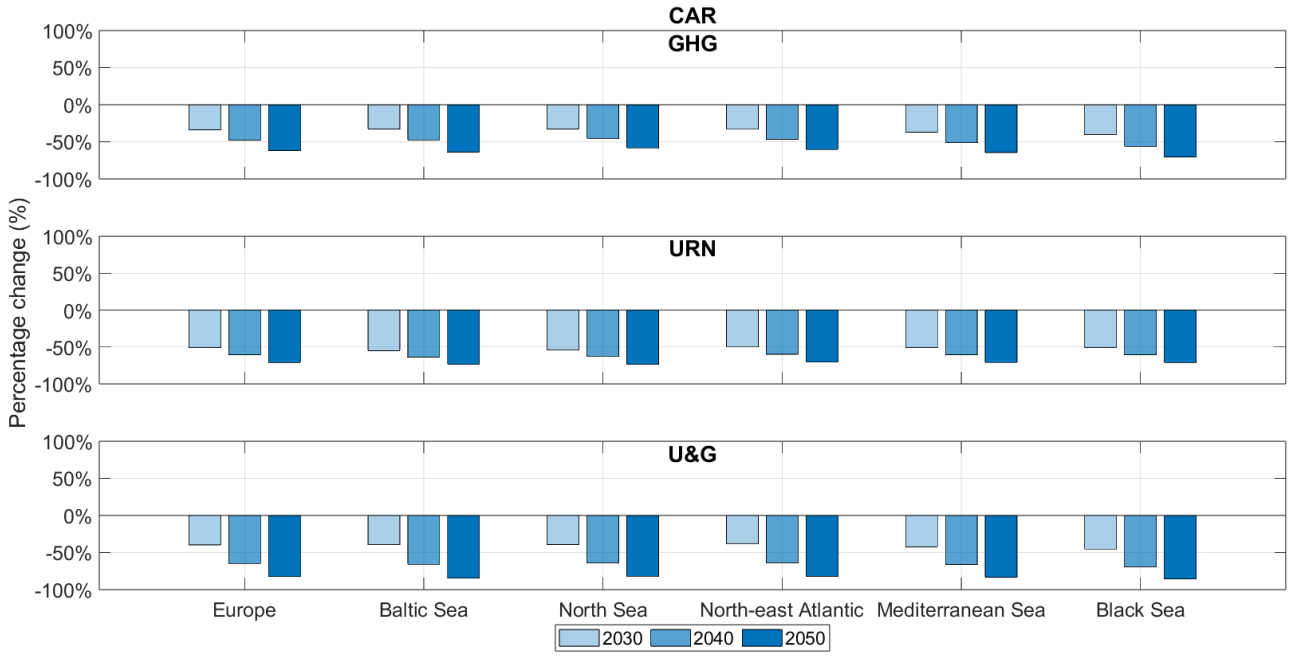

Figure 81 Comparing the percentage change in the sound energy density at different regions for CAR vessel category at 63 Hz. GHG (top), URN (middle), and U&G (bottom) forecast scenarios are shown in 2030, 2040, and 2050.

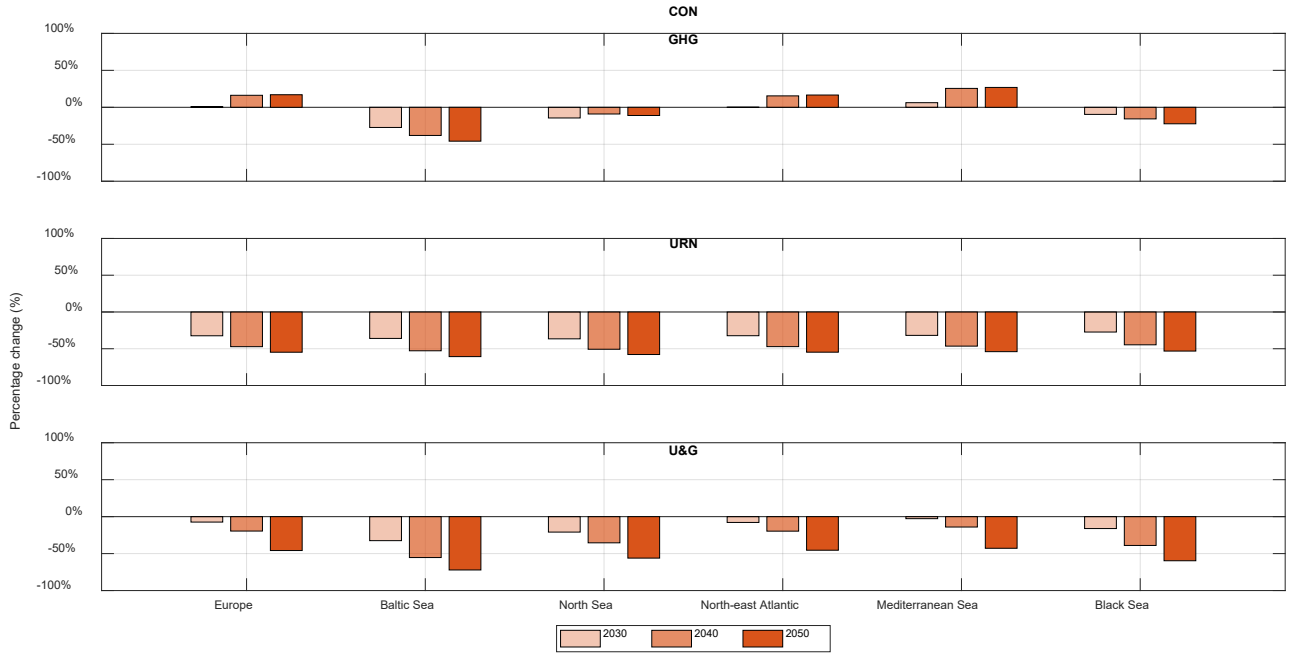

Figure 82 Comparing the percentage change in the sound energy density at different regions for CON vessel category at 63 Hz. (top) GHG, (middle) URN, and (bottom) U&G forecast scenarios are shown in 2030, 2040, and 2050.

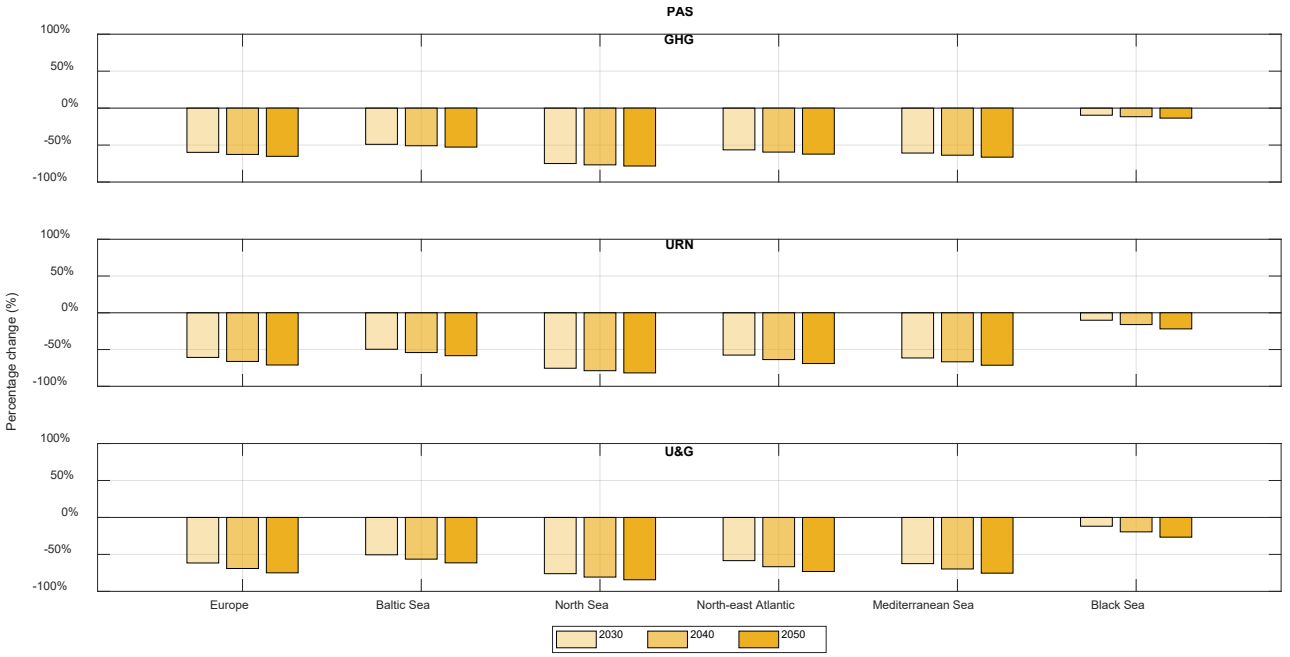

Figure 83 Comparing the percentage change in the sound energy density at different regions for PAS vessel category at 63 Hz. (top) GHG, (middle) URN, and (bottom) U&G forecast scenarios are shown in 2030, 2040, and 2050.

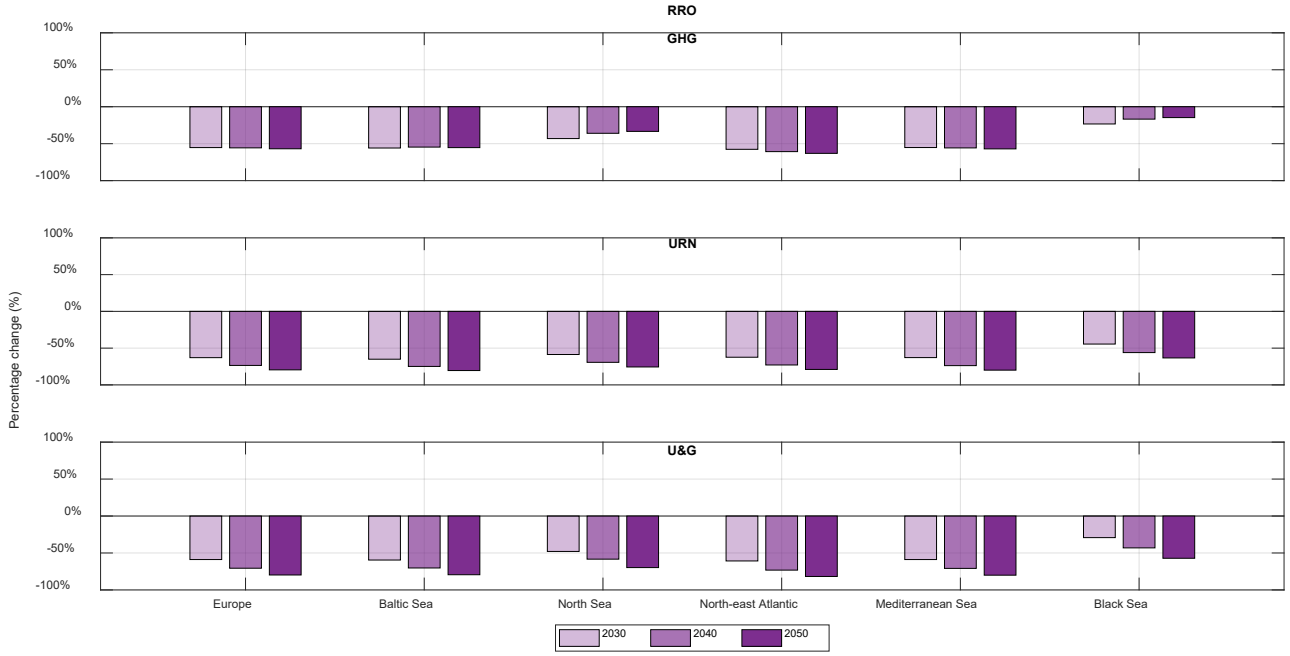

Figure 84 Comparing the percentage change in the sound energy density at different regions for RRO vessel category at 63 Hz. (top) GHG, (middle) URN, and (bottom) U&G forecast scenarios are shown in 2030, 2040, and 2050.

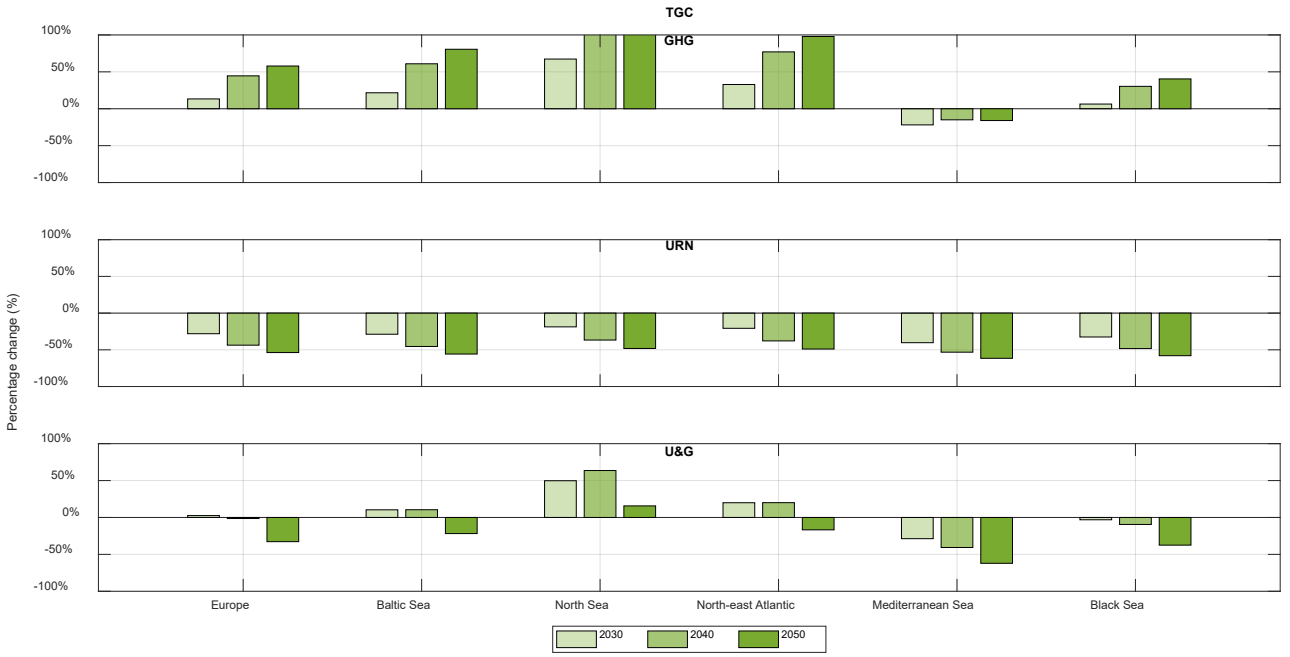

Figure 85 Comparing the percentage change in the sound energy density at different regions for TGC vessel category at 63 Hz. (top) GHG, (middle) URN, and (bottom) U&G forecast scenarios are shown in 2030, 2040, and 2050.

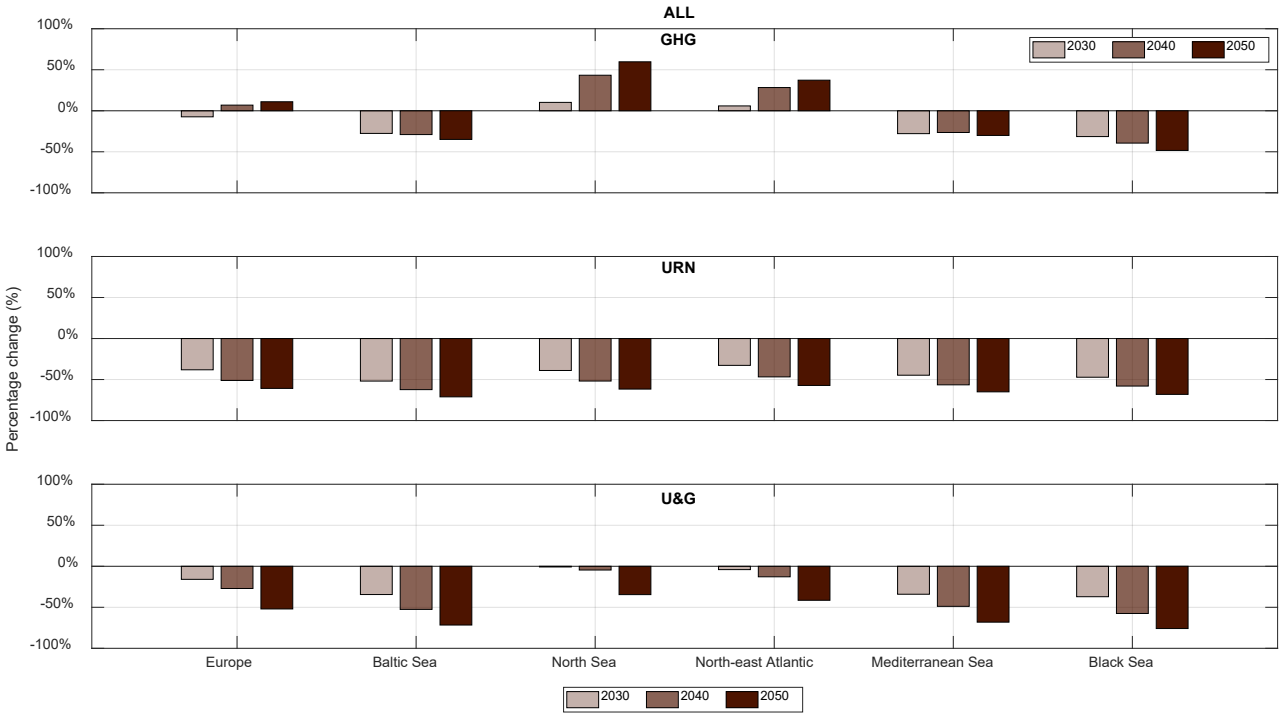

Figure 86 Comparing the percentage change in the sound energy density at different regions for ALL vessel categories at 63 Hz. (top) GHG, (middle) URN, and (bottom) U&G forecast scenarios are shown in 2030, 2040, and 2050.

The forecast sound energy density of CAR, PAS, and RRO vessels decreased in all regions.

For CAR vessels, the largest declines in forecast sound energy density for GHG scenarios are observed in the Black Sea (40.5 % in 2030 and 70.4 % in 2050) and the Mediterranean Sea (37.1 % in 2030 and 64.5 % in 2050). The largest declines for URN scenarios are observed in the Baltic Sea (55.0 % in 2030 and 73.4 % in 2050) and the North Sea (53.9 % in 2030 and 73.3 % in 2050). For U&G scenarios, although the largest decline is observed in the Black Sea (45.2 % in 2030 and 85.6 % in 2050), the declines in all other regions were very close (varying between 81.9 % and 84.7 % in 2050). A decline of 20 %, 50 % and 80 % in energy density corresponds, respectively, to a reduction of 1 dB, 3 dB and 7 dB in level.

For PAS vessels, the largest declines in forecast sound energy density for GHG scenarios are observed in the North Sea (75.0 % in 2030 and 78.3 % in 2050) and the Mediterranean Sea (60.8 % in 2030 and 66.3 % in 2050). The largest declines for URN scenarios are observed in the North Sea (75.4 % in 2030 and 81.8 % in 2050) and the Mediterranean Sea (61.5 % in 2030 and 71.3 % in 2050). For U&G scenarios, the largest declines are observed in the North Sea (76.1 % in 2030 and 84.3 % in 2050) and the Mediterranean Sea (69.7 % in 2030 and 75.4 % in 2050).

For RRO vessels, the largest declines in forecast sound energy density for GHG scenarios are observed in the northeast Atlantic (57.6 % in 2030 and 63.1 % in 2050), the Mediterranean Sea (55.2 % in 2030 and 57.0 % in 2050), and the Baltic Sea (55.9 % in 2030 and 55.3 % in 2050). The largest declines for URN scenarios are very close to each other (varying from 62.4 % to 65.1 % in 2030 and from 79.0 % to 80.5 % in 2050) in the Baltic Sea, northeast Atlantic, and Mediterranean Sea. This change is the lowest in the Black Sea (44.5 % in 2030 and 63.3 % in 2050). For U&G scenarios, the largest percentage declines are again very close to each other (varying from 58.9 % to 60.8 % in 2030 and from 79.4 % to 81.8 % in 2050) in the Baltic Sea, northeast Atlantic Ocean, and Mediterranean Sea. This change is the lowest in the Black Sea (29.2 % in 2030 and 57.2 % in 2050).

For CON vessels, the forecast sound energy density increased in Europe (0.8 % in 2030 and 17.0 % in 2050), the northeast Atlantic Ocean (0.1 % in 2030 and 16.6 % in 2050), and the Mediterranean Sea (6.3 % in 2030 and 26.9 % in 2050) for GHG scenarios but decreased in other regions (the largest decline in the Baltic Sea as 27.2 % in 2030 and 45.8 % in 2050) and other scenarios. For URN scenarios, all regions have a similar amount of decline varying from 31.8 % to 35.0 % in 2030 and from 53.2 % to 60.7 % in 2050. For U&G scenario, the largest decline is observed in the Baltic Sea (32.5 % in 2030 and 72.1 % in 2050).

For TGC vessels, the forecast sound energy density increased in all regions except the Mediterranean Sea for GHG scenarios while decreasing under URN scenarios. The largest increase in the sound energy density for this vessel category is observed in the North Sea (exceeding 100 % in 2050), northeast Atlantic Ocean (97.9 % in 2050) and Baltic Sea (57.9 % in 2050). For U&G scenarios, the sound energy density of TGC vessels increased during 2030 and 2040 in the Baltic Sea, North Sea, and the northeast Atlantic Ocean.

When the contributions of all vessel categories are considered, the sound energy density decreased for URN and U&G in all regions while increasing in Europe (only in 2040 and 2050), the North Sea, and the northeast Atlantic Ocean.

It is important to note that these results are valid for the 63 Hz decidecade band. Comparisons and rankings could differ at other frequencies. Therefore, similar simulations should be conducted for different frequencies covering a broad frequency band relevant to the source levels of the considered vessel categories. Such research could help to identify the effects of mitigation measures in more detail in future studies.

4. Limitations, Artefacts and Caveats

This section explains the limitations of the model concerning the modelling and use of map layers, providing examples. The following model limitations and artefacts were identified for hindcast map layers:

- The AIS data provided by EMSA follow two distinct data storage protocols. Long-term storage covers data from 2016 until June 2020, while recent data storage includes information from July 2020 onwards. The long-term storage includes both satellite and terrestrial data. The recent data storage includes only terrestrial-based AIS data although for NAVISON satellite data was provided separately for 2022 and 2023. In addition, there are some AIS data gaps since the UK no longer delivers terrestrial AIS data to EMSA following Brexit in 2020. An overview of the AIS data, in terms of number of messages per month, is provided in Appendix B. The absence of satellite AIS data introduces limitations in the accuracy of sound map layers, presenting an obstacle to analysing the temporal patterns of shipping sound. As an example of this limitation, the sound maps layers for the third quarter of 2019 and 2020 are compared in Figure 87.

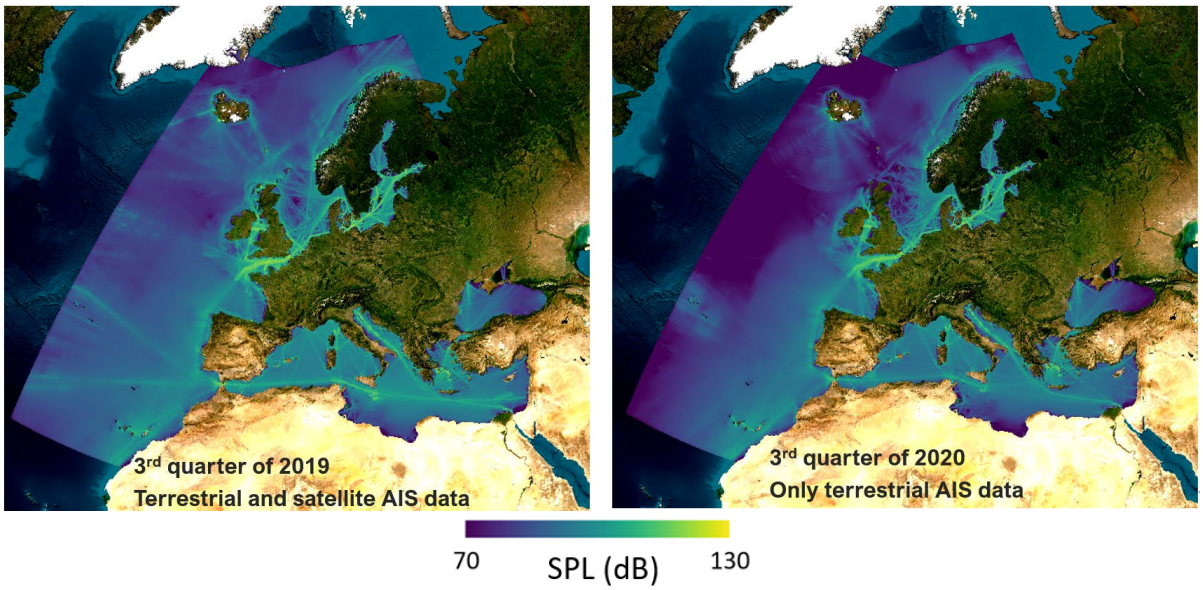

Figure 87 Comparison of hindcast sound map layers (SPL re 1 µPa^2, in dB) for the third quarters of 2019 and 2020.

- The sound map layers only include ship sound sources based on the AIS track data within the individual NAVISON regions, even though ships located outside of the region may still contribute to overall sound pressure level. Similarly, the contribution of ships outside of the NAVISON regions are also not included (such as the contribution of ship sound sources in north-west Atlantic Ocean to the sound map layers of the northeast Atlantic Ocean).
- Related to the previous bullet point regarding the use of ship AIS data within individual NAVISON regions and the integration of sound map layers with different meshing resolutions, some artefacts may become apparent at the boundaries of each NAVISON region when visualising all map layers together with GIS software. In most cases, boundaries between regions have been carefully selected to avoid artefacts. However, the North Sea presents a particular challenge. For example, the sound map layers of the North Sea solely use AIS data within the North Sea boundaries, disregarding any contributions from the Baltic Sea and the northeast Atlantic Ocean. These artefacts are indicated by the white circles in Figure 88.

Figure 88 Sound pressure level re 1 µPa^2 (dB). The artefacts that appear as straight blue lines (highlighted in the white circles) for the visualisation of individual hindcast sound pressure level map layers in QGIS.

- Although the sound propagation computations were accelerated using high-performance computing clusters, the computational power is not sufficient to make the calculations for very long ranges due to limited computation time nonetheless limiting the maximum propagation distance in some regions due to the size of the area and the number of source points included. Therefore, underwater sound propagation has been modelled up to a specific maximum distance in each region, as listed in Table 6. In some instances, the distance cutoff in the propagation calculation introduced artefacts into the sound map layers. For example, such an artefact in the sound map layers can be seen around Iceland for the third quarter of 2020 in Figure 87.

Table 6 Maximum distances used in sound propagation modelling.

Region	Maximum distance
Baltic Sea	300 km
North Sea	400 km
Black Sea	500 km
Mediterranean Sea	600 km
Northeast Atlantic Ocean	900 km

- The modelling approach, which is implemented for the calculation of the forecast sound map layers, uses the baseline sound map layers from 2022. Consequently,
  - All forecast map layers are based on the same shipping distribution in the selected baseline map layers.
  - In BAU scenarios, uniform volume traffic changes are applied to entire map layers, resulting in the same amount of sound pressure level (SPL) change across the entire sound map layers. Potential new shipping lanes, which may be planned in the future, or changes to existing lanes, are not included in the forecast sound map layers.
  - All sound maps use the same sound speed profile (without considering the effect of climate change (Possenti et al. 2024)) and sediment data from 2022. Any specific changes in environmental parameters during the forecast years are not taken into consideration in the forecast map layers.

- If there are any artefacts due to incomplete AIS data coverage in the baseline sound maps, they will also be visible in the forecast maps. The visibility of these artefacts may vary after applying noise mitigation measures that are specific to vessel categories, making them less or more noticeable as shown in Figure 89.

- All limitations and caveats mentioned for the hindcast map layers in the D2.1 report (Sertlek and MacGillivray 2024) also apply to the forecast map layers. As a reminder, since each region has a different SOW, spatial statistics of SPL (e.g., quantiles, mean, and standard deviation) can be misleading for the comparisons of the sound map layers in different regions. When comparing map layers between regions, mean sound energy density provides more reliable results, as it is independent of SOW.

Examining only difference maps (Forecast-BAU) can sometimes be misleading, especially in areas with low shipping density or incomplete AIS coverage. Therefore, they should be interpreted together with the forecast sound map layers to understand the details of shipping density and sound levels. For instance, in Figure 90, there are some increases in SPL (red areas) visible in the difference map for the Black Sea. However, when comparing the same map with the same vessel category and time period, it becomes evident that the SPL is very low and AIS coverage is sparse in the same area where positive differences are observed.

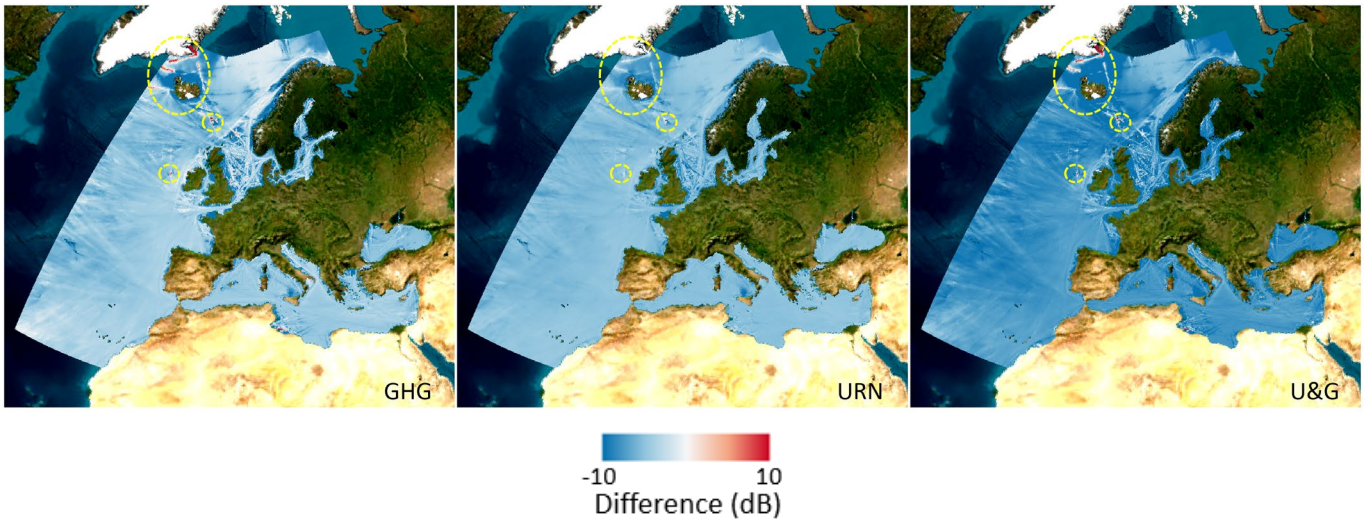

Figure 89 Artefacts in level difference (dB) in the forecast map layers (yellow circles), which could become more or less visible for different forecast scenarios.

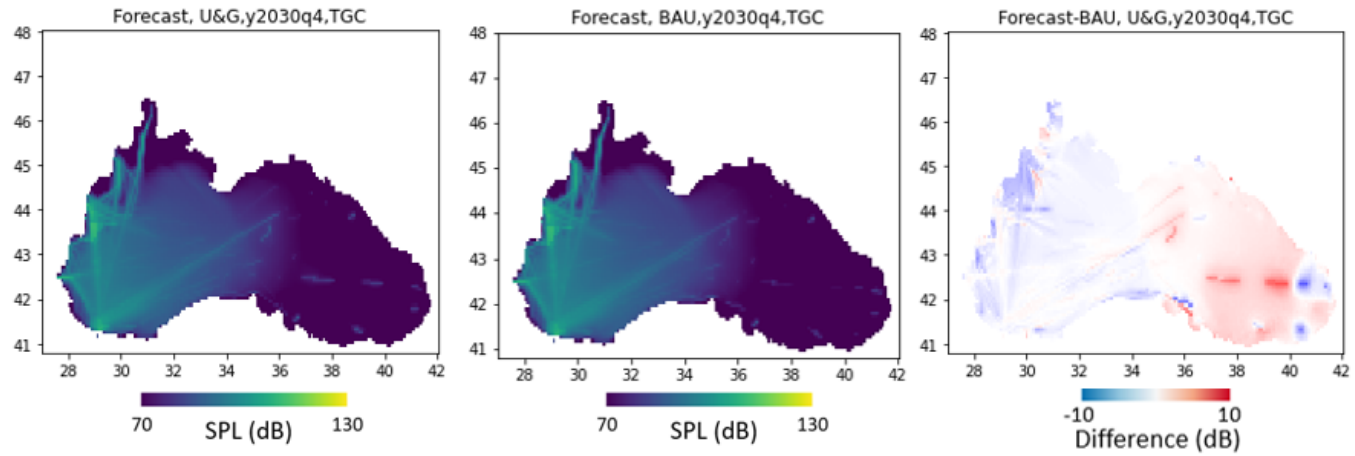

Figure 90 TGC: Forecast sound map layers (SPL re 1 μPa^2) for (left) U&G and (middle) BAU scenarios. Example of localised increases (red areas) corresponding to locations with sparse AIS coverage in the (right) difference map layers

- The conclusions drawn from the forecast scenarios are based on results for a single decidecade frequency band. When applying the PIANO model, it is possible that the effect of mitigation measures on source levels will be different in frequency bands other than 63 Hz, which could lead to different trends and/or conclusions than those derived here.

- The sound map layers include continuous sounds from ships with AIS. Ships not fitted with AIS (e.g. recreational vessels) are excluded, as are operational wind farms. Impulsive sounds are out of scope, such as produced by seismic airguns and pile driving). Also excluded are all biological sources, such as biotic sounds from whales and fish and other natural sources such as wind and rain.
- AIS data are used only for selected vessel categories. This means that map layers exclude, for example, fishing vessels, and some specialised activities (such as dredging, construction, and hydrocarbon development) that may make a substantial contribution in certain areas where these activities are concentrated.

5. Comparisons with Other Sound Mapping Projects

Past research projects in European seas have demonstrated different approaches for producing shipping sound maps and used different underwater sound metrics (Table 7). Consequently, direct comparisons are not straightforward. By contrast, the NAVISON project applies a consistent sound mapping approach for all regions in the Europe, thus permitting quantitative like-with-like comparisons of shipping contributions to ambient sound between regions, vessel categories, years, and forecast scenarios, as discussed in the previous sections.

Table 7 International joint monitoring projects for continuous sound in Europe (based on Merchant et al. (2022)).

Project	Years	Region
BIAS	2012–2016	Baltic Sea
CeNoBS	2019–2016	Black Sea
COMPASS	2017–2021	Ireland, Northern Ireland, Scotland
JOMOPANS	2019–2021	North Sea
JONAS	2018–2022	Northeast Atlantic Ocean
Soundscape	2019–2021	Northern Adriatic Sea
QUIETSEAS	2021–2023	Black Sea and Mediterranean Sea

In addition to these programmes in Europe, there are other monitoring projects in various regions worldwide. The National Park Service (NPS) Ocean Noise Reference Station (NRS) Network consists of twelve calibrated autonomous passive acoustic recorders (10 to 2000 Hz) that help quantify baseline levels and multi-year trends in ocean ambient sound across the continental United States, Alaska, Hawaii, and island territories within and near the United States Exclusive Economic Zone (US EEZ) (Haver et al. 2018, Haver et al. 2019). The Atlantic Deepwater Ecosystem Observatory Network (ADEON) project measured the natural and anthropogenic sound of the Mid-South-Atlantic Outer Continental Shelf (OCS) from November 2017 to December 2020 (Heaney et al. In press). Especially, ADEON and JOMOPANS produced several project standards, and these form the basis of ISO 7605 (under development at the time of writing).

In the following subsections, we focus on projects in Europe. The sound maps from the BIAS, JOMOPANS, and HOLAS 3 projects are compared with the closest corresponding NAVISON sound map layers. Although these projects all nominally calculate “sound pressure level”, important quantitative differences arise due to use of different metrics by different projects. Table 8 summarizes the differences in their output metrics. In NAVISON sound map layers, spatially averaged sound pressure level is used, which is defined as

$$L_{\mathrm{sa}} = 10 \log_{10} \frac{\langle \overline{p^2} \rangle}{p_0^2} \ \mathrm{dB},$$

where <> indicates a spatial average. Depth averaged sound pressure level is a special case of spatially averaged sound pressure level, where the spatial average is conducted over depth only, and not over latitude or longitude. The calculation of spatially averaged mean-square sound pressure is also helpful for the calculation of sound energy density as described in Appendix D. In the other projects, instead of a metric based on an arithmetic average, spatio-temporal N% exceedance level (BIAS and HOLAS 3) and temporal N% exceedance level of depth-averaged sound pressure level (JOMOPANS) are used. For N=50, the median SPL is obtained. Due to the use of different metrics (Table 8), it is not possible to make a direct comparison between the sound maps of BIAS, JOMOPANS, HOLAS 3, and NAVISON. The arithmetic mean (AM) was recommended by TG Noise (Dekeling et al. 2014) and IQOE 2019 (Ainslie et al. 2019). The benefit of AM is its inherent robustness to the choice of TOW (AM is independent of TOW). By choosing $\mathrm{L}_{\{\mathrm{p,3mo}\}}$, NAVISON obtains the same result as calculating AM from a smaller TOW (ref ADEON soundscape spec), consistent with the recommendations of TG Noise (Dekeling et al. 2014) and IQOE 2019 recommendations (Ainslie et al. 2019), both of which indicated AM as a robust metric for differences in TOW. Therefore, the comparisons between median sound pressure level and spatially averaged sound pressure level are presented in the next subsections.

Table 8 Comparison of output metrics of BIAS, HELCOM BLUES/HOLAS 3, JOMOPANS, and NAVISON.

Project	Metric	Frequency	TOW
BIAS	L_{BIAS}: Spatio-temporal N% exceedance level (N=5, 10, 25, 50[7], 75, 90, 95)	63 Hz, 125 Hz, and 2 kHz (one-third octave bands)	Unstated
HOLAS 3 (HELCOM BLUES)	$L_{HOLAS} = L_{BIAS}$	63 Hz, 125 Hz, and 500 Hz (decidecade bands)	Unstated
JOMOPANS	$L_{JOMOPANS}$: temporal N% exceedance level of depth-averaged sound pressure level (N=10, 50)	63 Hz and 125 Hz (decidecade bands) Broadband (10 Hz to 20 kHz)	Unstated
NAVISON	$L_{NAVISON}$: Spatially averaged sound pressure level ($L_{p,3mo}$)	63 Hz and 125 Hz (decidecade bands)	3 months

5.1 Processing Windows

The temporal and spatial observation and analysis windows used to produce sound maps are important metrics that affect the modelling outputs; where available, these are described and compared for the different projects in the following subsections.

5.1.1 Temporal Observation and Analysis Windows

The TOW duration for NAVISON is 3 months (mo), as stated in Table 8. Although the NAVISON methodology does not require a value of TAW, if the AM had been used with a shorter duration than 3 mo, the sound maps would then correspond quantitatively to a TAW duration of 3 mo.

For other projects it is unstated, but for BIAS and HOLAS 3 an empirical adjustment is made to ensure agreement with measurements made using TOW = 20 s (Betke et al. 2015). Thus, the plotted sound maps for BIAS and HOLAS 3 correspond quantitatively with a TOW duration of 20 s.

According to TG Noise (Borsani et al. 2023), for BIAS, HOLAS 3 and JOMOPANS, the temporal analysis window (TAW) is 1 month.

5.1.2 Spatial observation and analysis windows

Another novel aspect of NAVISON is the specification of an explicit SOW when computing the SPL maps. It is important to consider the choice of SOW size when computing sound maps since the SOW area influences the results of the sound map calculations. To illustrate the effect of SOW size on the sound maps, curves of the area exceeding a specified spatially averaged sound pressure level threshold (exceedance area) are computed versus the spatially averaged sound pressure level threshold for different SOW areas (Figure 91). To see the differences more clearly, the percentage change in the exceedance area is calculated relative to the sound map layer with the finest resolution (Figure 92). The calculations for both the Baltic Sea and North Sea showed that, as the size of the SOW increased by a factor of 16, exceedance areas for lower SPL values increase by up to 20 % while exceedance areas for higher SPL values decrease by up to 100 %. This analysis demonstrates that, in addition to the known sensitivity of SPL to TOW (Merchant et al. 2012), the exceedance area is sensitive to UNLV when UNLV exceeds 110 dB for these examples (Figure 92).

[7] Median SPL is calculated for N=50 and shown as $L_{p,T,50\,\%}$

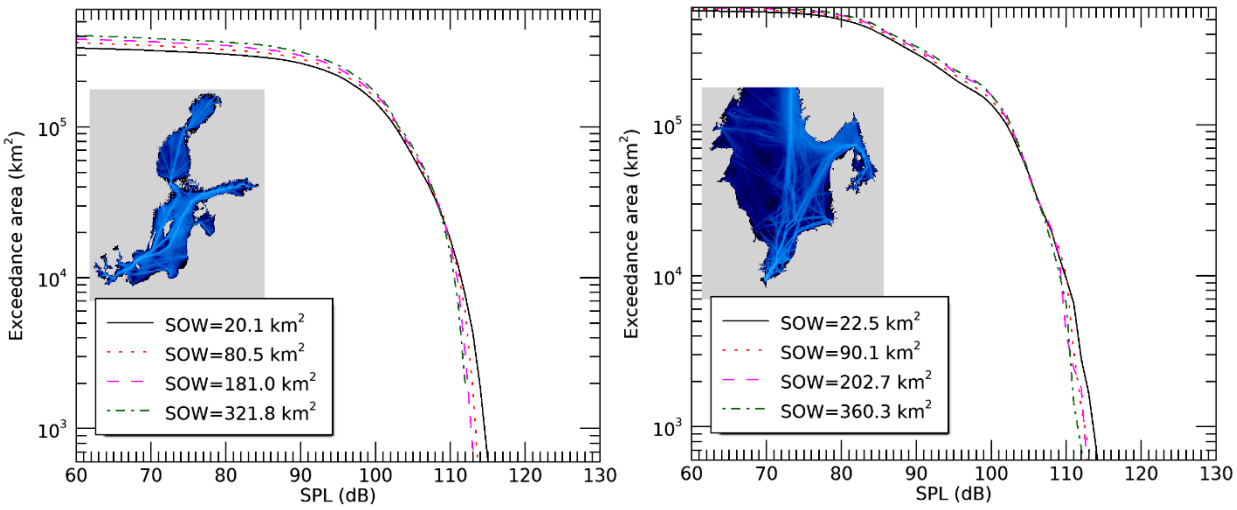

Figure 91 Exceedance area versus UNLV in the Baltic Sea (left) and North Sea (right) for different sizes of spatial observation window (SOW). Exceedance areas are calculated from the NAVISON 2022 yearly average sound maps. The exceedance area is plotted on a logarithmic scale.

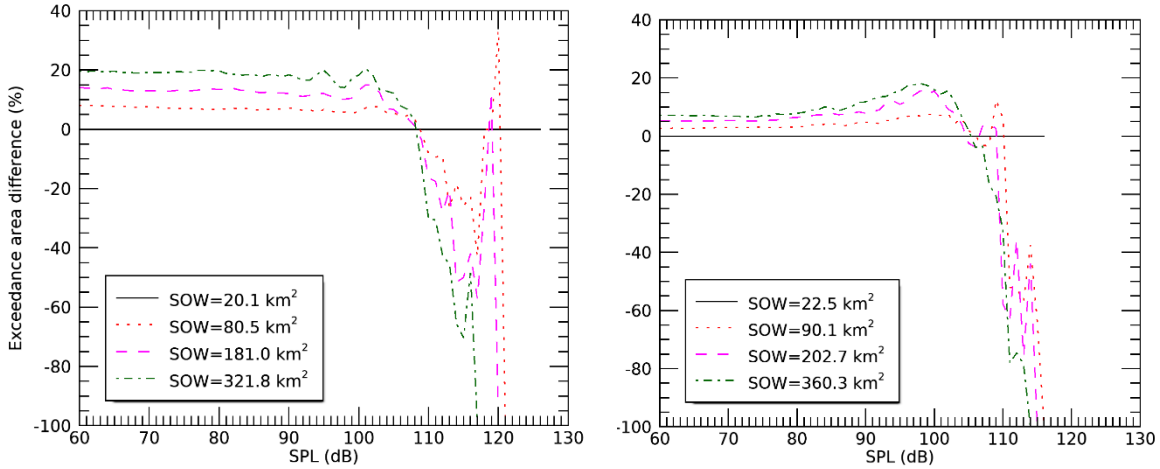

Figure 92 Percentage difference in exceedance area versus UNLV in the Baltic Sea (left) and North Sea (right) for different sizes of spatial observation window (SOW).

For NAVISON, the horizontal SOW is specified in Table 4. The vertical SOW is from the surface to the shallow of 200 m and the water depth.

While the concept of SAW is not generally used for NAVISON, for the purpose of Figure 91 and Figure 92 the SAW can be thought of as entire the region (i.e., Baltic Sea or North Sea).

For JOMOPANS, an average of mean-square sound pressure is calculated in depth, with no horizontal averaging. Thus, SOW is a vertical line from the surface to the seabed.

SOW is not specified in the BIAS or HOLAS 3 project reports. In our interpretation based on the reports and publications of these projects, no spatial averaging is applied in this sense.

The BIAS and HOLAS 3 projects do apply spatial averaging in depth but in a different sense. The spatio-temporal statistics calculated (Table 8) (Folegot et al. 2016) can be thought of as adopting a SAW in depth corresponding to the range of depths considered for the spatial part of the statistical processing.[8]

[8] The BIAS sound maps were calculated for different receiver depth categories as surface layer (0 to 15 m), bottom layer (30 m to the bottom) and full water column. HOLAS 3 also considers three different receiver depth categories: surface layer, deep layer, and entire water column.

5.2 Comparisons with Other Programmes

As pointed out above, the use of different metrics by different projects complicates quantitative comparisons between them, and harmonisation of the output metric is considered an urgent priority. Furthermore, these projects use different source and propagation modelling approaches, as well as different inputs (i.e., AIS data set, bathymetry, and sediment parameters). For example, the hybrid mode energy flux model used in JOMOPANS does not incorporate the elastic properties of sediments and the sound speed profile in water, whereas these factors are accounted for in NAVISON maps. The AIS data coverage could also differ between both projects. These differences in both modelling and inputs provide an additional explanation for the variations in the sound map results from these projects.

The following subsections provide more details about the BIAS, JOMOPANS, and HELCOM BLUES/HOLAS 3 projects, along with some examples.

5.2.1 BIAS Programme

The Baltic Sea Information on the Acoustic Soundscape (BIAS) programme was a pioneering joint sound monitoring programme in EU waters (Sigray et al. 2016). During the BIAS programme, monthly averaged sound maps of Baltic Sea were calculated with a parabolic equation model for various receiver depths during 2014 at 63, 125, and 2000 Hz (in one-third octave frequency bands).

In BIAS, the measured data were stored as 20-s averages (Folegot et al. 2016, Nikolopoulos et al. 2016). Time snapshots based on AIS data are used to calculate these sound maps. The BIAS sound maps were produced with 1 h temporal resolution. The temporal analysis window (TAW) duration is 1 month, as used in the time statistics for calculating SPL at various percentiles. The SOW size of BIAS maps was not reported in Folegot et al. (2016) or Nikolopoulos et al. (2016). The map resolution in the provided netCDF files is 0.008° longitude × 0.005° latitude. A modified version of RANDI3 model based on an empirical adjustment applied to calculate source level for each vessel. The empirical adjustment is calculated from the measurements (for each month and frequency) by minimising the difference between the measured and modelled SPL at 15th and 5th percentiles (85 % and 95 % exceedance levels).

The BIAS sound maps are downloaded in netCDF format (ICES, 2024) and plotted with the same NAVISON colormap. The BIAS map layers are available for all months of 2014. There were also no separate netCDF files for each vessel category. In Figure 93, a comparison is shown between NAVISON and BIAS sound maps including all vessel categories. Expected differences between the BIAS and NAVISON maps, considering the known difference between mean and median, are confirmed.

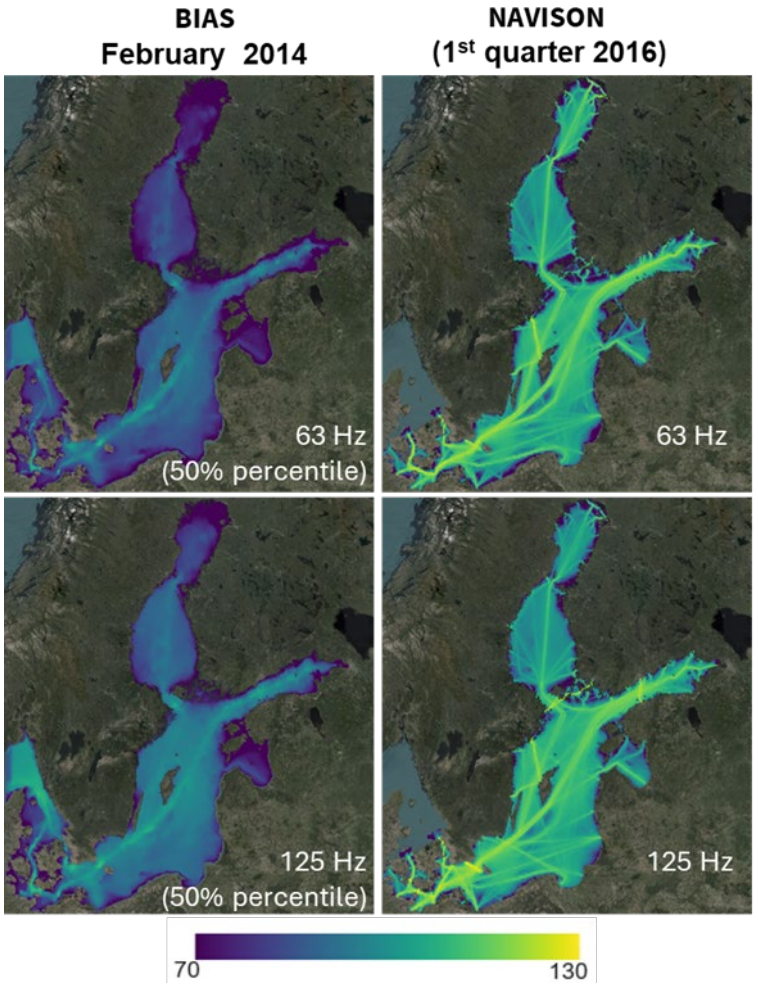

Figure 93 Comparison between BIAS (left) and NAVISON (right) sound maps (SPL re 1 μPa^2, in dB) at (top) 63 Hz and (bottom) 125 Hz. The NAVISON results are based on the spatially averaged sound pressure level while the BIAS results are for the median (spatio-temporal 50 % exceedance level). See Table 8 for detailed description of the metrics for each project.

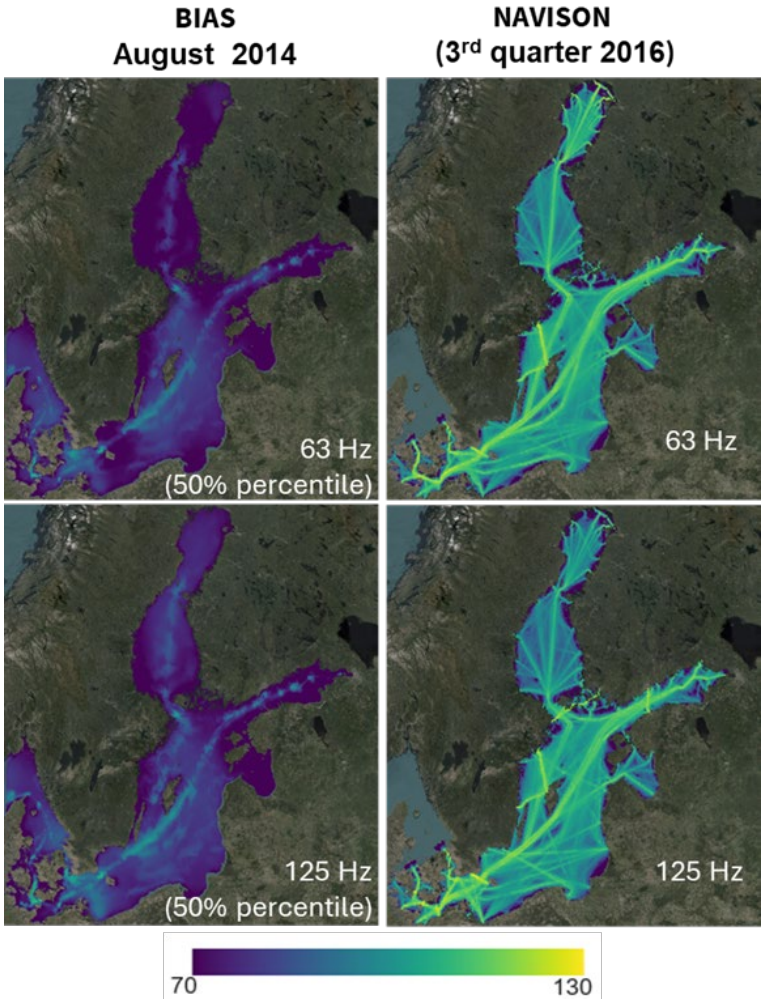

Figure 94 Comparison between BIAS (left) and NAVISON (right) sound maps (SPL re 1 μPa^2, in dB) at (top) 63 Hz and (bottom) 125 Hz. The NAVISON results are based on spatially averaged sound pressure level while the BIAS results are for the median (spatio-temporal 50 % exceedance level). See Table 8 for detailed description of the metrics for each project.

5.2.2 JOMOPANS Programme

The Joint Monitoring Programme for Ambient Noise in the North Sea (JOMOPANS) programme calculated monthly and annual depth-averaged sound maps (for individual ship types and wind,) for one-tenth decade (decidecade) bands between 10 Hz to 20 kHz (de Jong et al. 2022). The different versions of these maps are shown with different metrics as excess level and dominance. The spatial resolution of JOMOPANS maps is 0.05° longitude × 0.025° latitude (approximately 3.2 × 2.8 km^2). The propagation loss is based on hybrid mode-energy flux mode, which could reproduce similar results as adiabatic normal mode models with iso-velocity assumption (Sertlek et al. 2019a). The propagation loss calculations are performed for 16 radials per source, starting from 100 metres from the source grid location up to a maximum distance of 400 km, with a resolution of 100 m. The depth-averaged mean square sound pressure is calculated for ten uniformly spaced points from 1 m above the seabed to 1 metre below the sea surface. To accelerate the calculations using a look-up table for propagation loss (PL) calculations, the source grid is defined by shifting the receiver grid by one-half of the grid resolution (de Jong et al. 2021).

De Jong et al. (2021) states that JOMOPANS North Sea sound maps were calculated at a 10-min resolution. However, the modelling report does not clearly state the TOW used for modelling. On the other hand, as stated as in Wang and Robinson (2021) for the JOMOPANS measurements:" The temporal observation window and the temporal analysis window are both defined as being equal to 1 second."). Source levels of vessels are calculated based on (MacGillivray and de Jong 2021). JOMOPANS' categorisation for the vessel types is different from the categorisation in NAVISON.

The JOMOPANS sound maps are also available from ICES (2024) in netCDF format.

In Figure 95, NAVISON and JOMOPANS sound maps (including all vessel categories) are compared. Both maps use the NAVISON colormap. JOMOPANS sound maps have different versions with and without the contribution of

wind noise. In the following comparison, the sound maps without the contribution of wind noise are shown. Expected differences between the JOMOPANS and NAVISON maps, considering the known difference between mean and median, are confirmed.

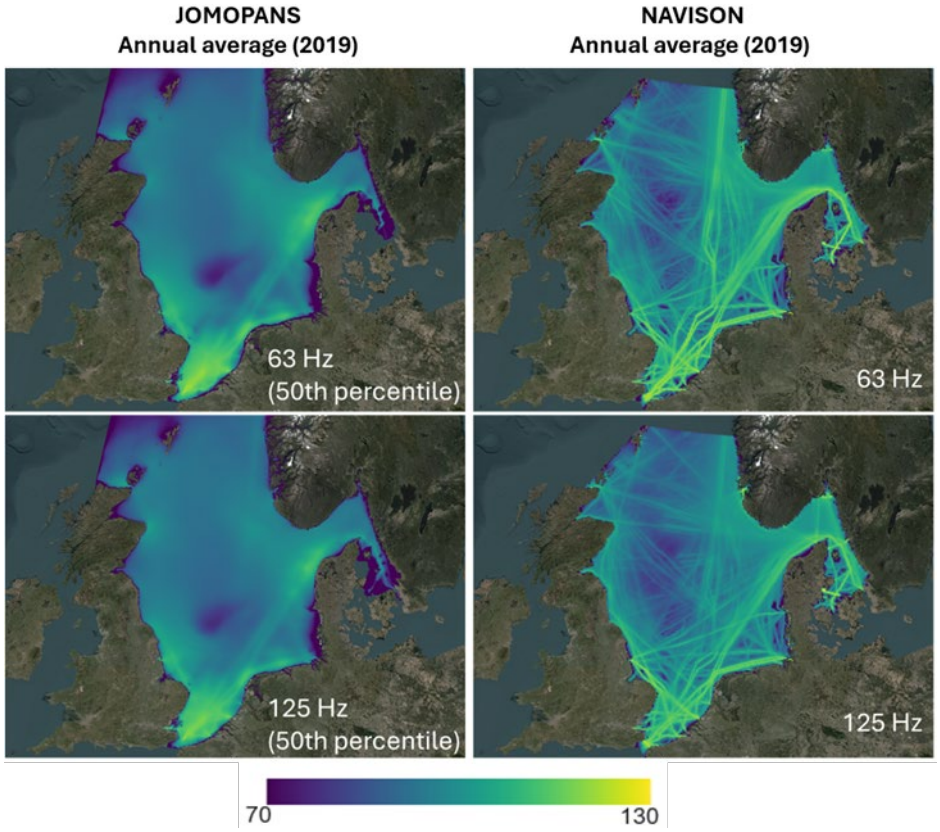

Figure 95 Comparison between JOMOPANS (left) and NAVISON (right) and sound maps (SPL re 1 μPa^2, in dB) at (top) 63 Hz and (bottom) 125 Hz. The NAVISON results are based on spatially averaged sound pressure level while the JOMOPANS results are for the median (temporal 50 % exceedance level of depth-averaged sound pressure level). See Table 8 for detailed description of the metrics for each project.

JOMOPANS sound maps also adopt a time-statistics approach and calculates the sound maps at different percentiles. Consequently, the metrics differ once more between NAVISON (arithmetic mean) and JOMOPANS (median).

Another comparison with JOMOPANS is added to show the differences between different percentiles in Figure 96. JOMOPANS maps with different percentiles are only available for consider the contribution of wind in the shipping sound maps. The shipping sound maps without wind were only available for 50^{th} percentiles.

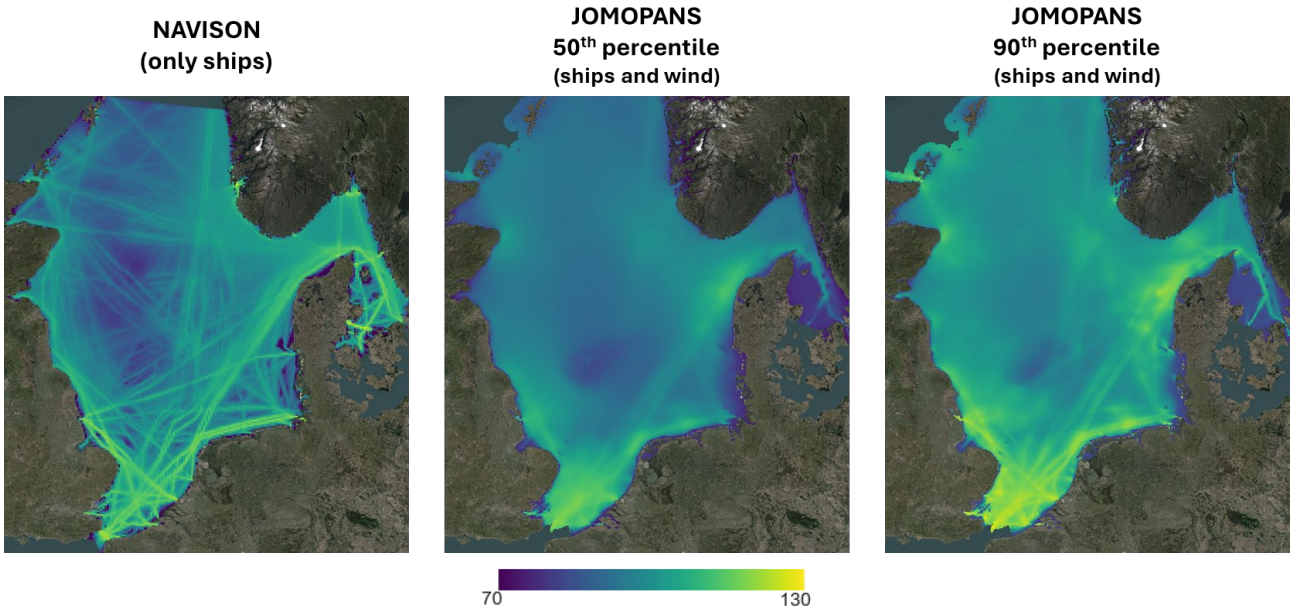

Figure 96 Comparison between NAVISON (only ships) and JOMOPANS (ships and wind) sound maps (SPL re 1 μPa^2, in dB) at 125 Hz. The NAVISON results are based on spatially averaged sound pressure level while the JOMOPANS results are for 50 and 10 % exceedance levels.

In the 10 % exceedance (90th percentile) sound map of JOMOPANS, the vessel tracks on the northern part of the sound map become more visible. The effect of wind is mainly visible at Dogger Bank and does not seem large at 125 Hz. However, a larger contribution from the wind is expected at higher frequencies.(Sertlek et al. 2019b).

5.2.3 HELCOM BLUES/ HOLAS 3 Project

The third HELCOM holistic assessment (HOLAS 3) examines the ecosystem health of the Baltic Sea from 2016 to 2021 (HELCOM BLUES 2023). As part of this analysis, sound maps of the Baltic Sea were computed at 63, 125, and 500 Hz (decidecade bands). The modelling was performed for four different layers: transport noise, natural sound pressure level (SPL), excess level, and total SPL. The RANDI3 source model is used to calculate the source level of commercial vessels. Monthly sound maps (corresponding to TAW) were calculated with a spatial resolution of 400 × 400 m (SOW is unstated) and a temporal resolution of 1 h (TOW is unstated) (HELCOM BLUES 2023).

Monthly, quarterly, and annually sound maps of 2018 are available from ICES (2024) in netCDF format. Figure 97 shows HOLAS 3 (HELCOM BLUES) and NAVISON sound maps for 2018. Expected differences between the HOLAS 3 and NAVISON maps, considering the known difference between mean and median, are confirmed.

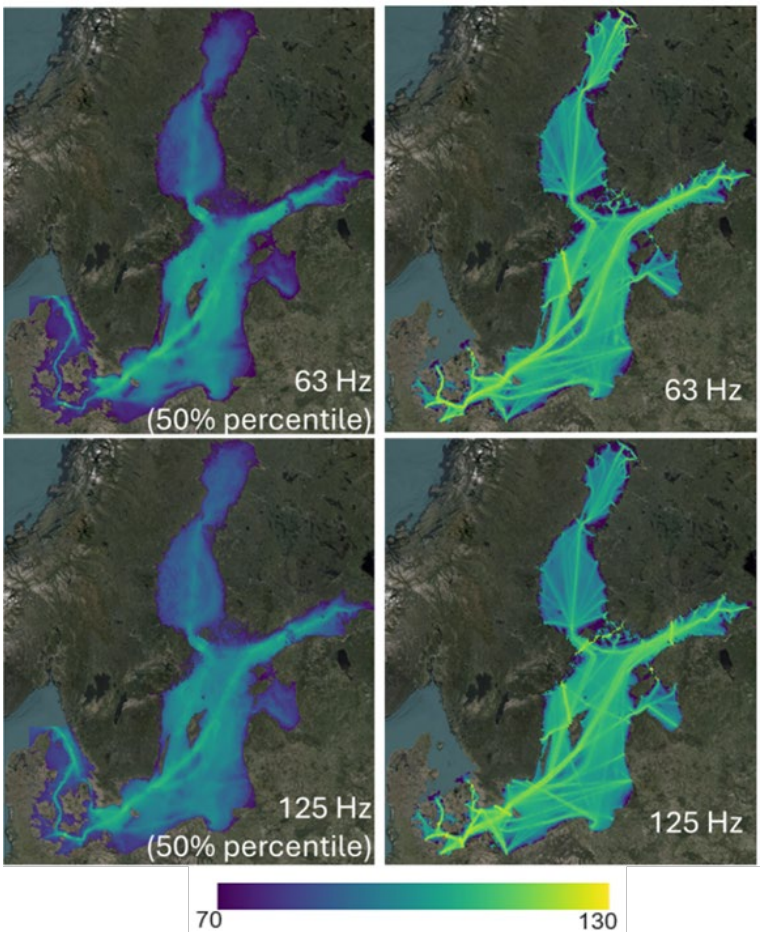

Figure 97 Comparison between HOLAS 3 (HELCOM BLUES) (left) and NAVISON (right) sound maps at (top) 63 Hz and (bottom) 125 Hz. The NAVISON results are based on spatially averaged sound pressure level while the HOLAS 3 (HELCOM BLUE) results are for the median (50th percentile) of SPL.

6. Discussion and Conclusions

6.1 Innovations during the NAVISON projects

The NAVISON project has developed methods and tools for producing large-scale shipping sound maps in European waters. These include tools for the following:

- Vessel traffic data processing,
- Source level computations,
- Acoustic environmental model automation,
- Source density processing,
- Ship sound propagation, and
- Sound map post-processing.

In most cases, these tools are based on MARIN and JASCO's existing software (such as DECS and ARTEMIA), which have been augmented with new capabilities and databases to meet EMSA's requirements for the NAVISON project. The sound mapping methodology developed using an efficient energy-based modelling approach, computes time-averaged SPL over large spatial scales using source density grids derived from AIS ship track data. Spatial averaging of the mean-square sound pressure in the receiver grid captures the received sound pressure levels in more detail within each grid cell, leading to more accurate estimates of total acoustic energy. This approach is expected to significantly improve sound pressure level predictions near source locations, where propagation loss changes rapidly with position. Applying the same source, propagation, and sound mapping approach across all European regions facilitates comparisons between regions, years, traffic scenarios, and technical/operational measures. Sound energy density is a linear quantity, to which the principle of conservation of energy applies, thus providing a practical way to perform the following:

- Analyse the time trend of the underwater sound in a selected region/frequency band/averaging time (quarter and year),
- Quantify the relative contribution of the different vessel categories,
- Quantify the performance of mitigation measures for the forecast scenarios, and
- Visualise the information in the large set of sound maps with simplified graphs.

The NAVISON project involves a novel, state-of-the-art, semi-empirical, source-level model (PIANO) for machinery and cavitation, which was described in the Task 1.1 progress report (Lloyd et al. 2024a). Many previous studies used the RANDI (Breeding et al. 1996) and Wales and Heitmeyer (2002) reference spectrum models to estimate the source levels of different ships. These methods have been shown to have relatively poor accuracy at low frequency (<500 Hz) when validated against to the ECHO data set (MacGillivray and de Jong 2021). The accuracy of the RANDI model was improved upon by JOMOPANS, which developed a modified RANDI model based on ECHO data. The NAVISON model, which builds on previous work, can provide even more accurate predictions of source levels for commercial vessels.

Another new development for the NAVISON project is the method to combine component sound map layers to produce forecast scenarios for arbitrary combinations of mitigation measures. The method introduced for this project is based on a probabilistic approach, whereby sound level changes associated with different combinations of measures are calculated by combining reduction layers ($\Delta L_M(x,y)$) according to joint probability tables for the different measures. The probability tables are computed according to the penetration rates of the different measures, rules for their implementation, and their probabilities of overlap. This method requires only that two SPL reduction layers, one for machinery noise and one for cavitation noise, be computed for each measure (corresponding to the 100 % penetration rate). For example, for the six reduction measures considered by NAVISON, a set of 12 reduction layers (6 for cavitation, 6 for machinery) must be produced for each vessel category. By combining this set of 12 reduction layers with two baseline layers, changes in sound levels may be evaluated for scenarios involving any combination of measures and penetration rates. Unlike existing approaches, which are restricted to static scenarios, this method allows for an arbitrary number of forecast scenarios to be evaluated for NAVISON. Furthermore, the capabilities of the NAVISON source model allow the various mitigation measures to be modelled in ways that were not previously possible using existing ship point-source models.

The following are examples of this for each of the mitigation measures:

- Under the speed reduction measure, differences in how fixed pitch and controllable pitch propellers are modelled mean that source level does not always decrease with a reduction in operating speed.
- For hull and propeller cleaning, separate changes in power requirement and rotation rate can be included.
- When considering an optimised hull form, not only could the gross effect on power requirement to accounted for, but also the improvement in propeller inflow, modelled by the propeller-tip, loading-wake, peak parameter.
- An additional advancement when modelling changes in propeller design is the adjustment of the estimated cavitation inception speed, which is derived from the speed dependency of the cavitation source model.

Finally, all these changes are modelled for cavitation and machinery noise separately, leading to more accurate predictions of the effect of mitigation on the total soundscape. This is due to the cavitation and machinery source models having different dependencies on different input parameters, with operating speed being perhaps the most important example.

Sound map layers are provided individually for each region and can be loaded with a uniform colormap for all regions using the provided PyQGIS scripts in QGIS. One of the potential benefits of using GIS software is the ability to overlay different properties on the maps. Figure 98 shows the sound map layer for the first quarter of 2022 at 63 Hz, including the marine protected areas (MPAs) in the Mediterranean Sea. By loading the map layers for different time periods, variations in the MPAs can be visually investigated.

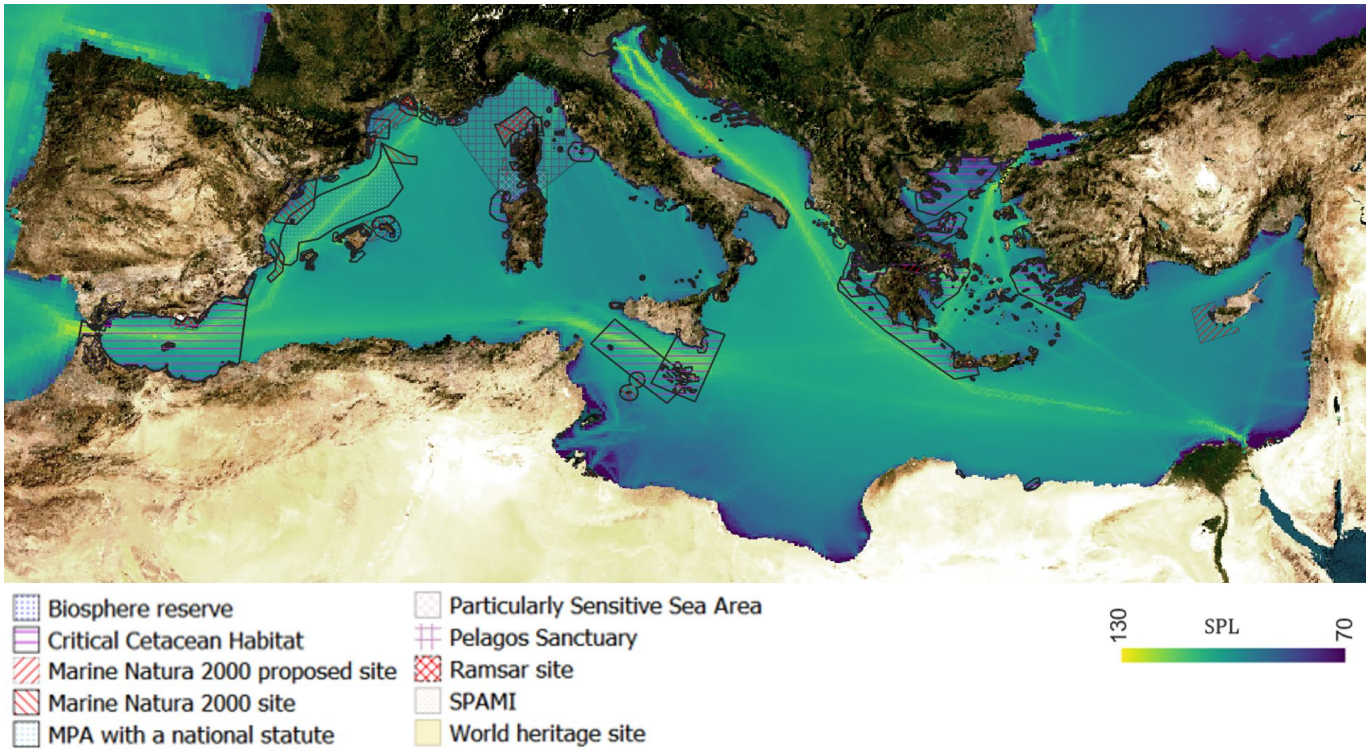

Figure 98 Sound map layer of Mediterranean Sea during the first quarter of 2022 at 63 Hz including marine protected areas (MPAs).

6.2 Discussion of Hindcast Results

After a detailed analysis of the sound map layers in both SPL and sound energy density metrics, answers were found for the questions listed in the introduction section, such as where are the regions with the highest and lowest SPL values, what are the temporal changes related to environmental (effects of seasonal changes and bathymetry) and non-environmental factors (including COVID-19 effects, changes in ship routes, etc.), and what are the rankings of different vessel categories and regions based on sound energy density.

The areas with the highest SPL values in Europe appear to be the English Channel, Strait of Gibraltar, Adriatic Sea, Dardanelles (Strait of Çanakkale), and some regions in the Baltic Sea (Kattegat, Arkona Basin, and Gulf of Finland), where SPL is above 120 dB for most of the years from 2016 to 2023.

The areas with the lowest SPL values seem like the northwest part of the northeast Atlantic Ocean (around Denmark strait and Irminger Sea), southern part of Mediterranean Sea (Gulf of Gabes and Gulf of Sidra), and east of Black Sea. However, having low SPL values outside of Europe regions could be related to limited AIS coverage in these regions. Furthermore, no vessel inputs are used outside of the NAVISON regions (i.e., from northwest Atlantic Ocean, beyond the Mid-Atlantic Ridge). Appendix A provides the boundaries of NAVISON regions.

The seasonal changes in the sound energy density can be explained by the variations in the sound speed profile. The largest sound energy density is observed in the quarters including winter and spring (quarters 1 and 2). The lowest sound energy density is observed in the quarter including summer (quarter 3). In shallow water regions (Baltic Sea and North Sea), the effect of the sound speed profile on propagation does not seem strong, as supported by detailed parametric analysis from earlier research (Sertlek et al. 2016b).

In some regions, the seasonal cycles in sound energy density are interrupted. One possible reason for this is related to the COVID-19 pandemic, which is mostly observed in the PAS vessel category. Additionally, changes in shipping routes, volume of traffic, and speed can cause variations in ASL map inputs. Consequently, these changes affect the sound map layers and sound energy density, as shown in Figures 32 and 36. The largest changes in ASL are mostly observed for TGC and PAS vessels. The contribution of the PAS vessel category to total sound energy is very low in most regions. However, changes in TGC vessels' sound energy density can have a large impact on the temporal pattern across all vessel categories Furthermore, the temporal changes in AIS data coverage can impact the results, as discussed in more detail in Section 4.

For Europe, the largest contribution to sound energy density at 63 Hz is from TGC (56.7 to 71.8 %) and CAR (21.5 to 34.2 %) vessel categories. The lowest contributions at 63 Hz are from RRO (3.7 to 5.7 %). CON (2.0 to 3.0 %) and PAS (0.4 to 1.9 %) vessel categories. At 125 Hz, the largest contribution to sound energy density is from CAR (26.9 to 35.3 %), RRO (29.2 to 35.0 %), and TGC (25.8 to 37.3 %). The lowest contributions at 125 Hz are from CON (2.6 to 3.9 %) and PAS (1.1 to 4.4 %). Appendix E provides a detailed analysis for each region, category, and frequency.

The ship type making the largest contribution to the total sound energy density differs between 63 and 125 Hz, and this can also be expected to be true for other frequency bands. While CON vessels were found to give a small contribution to the total sound energy density in NAVISON, their peak source level occurs at a lower frequency than for other vessel categories considered. This is because the frequency of the highest (broadband) cavitation source levels reduces as ship speed increases, an effect which is included in the PIANO model. This results in container ships typically exhibiting their highest source levels at lower frequencies than other ship types such as tankers and bulkers, as they have a higher design speed. This is illustrated in Figure 99 by comparing typical source level spectra for a tanker and a container ship.

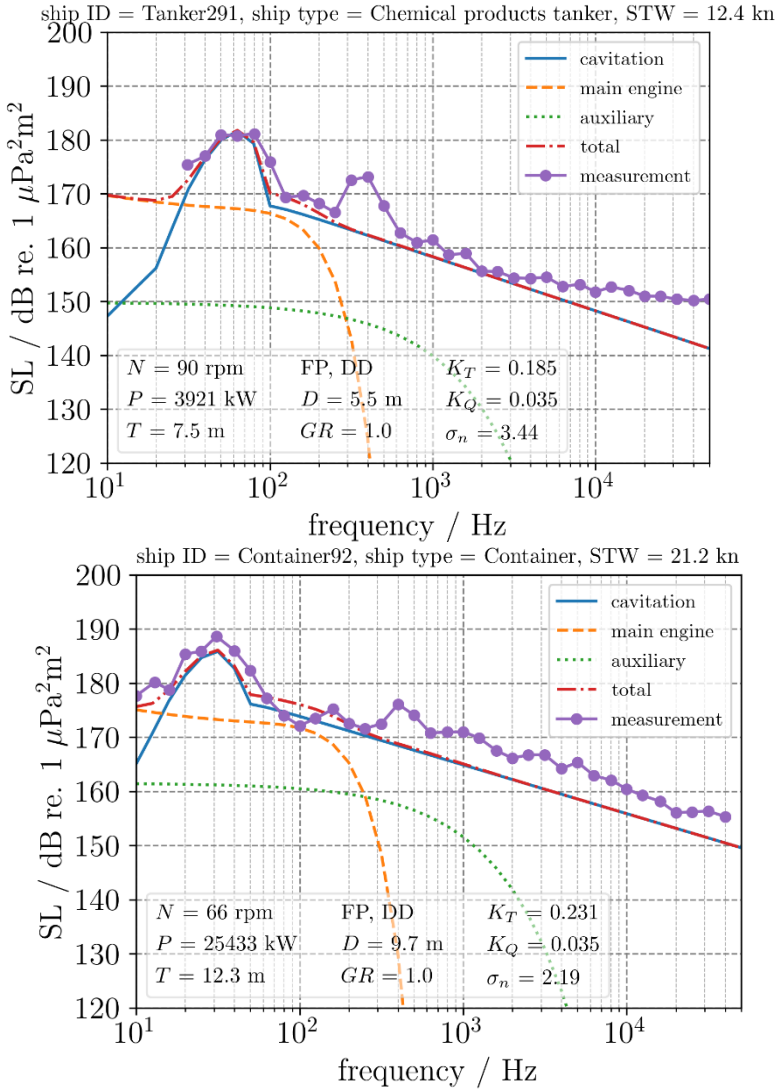

Figure 99 Example comparisons of source level in decibels (dB) as a function of frequency in Hertz (Hz) between the PIANO model and ECHO database measurement for (top) tanker and (bottom) container ship. The maximum modelled source levels of the two vessels occur at 63 and 32 Hz, respectively.

For both vessels, the highest broadband source levels predicted by the PIANO model are due to the cavitation noise spectral hump, typical of cargo vessels operating close to their design speed. While this occurs in the 63 Hz frequency band for the tanker, this reduces to 32 Hz for the container ship. For comparison purposes, the frequency bands of the peak source levels for tankers and container ships as predicted by the JOMOPANS-ECHO model (MacGillivray and de Jong 2021) are 63 and 40 Hz, respectively.

In addition, the height of the cavitation spectral hump relative to the rest of the spectrum affects the distribution of energy between frequency bands. In the PIANO model, tankers are modelled as having a more pronounced hump than container ships, resulting in the spectrum either side of the hump being 4 dB lower. This (partly) explains the higher difference in sound energy density between the 63 and 125 Hz frequency bands for tankers compared to container ships (Figure 16), further motivating the study of additional frequency bands.

For the example of Figure 99, the CON source level is 13 dB higher than TGC at 32 Hz, and 3 dB lower at 63 Hz, implying a 16 dB difference overall. Thus, if these differences are found to be representative of CON and TGC vessels generally, the contribution from CON vessels is likely to be larger than the contribution from TGC vessels at 32 Hz. Any statement about the relative contribution of CON vessels at frequencies below 63 Hz would, therefore, need further investigation.

The Baltic Sea has the highest sound energy density of the regions considered. This is a consequence of the high vessel density and shallow water (low sea water volume). Conversely, in the northeast Atlantic Ocean, when the sea water volume size increases, the sound energy density decreases.

The AIS coverage plays an important role in obtaining accurate results based on the sound energy density analysis. As mentioned in the limitations, there were also some temporal variations in the amount of AIS data, separate from any seasonal fluctuations and changes in traffic. For instance, only terrestrial-based AIS data were available between July 2020 and December 2021, both satellite and terrestrial AIS data included outside of this period. Additionally, terrestrial AIS data were missing in UK waters following Brexit in 2020. Due to these limitations, it is difficult to separate the effects of the COVID-19 pandemic in the same years or the recovery from COVID-19 after 2021.

6.3 Discussion of Forecast Scenario Results

The overall trends of the changes in sound energy density over time are generally as expected, considering the modelling framework and inputs used. Taking Europe as a whole, increases in sound energy density until 2050 are observed under the GHG scenario, reflecting the fact that not all mitigation measures represent a “win-win” situation for both GHG and URN. However, this small net increase can be attributed to a couple of regions (North Sea and northeast Atlantic Ocean) and ship types (TGC and CON). In general, increases in sound energy density are driven by the effect of the More Efficient Propeller measure, for which an increase in vessel cavitation source level is modelled. As may be expected in the URN scenario, the sound energy density decreases consistently over time for all regions and ship types, primarily because the MEP measure has been replaced by the Quieter Propeller measure. However, this scenario is less realistic given that it ignores the existing regulations for GHG emissions. The U&G scenario can be considered the most realistic, being inspired by the mandatory GHG regulations and the assumption of future noise policy becoming stricter over time. This is reflected in the results, whereby the rate of sound energy density reduction increases between 2030 and 2050. Even for the TGC category, which has the largest contribution to the total sound energy density, initial increases in sound energy density in certain regions give way to decreases by 2050. This reflects the trade-off between efficiency and URN in propeller design, modelled here by blending the effects of the MEP and QRP measures, while also accounting for improvements in propeller design over time, which is achieved by adjusting the penetration rates such that QRP are more widely adopted in 2050 than MEP (see Table 19).

Since the mitigation measures are modelled in the same way for all regions and ship types, changes in the results across regions and ship types derive from differences in the input data used in the modelling. For example. the noticeable increases in sound energy density for the TGC category (and in a couple of cases for CON) can be explained by examining the results for the percentage change in sound energy density for each mitigation measure, for the case of 100 % penetration rate. In general, the sound energy density is estimated to increase more for TGC when applying a MEP than for other ship types. This is because a higher proportion of vessels within this category were modelled as being eligible for a new propeller offering a larger increase in efficiency, with an associated higher increase in cavitation source level. Of all ship type categories, TGC also has the lowest proportion of vessels assumed to not need to retrofit their propeller. Since the loudest vessels contribute more to the soundscape, the MEP measure can have a stronger effect on the results than other measures for which the source levels decrease. An additional factor is the relative effect of the other mitigation measures included in the scenario. Recall that the GHG scenario is modelled using a combination of the HPC, MEP and SRD measures. For all regions apart from the Mediterranean, the modelled effect of HPC and SRD measures (together with the chosen penetration rates) is not sufficient to cancel the effect of MEP, resulting in an increase in sound energy density compared to BAU. However, the Mediterranean Sea, the relative increase due to MEP is smaller, while the decreases due to HPC and SRD are larger, resulting in a net decrease in sound energy density in this case. The same explanation holds for the CON category in the northeast Atlantic Ocean and North Sea.

The effect of TGC also has a large effect on the results for all ship types due to this ship type category having the highest sound energy density, despite there being fewer individual TGC vessels than in the CAR category. This is thought to be related to gross differences between the ship types included within each of these two categories. The CAR category contains relatively more vessels with four-stroke engines, which are more likely to contribute more at frequencies above 63 Hz due to their higher engine/propeller rotation rate (this can be seen in, for example, Figure 16).This also means that one of the dominant effects leading to changes in vessel source levels under the forecast scenarios – changes in magnitude and frequency of the cavitation spectral hump – are not as pronounced at 63 Hz than they would be at higher frequency bands such as 125 Hz. This motivates inclusion of multiple frequency bands in future projects looking at forecast scenarios, in order to gain additional insights into the effectiveness of mitigation measures. This is expected to be even more relevant when using the PIANO model, in which cavitation and machinery source levels are modelled separately, resulting in different (relative) changes in these contributions to the total source levels when applying mitigation measure modelling (as summarised in Lloyd et al. (2024c)) while the centre frequency of the cavitation spectral hump shifts as a function of vessel operating condition – this shift being inversely proportional to propeller rotation rate for fixed-pitch propellers. Since the cavitation hump dominates over a

relatively small frequency range and exhibits a high slope compared to the rest of the total spectrum, changes in source level can be strongly dependent on frequency. This implies that the effectiveness of mitigation measures involving changes in propeller rotation rate will also be frequency-dependent, and source levels may decrease in one frequency band while increasing in another. This effect is illustrated in Figure 100, which can be considered representative of the case of speed reduction from design speed to 75 % of design speed, as was assumed in NAVISON. Although the magnitude of the hump reduces under SRD, part of the mitigation effect at 63 Hz results from the hump shifting to higher frequencies, leading in this example to an increase in source level at 125 Hz. While it is not suggested that this will occur for all vessels all the time, it is recommended to study this effect in more detail.

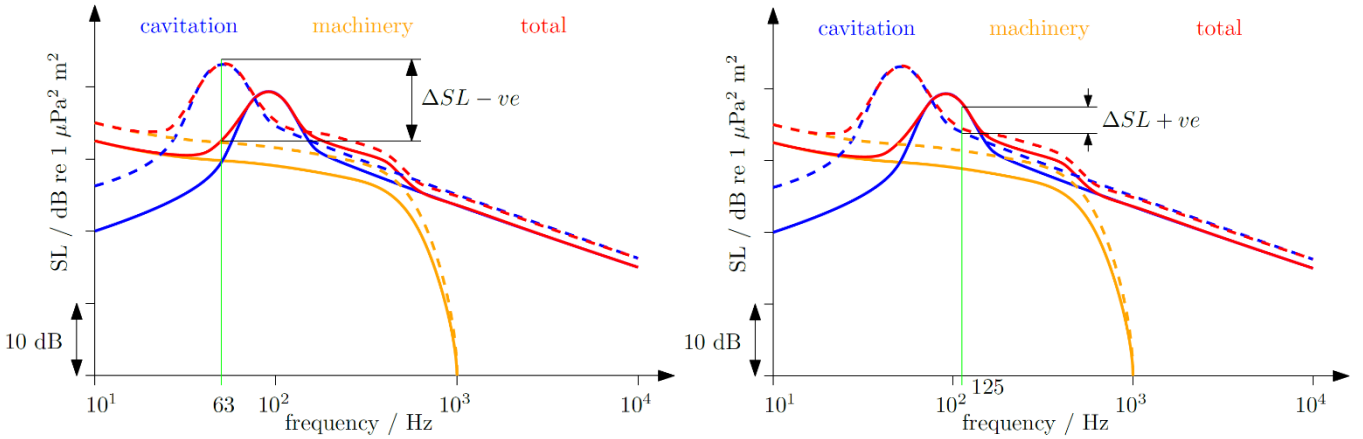

Figure 100 Illustrative changes in PIANO model source levels for a large cargo vessel equipped with two-stroke engine and fixed-pitch propeller, under mitigation scenarios involving reductions in propeller/engine rotation rate. Source levels due to cavitation and machinery shown in blue and yellow, with the total source level in red. Solid and dashed lines indicate the source levels with and without mitigation. The left plot highlights the total source level reduction at 63 Hz, while the right plot shows the source level increase at 125 Hz, when applying mitigation.

The mitigation measures selected for modelling allowed scenarios to be simulated based on expected developments in GHG and URN management. Six mitigation measures were selected out of 16 initially considered (see Lloyd et al. (2024c)). Under each of the GHG and URN scenarios three measures were applied concurrently, while all six measures were included in the more realistic U&G scenario. In reality, a higher number of measures will be implemented across the fleet and European region.

Since the novel modelling approach adopted by NAVISON allows the generation of an unlimited number of sound maps using an existing set of input map layers, new results can be obtained under modified scenarios at relatively low effort. For example, using only the existing input map layers, new results for the GHG scenario that consider revisions to IMO's GHG reduction strategy could be generated.

A pragmatic approach to account for the effects of additional mitigation measures not included in NAVISON could be to identify measures that have a similar effect on vessel source levels as those already modelled (e.g., reductions in operating power and rotation rate). New scenarios could then be developed by adjusting (increasing) the penetration rate of the relevant measures, with this increase acting as a proxy of the measure(s) not explicitly modelled. In this way, no new input map layers need to be generated. Alternatively, additional map layers for other mitigation measures could be produced as part of future work in order to increase the realism of the scenarios. Although accounting for mitigation effects in a gross sense, the former approach omits certain modelling details and is, therefore, expected to result in a higher uncertainty than the later approach.

6.4 Analysis with Different UNLV Values

TG Noise 2023 (Borsani et al. 2023) suggests a framework to assess impact of continuous sound. This framework includes the calculation of the level of onset of biologically adverse effects (LOBE), which is related to an indicator species in the region. TG Noise defines LOBE as "The noise level at which individual animals start to have adverse effects that could affect their fitness." Their definition also includes the following clarifications:

- "Examples of adverse effect include behavioural disturbance, stress, reduced communication space, and temporary or permanent habitat loss.

- Fitness is the ability of an individual to successfully reproduce relative to other individuals in the population. If an animal experiences a loss in fitness, it means that its reproductive output is affected negatively, even if only slightly.
- For continuous noise D11C2, noise level that can be spatially averaged sound pressure level or excess level."

As recently discussed in the SATURN Acoustical Terminology Standard report (Ainslie et al. 2024), TG Noise definition lead some questions as below:

- What is "noise level"?
- What is meant by "start to have"?
- What is meant by "adverse effects"?
- What is meant by "could affect their fitness"?

SATURN D2.3 (Ainslie et al. 2024) explains the ambiguities in the TG Noise definition of LOBE and proposes the alternative term 'underwater noise limit value' (UNLV), which is defined as "value of a specified underwater noise metric, as determined by an appropriate authority, above which management action is considered".

In the following examples, the term UNLV is used. The analysis has been performed using three limit values (re 1 μPa²): 100, 110, and 120 dB. While no specific animal groups or adverse effects of sound on them are investigated, the changes in areas below and above these limit values have been examined from 2016 to 2023 for all of Europe at 63 Hz. The TOW is chosen as 1 year for the results shown. Figures 101, 102, and 103 illustrate sound map layers for UNLV values of 100, 110, and 120 dB, respectively. The areas above UNLV are shown in red, while a blue gradient is used for areas below the limit value. Specifically, areas up to 1 dB below the limit value are shown in white to mark areas at risk of exceeding UNLV in the event of an increasing trend.

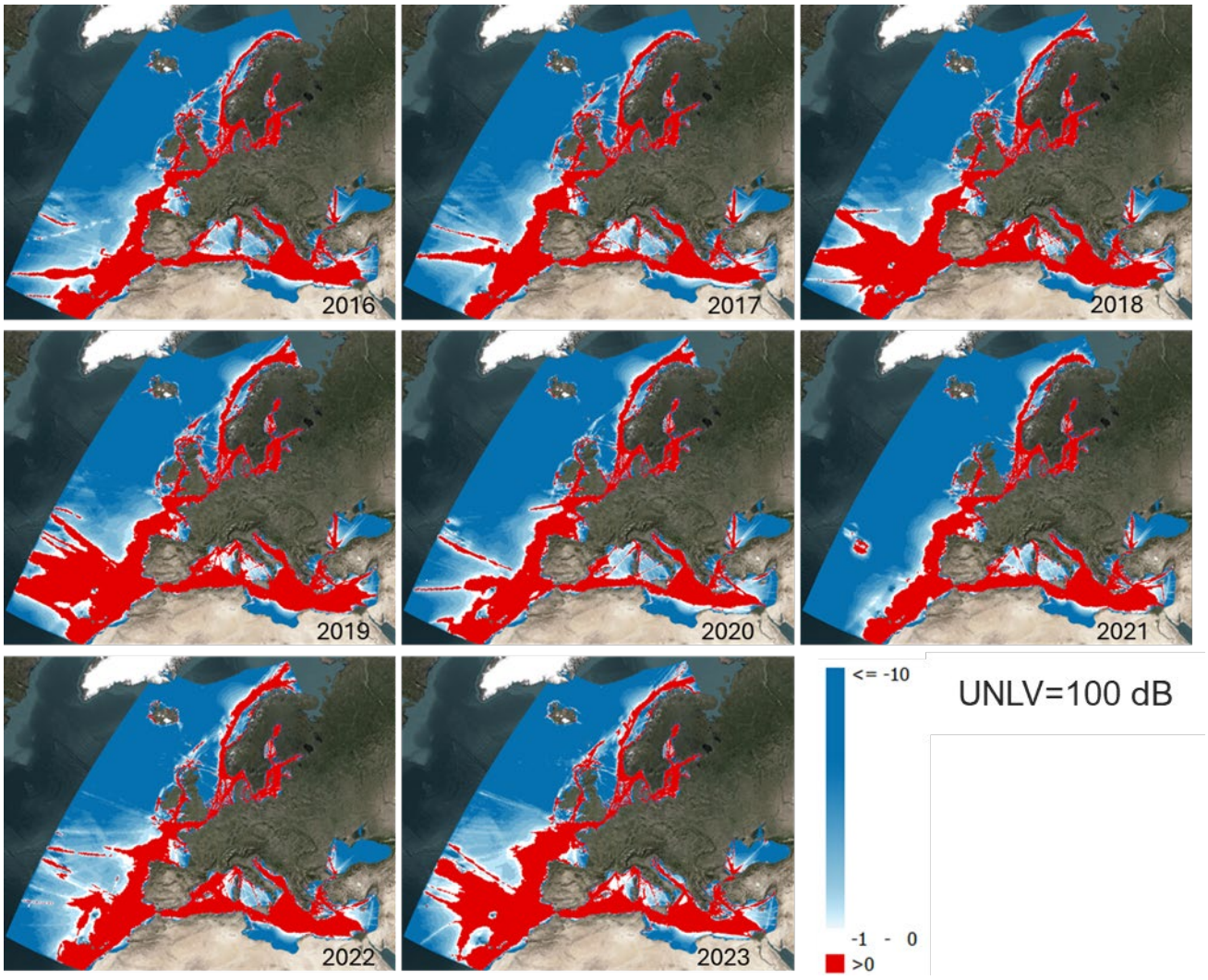

Figure 101 Sound map layers of Europe with an underwater noise limit value (UNLV; re 1 μPa²) of 100 dB (63 Hz band).

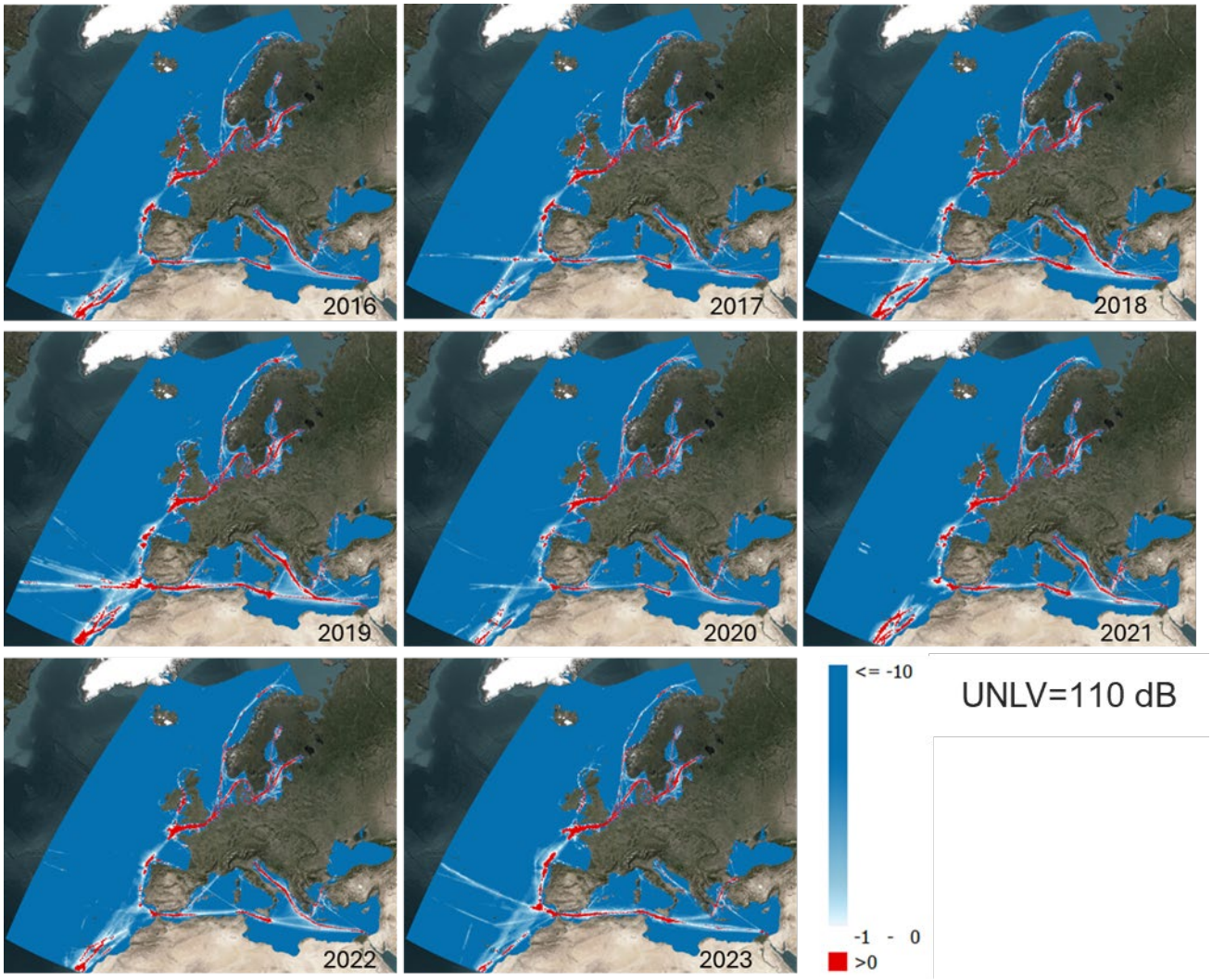

Figure 102 Sound map layers of Europe with an underwater noise limit value (UNLV; re 1 μPa^2) of 110 dB (63 Hz band).

When the UNLV is 110 dB, the main shipping lanes in the southern North Sea, English Channel, Baltic Sea, Adriatic Sea, Alboran Sea, Strait of Gibraltar, Sea of Sicily, Libyan Sea, Aegean Sea, and Marmara Sea can be identified as areas with SPL above 110 dB.

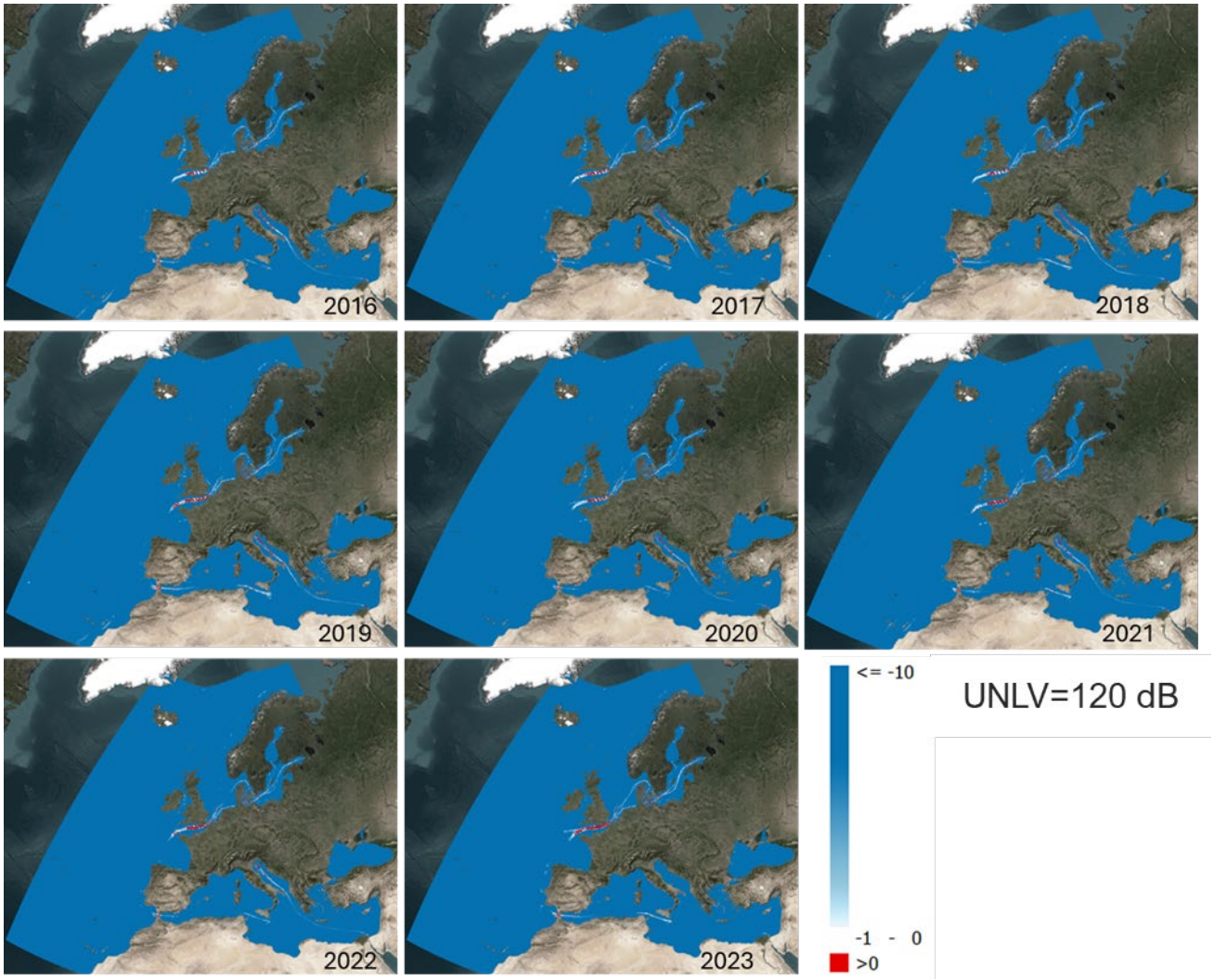

Figure 103 Sound map layers of Europe with an underwater noise limit value (UNLV; re 1 μPa^2) of 120 dB (63 Hz band).

The sound map layers of Europe with UNLV of 120 dB also helped to identify the spots with the largest SPL values in the Europe. These areas appear to be the English Channel, Strait of Gibraltar, Adriatic Sea, Dardanelles (Strait of Çanakkale), and some regions in the Baltic Sea (Kattegat, Arkona Basin, and Gulf of Finland), where SPL was above 120 dB for most of the years from 2016 to 2023.

6.5 On the Need for International Standards for Ambient Sound Monitoring

A successful coordinated implementation of MSFD Descriptor 11 (D11) by EU member states (MS) requires harmonised regional ambient sound monitoring programmes. Ambient sound monitoring involves both measurements and modelling, as described by the TG Noise report published in 2023 (Borsani et al. 2023), henceforth referred to as TG Noise (2023), which entails the need for model verification and model validation procedures. Thus, the measurement and modelling of ambient sound require common standards rooted in a harmonised terminology.

The SATURN project has issued a policy brief that emphasises the urgent need for appropriate terminology:

> "The SATURN project urgently recommends the adoption of existing international terminology standards and the development of standardised and agreed-upon terminology to facilitate effective communication, a pre-requisite for monitoring and mitigation efforts worldwide".

6.5.1 Ambient Sound Terminology and Underwater Noise Metrics

Clear definitions of the terms used for assessing underwater noise are essential for effective communication, without which there can be no effective implementation. Progress by MS in their implementation of MSFD D11 is presently hampered by the absence of clear terms and definitions.

Terminology provides the foundation upon which other standards can be developed. ISO 18405 provides basic acoustical terminology (e.g., sound pressure level), but specialised terms used for ambient sound monitoring (e.g., temporal observation window, spatial observation window, excess level) are not included in that standard.

The Environmental Noise Directive (END) includes, in Article 3, a list of terms and clear definitions that has no counterpart in the MSFD itself (EC 2008), in the 2017 Commission Decision (EC 2017), or in TG Noise (2023) . As a result, some terms in the latter documents can be interpreted in different ways by different MS, potentially leading to misunderstandings.

'Noise Indicator' and 'Limit Value' in the Environmental Noise Directive (END)

The END defines the concepts of a noise indicator and a limit value. Four noise indicators, L_{day} (day-noise indicator, for annoyance during the day period), $L_{evening}$ (evening-noise indicator, for annoyance during the evening period), L_{night} (night-time noise indicator, for sleep disturbance) and L_{den} (day-evening-night noise indicator, for overall annoyance), are introduced. All are defined, via Annex I of the END, by ISO 1996-2:1987. While use of L_{day} and $L_{evening}$ is optional, use of L_{den} and L_{night} by MS is mandated by the END.

The END does not specify the noise limits, as it is the responsibility of individual MS to set appropriate values of these. If the noise limits are exceeded, competent authorities are then required to consider or enforce mitigation measures.

The MSFD and LOBE

In the MSFD, the conceptual parallels of the END's noise indicator and limit values are intertwined. TG Noise (2023), which provides MS with guidance to implementation, introduces the concept of level of onset of adverse biological effects (LOBE), the logical equivalent of the END's *limit value*. What is missing is a clear description of the corresponding *noise indicator*.

The Noise Indicator: Noise Level

According to the TG Noise 2023 report, LOBE is the "noise level at which individual animals start to have adverse effects that could affect their fitness", suggesting that a specified limit on 'noise level' is the quantity above which mitigation action is to be considered, and hence the term most closely related to the END's noise indicator. TG Noise (2023) describes two metrics that can be reasonably interpreted as 'noise level'. These are SPL and excess level (EL):

- *sound pressure level* (SPL) is defined by ISO 18405:2017, which requires one to specify an averaging time (temporal observation window, or TOW) and a frequency band. Further, while ISO 18405 does not mention spatial averaging, the quantity plotted on maps is nearly always spatially averaged, creating a further need to specify the spatial observation window (SOW).
- *excess level* (EL) is defined by SATURN D2.3 (Ainslie et al. 2024)[9] as "SSSPL (for all ambient sound) minus SSSPL (for natural ambient sound) at the same position and time", where SSSPL is an abbreviation for *steady state sound pressure level*.[10] This definition is supplemented by the remark: "Sometimes a statistic of excess level, such as the median in space and time, is represented on a map."

Thus, SPL and EL in the MSFD take the place of L_{den} and Lnight in the END, with an important difference. While L_{den} and Lnight are clearly specified (Annex I of END), there is no comparable specification of SPL and EL. Specifically, there is no guidance on a suitable choice of TOW or SOW. This absence of guidance on TOW leads to an uncertainty that can be in the region of 10–15 dB (TG Noise 2023). There is no such ambiguity in the END, which specifies a TOW duration of one year.

A further source of confusion is the mention of '1/3-octave bands' in CD 2017/848/EU by the European Commission (2017). In 2010, when MSFD indicators were first specified in 2010/477/EU (EC, 2010), one-third octave (1/3 oct) and one-tenth decade (1/10 dec) frequency bands were compliant with international standards. The advice of TG Noise (van der Graaf et al. 2012), consistent with modern standards (e.g., IEC 61260-1:2014, ISO 17208-2:2019, ISO/DIS 7605:2024), to use 1/10 dec (decidecade) bands was followed by some projects, including NAVISON, while 1/3 oct was adopted by others (Table 8). Thus, the mention of '1/3-octave bands' in CD 2017/848/EU, when TG Noise advice (and international standards) require 1/10 dec bands, creates unnecessary confusion.

Progress Towards Standard Terminology

Existing international standards relevant to underwater acoustics include ISO 80000-8:2020 Quantities and units – Acoustics and ISO 18405:2017 Underwater acoustics – Terminology.

A standard specific to bio-acoustical terminology is under development (ISO/AWI 23990 'Underwater acoustics – Bioacoustical terminology'). The project held its kick-off meeting in February 2024. The standard ISO 23990 is scheduled for publication in 2026.

Choice of Underwater Noise Metric

The selection of an underwater noise metric would facilitate quantitative comparison between sound maps from different projects. The main priority is the choice of TOW, to avoid the aforementioned ambiguity. A choice of SOW is also needed.

6.5.2 Ambient Sound Measurement

No international standards for ambient sound measurement presently exist. Project standards were developed by the ADEON and JOMOPANS projects, and these project standards – together with measurement guidelines

[9] According to TG Noise (2023), "TG Noise has decided to follow the SATURN terminology standard, which is based on and fully compatible with ISO 18405"

[10] *steady state sound pressure level* is defined by SATURN D2.3 as "for specified sources, sound pressure level that would arise (at position x) if the specified sources were stationary at their actual positions, but with the same steady state source level that the sources would have had if they had remained moving at their actual speed". This definition is supplemented by the following remarks:

- "SSSPL is a hypothetical construct. It is not physically realisable."
- "The term SSSPL applies to various anthropogenic and natural sources, including ships and wind."
- "The steady state sound pressure level can be spatially averaged."
- "The spatial observation window shall be specified."

developed by NPL (Robinson et al. 2014) – are being used as the basis for an international standard under development (ISO/DIS 7605 'Underwater acoustics – Ambient sound measurement'). The project started in 2021, and the standard is scheduled for publication in 2025.

6.5.3 Ambient Sound Modelling

Many different modelling methods are applied to produce sound maps. There is no single method generally acknowledged as the most appropriate, and in fact there is no need in the short term to standardise the method. Instead, it is appropriate to develop harmonised procedures for verification and validation, enabling one to quantify the accuracy and uncertainty of the sound maps.

No international standards for ambient sound modelling presently exist. Guidelines were developed by JOMOPANS (de Jong et al. 2021). The Aquatic Noise workshop (Berlin, July 2022) addressed the need for model verification, and some of the results have been published in a special issue of JASA/JASA-EL (Church 2024):

- Chapman (2024) provides measurements of source level for wind, and
- Martin (2024) addresses model verification for ships.

Other manuscripts are currently in the publication process, including one addressing model verification for wind.

A validation procedure is also needed to quantify the accuracy of a sound map.

7. Recommendations

Based on lessons learned during the NAVISON project, the following recommendations could be considered for harmonisation and general improvement of future studies.

7.1 Harmonisation

Terminology for Underwater Ambient Sound

Recommendations related to standardising terminology are:

- Follow general acoustical terminology of ISO 80000-8.
- Follow underwater acoustical terminology of ISO 18405.
- Support and facilitate the completion and publication of ISO 23990, for bio-acoustical terminology.
- Avoid use of “one-third octave” to mean one tenth of a decade (1/10 dec); specifically, update the language of CD 2017 to replace any mention of “1/3 oct” with “1/10 dec”, one-tenth decade or decidecade.
- Provide clear and unambiguous definitions of terms needed for underwater noise assessment (e.g., UNLV, UNM, TOW).

Underwater Noise Metric

Recommendations related to standardising the underwater noise metric are:

- Harmonize the metrics to eliminate difficulties in comparing different projects as mentioned in Section 4:
  - In the short term, follow recommendation from TG Noise (2014) to adopt a universal metric for all projects (the arithmetic mean) to facilitate quantitative inter-project comparisons. The arithmetic mean is easy to calculate and robust to the choice of TOW.
  - In the long term, seek consensus on other harmonized metrics.
- Consider the need for additional underwater noise metrics to complement the arithmetic mean (UNM).
- Select and specify a harmonised value of TOW for the selected UNM.
- Provide clear guidance for the choice of SOW.

Underwater Ambient Sound Measurement Standard

Recommendations related to standardising measurement of underwater ambient sound are:

- Facilitate successful completion and publication of ISO 7605.
- Promote use of ISO 7605.

Underwater Ambient Sound Modelling Standard

Recommendations related to standardising modelling of underwater ambient sound are:

- Develop harmonised procedures for model verification.
- Develop harmonised procedures for model validation.

7.2 General Recommendations

The following guidance points apply to using map layers:

- When comparing map layers between regions, use mean sound energy density, not spatial statistics of SPL. Spatial statistics of SPL (e.g., quantiles, mean, and standard deviation) should be avoided when comparing the provided map layers between regions since variations in SOW between regions can yield misleading results.

The following future improvements to the PIANO model are desirable:

- Improve accessibility and usability of the model by simplifying the input parameters required.
- Validate the model for other ship types carrying AIS(-like) transponders, such as fishing vessels.
- Model the contributions of additional sources, such a low-frequency tonal sound from propellers and propulsion machinery.

Changes in model accuracy and uncertainty resulting from the above could be assessed using a similar approach as was used in NAVISON (i.e., using a ship source-level database).

Future projects expanding on NAVISON should encompass the following aims:

- Produce hindcast and forecast sound maps for a wider range of decidecade bands. Of special interest are frequencies below 63 Hz (to investigate the contribution of container ships) and between the MSFD frequencies (i.e., at 80 and 100 Hz) to aid in the interpretation of the 63 and 125 Hz maps.
- Model additional mitigation measures, e.g., wind propulsion, just-in-time arrival, and optimised controllable pitch propeller operation (combinator curve), to improve the realism of forecast scenario results.
- Calculate contribution from wind, which is essential for quantifying exceedance level and potentially important for higher frequencies.
- Validate the existing maps with measurements and quantify the difference between modelled and measured SPL.

Literature Cited

[CMEMS] Copernicus Marine Environment Monitoring Service. 2023. Global Ocean Physics Reanalysis. https://doi.org/10.48670/moi-00021 (Accessed 2023).

[DNV] Det Norske Veritas. 2022. *Maritime forecast to 2050. Energy transition outlook 2022*. Høvik, Norway.

[ICES] International Council for the Exploration of the Sea. 2024. Continuous Noise Database. https://www.ices.dk/data/data-portals/Pages/Continuous-Noise.aspx (Accessed 2024).

[IMO] International Maritime Organization. 2021. *Fourth IMO GHG Study 2020*. Technical report by IMO, London, UK. https://www.imo.org/en/ourwork/Environment/Pages/Fourth-IMO-Greenhouse-Gas-Study-2020.aspx.

[IMO] International Maritime Organization. 2022. *Improving energy efficiency of ships* (web page). https://www.imo.org/en/OurWork/Environment/Pages/Improving%20the%20energy%20efficiency%20of%20ships.aspx. (Accessed 2023).

[IMO] International Maritime Organization. 2023a. *MEPC 80/WP.12, Annex 1, Resolution MEPC.377(80). IMO Strategy on Reduction of GHG Emissions from Ships*. p. 17. https://wwwcdn.imo.org/localresources/en/MediaCentre/PressBriefings/Documents/Resolution%20MEPC.377(80).pdf.

[IMO] International Maritime Organization. 2023b. *MEPC.1/Circ.906, Revised guidelines for the reduction of underwater radiated noise from shipping to address adverse impacts on marine life*. p. 21. https://wwwcdn.imo.org/localresources/en/Documents/MEPC.1-Circ.906%20-%20Revised%20Guidelines%20For%20The%20Reduction%20Of%20Underwater%20Radiated%20Noise From%20Shipping%20To%20Address...%20(Secretariat).pdf.

[IQOE] International Quiet Ocean Experiment. 2019. *Guidelines for Observation of Ocean Sound*. *IQOE Workshop*, 13 Jul 2019, Den Haag, Netherlands, p. 18. https://scor-int.org/wp-content/uploads/2022/08/IQOE_2019_Standards_Workshop_Report.pdf.

[ISO] International Organization for Standardization. 1987. *ISO 1996-2:1987. Acoustics — Description and measurement of environmental noise — Part 2: Acquisition of data pertinent to land use*. https://www.iso.org/standard/6749.html.

[ISO] International Organization for Standardization. 2020. *ISO 80000-8:2020. Quantities and units — Part 8: Acoustics*. https://www.iso.org/standard/64978.html.

[ISO] International Organization for Standardization. 2024a. *ISO/DIS 7605. Underwater acoustics — measurement of underwater ambient sound*. https://www.iso.org/standard/87649.html.

[ISO] International Organization for Standardization. 2024b. *ISO/AWI 23990. Underwater acoustics — bioacoustical terminology (under development)*. https://www.iso.org/standard/87649.html.

Ainslie, M.A. 2010. *Principles of Sonar Performance Modeling*. Praxis Books. Springer, Berlin. https://doi.org/10.1007/978-3-540-87662-5.

Ainslie, M.A., J.L. Miksis-Olds, S.B. Martin, K.D. Heaney, C.A.F. de Jong, A.M. von Benda-Beckmann, and A.P. Lyons. 2018. *ADEON Underwater Soundscape and Modeling Metadata Standard*. Version 1.0. Technical report by JASCO Applied Sciences for ADEON Prime Contract No. M16PC00003. 35 p. https://doi.org/10.6084/m9.figshare.6792359.v2.

Ainslie, M.A., R.K. Andrew, B.M. Howe, and J.A. Mercer. 2021a. Temperature-driven seasonal and longer term changes in spatially averaged deep ocean ambient sound at frequencies 63–125 Hz. *Journal of the Acoustical Society of America* 149(4): 2531–2545. https://doi.org/10.1121/10.0003960.

Ainslie, M.A., C.A.F. de Jong, S.B. Martin, J.L. Miksis-Olds, J.D. Warren, K.D. Heaney, C.A. Hillis, and A.O. MacGillivray. 2021b. *ADEON Project Dictionary: Terminology Standard*. OCS Study BOEM 20xx-xxx. 40 p.

Ainslie, M.A., R.M. Laws, M.J. Smith, and A.O. MacGillivray. 2022. *JIP Acoustic Modelling Workshop: Verification Scenarios*. Version 2.0. Submitted on 11 Aug 2023 as 'Source and propagation modelling scenarios for environmental impact assessment: Verification', by Ainslie, M.A., R.M. Laws, M.J. Smith, and A.O. MacGillivray; to JASA/JASA-EL Special Issue: Verification and Validation of Source and Propagation Models for Underwater Sound.

Ainslie, M.A., F.-A. Bruliard, C.A.F. de Jong, J.A. Díaz, T. Folegot, M. Ghasemi, M.B. Halvorsen, H. Slabbekoorn, J. Tougaard, et al. 2024. *SATURN Acoustical Terminology Standard (Deliverable D2.3)*. Report by TNO, BV, ULEI, AU, PLOCAN, JASCO, UPC, DNV, and QO. https://1079319b-6fc4-4f45-badb-9450d454ef1c.usrfiles.com/ugd/a39dff_f438b2c6a3e240f29b04da42ca973ae4.pdf.

Betke, K., T. Folegot, R. Matuschek, J. Pajala, L.K.G. Persson, J. Tegowski, J. Tougaard, and M. Wahlberg. 2015. *BIAS Standards for Signal Processing. Aims, Processes and Recommendations*. Amended version. Editors: U.K. Verfuß and P. Sigray. https://biasproject.wordpress.com/wp-content/uploads/2016/01/bias_sigproc_standards_v5_final.pdf.

Borsani, J.F., M.H. Andersson, M. André, A. Azzellino, M. Bou, M. Castellote, L. Ceyrac, D. Dellong, T. Folegot, et al. 2023. *Setting EU Threshold Values for continuous underwater sound*. *In*: Druon, J.-N., G. Hanke, and M.

Casier (eds.). Document JRC133476. Publications Office of the European Union, Luxembourg. https://doi.org/10.2760/690123.

Bosschers, J. 2018. A Semi-Empirical Prediction Method for Broadband Hull-Pressure Fluctuations and Underwater Radiated Noise by Propeller Tip Vortex Cavitation. *Journal of Marine Science and Engineering* 6(2): 49. https://doi.org/10.3390/jmse6020049.

Breeding, J.E., Jr., L.A. Pflug, M. Bradley, M.H. Walrod, and W. McBride. 1996. *Research Ambient Noise DIrectionality (RANDI) 3.1 Physics Description: Planning System Incorporated*. Document NRL/FR/7176--95-9628. Report by Naval Research Library. https://apps.dtic.mil/sti/pdfs/ADA316034.pdf.

Chapman, N.R., M.A. Ainslie, and M. Siderius. 2024. Source level of wind-generated ambient sound in the ocean. *JASA Express Letters* 4(1): 010001. https://doi.org/10.1121/10.0024517.

Church, C.C. (ed.) 2024. *Special Issue on Verification and Validation of Source and Propagation Models for Underwater Sound*. Volume 4. *JASA Express Letters*. https://pubs.aip.org/asa/jel/issue/4/1.

Collins, M.D. 1993a. A split-step Padé solution for the parabolic equation method. *Journal of the Acoustical Society of America* 93(4): 1736–1742. https://doi.org/10.1121/1.406739.

Collins, M.D. 1993b. The adiabatic mode parabolic equation. *Journal of the Acoustical Society of America* 94(4): 2269–2278. https://doi.org/10.1121/1.407498.

Dahl, P.H. and D.R. Dall'Osto. 2022. Potential and kinetic energy of underwater noise measured below a passing ship and response to sub-bottom layering. *Journal of the Acoustical Society of America* 152(6): 3648–3658. https://doi.org/10.1121/10.0016510.

de Jong, C.A.F., B. Binnerts, S. Robinson, and L.S. Wang. 2021. *Guidelines for modelling ocean ambient noise*. Joint Monitoring Programme for Ambient Noise North Sea 2018 – 2021. Report by TNO and NPL for the EU INTERREG Joint Monitoring Programme for Ambient Noise North Sea (Jomopans). https://northsearegion.eu/media/17953/jomopans-guidelines-for-modelling-ocean-ambient-noise_final.pdf.

de Jong, C.A.F., B. Binnerts, P. de Krom, and T. Gaida. 2022. *North Sea Sound Maps 2019-2020*. Report by TNO (NL) for the EU INTERREG Joint Monitoring Programme for Ambient Noise North Sea (Jomopans). https://northsearegion.eu/media/21823/jomopans-north-sea-sound-maps-2019-2020.pdf.

Dekeling, R.P.A., M.L. Tasker, M.A. Ainslie, M. Andersson, M. André, M. Castellote, J.F. Borsani, J. Dalen, T. Folegot, et al. 2014. *Monitoring Guidance for Underwater Noise in European Seas, Part II: Monitoring Guidance Specifications*. *In*: Dekeling, R.P.A., M.L. Tasker, M. Ferreira, and N. Zampoukas (eds.). EUR 26555. Publications Office of the European Union, Luxembourg. https://doi.org/10.2788/27158.

European Commission. 2008. Directive 2008/56/EC of the European Parliament and of the Council of 17 June 2008 establishing a framework for community action in the field of marine environmental policy (Marine Strategy Framework Directive). *Official Journal of the European Union* L 164/19. https://eur-lex.europa.eu/eli/dir/2008/56/oj.

European Commission. 2010. Commission Decision of 1 September 2010 on criteria and methodological standards on good environmental status of marine waters (notified under document C(2010) 5956). *Official Journal of the European Union* L 232/14. https://eur-lex.europa.eu/eli/dec/2010/477(2)/oj.

European Commission. 2017. Commission Decision 2017/848/EU of 17 May 2017 laying down criteria and methodological standards on good environmental status of marine waters and specifications and standardised methods for monitoring and assessment, and repealing Decision 2010/477/EU. *Official Journal of the European Union* L125/43. https://eur-lex.europa.eu/eli/dec/2017/848/oj.

Flamant, J. and J. Bonnel. 2023. Broadband properties of potential and kinetic energies in an oceanic waveguide. *Journal of the Acoustical Society of America* 153(5): 3012. https://doi.org/10.1121/10.0019545.

Folegot, T., D. Clorennec, R. Chavanne, and R. Gallou. 2016. *Mapping of ambient noise for BIAS*. Document QO.20130203.01.RAP.001.01B. Technical report by Quiet-Oceans, Brest, France. https://biasproject.files.wordpress.com/2017/01/qo-20130203-01-rap-001-01b-foi-bias-modelingreport.pdf.

Hamilton, E.L. 1980. Geoacoustic modeling of the sea floor. *Journal of the Acoustical Society of America* 68(5): 1313–1340. https://doi.org/10.1121/1.385100.

Haver, S.M., J. Gedamke, L.T. Hatch, R.P. Dziak, S. Van Parijs, M.F. McKenna, J. Barlow, C. Berchok, E. DiDonato, et al. 2018. Monitoring long-term soundscape trends in U.S. Waters: The NOAA/NPS Ocean Noise Reference Station Network. *Marine Policy* 90: 6–13. https://doi.org/10.1016/j.marpol.2018.01.023.

Haver, S.M., M.E.H. Fournet, R.P. Dziak, C. Gabriele, J. Gedamke, L.T. Hatch, J. Haxel, S.A. Heppell, M.F. McKenna, et al. 2019. Comparing the Underwater Soundscapes of Four U.S. National Parks and Marine Sanctuaries. *Frontiers in Marine Science* 6: 500. https://doi.org/10.3389/fmars.2019.00500.

Heaney, K.D. In press. Basin Scale Soundscape Modelling: Wind and Ships. *Journal of the Acoustical Society of America*.

HELCOM BLUES. 2023. A4.1 Support for the assessment of continuous noise. Main report. *Baltic Sea Environment Proceedings 190*. https://helcom.fi/wp-content/uploads/2023/03/HELCOM-Thematic-assessment-of-hazardous-substances-marine-litter-underwater-noise-and-non-indigenous-species-2016-2021.pdf.

Hoffmann, J. 2020. Decarbonizing maritime transport: Estimating fleet renewal trends based on ship scrapping patterns. *UNCTAD Transport and Trade Facilitation Newsletter* 85: 45. https://unctad.org/news/decarbonizing-maritime-transport-estimating-fleet-renewal-trends-based-ship-scrapping-patterns.

Jensen, F.B., W.A. Kuperman, M.B. Porter, and H. Schmidt. 2011. *Computational Ocean Acoustics*. 2nd edition. AIP Series in Modern Acoustics and Signal Processing. AIP Press - Springer, New York. 794 p. https://doi.org/10.1007/978-1-4419-8678-8.

Lloyd, T. 2024. 'PIANO': A physics-based semi-empirical source model for fleet-scale ship URN prediction. *8th International Symposium on Marine Propulsors*. 17–20 Mar 2024, Berlin, Germany. https://doi.org/10.15480/882.9335.

Lloyd, T., J. Daniel, J. Bosschers, and M. Schuster. 2024a. *NAVISON Task 1.1 Progress Report: Development of a Semi-empirical Source Level Model for Machinery and Cavitation Underwater Radiated Noise from Ships*. Document 02912, Version 4.0. Technical report by Maritime Research Institute Netherlands and DW-ShipConsult for the European Maritime Safety Agency (EMSA).

Lloyd, T., F.H. Lafeber, and J. Bosschers. 2024b. Ship URN mitigation by air injection: Model-scale experiments and application to full-scale measurement data. *8th International Symposium on Marine Propulsors (SMP 2024)*. 17–20 Mar 2024, Berlin, Germany. pp. 237–247. https://doi.org/10.15480/882.9336.

Lloyd, T., A.O. MacGillivray, and H.Ö. Sertlek. 2024c. *NAVISON Task 1.4 Progress Report: Integrated vessel URN soundscape forecasting model*. Document 03137, Version 2.1. Technical report by JASCO Applied Sciences (Deutschland) GmbH and Maritime Research Institute Netherlands for European Maritime Safety Agency (EMSA).

MacGillivray, A.O. and C.A.F. de Jong. 2021. A Reference Spectrum Model for Estimating Source Levels of Marine Shipping Based on Automated Identification System Data. *Journal of Marine Science and Engineering* 9(4): 369. https://doi.org/10.3390/jmse9040369.

MacGillivray, A.O., M. Hermans, T. Lloyd, M.A. Wood, and H.Ö. Sertlek. 2023. *NAVISON Task 1.3 Progress Report: Integrated Vessel URN Soundscape Model*. Document 02912, Version 2.0. Technical report by JASCO Applied Sciences (Deutschland) GmbH and Maritime Research Institute Netherlands for European Maritime Safety Agency (EMSA).

Martin, S.B., M. Siderius, M.A. Ainslie, M.B. Halvorsen, L.T. Hatch, M.K. Prior, D. Brooker, J. Caplinger, C. Erbe, et al. 2024. Verifying Models of the Underwater Soundscape from Wind and Ships with Benchmark Scenarios. *JASA Express Letters* 4(1).

Mathieu, E., H. Ritchie, L. Rodés-Guirao, C. Appel, D. Gavrilov, C. Giattino, J. Hasell, B. Macdonald, S. Dattani, et al. 2024. Coronavirus Pandemic (COVID-19): Research and data. Our World in Data https://ourworldindata.org/coronavirus (Accessed 2024).

Merchant, N.D., P. Blondel, D.T. Dakin, and J. Dorocicz. 2012. Averaging underwater noise levels for environmental assessment of shipping. *Journal of the Acoustical Society of America* 132(4): EL343–EL349. https://doi.org/10.1121/1.4754429.

Merchant, N.D., R.L. Putland, M. André, E. Baudin, M. Felli, H. Slabbekoorn, and R. Dekeling. 2022. A decade of underwater noise research in support of the European Marine Strategy Framework Directive. *Ocean & Coastal Management* 228: 106299. https://doi.org/10.1016/j.ocecoaman.2022.106299.

Nelissen, D., J. Kiraly, and C. Meijer. 2022. *Blue Speeds for shipping. Economic analysis and legal framework to achieve environmental benefits*. Document 22.210439.096. Technical report by CE Delft, Delft, Netherlands.

Nikolopoulos, A., P. Sigray, M.H. Andersson, J. Carlström, and E. Lalander. 2016. *BIAS Implementation Plan - Monitoring and assessment guidance for continuous low frequency sound in the Baltic Sea*. Report by Swedish Defence Research Agency (FOI). 39 p. https://doi.org/10.25607/OBP-748.

Possenti, L., L. de Nooijer, C.A.F. de Jong, F.-P. Lam, S. Beelen, J. Bosschers, T. van Terwisga, R. Stigter, and G.-J. Reichart. 2024. The present and future contribution of ships to the underwater soundscape. *Frontiers in Marine Science* 11. https://doi.org/10.3389/fmars.2024.1252901.

Robinson, S., P. Lepper, and R. Hazelwood. 2014. *Good Practice Guide for Underwater Noise Measurement*. NPL Good Practice Guide No. 133. National Measurement Office, Marine Scotland, The Crown Estate. https://www.npl.co.uk/gpgs/underwater-noise-measurement.

Sertlek, H.Ö., G. Aarts, S. Brasseur, H. Slabbekoorn, C. ten Cate, A.M. von Benda-Beckmann, and M.A. Ainslie. 2016a. Mapping underwater sound in the Dutch part of the North Sea. *In* Popper, A.N. and A.D. Hawkins (eds.). *The Effects of Noise on Aquatic Life II*. Springer, New York. pp. 1001–1006. https://doi.org/10.1007/978-1-4939-2981-8_124.

Sertlek, H.Ö., B. Binnerts, and M.A. Ainslie. 2016b. The effect of sound speed profile on shallow water shipping sound maps. *Journal of the Acoustical Society of America* 140(1): EL84–EL88. https://doi.org/10.1121/1.4954712.

Sertlek, H.Ö., M.A. Ainslie, and K.D. Heaney. 2019a. Analytical and Numerical Propagation Loss Predictions for Gradually Range-Dependent Isospeed Waveguides. *IEEE Journal of Oceanic Engineering* 44(4): 1240–1252. https://doi.org/10.1109/JOE.2018.2865640.

Sertlek, H.Ö., H. Slabbekoorn, C. ten Cate, and M.A. Ainslie. 2019b. Source specific sound mapping: Spatial, temporal and spectral distribution of sound in the Dutch North Sea. *Environmental Pollution* 247: 1143–1157. https://doi.org/10.1016/j.envpol.2019.01.119.

Sertlek, H.Ö. 2021. Hindcasting Soundscapes before and during the COVID-19 Pandemic in Selected Areas of the North Sea and the Adriatic Sea. *Journal of Marine Science and Engineering* 9(7): 702. https://doi.org/10.3390/jmse9070702.

Sertlek, H.Ö. and A.O. MacGillivray. 2024a. *NAVISON Task 2.2 Progress Report: Calculating forecast sound map layers*. Document 03296, Version 1.9. Technical report by JASCO Applied Sciences (Deutschland) GmbH for the European Maritime Safety Agency (EMSA).

Sertlek, H.Ö. and A.O. MacGillivray. 2024b. *NAVISON Task 2.1 Progress Report: Hindcasting shipping source level and sound map layers*. Document 03264, Version 1.9. Technical report by JASCO Applied Sciences (Deutschland) GmbH for the European Maritime Safety Agency (EMSA).

Sigray, P., M. Andersson, J. Pajala, J. Laanearu, A. Klauson, J. Tegowski, M. Boethling, J. Fischer, J. Tougaard, et al. 2016. *BIAS: A Regional Management of Underwater Sound in the Baltic Sea*. Springer, New York, pp. 1015–1023. https://doi.org/10.1007/978-1-4939-2981-8_126.

Straume, E.O., C. Gaina, S. Medvedev, K. Hochmuth, K. Gohl, and J.M. Whittaker. 2019. *NGDC Total Sediment Thickness of the World's Oceans & Marginal Seas, Version 3 (GlobSed)* (web page). ArcGIS files. https://www.ngdc.noaa.gov/mgg/sedthick/index.html. (Accessed DD Mon YYYY).

Tasker, M.L., M. Amundin, M. André, A.D. Hawkins, W. Lang, T. Merck, A.R. Scholik-Schlomer, J. Teilmann, F. Thomsen, et al. 2010. *Marine strategy framework directive: Task Group 11 report: Underwater noise and other forms of energy*. Report EUR 24341 EN - 2010. European Commission and International Council for the Exploration of the Sea. JRC Scientific and Technical Report, Luxembourg. https://dx.doi.org/10.2788/87079.

van der Graaf, A.J., M.A. Ainslie, M. André, K. Brensing, J. Dalen, R.P.A. Dekeling, S. Robinson, M.L. Tasker, F. Thomsen, et al. 2012. *European Marine Strategy Framework Directive - Good Environmental Status (MSFD GES)*. Report of the Technical Subgroup on Underwater Noise and Other Forms of Energy, Brussels. https://environment.ec.europa.eu/topics/marine-environment_en.

Wales, S.C. and R.M. Heitmeyer. 2002. An ensemble source spectra model for merchant ship-radiated noise. *Journal of the Acoustical Society of America* 111(3): 1211–1231. https://doi.org/10.1121/1.1427355.

Wang, L. and S. Robinson. 2020. *JOMOPANS standard: Terminology for ambient noise monitoring*. Version 2.0. Report by the National Physical Laboratory for JOMOPANS. Deliverable/Task: 3.1, The Netherlands. 31 p. https://northsearegion.eu/media/13062/jomopans_wp3-standard-terminology_version_-2.pdf.

Wittekind, D.K. 2014. A simple model for the underwater noise source level of ships. *Journal of Ship Production and Design* 30(1): 7–14.

Wood, M.A., H.P. Wecker, and A.O. MacGillivray. 2022. *NAVISON Task 1.2 Progress Report: Sound Propagation Modelling and Environmental Processing*. Document 02911, Version 2.0. Technical report by JASCO Applied Sciences (Deutschland) GmbH for the European Maritime Safety Agency (EMSA).

Zhang, Z.Y. and C.T. Tindle. 1995. Improved equivalent fluid approximations for a low shear speed ocean bottom. *Journal of the Acoustical Society of America* 98(6): 3391–3396. https://doi.org/10.1121/1.413789.

Appendix A Regions

For the NAVISON project, European waters were divided into five distinct regions. Where possible, boundaries were based on natural sound barriers to limit the influence of sound emanating from outside of the regions. The regions were:

- Baltic Sea,
- Black Sea,
- Mediterranean Sea,
- Northeast Atlantic Ocean, and
- North Sea.

Figure 104 provides an overview of the regions.

Figure 104 Defined regions for the NAVISON project (EPSG:3035)

The rationale applied in determining the region boundaries was as follows:

- The western boundary of the northeast Atlantic Ocean was defined as being the approximate position of the mid-Atlantic ridge at 30°W,
- The northern boundary of the northeast Atlantic Ocean:
    - has a minimum latitude of 71°N, defined by the location of Jan Mayen (island),
    - follows Mohns Ridge,
    - has a maximum latitude defined by the Norwegian EEZ (74.5°N).
- The eastern boundary of the northeast Atlantic Ocean is defined by the Norwegian EEZ (36.5°E),
- The southern boundary of the northeast Atlantic Ocean is defined by the Canary Islands EEZ (24°N),

- The northern boundary between the North Sea and the northeast Atlantic Ocean is defined by a straight line through Orkney and Shetland, and limited to the northernmost point of Shetland (60.7°N),
- The divide between the North Sea and the Baltic Sea is defined as a line through the northern edge of Zealand and Funen islands,
- The southern boundary between the North Sea and the northeast Atlantic Ocean is at the narrowest section of the English Channel (Dover-Calais crossing),
- The boundary between the Black Sea and the Mediterranean Sea is across the Bosphorus Strait at its midpoint,
- The boundary between the Mediterranean Sea and the northeast Atlantic Ocean is defined as the narrowest point across the Strait of Gibraltar.

The boundary coordinates for all regions are listed in Table 9.

Table 9 Boundary coordinates for NAVISON regions (WGS84)

Northeast Atlantic Ocean		North Sea		Mediterranean Sea		Baltic Sea		Black Sea	
Lon.	Lat.	Lon.	Lat.	Lon.	Lat.	Lon.	Lat.	Lon.	Lat.
5°30'W	24°00'N	0°48'W	60°48'N	19°00'E	29°00'N	30°30'E	60°00'N	27°00'E	48°00'N
30°00'W	24°00'N	3°24'W	58°42'N	37°00'E	31°00'N	20°00'E	53°00'N	42°00'E	48°00'N
30°00'W	71°00'N	5°00'W	57°30'N	37°00'E	37°00'N	11°00'E	53°00'N	42°00'E	40°48'N
8°30'W	71°00'N	3°30'W	55°30'N	30°30'E	40°48'N	9°00'E	55°00'N	30°30'E	40°48'N
14°00'E	74°30'N	2°30'W	55°30'N	27°00'E	41°36'N	13°30'E	56°30'N	27°00'E	41°36'N
36°30'E	74°30'N	0°00'E	51°12'N	15°00'E	47°00'N	13°30'E	60°48'N	27°00'E	48°00'N
36°30'E	68°00'N	1°24'E	51°09'N	2°00'W	42°00'N	25°00'E	68°00'N		
25°00'E	68°00'N	1°36'E	50°51'N	5°30'W	36°03'N	30°30'E	60°00'N		
13°30'E	60°48'N	3°00'E	50°00'N	5°30'W	35°54'N				
4°36'E	60°48'N	11°00'E	53°00'N	5°30'W	35°00'N				
0°48'W	60°48'N	9°00'E	55°00'N	19°00'E	29°00'N				
3°24'W	58°42'N	13°30'E	56°30'N						
5°00'W	57°30'N	13°30'E	60°48'N						
3°30'W	55°30'N	4°36'E	60°48'N						
2°30'W	55°30'N	0°48'W	60°48'N						
0°00'E	51°12'N								
1°24'E	51°09'N								
1°36'E	50°51'N								
3°00'E	50°00'N								
2°00'W	42°00'N								
5°30'W	36°03'N								
5°30'W	35°54'N								
5°30'W	24°00'N								

Appendix B AIS Data Overview

This appendix provides an overview of the temporal variations in the number of Vessel Data Messages (VDM) contained in the Automatic Identification System data set used to generate the ship tracks for NAVISON. Figure 105 shows the monthly total number of messages from all terrestrial originators combined and the different satellite originators.

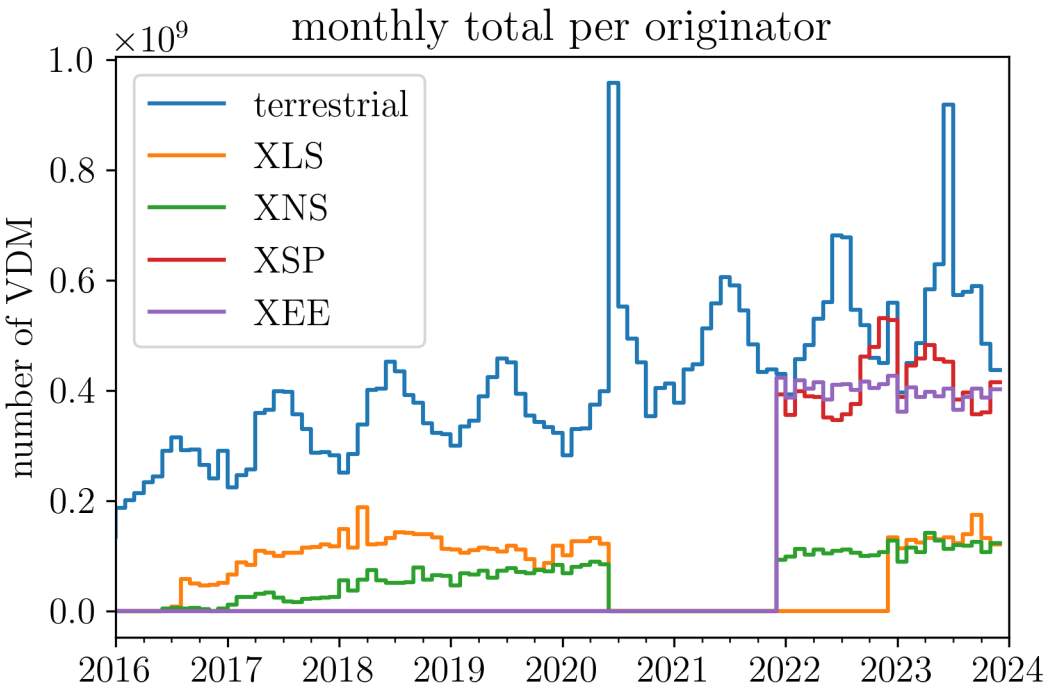

Figure 105 Monthly total VDM per originator for the entire AIS data set used to generate the ship tracks. The terrestrial data is the sum of all messages provided by Member States' land-based receiver stations. The other originators are all satellite. NB: Number of messages does not directly correspond to the number of data points in the processed ship tracks.

Annual variations are observable in the terrestrial data due seasonal changes in ship traffic. Despite this, the average number of messages increases over time, roughly doubling over the timeframe of the data set. Furthermore, two months contain a much higher number of messages than the rest: July 2020 and July 2023. These are both due to a peak in the number of messages contributed by a single Member State. This is shown in Figure 106 from which it can be seen that messages from Germany (DEU) are only present from July 2020, peaking sharply in this month before dropping to more consistent levels over the rest of the time period. The peak in July 2023 results from a similar occurrence in the data from Norway (NOR). The peak in the data from Germany was attributed to a faster update rate than the usual 6 min found in most of the complete dataset. It is also notable that Great Britain (GBR) stops reporting data in July 2023, presumably due to Brexit.

The satellite data in Figure 105 was reported by several different originators. Before July 2020, only two originators are present, while from January 2022 two additional originators contribute messages. In the intervening period no satellite data is included in the AIS data set, due to a change in the data storage system at EMSA.

It is emphasised that the number of messages from each originator is not a direct indicator of the AIS data coverage, for several reasons. Firstly, the temporal resolution of the satellite data varies from order of minutes to order of hours, while for terrestrial data this is typically 6 min. Secondly, the satellite data represents a global data set, which was subsequently filtered to obtain the messages relevant for European seas. Finally, there is overlap between the various data subsets, i.e. the same vessel is reported multiple times through different originators. Any duplicate information is removed when processing the ship tracks.

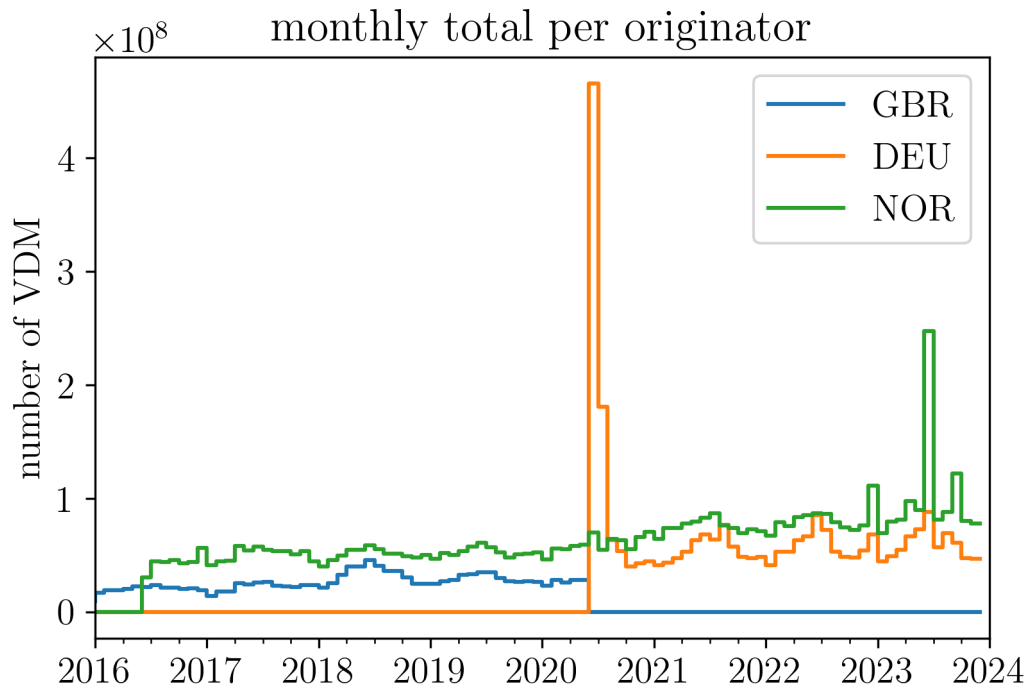

Figure 106 Monthly total VDM per originator for selected Member States. Germany (DEU) only starts to contribute data from Q3 2020, while at the same time Great Britain (GBR) stops, due to Brexit.

Appendix C Number of AIS Vessels by Region

The mean number of AIS vessels in each region was computed by integrating per-category vessel density, as computed from the vessel track data (Figure 107). The vessel density (in units of vessels/m²) is equal to the total accumulated AIS vessel time within each grid cell, divided by the total time over a given period (equal to a quarter year). Given the vessel density data, the mean vessel count is simply equal to the integral of the vessel density grid over area. The resulting quantity is equal to the average number of AIS vessels present, at any instant, within the specified region and quarter. Time-dependent changes in the number of vessels represent time-dependent changes in traffic volume, as well as changes in overall AIS coverage within the study area.

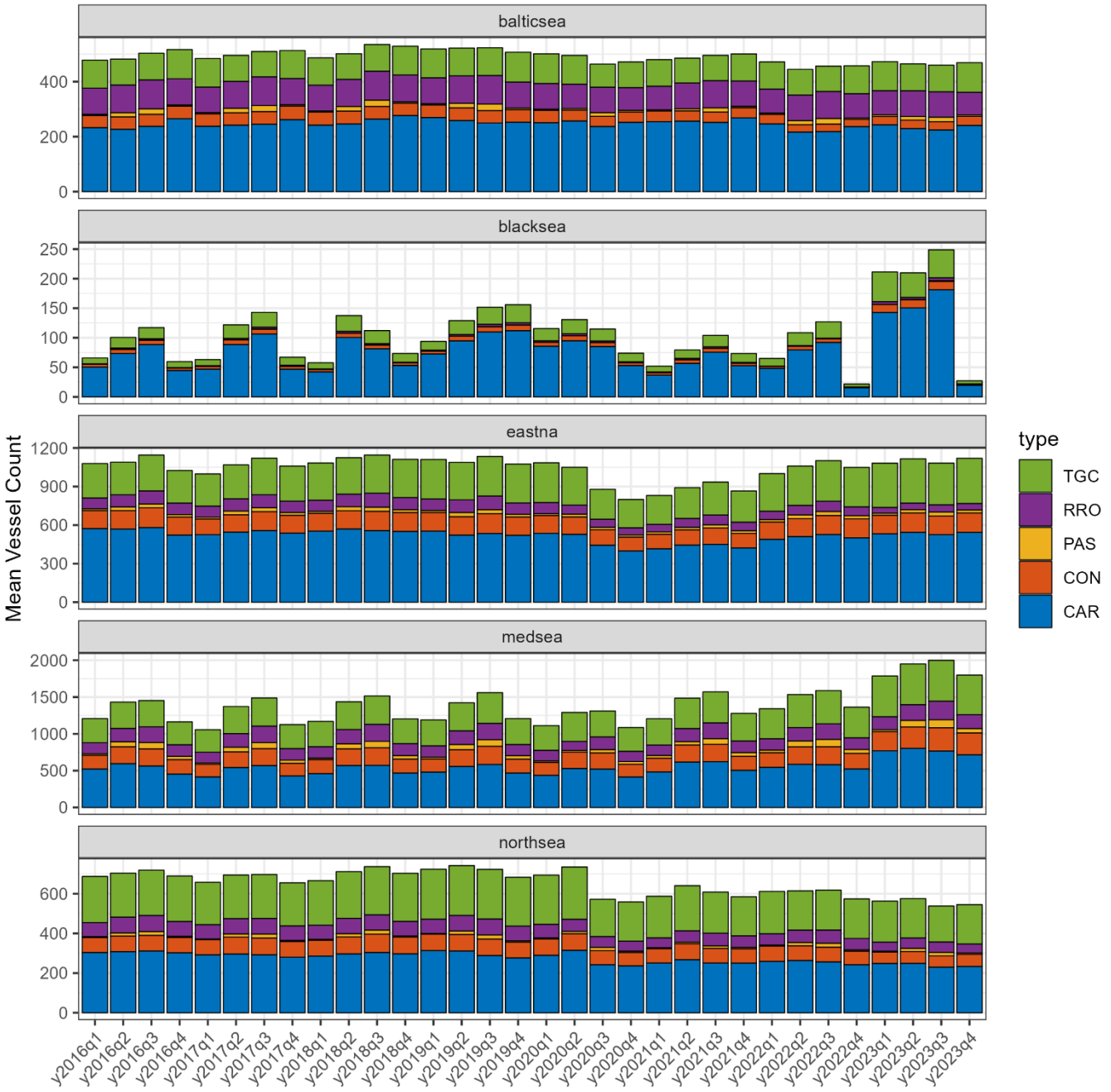

Figure 107 Mean number of vessels versus quarter and year, by region.

Appendix D Sound Energy Density

When analysing multiple sound map layers, applying statistical methods for post-processing may be not straightforward. Statistics of sound pressure level (SPL) are notoriously sensitive to the choice of temporal (Merchant et al. 2012, van der Graaf et al. 2012) and spatial averaging windows (Sigray et al. 2023). Spatial statistics concerning acoustic metrics like SPL and SEL might lead to misleading results if different sizes of spatial observation windows (SOWs) are used for each NAVISON region. Thus, it is essential to employ a robust metric for analysing sound map layers. If there is no spatial averaging, the problem is solved by using the arithmetic mean of squared sound pressure is used to evaluate the level (Merchant et al. 2012, van der Graaf et al. 2012), and for this reason TG Noise proposed use by EU Member States of the arithmetic mean in addition to other statistics (Dekeling et al. 2014). The concept of arithmetic mean can be extended spatially by introducing the spatially averaged mean-square sound pressure (SAMSP) (Ainslie et al. 2021a):

$$\langle \overline{p^2} \rangle = \frac{1}{V} \int_V \overline{p^2} \, \mathrm{d}V$$

where $\overline{p^2}$ is the arithmetic mean of the squared sound pressure and T is the averaging time.

$$\overline{p^2} = \frac{1}{T} \int_0^T p^2 \, \mathrm{d}t \, .$$

This integration for SAMSP is performed over the volume of water (V). The spatially averaged mean-square sound pressure is independent of TOW and SOW, making it a convenient metric for characterising a sound map. The SAMSP is related to mean sound energy density (E_V) via:

$$E_V = \frac{\langle \overline{p^2} \rangle}{\rho c^2}$$

where ρ is the density of water, c is the sound speed in the water. The total sound energy (E) and mean sound energy density are related via:

$$E_V = \frac{E}{V} .$$

When calculated over a wide band, this includes both the potential and kinetic energy of the acoustic field (Flamant and Bonnel 2023). Sound energy density, which is independent of the SOW, is one such metric. The energy density is more intuitive than the spatially averaged mean-square sound pressure, and is also independent of TOW and SOW. It is therefore used here to analyse the sound map layers. The sound energy was first applied to sound mapping, including the bathymetry and sound speed profiles by modelling underwater sound propagation, by (Sertlek et al. 2016a). The sound energy density may be used for different purposes such as:

- Tracking the time-trend of shipping sound (for each quarter or year).
- Comparing the contributions of individual vessel categories.
- Quantifying the effect of the mitigation measures.

As an examples of the use of sound energy density, various publications are available in the literature. The sound energy and sound energy density were previously both used for examining the temporal patterns of sound and ranking the different source sources in the Dutch part of North Sea, as explored by Sertlek et al. (2019b). Likewise, Sertlek (2021) utilises sound energy density to measure variations in shipping sound during the Covid-19 pandemic and compare the changes in two regions in the southern North Sea and northern Adriatic Sea. (Ainslie et al. 2021a) used the sound energy concept to derive a formula which describes the relation between the total radiated power of all ocean sound sources and the spatially averaged mean-square sound pressure. This formula is used to quantify the temperature-driven seasonal and long-term changes in the ambient sound. Dahl and Dall'Osto (2022) used potential and kinetic energy to quantify the sound field below a passing ship and the measured and modelled potential to kinetic energy ratios for different seabed impedances.

Total sound energy and mean sound energy density can be used to quantify the provided information in the sound map layers with a single value for each map layer. Furthermore, since the energy is a linear metric, it is possible to

apply linear mathematical operations without any logarithmic sum. Therefore, the energy contributions of each vessel category can be directly summed or subtracted directly whenever it is necessary for the analysis of sound map layers.

Appendix E Percentage Distribution of Sound Energy Density for Each Vessel Category

Another analysis could be performed to quantify the percentage distribution of sound energy density for each vessel category for the selected years. It is important to note that the percentage values cannot be used to compare temporal trends. Instead, they provide insight into the percentage distribution specific to the selected year. This analysis helps to understand the proportional contribution of each vessel category to the total sound energy density for a given year, offering valuable insights into the composition of shipping sound during that period.

The percentage distribution of sound energy density for each vessel category in each region is calculated and listed in the following tables.

Table 10 Percentage distribution of sound energy density for each vessel category in Europe at 63 Hz

	63 Hz				
year	CAR	CON	PAS	RRO	TGC
2016	33.54 %	2.79 %	0.69 %	5.53 %	57.45 %
2017	33.85 %	3.02 %	0.75 %	5.70 %	56.69 %
2018	25.89 %	2.35 %	0.63 %	4.30 %	66.82 %
2019	21.54 %	2.02 %	0.94 %	3.73 %	71.77 %
2020	29.24 %	2.64 %	0.37 %	4.26 %	63.49 %
2021	32.24 %	2.75 %	0.47 %	4.65 %	59.89 %
2022	34.16 %	2.80 %	1.62 %	4.71 %	56.71 %
2023	32.72 %	2.94 %	1.88 %	4.02 %	58.45 %

Table 11 Percentage distribution of sound energy density for each vessel category in Europe at 125 Hz

	125 Hz				
year	CAR	CON	PAS	RRO	TGC
2016	33.63 %	3.17 %	2.31 %	32.51 %	28.38 %
2017	34.88 %	3.05 %	2.40 %	33.10 %	26.56 %
2018	29.45 %	2.90 %	2.28 %	30.37 %	34.99 %
2019	26.87 %	2.60 %	3.19 %	30.04 %	37.31 %
2020	32.05 %	2.90 %	1.07 %	32.16 %	31.82 %
2021	32.29 %	2.75 %	1.39 %	33.51 %	30.07 %
2022	32.40 %	2.64 %	4.18 %	34.97 %	25.81 %
2023	35.32 %	3.92 %	4.38 %	29.23 %	27.16 %

Table 12 Percentage distribution of sound energy density for each vessel category in Baltic Sea at 63 Hz

	63 Hz				
year	CAR	CON	PAS	RRO	TGC
2016	52.01 %	3.04 %	0.46 %	26.53 %	17.96 %
2017	51.89 %	3.09 %	0.63 %	25.80 %	18.58 %
2018	54.57 %	2.95 %	0.59 %	24.70 %	17.20 %
2019	54.03 %	2.73 %	1.20 %	22.99 %	19.06 %
2020	58.38 %	2.69 %	0.32 %	18.28 %	20.32 %
2021	62.90 %	2.47 %	0.53 %	17.70 %	16.40 %
2022	61.62 %	1.96 %	0.34 %	18.55 %	17.53 %
2023	53.22 %	1.47 %	0.26 %	11.23 %	33.82 %

Table 13 Percentage distribution of sound energy density for each vessel category in Baltic Sea at 125 Hz

	125 Hz				
year	CAR	CON	PAS	RRO	TGC
2016	38.28 %	1.74 %	1.01 %	49.28 %	9.69 %
2017	36.22 %	1.79 %	1.14 %	51.21 %	9.65 %
2018	35.19 %	1.82 %	1.11 %	52.78 %	9.10 %
2019	36.74 %	1.69 %	1.76 %	50.28 %	9.53 %
2020	41.01 %	1.63 %	0.64 %	46.70 %	10.02 %
2021	38.97 %	1.47 %	0.90 %	49.31 %	9.35 %
2022	36.10 %	0.95 %	0.85 %	52.78 %	9.32 %
2023	36.56 %	0.98 %	0.70 %	46.74 %	15.03 %

Table 14 Percentage distribution of sound energy density for each vessel category in Black Sea at 63 Hz

	63 Hz				
year	CAR	CON	PAS	RRO	TGC
2016	81.98 %	1.93 %	0.02 %	0.91 %	15.16 %
2017	83.17 %	1.92 %	0.02 %	1.19 %	13.71 %
2018	84.15 %	1.99 %	0.00 %	0.97 %	12.89 %
2019	82.98 %	2.01 %	0.00 %	0.97 %	14.04 %
2020	83.31 %	1.94 %	0.00 %	1.22 %	13.53 %
2021	84.60 %	2.13 %	0.00 %	1.06 %	12.20 %
2022	80.19 %	2.05 %	0.00 %	0.29 %	17.47 %
2023	75.28 %	6.82 %	0.05 %	0.62 %	17.23 %

Table 15 Percentage distribution of sound energy density for each vessel category in Black Sea at 125 Hz

	125 Hz				
year	CAR	CON	PAS	RRO	TGC
2016	76.20 %	3.17 %	0.15 %	6.84 %	13.64 %
2017	76.79 %	3.24 %	0.08 %	7.46 %	12.43 %
2018	77.01 %	3.22 %	0.01 %	8.20 %	11.55 %
2019	75.69 %	3.03 %	0.02 %	7.69 %	13.57 %
2020	76.08 %	2.82 %	0.01 %	8.10 %	12.98 %
2021	78.86 %	3.04 %	0.01 %	7.14 %	10.95 %
2022	82.50 %	2.53 %	0.01 %	1.48 %	13.49 %
2023	66.11 %	13.13%	0.40 %	2.48 %	17.88 %

Table 16 Percentage distribution of sound energy density for each vessel category for Mediterranean Sea at 63 Hz

	63 Hz				
year	CAR	CON	PAS	RRO	TGC
2016	19.22 %	2.42 %	0.90 %	6.40 %	71.06 %
2017	20.17 %	2.66 %	0.84 %	6.90 %	69.43 %
2018	14.86 %	1.95 %	0.71 %	4.88 %	77.61 %
2019	13.72 %	1.75 %	0.91 %	4.50 %	79.12 %
2020	21.18 %	2.63 %	0.32 %	5.76 %	70.11 %
2021	23.18 %	2.58 %	0.54 %	5.23 %	68.48 %
2022	27.14 %	2.93 %	1.46 %	6.52 %	61.95 %
2023	31.23 %	4.18 %	2.04 %	7.40 %	55.15 %

Table 17 Percentage distribution of sound energy density for each vessel category for Mediterranean Sea at 125 Hz

	125 Hz				
year	CAR	CON	PAS	RRO	TGC
2016	16.12 %	3.38 %	2.92 %	37.12 %	40.46 %
2017	16.85 %	3.41 %	2.61 %	39.49 %	37.65 %
2018	13.87 %	2.90 %	2.30 %	31.63 %	49.30 %
2019	13.08 %	2.57 %	2.81 %	31.58 %	49.96 %
2020	18.43 %	3.37 %	0.96 %	37.62 %	39.63 %
2021	19.22 %	3.26 %	1.65 %	36.02 %	39.85 %
2022	19.34 %	3.19 %	3.70 %	42.58 %	31.19 %
2023	22.65 %	6.01 %	4.13 %	40.63 %	26.59 %

Table 18 Percentage distribution of sound energy density for each vessel category in North Sea at 63 Hz

	63 Hz				
year	CAR	CON	PAS	RRO	TGC
2016	59.97 %	3.04 %	0.96 %	9.28 %	26.75 %
2017	55.17 %	3.10 %	1.18 %	9.60 %	30.95 %
2018	56.30 %	3.15 %	1.74 %	9.12 %	29.69 %
2019	47.49 %	2.95 %	1.56 %	9.02 %	38.98 %
2020	40.50 %	2.51 %	0.35 %	6.40 %	50.24 %
2021	44.73 %	2.70 %	0.47 %	7.21 %	44.90 %
2022	40.50 %	2.28 %	5.14 %	7.16 %	44.92 %
2023	39.40 %	1.81 %	5.21 %	5.93 %	47.64 %

Table 19 Percentage distribution of sound energy density for each vessel category in North Sea at 125 Hz

	125 Hz				
year	CAR	CON	PAS	RRO	TGC
2016	45.86 %	2.53 %	1.50 %	31.27 %	18.84 %
2017	44.39 %	2.48 %	1.64 %	32.43 %	19.07 %
2018	43.47 %	2.65 %	2.24 %	32.96 %	18.68 %
2019	40.35 %	2.54 %	2.23 %	34.76 %	20.13 %
2020	40.82 %	2.53 %	0.46 %	27.70 %	28.50 %
2021	42.75 %	2.36 %	0.55 %	26.99 %	27.35 %
2022	37.80 %	1.93 %	5.93 %	30.39 %	23.95 %
2023	41.12 %	1.84 %	6.13 %	26.63 %	24.27 %

Table 20 Percentage distribution of sound energy density for each vessel category in the northeast Atlantic Ocean at 63 Hz

	63 Hz				
year	CAR	CON	PAS	RRO	TGC
2016	38.42 %	3.00 %	0.57 %	2.17 %	55.84 %
2017	38.04 %	3.24 %	0.68 %	2.16 %	55.88 %
2018	28.88 %	2.55 %	0.53 %	1.66 %	66.38 %
2019	22.34 %	2.10 %	0.92 %	1.48 %	73.16 %
2020	29.57 %	2.66 %	0.40 %	1.87 %	65.50 %
2021	33.95 %	2.93 %	0.40 %	2.39 %	60.33 %
2022	35.15 %	2.84 %	1.62 %	2.20 %	58.19 %
2023	30.61 %	2.51 %	1.77 %	1.60 %	63.52 %

Table 21 Percentage distribution of sound energy density for each vessel category in the northeast Atlantic Ocean at 125 Hz

	125 Hz				
year	CAR	CON	PAS	RRO	TGC
2016	41.87 %	3.63 %	2.51 %	23.73 %	28.27 %
2017	44.04 %	3.38 %	2.90 %	22.58 %	27.10 %
2018	37.22 %	3.29 %	2.71 %	21.98 %	34.82 %
2019	31.88 %	2.93 %	4.11 %	22.09 %	38.99 %
2020	35.51 %	3.10 %	1.36 %	24.93 %	35.11 %
2021	37.25 %	2.88 %	1.51 %	27.26 %	31.11 %
2022	39.23 %	2.85 %	5.41 %	24.95 %	27.55 %
2023	43.31 %	3.24 %	5.56 %	16.18 %	31.71 %

Appendix F Forecast Scenario Inputs

Table 22 BAU: Forecast scenario in 2030, 2040, and 2050. Penetration rates for each mitigation measure and change in the traffic volumes are shown for different vessel categories.

Year	Mitigation measure	CAR (%)	CON (%)	PAS (%)	RRO (%)	TGC (%)
BAU 2030	Total change in ship traffic volume (ΔN)	17.1	29.3	16.4	19.6	20.5
	Penetration rate of hull and propeller cleaning (P(HPC))	0.0	0.0	0.0	0.0	0.0
	Penetration rate of air injection (P(AIN))	0.0	0.0	0.0	0.0	0.0
	Penetration rate of optimised hull form (P(OHF))	0.0	0.0	0.0	0.0	0.0
	Penetration rate of speed reduction (P(SRD))	0.0	0.0	0.0	0.0	0.0
	Penetration rate of more efficient propeller (P(MEP))	0.0	0.0	0.0	0.0	0.0
	Penetration rate of quieter propeller (P(QRP))	0.0	0.0	0.0	0.0	0.0
	Joint probability of speed reduction and more efficient propeller (P(SRD & MEP))	0.0	0.0	0.0	0.0	0.0
	Joint probability of speed reduction and quieter propeller (P(SRD & QRP))	0.0	0.0	0.0	0.0	0.0
BAU 2040	Total change in ship traffic volume (ΔN)	29.9	53.1	26.0	32.8	38.0
	Penetration rate of hull and propeller cleaning (P(HPC))	0.0	0.0	0.0	0.0	0.0
	Penetration rate of air injection (P(AIN))	0.0	0.0	0.0	0.0	0.0
	Penetration rate of optimised hull form (P(OHF))	0.0	0.0	0.0	0.0	0.0
	Penetration rate of speed reduction (P(SRD))	0.0	0.0	0.0	0.0	0.0
	Penetration rate of more efficient propeller (P(MEP))	0.0	0.0	0.0	0.0	0.0
	Penetration rate of quieter propeller (P(QRP))	0.0	0.0	0.0	0.0	0.0
	Joint probability of speed reduction and more efficient propeller (P(SRD & MEP))	0.0	0.0	0.0	0.0	0.0
	Joint probability of speed reduction and quieter propeller (P(SRD & QRP))	0.0	0.0	0.0	0.0	0.0
BAU 2050	Total change in ship traffic volume (ΔN)	35.6	77.7	29.9	43.0	49.6
	Penetration rate of hull and propeller cleaning (P(HPC))	0.0	0.0	0.0	0.0	0.0
	Penetration rate of air injection (P(AIN))	0.0	0.0	0.0	0.0	0.0
	Penetration rate of optimised hull form (P(OHF))	0.0	0.0	0.0	0.0	0.0
	Penetration rate of speed reduction (P(SRD))	0.0	0.0	0.0	0.0	0.0
	Penetration rate of more efficient propeller (P(MEP))	0.0	0.0	0.0	0.0	0.0
	Penetration rate of quieter propeller (P(QRP))	0.0	0.0	0.0	0.0	0.0
	Joint probability of speed reduction and more efficient propeller (P(SRD & MEP))	0.0	0.0	0.0	0.0	0.0
	Joint probability of speed reduction and quieter propeller (P(SRD & QRP))	0.0	0.0	0.0	0.0	0.0

Table 23 GHC: Forecast scenario in 2030, 2040, and 2050. Penetration rates for each mitigation measure and change in the traffic volumes are shown for different vessel categories.

Year	Mitigation measure	CAR (%)	CON (%)	PAS (%)	RRO (%)	TGC (%)
GHC 2030	Total change in ship traffic volume (ΔN)	17.1	29.3	16.4	19.6	20.5
	Penetration rate of hull and propeller cleaning (P(HPC))	55.0	55.0	55.0	55.0	55.0
	Penetration rate of air injection (P(AIN))	0.0	0.0	0.0	0.0	0.0
	Penetration rate of optimised hull form (P(OHF))	12.7	34.8	23.9	27.6	32.7
	Penetration rate of speed reduction (P(SRD))	100.0	100.0	100.0	100.0	100.0
	Penetration rate of more efficient propeller (P(MEP))	35.0	40.0	33.0	35.0	35.0
	Penetration rate of quieter propeller (P(QRP))	0.0	0.0	0.0	0.0	0.0
	Joint probability of speed reduction and more efficient propeller (P(SRD & MEP))	35.0	40.0	33.0	35.0	35.0
	Joint probability of speed reduction and quieter propeller (P(SRD & QRP))	0.0	0.0	0.0	0.0	0.0
GHC 2040	Total change in ship traffic volume (ΔN)	29.9	53.1	26.0	32.8	38.0
	Penetration rate of hull and propeller cleaning (P(HPC))	67.5	67.5	67.5	67.5	67.5
	Penetration rate of air injection (P(AIN))	0.0	0.0	0.0	0.0	0.0
	Penetration rate of optimised hull form (P(OHF))	55.6	79.3	50.0	69.8	70.9
	Penetration rate of speed reduction (P(SRD))	100.0	100.0	100.0	100.0	100.0
	Penetration rate of more efficient propeller (P(MEP))	60.0	85.0	58.0	75.0	75.0
	Penetration rate of quieter propeller (P(QRP))	0.0	0.0	0.0	0.0	0.0
	Joint probability of speed reduction and more efficient propeller (P(SRD & MEP))	60.0	85.0	58.0	75.0	75.0
	Joint probability of speed reduction and quieter propeller (P(SRD & QRP))	0.0	0.0	0.0	0.0	0.0
GHC 2050	Total change in ship traffic volume (ΔN)	35.6	77.7	29.9	43.0	49.6
	Penetration rate of hull and propeller cleaning (P(HPC))	80.0	80.0	80.0	80.0	80.0
	Penetration rate of air injection (P(AIN))	0.0	0.0	0.0	0.0	0.0
	Penetration rate of optimised hull form (P(OHF))	90.0	96.7	73.9	89.3	91.8
	Penetration rate of speed reduction (P(SRD))	100.0	100.0	100.0	100.0	100.0
	Penetration rate of more efficient propeller (P(MEP))	96.0	100.0	80.0	96.0	96.0
	Penetration rate of quieter propeller (P(QRP))	0.0	0.0	0.0	0.0	0.0
	Joint probability of speed reduction and more efficient propeller (P(SRD & MEP))	96.0	100.0	80.0	96.0	96.0
	Joint probability of speed reduction and quieter propeller (P(SRD & QRP))	0.0	0.0	0.0	0.0	0.0

Table 24 URN: Forecast scenario in 2030, 2040, and 2050. Penetration rates for each mitigation measure and change in the traffic volumes are shown for different vessel categories.

Year	Mitigation measure	CAR (%)	CON (%)	PAS (%)	RRO (%)	TGC (%)
URN 2030	Total change in ship traffic volume (ΔN)	17.1	29.3	16.4	19.6	20.5
	Penetration rate of hull and propeller cleaning (P(HPC))	0.0	0.0	0.0	0.0	0.0
	Penetration rate of air injection (P(AIN))	5.0	5.0	5.0	5.0	5.0
	Penetration rate of optimised hull form (P(OHF))	0.0	0.0	0.0	0.0	0.0
	Penetration rate of speed reduction (P(SRD))	100.0	100.0	100.0	100.0	100.0
	Penetration rate of more efficient propeller (P(MEP))	0.0	0.0	0.0	0.0	0.0
	Penetration rate of quieter propeller (P(QRP))	35.0	40.0	33.0	35.0	35.0
	Joint probability of speed reduction and more efficient propeller (P(SRD & MEP))	0.0	0.0	0.0	0.0	0.0
	Joint probability of speed reduction and quieter propeller (P(SRD & QRP))	35.0	40.0	33.0	35.0	35.0
URN 2040	Total change in ship traffic volume (ΔN)	29.9	53.1	26.0	32.8	38.0
	Penetration rate of hull and propeller cleaning (P(HPC))	0.0	0.0	0.0	0.0	0.0
	Penetration rate of air injection (P(AIN))	17.5	17.5	17.5	17.5	17.5
	Penetration rate of optimised hull form (P(OHF))	0.0	0.0	0.0	0.0	0.0
	Penetration rate of speed reduction (P(SRD))	100.0	100.0	100.0	100.0	100.0
	Penetration rate of more efficient propeller (P(MEP))	0.0	0.0	0.0	0.0	0.0
	Penetration rate of quieter propeller (P(QRP))	60.0	85.0	58.0	75.0	75.0
	Joint probability of speed reduction and more efficient propeller (P(SRD & MEP))	0.0	0.0	0.0	0.0	0.0
	Joint probability of speed reduction and quieter propeller (P(SRD & QRP))	60.0	85.0	58.0	75.0	75.0
URN 2050	Total change in ship traffic volume (ΔN)	35.6	77.7	29.9	43.0	49.6
	Penetration rate of hull and propeller cleaning (P(HPC))	0.0	0.0	0.0	0.0	0.0
	Penetration rate of air injection (P(AIN))	30.0	30.0	30.0	30.0	30.0
	Penetration rate of optimised hull form (P(OHF))	0.0	0.0	0.0	0.0	0.0
	Penetration rate of speed reduction (P(SRD))	100.0	100.0	100.0	100.0	100.0
	Penetration rate of more efficient propeller (P(MEP))	0.0	0.0	0.0	0.0	0.0
	Penetration rate of quieter propeller (P(QRP))	96.0	100.0	80.0	96.0	96.0
	Joint probability of speed reduction and more efficient propeller (P(SRD & MEP))	0.0	0.0	0.0	0.0	0.0
	Joint probability of speed reduction and quieter propeller (P(SRD & QRP))	96.0	100.0	80.0	96.0	96.0

Table 25 U&G: Forecast scenario in 2030, 2040, and 2050. Penetration rates for each mitigation measure and change in the traffic volumes are shown for different vessel categories.

Year	Mitigation measure	CAR (%)	CON (%)	PAS (%)	RRO (%)	TGC (%)
U&G 2030	Total change in ship traffic volume (ΔN)	17.1	29.3	16.4	19.6	20.5
	Penetration rate of hull and propeller cleaning (P(HPC))	55.0	55.0	55.0	55.0	55.0
	Penetration rate of air injection (P(AIN))	5.0	5.0	5.0	5.0	5.0
	Penetration rate of optimised hull form (P(OHF))	12.7	34.8	23.9	27.6	32.7
	Penetration rate of speed reduction (P(SRD))	100.0	100.0	100.0	100.0	100.0
	Penetration rate of more efficient propeller (P(MEP))	30.0	35.0	28.0	30.0	30.0
	Penetration rate of quieter propeller (P(QRP))	5.0	5.0	5.0	5.0	5.0
	Joint probability of speed reduction and more efficient propeller (P(SRD & MEP))	30.0	35.0	28.0	30.0	30.0
	Joint probability of speed reduction and quieter propeller (P(SRD & QRP))	5.0	5.0	5.0	5.0	5.0
U&G 2040	Total change in ship traffic volume (ΔN)	29.9	53.1	26.0	32.8	38.0
	Penetration rate of hull and propeller cleaning (P(HPC))	67.5	67.5	67.5	67.5	67.5
	Penetration rate of air injection (P(AIN))	17.5	17.5	17.5	17.5	17.5
	Penetration rate of optimised hull form (P(OHF))	55.6	79.3	50.0	69.8	70.9
	Penetration rate of speed reduction (P(SRD))	100.0	100.0	100.0	100.0	100.0
	Penetration rate of more efficient propeller (P(MEP))	35.0	55.0	28.0	42.5	50.0
	Penetration rate of quieter propeller (P(QRP))	25.0	30.0	30.0	32.5	25.0
	Joint probability of speed reduction and more efficient propeller (P(SRD & MEP))	35.0	55.0	28.0	42.5	50.0
	Joint probability of speed reduction and quieter propeller (P(SRD & QRP))	25.0	30.0	30.0	32.5	25.0
U&G 2050	Total change in ship traffic volume (ΔN)	35.6	77.7	29.9	43.0	49.6
	Penetration rate of hull and propeller cleaning (P(HPC))	80.0	80.0	80.0	80.0	80.0
	Penetration rate of air injection (P(AIN))	30.0	30.0	30.0	30.0	30.0
	Penetration rate of optimised hull form (P(OHF))	90.0	96.7	73.9	89.3	91.8
	Penetration rate of speed reduction (P(SRD))	100.0	100.0	100.0	100.0	100.0
	Penetration rate of more efficient propeller (P(MEP))	36.0	35.0	30.0	36.0	36.0
	Penetration rate of quieter propeller (P(QRP))	60.0	65.0	50.0	60.0	60.0
	Joint probability of speed reduction and more efficient propeller (P(SRD & MEP))	36.0	35.0	30.0	36.0	36.0
	Joint probability of speed reduction and quieter propeller (P(SRD & QRP))	60.0	65.0	50.0	60.0	60.0

Appendix G NetCDF File Format

Table 26 shows an example of netCDF file format used for the sound map layers.

Table 26 Example of netCDF file format metadata for the northeast Atlantic Ocean sound map layer, quarter 1 of 2016, and 63 Hz frequency.

Main field name	Subfield name	Description
Global Attributes:	**title**	NAVISON Sound Maps
	Institution	EMSA (European Maritime Safety Agency)
	comment	This data set contains shipping sound maps calculated by the NAVISON project
	version	0.1
	Descriptions	region=eastna, year=2016, quarter=1, ship category=ALL, frequency= 00063 Hz, minimum receiver depth=5 m, maximum receiver depth=195 m, spatial observation window (SOW)= 0.22 degree x 0.14 degree , temporal observation window (TOW) = 7889400 s (91 days= 3 months)
crs	**standard_name**	'crs'
	grid_mapping_name	'latitude_longitude'
	epsg_code	'EPSG:4326'
	semi_major_axis	'6378137.0'
	inverse_flattening	'298.257223563'
lat	**standard_name**	'lat'
	long_name	'latitude'
	units	'degrees_north'
	axis	'y'
	_CoordinateAxisType	'Lat'
lon	**standard_name**	'lon'
	long_name	'longitude'
	units	'degrees_east'
	axis	'x'
	_CoordinateAxisType	'Lon'
SPL	**standard_name**	'SPL'
	long_name	'Sound Pressure Level (dB re 1 μPa^2 '
	units	'decibel'
	dBreferencevalue	'1 μPa^2
	_FillValue	NaN
	grid_mapping	'crs'

For the calculation of source level and sound map layers, some abbreviations are used in the expressions following the conventions in the previous NAVISON reports. The source level and sound map layer names encode the following information:

- Region name.
- Year and quarter name (only year name for the annual averages).
- Quantity.
- Vessel category.
- Frequency.

The region names and vessel categories as used in the filenames are shown in Table 27.

Table 27 Region name format.

Region	Region name format
Baltic Sea	balticsea
North Sea	northsea
Black Sea	blacksea
Mediterranean Sea	medsea
Northeast Atlantic Ocean	eastna

The second field in the filename contains the year and quarter information, or just the year in the case of annual averaged layers. The letters 'y' and 'q' precede the year and quarter number fields, marking respectively the start of the year and quarter information in the filename. For example, the third quarter of 2018 is expressed as 'y2018q3.' In cases where map layers are averaged annually, the 'q' letter and subsequent number are replaced with 'avg,' resulting in terms like 'y2018avg' for the annual average for 2018. The third field in the filename is reserved for the metric. The source level and sound map layers represent ASL and sound pressure level (SPL) metrics, respectively, and are identified by 'ASL' and 'SPL' in the filenames. The fourth field in the filename contains the vessel category, encoded with the abbreviations listed in Table 28.

Table 28 Vessel category identifiers.

Vessel category	Abbreviation	Full description
cargo vessel	CAR	cargo vessels and bulk carriers
container ship	CON	container ships
passenger vessel	PAS	cruise and passenger vessels (except ro-ro)
tanker	TGC	tankers and gas carriers
roll on-roll off	RRO	ro-ro vessels (cargo and passenger)
all vessel categories as included in NAVISON	ALL	Includes all ship categories listed above

At the tail end of the filenames, the frequencies are represented with 5-digit and unit fields, such as '00063Hz' and '00125Hz.' Examples of the output netCDF filename format for selected regions, vessel categories, time periods, and frequencies are shown in Table 29.

Table 29 Examples of netCDF filenames.

Region	Time period	Metric	Vessel category	decidecade band centre frequency	netCDF file name
Black sea	First quarter of 2016	SPL	PAS	63 Hz	blacksea_y2016q1_SPL_PAS_00063Hz.nc
Mediterranean Sea	Third quarter of 2018	ASL	CAR	125 Hz	medsea_y2018q3_ASL_CAR_00125Hz.nc
Baltic Sea	Annual averaged of 2020	SPL	ALL	125 Hz	balticsea_y2017avg_SPL_ALL_00125Hz.nc

The filename for the forecast map layers includes an additional field for the forecast scenarios as a prefix before the vessel category as shown in Table 30.

Table 30 Examples of netCDF filenames for the forecast sound map layers

Region	Time period	Forecast Scenario	Vessel category	Decidecade frequency band	netCDF file name
North Sea	Annual average of 2050	GHG	TGC	63 Hz	northsea_y2050avg_SPL_GHG_TGC_00063Hz.nc
Mediterranean Sea	Second quarter of 2030	U&G	CAR	63 Hz	medsea_y2030q2_SPL_U&G_CAR_00063Hz.nc

European Maritime Safety Agency
Praça Europa 4
1249-206 Lisbon, Portugal
Tel +351 21 1209 200
Fax +351 21 1209 210
emsa.europa.eu